Lars Chresten Lund-Hansen
Dorte Haubjerg Søgaard
Brian Keith Sorrell · Rolf Gradinger
Klaus Martin Meiners

Arctic Sea Ice Ecology

Seasonal Dynamics in Algal and Bacterial Productivity

MOREMEDIA ▶

Springer

Springer Polar Sciences

Springer Polar Sciences

Springer Polar Sciences is an interdisciplinary book series that is dedicated to research in the Arctic, sub-Arctic regions, and the Antarctic. In recent years, the polar regions have received increased scientific and public interest. Both the Arctic and Antarctic have been recognized as key regions in the regulation of the global climate, and polar ecosystems have been identified to be particularly susceptible to the ongoing environmental changes. Consequently, the international efforts in polar research have been enhanced considerably, and a wealth of new findings is being produced at a growing rate by the international community of polar researchers.

   Springer Polar Sciences aims to present a broad platform that will include state-of-the-art research, bringing together both science and humanities to facilitate an exchange of knowledge between the various polar science communities. The Series offers an outlet to publish contributions, monographs, edited works, conference proceedings, etc. Topics and perspectives will be broad and will include, but not be limited to: climate change impacts, environmental change, polar ecology, governance, health, economics, indigenous populations, tourism and resource extraction activities. Books published in the series will appeal to scientists, students, polar researchers and policy makers.

More information about this series at http://www.springer.com/series/15180

Lars Chresten Lund-Hansen
Dorte Haubjerg Søgaard
Brian Keith Sorrell • Rolf Gradinger
Klaus Martin Meiners

Arctic Sea Ice Ecology

Seasonal Dynamics in Algal and Bacterial
Productivity

Lars Chresten Lund-Hansen
Department of Bioscience,
Arctic Research Centre, Bioscience
Aarhus University
Aarhus C, Denmark

Brian Keith Sorrell
Aquatic Biology,
Department of Bioscience
Aarhus University
Aarhus C, Denmark

Klaus Martin Meiners
Antarctic Climate and Ecosystems CRC
University of Tasmania
Hobart, TAS, Australia

Dorte Haubjerg Søgaard
Greenland Climate Research Centre
Greenland Institute of Natural Resources
Nuuk, Greenland

Rolf Gradinger
Department of Arctic and Marine Biology
UiT, the Arctic University of Norway
Tromsø, Norway

Foreword

The sea ice ecosystem in the remote Arctic Ocean is the fastest changing habitat on Earth yet it is the least studied. To forecast its fate in a future ocean impacted by anthropogenic change we need to understand how organisms adapt and thrive under highly unpredictable conditions where thermodynamics, divergence and deformation processes continuously alter habitat characteristics.

Life in the ocean begins at its surface as one-way energy from sunlight supports primary production at the base of the marine trophic network – a phenomenon that is constrained in the Arctic Ocean by the presence of sea ice as well as extreme seasonal changes that limit the amount of light available in the upper ocean. The sea ice biota consists of a complete food web with primary and secondary producers, a microbial loop and three to four trophic levels. The bottom ice layer is typically the most biologically productive habitat as nutrients are mostly provided by the underlying water column.

Sea ice algae constitute a major carbon source in the Arctic food chain during early spring before ice melt, and understanding the dynamics and drivers of ice algae carbon production is absolutely essential as they, to a large extent, dictate the response of the entire Arctic marine ecosystem.

A cornerstone of the book is the concept that sea ice is an ecosystem on its own, and the only ecosystem which melts and partly disappears every summer to be reestablished during autumn and winter. The authors take the reader on a journey to the Arctic covering the different seasons from ice formation where algae and bacteria are incorporated into the newly formed sea ice, to maximum ice thickness and optimal growth conditions for ice algae during spring, to summer conditions where sea ice melt away and organisms are released to the underlying water.

A large part of the research presented in the book is based on extensive fieldwork in Greenland by the authors, and four case studies from the field are included to examine different complex phenomena under natural settings to further our understanding of the dynamic nature of sea ice and its inhabitants. A thorough description of methods and techniques provides information on how to sample and handle sea ice and how to process, analyse and quantify various physical, chemical and biological parameters in sea ice.

Finally, a description of the role and importance of sea ice and sea ice biota at large scales and in relation to the effects of climate change is included. Given the rapid changes in sea ice conditions, the question is whether more light in an ice-free water column will increase pelagic primary production in the Arctic Ocean. There is still a lot to be discovered in the Arctic and hopefully the book will inspire a new generation of researchers with interest for the Arctic.

Arctic Research Centre, Aarhus University   Søren Rysgaard
Aarhus, Denmark
1 June 2020

Preface

This book deals with sea ice ecology, with a focus on sea ice algae and other microbes such as bacteria and small metazoans (meiofauna) residing inside or at the bottom of the sea ice, all referred to as the sympagic biota of the ice. Sea ice also provides a habitat for a wide and ecologically important range of organisms including zooplankton, fish, seals, whales, walruses, birds, and polar bears. Some of these organisms are entirely dependent on sea ice for feeding, resting, and/or breeding but are not part of the sympagic biota. These organisms may also depend on the existence of the bacteria and ice algae which form the basis of the ice-associated Arctic food webs. This book is organized by season, describing the physical, optical, biological, and geochemical conditions typical for each specific season, recognizing that a large part of this ecosystem actually disappears (melts) in summer and is reestablished again in autumn and winter. This book, its case studies, and its descriptions of seasonal processes are very much focused on the Arctic. There are significant differences in sea ice types and conditions between the Arctic and Antarctic though sampling and methods are similar for both polar regions. This book targets university students at the master's or PhD level and scientists in general.

Aarhus C, Denmark   Lars Chresten Lund-Hansen
Nuuk, Greenland   Dorte Haubjerg Søgaard
Aarhus C, Denmark   Brian Keith Sorrell
Tromsø, Norway   Rolf Gradinger
Hobart, Australia   Klaus Martin Meiners

Acknowledgments

Contents

Chapter 1
The Book, and Ecology of Sea Ice

Abstract This chapter describes the structure of the book and the diverse significance and importance of sea ice. The first section explains how and why the book is structured following the seasonal events governing the abiotic and biotic parameters in sea ice (1.1). The second section places sea ice into a physical and geopolitical perspective with the new and developing international borders in the Arctic Ocean (1.2). Sea ice ecosystems are then compared to other ecosystems (1.3), followed by a section describing the important and global ecological features of sea ice (1.4).

Keywords Seasonal variability · Arctic marine ecosystem · Ecological role of sea ice

1.1 Follow the Seasons

In this book, we emphasize the seasonal sea ice dynamics, highlighting the strong seasonal signal from development of the ice during autumn, all through the winter, and through to the melt and eventual disappearance of the ice in summer. Most ecosystems on Earth experience seasonal variations in the physical environment as with light or temperature, but it is difficult to envisage any other system where such a large part of the ecosystem simply disappears during spring and summer to be regenerated the following autumn and winter. The book is therefore organized differently to a traditional "The Ecology of …." textbook, which in different chapters would focus on the physical, chemical, and biological components. Here we have strongly emphasized the seasonal variation in all parameters, considering that a large part of this ecosystem melts and disappears in spring and summer, and is re-established again in autumn and winter. The physical, optical, biological, and chemical conditions are then described in each chapter according to their seasonal context. For instance, physical ice growth and ice formation are more prominent features during autumn compared to winter when there is solid ice with minor variations in the physical conditions. Accordingly, the book is organized in three seasonal chapters: autumn, winter, and spring/summer, with focus on important and dominant seasonal parameters, and how these affect and relate to the sympagic biota of ice algae, bacteria, and meiofauna. The chapters also include several case studies based on the authors fieldwork
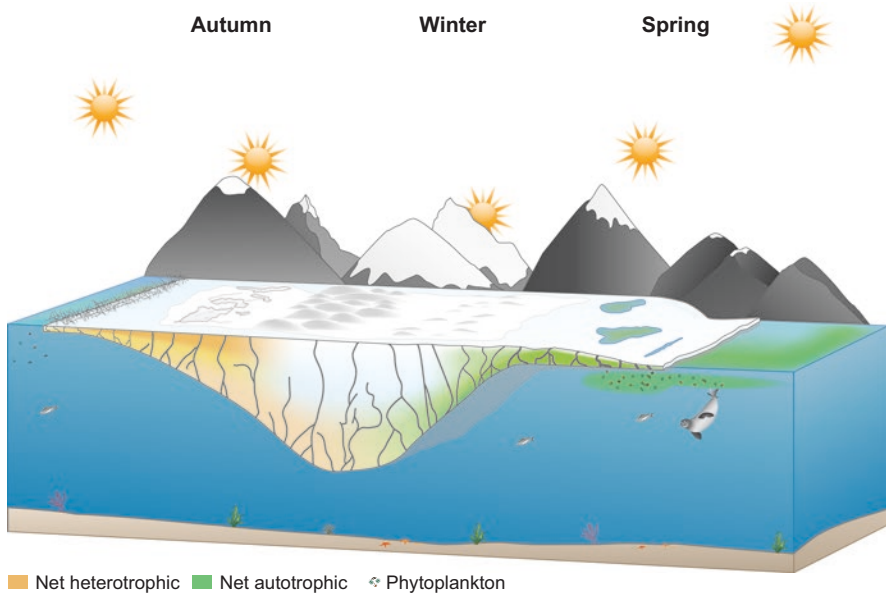
Fig. 1.1 Schematic representation of the evolution of bacterial productivity (net heterotrophic in orange) and algal productivity (net autotrophic in green) in ice-covered seas during all phases of the sea ice formation and decay cycle in the Arctic

in Greenland, the Arctic Ocean, Fram Strait, and Antarctica to exemplify themes and topics from the general text. The final chapter is a methods section, where methods commonly applied in sea ice ecology research are described in more detail, for the benefit of readers seeking a deeper understanding. The scenario of the book is envisaged in Fig. 1.1, which depicts the seasonal progress of the sea ice from its establishment in autumn, through a period of thick ice with a snow cover in winter. This is followed by the decay cycle of thinner ice and snow, and development of melt ponds on the surface of the ice, and finally the complete ice melt. The seasonal succession from yellow/orange colours to greenish depicts the change from a net heterotrophic bacteria-based activity in autumn/winter, to a net autotrophic ice algae-based activity in spring/summer. Grey and branched lines in the ice are the brine channels illustrating that the ice is a porous medium.

1.2   Physical and Geopolitical Perspectives of Sea Ice

Sea ice is an inherent, characteristic, and extremely important entity in polar regions, from physical, chemical, biological, economical, and political perspectives. Sea ice in the Arctic and Antarctic together covers about 10% of the world's oceans at its average winter maximum extent of about 34 million km², an area larger than Africa (30.4 million km²). The Arctic sea ice extent varies between a minimum of

4.7–7.7 million km^2 and a maximum of 14.3–16.3 million km^2 (median values, 1981–2010). The seasonal difference of about 8.0 million km^2 between summer and winter extent is comparable to the total area of the USA (9.6 million km^2). Sea ice cover is also an important indicator and mediator of climate change, as seen from the significant decrease in sea ice extent and volume over recent decades in the Arctic Ocean. Changes in sea ice extent have far-reaching consequences. For example, ice and snow reflect light and radiation back into space, while most of this radiation would otherwise be absorbed in an ice-free water column. It is foreseen that the entire Arctic Ocean will reach an ice-free state for several weeks in summer within three to four decades, except for a few remaining areas of multiyear ice north of Greenland. The sea ice extent during winter is also decreasing, but at a lower rate compared to the rate of the summer ice extent. This decrease in sea ice extent is also driving a growing economical and thereby political interest in the Arctic, with less and less summer ice opening up both the Northeast and Northwest Passages for commercial shipping. These routes are shorter and safer than classical shipping routes and would save expensive fuel. The decreasing extent of summer sea ice has also opened the extensive and shallow (<200 m) Arctic shelf areas, many of which contain huge amounts of oil and gas reserves. Nearly 50% of the Arctic Ocean consists of such shelf areas. Deep-sea mining in the Arctic Ocean for rare elements will also be an issue in the future, and a reduced sea ice cover with more light and more photosynthesis in the water column is predicted to increase fishery catches in the Arctic Ocean. All of the five Arctic countries (USA, Canada, Russia, Greenland, and Norway) have borders in the central Arctic Ocean. These countries have a 200 nautical mile wide zone from their coast and outwards as their sovereign region. However, borders in the central Arctic Ocean have not yet been agreed upon and the countries have specified their territorial claims based on several years of geological exploration in the Arctic Ocean. The UN-founded organization United Nations Law of the Sea Convention (UNCLOS) validates the data presented to support the territorial claims.

1.3   Sea Ice as an Ecosystem

Sea ice ecosystems comprise a physical environment of ice, snow, brine channels and seawater at a particular location with specific pathways and exchanges of energy and matter, and with a variety of organisms that live and thrive there. Organisms living inside the ice in the brine channels or at the bottom of the ice are called sea ice or sympagic biota, and include bacteria, viruses, algae, fungi, ciliates, heterotrophic flagellates, amphipods, copepods, and several others as shown in Fig. 1.2. These organisms form a unique food-web inside the ice, and facilitate specific pathways of matter and transport of energy, as heterotrophic bacteria digest particulate organic material (POM) and or dissolved organic matter (DOM) excreted by the ice algae. Ciliates and flagellates ingest ice algae and bacteria, and their breakdown of organic material also generates inorganic nutrients available for the ice algae and their
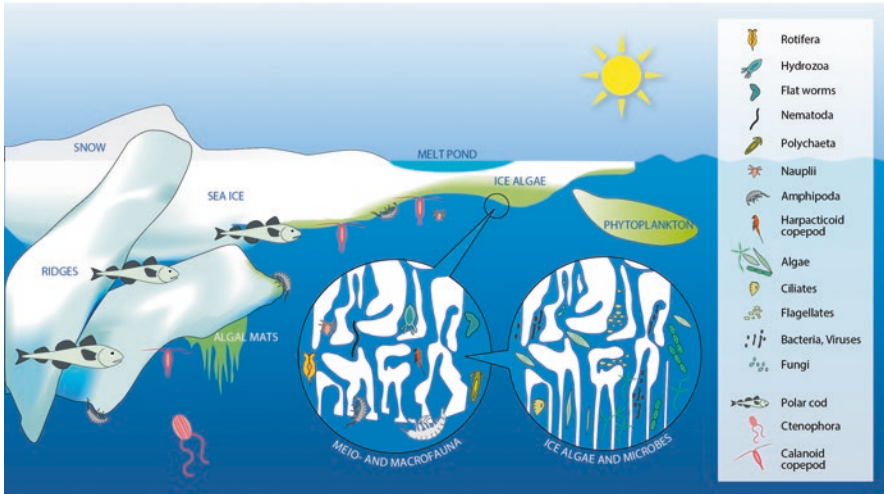
Fig. 1.2 Sea ice ecosystem with microhabitats for a variety of biota including single-celled eukaryotes (labelled algae), meio- and macrofauna, bacteria and viruses, under-ice fauna (amphi-pods and copepods), and polar cod (*Boreogadus saida*). (Courtesy: State of the Arctic Marine Biodiversity Report, https://www.caff.is/marine/marine-monitoring-publications/state-of-the-arctic-marine-biodiversity-report)

photosynthesis. Metazoans small enough to fit into the brine channel network are termed meiofauna and are mainly herbivores. In addition to the brine channel community, other organisms also inhabit the ice-water interface. Here the in-ice biota interact with other organisms such as larger zooplankton in the water column that also graze on ice algae (Fig. 1.2). The focus of this book is the in-ice biota and especially the ice algae and bacteria. An understanding of the living conditions for ice algae and bacteria implies descriptions of **(1)** the physical growth and structure of the sea ice as a habitat, **(2)** the optical properties of the ice and the overlying snow, especially concerning how much light reaches the ice algae for photosynthesis, and **(3)** the availability and concentrations of nutrients. Sea ice is an extreme environment where survival is challenging for most organisms, though bacteria and ice algae are both halophiles i.e. can live at very high salinities and cryophiles i.e. can live at very low temperatures. Oceans covered with ice are also found elsewhere in the solar system, such as on Saturn's moon Enceladus, and given this resemblance, sea ice is also of great interest in an astrobiological context given that sampling there is not an option yet (Martin and McMinn 2018). Ice algae attached to the sea ice or inside the brine channels are species of microalgae that have adapted to this high saline, low light, and cold environment. Some of the ice algae species also occur as drifting organisms in the water column below termed phytoplankton, where the main difference is that ice algae are fixed in position in or on the ice. It is estimated that sea ice algae account for a modest 4–6% of the pelagic primary production in the entire Arctic Ocean, but their major importance is being the only carbon source during late winter and early spring for higher trophic levels in the Arctic food chain (i.e. ice algae → zooplankton → fish → seals → polar bears). The pelagic carbon production

is based on phytoplankton in the water column and commences after sea-ice surface melt and ice break-up. The important role of the sea ice algae is illustrated in a recent study suggesting that 70–100% of the polar bear diet is derived from sympagic ice algae rather than pelagic phytoplankton, meaning that 70–100% of their food intake occurs during the ice-covered season, and further emphasizes the animals dependence on sea ice (Brown et al. 2018).

1.4   Ecological Role of Sea Ice

Sea ice algae primary production in the Arctic Ocean is about 20 Tg C year^{-1} (Arrigo 2017) compared to a pelagic primary production in the Arctic Ocean of 350–500 Tg C year^{-1} (Sakshaug 2004). Primary production rates in Arctic sea ice vary between 0.2 and 463.0 mg C m^{-2} day^{-1} (Arrigo 2017) which is low compared to e.g., estuarine ecosystems with rates up to 4101.0 mg C m^{-2} day^{-1} (Stiling 1996). The highest ice algal production rates are comparable to the 342.0 mg C m^{-2} day^{-1} reported for oligotrophic open oceans (Stiling 1996). There is, on the other hand, considerable spatial variation in rates of ice algae primary production in the Arctic, with average rates of 116.8 mg C m^{-2} day^{-1} and 93.7 mg C m^{-2} day^{-1} reported for the Canadian Arctic Archipelago and the North Water polynya area in Northern Baffin Bay, respectively (Arrigo 2017). Much lower rates of 0.1 mg C m^{-2} day^{-1}, 8.6 mg C m^{-2} day^{-1} and 21 mg C m^{-2} day^{-1} have been reported from various areas around Greenland (Rysgaard et al. 2001; Mikkelsen et al. 2008; Lund-Hansen et al. 2018). Ice algae production data in Fig. 1.3 comprise mostly coastal and shelf areas, based on the ^{14}C incubation method (Sect. 6.6). These differences in production rates between Greenland and the Canadian Arctic Archipelago are significant despite possible minor methodological variations. The reasons for the differences
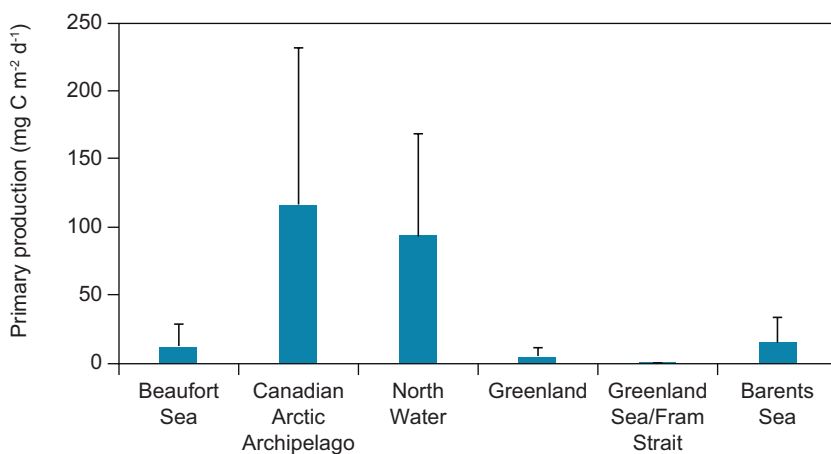
Fig. 1.3 Ice algae primary production in different Arctic regions. Data points represent treatment mean ± SD (Compiled from Barber et al. 2015; Leu et al. 2015; Arrigo 2017)

are unknown but studies have pointed towards the effects of nutrient availability and differences in water column stratification. A strong stratification inhibits vertical mixing and transport of nutrients from below to the surface layer (Schuback et al. 2017), and is important at points in time when the surface layer is depleted of nutrients. Exchange of sea ice brines and seawater between the ice and the water column induced by under-ice currents may additionally transport nutrients into the ice, and may be a key driver of productivity in land-fast sea ice regimes open to coastal currents and tidal influence (Cota and Horne 1989; Meiners and Michel 2017). Areas with high primary production rates as in the Canadian Arctic Archipelago (Fig. 1.3) are generally also areas of high Chlorophyll *a* (Chl *a*) concentrations as a proxy for ice algae biomass, which also varies between sites and over time (Fig. 1.4). Ice algal
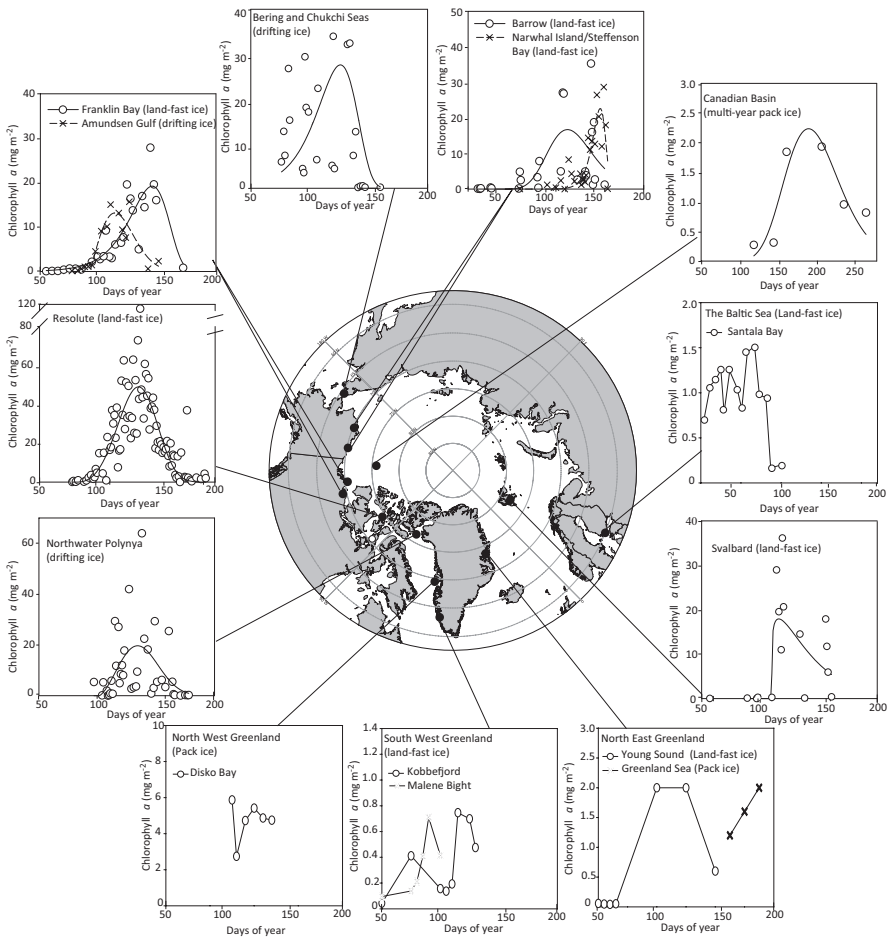
Fig. 1.4 Seasonal development of Chl *a* concentrations in sea ice in different regions of the Arctic. (Modified from: Leu et al. 2015) with additional data from the Baltic Sea (Kaartokallio 2004), Young Sound (Søgaard et al. 2019, Rysgaard and Glud 2007), Greenland Sea (Gradinger 1999), Disko Bay (Buck et al. 1998) and Malene Bight (Søgaard et al. 2010). (Note different ordinate scales for Chl *a*)

production, and the increase in biomass, can potentially start at first light and depends on snow and sea ice thickness as well as latitude. Time-series of seasonal irradiance (PAR) from three research stations at 81°, 74° and 64° N in Greenland demonstrate how the sun rises later and sets earlier with increasing latitude (Fig. 1.5). PAR is the photosynthetic active radiation between 400 and 700 nm (visible light)
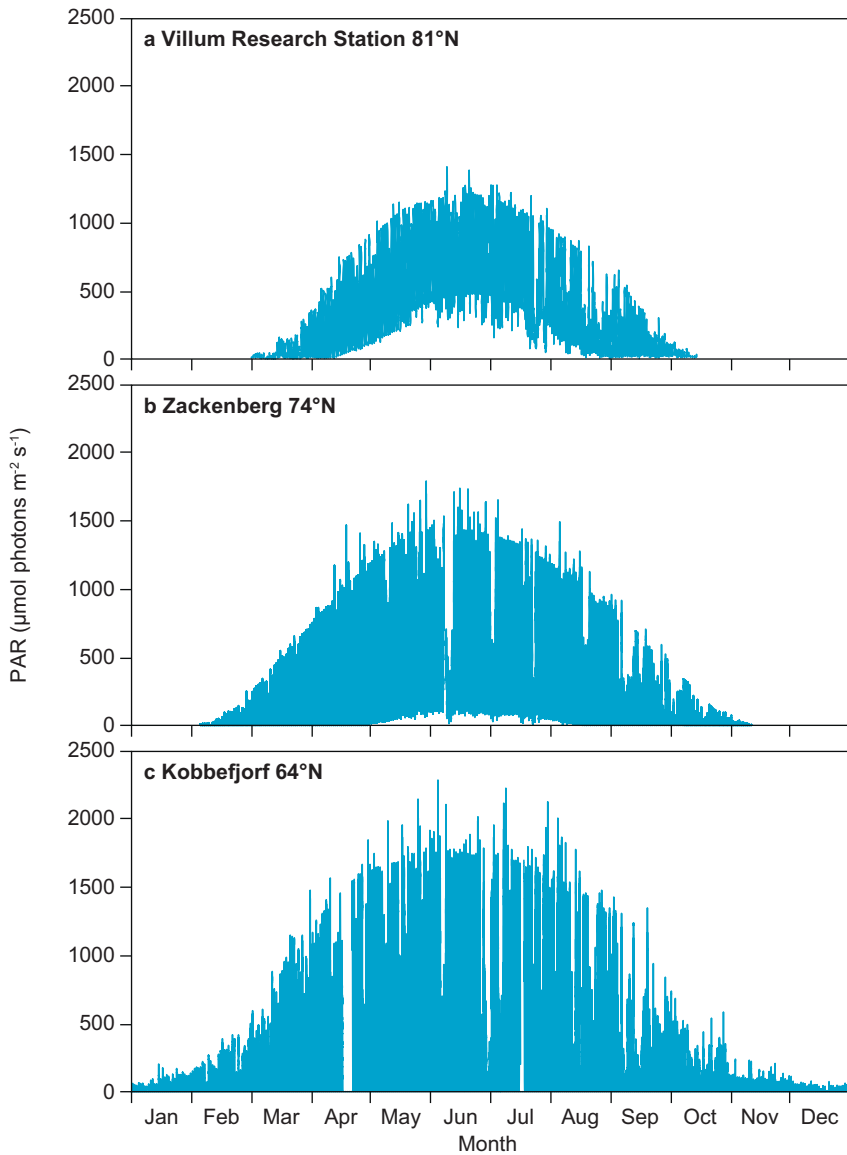
Fig. 1.5 Seasonal irradiance (PAR) at Villum Research Station, NE Greenland (81°N) (**a**), at Zackenberg Research Station, NE Greenland (74°N) (**b**), and at Kobbefjord, SW Greenland (64°N) (**c**)

utilized by the algae for photosynthesis. Midnight sun prevails between mid-April and the middle of August at 81° N but for a shorter period at Zackenberg at 74° N. In comparison there is no midnight sun at lower latitudes (64° N), but the sun is always above the horizon during winter. The summer PAR maximum decreases with latitude from a maximum of 1800 μmol m^{-2} s^{-1} at 64° N in Kobbefjord near Nuuk to about 1200 μmol m^{-2} s^{-1} at Station North. In accordance, there is a general increase in Chl *a* concentrations from mid to late April between latitudes 70°–80° N, and earlier at lower latitudes (Leu et al. 2015) (Fig. 1.4). This is exemplified by the beginning of April increase in Chl *a* in the Northwater Polynya (76° N), which starts in late February further south (64° N) in the Godthåbsfjord (Fig. 1.4). There is an average time span of about 90 days (3 months) between the initial increase in Chl *a* and when Chl *a* once again decreases to minimum concentrations. The size of the bloom varies significantly between a maximum of nearly 120 mg Chl *a* m^{-2} in Resolute Bay, Canada, and around 0.5 mg Chl *a* m^{-2} in Young Sound, NE Greenland. Organisms living inside the ice together form the sympagic communities and comprise taxonomically diverse groups including Eubacteria, Archaea, ice algae, viruses, fungi, ciliates, heterotrophic flagellates, amphipods, copepods, polychaetes, nematodes and more (Fig. 1.2). The communities can be divided into three main groups based on the size of the organisms (Bluhm et al. 2017). The first group is sea ice microbes including ice algae, Eubacteria, and Archaea; the second group is sea ice meiofauna consisting of multicellular organisms in the range 62–500 μm such as rotifers and nematodes; the third group comprises sea ice macrofauna organisms >500 μm such as amphipods and large copepods. The Eubacteria and Archaea use and decompose the organic material produced by ice algae, thereby remineralizing nutrients for primary production by the ice algae (Deming and Collins 2017). The sea ice meiofauna grazes on the ice algae as observed in Arctic Canada, where Grainger and Hsiao (1990) estimated that the meiofauna in the ice could consume about a quarter of the ice algal biomass. Typical estimates of meiofauna biomass from other areas in the Arctic and Antarctic are lower and often below 10% of the algal biomass (Gradinger 1999). Amphipods such as *Gammarus wilkitzkii*, *Onisimus glacialis* and *Apherusa glacialis* also graze directly on the ice algae, with relatively high grazing rates for all three species, e.g., *Gammarus wilkitzkii* can graze up to 73% of the ice algae biomass (Brown et al. 2017). The zooplankton species grazing on ice algae are generally *Calanus hyperboreus, C. finmarchius*, and *C. glacialis,* which are dominant species in the Arctic (Espinasse et al. 2017) but with different ecologies (Scott et al. 2000) (Fig. 1.6). Lønne and Gulliksen (1991) gave a comprehensive study of the sympagic fauna and food chain in the Barents Sea. Ice algae grazed by amphipods and zooplankton are consumed and establish a secondary pathway of organic material in the ice-pelagic-benthic coupling. Studies have established organic carbon budgets for the various components in the Arctic marine food web of the Barents Sea (Reigstad et al. 2011; Kortsch et al. 2015), where stable isotope compositions are often applied in carbon budget and food web structure analyses (Pineault et al. 2013). The zooplankton and the amphipods are again consumed by fish and especially the polar cod (*Boreogadus saida*), a circum-Arctic

Fig. 1.6 The Arctic copepod *Calanus hyperboreus*. (Photograph by: Authors)

Fig. 1.7 A deep sea
cucumber (*Kolga hyalina*)
(5–6 cm) feeding on
clumps of the ice algae
Melosira arctica at 3569 m
depth in the Arctic Ocean.
(Photograph by: Antje
Boetius)

species that occurs in high numbers near sea ice (David et al. 2016). The polar cod
is strongly dependent on the occurrence of ice algae, as stable isotope analyses have
shown that between 34% and 65% of the carbon taken up by polar cod is derived
from ice algae through grazing on amphipods and copepods (Kohlbach et al. 2017).
Much of the organic material produced by the ice algae and not grazed by the zoo-
plankton sinks towards the ocean bottom (Juul-Pedersen et al. 2008; Szymanski and
Gradinger 2016) where it is available for benthic organisms on the shelf (Tamelander
et al. 2006) and in the fjords (McMahon et al. 2006). It was recently observed that
ice algae contribute organic material to the deep sea where invertebrates (*Kolga
hyalina*) feed on clumps of the ice algal diatom *Melosira arctica* at 3569 m depth in
the Arctic Ocean (Boetius et al. 2013) (Fig. 1.7). During late spring or early summer

when the sea ice starts to break up, some of the ice algae leave the ice, either due to formation of larger brine channels and flushing at increased sea ice temperatures, or due to melting of the ice at the bottom. This transfer of ice algae from the sea ice to the pelagic water seeds the water column, and can initiate the pelagic primary production (Gradinger 2009; Selz et al. 2018). It was until very recently assumed that the pelagic primary production below the ice was extremely low and insignificant during the ice covered period, but several recent observations of pelagic phytoplankton blooms below sea ice have changed this view (e.g. Mundy et al. 2009; Arrigo et al. 2014). With younger and thinner sea ice, coupled with an earlier onset of snow melt and increased melt pond formation, it is foreseen that such under-ice blooms will be more frequent in the future (Arrigo et al. 2014; Horvat et al. 2017). It is, on the other hand, unknown how the under-ice blooms will affect ice algae communities and if this bloom is driven by seeding from the sea ice to the underlying water column.

References

Arrigo, K. R. (2017). Sea ice as a habitat for primary producers. In D. N. Thomas (Ed.), *Sea ice* (3rd ed., pp. 352–369, 652 pp). Oxford: Wiley Blackwell.

Arrigo, K. R., Perovich, D., Pickart, R. R., Brown, Z. W., Dijken, G. L., Lowry, K. E., Mills, M. M., Palmer, M. A., Balch, W. M., Bates, N. R., Benitez-Nelson, C. R., Brownlee, E., Frey, K. E., Laney, S. R., Mathis, J., Matsouka, A., Mitchell, B. G., Moore, G. W. K., Reynolds, R. A., Sosik, H. M., & Swift, J. H. (2014). Phytoplankton blooms beneath the sea ice in the Chukchi Sea. *Deep-Sea Research II, 105*, 1–16. https://doi.org/10.1016/j.dsr2.2014.03.018.

Barber, D. G., Hop, H., Mundy, C. J., Else, B., Dmitrenko, I. A., Tremblay, J. E., Ehn, J. K., Assmy, P., Daase, M., Candlish, L. M., & Rysgaard, S. (2015). Selected physical, biological and biogeochemical implications of a rapidly changing Arctic Marginal Ice Zone. *Progress in Oceanography, 139*, 122–150. https://doi.org/10.1016/j.pocean.2015.09.003.

Bluhm, B. A., Swadling, K. M., & Gradinger, R. (2017). Sea ice as a habitat for macrograzers. In D. N. Thomas (Ed.), *Sea ice* (3rd ed., pp. 394–414, 652 pp). Oxford: Wiley Blackwell.

Boetius, A., Albrecht, S., Bakker, K., Beinhold, C., Felden, J., Fernández-Méndez, Hendricks, S., Katlein, C., Lalande, C., Krumpen, T., Nicolaus, M., Peeken, I., Rabe, B., Rogacheva, A., Rybakova, E., Somavilla, R., & Wenzhöfer, F. (2013). Export of algal biomass from the melting Arctic sea ice. *Science, 339*. https://doi.org/10.1126/science.1231346.

Brown, T., Assmy, P., Hop, H., Wold, A., & Belt, S. T. (2017). Transfer of ice algae carbon to ice-associated amphipods in the high-Arctic pack ice. *Journal of Plankton Research, 39*, 664–674. https://doi.org/10.1093/plankt/fbx030.

Brown, T. A., Galicia, M. P., Thiemann, G. W., Belt, S. T., Yurkowski, D. J., & Dyck, M. G. (2018). High contributions of sea ice derived carbon in polar bear (*Ursus maritimus*) tissue. *PLoS ONE* 13(1): e0191631. https://doi.org/10.1371/journal.pone.0191631.

Buck, K. R., Nielsen, T. G., Hansen, B. W., Gastrup-Hansen, D., & Thomsen, H. A. (1998). Infiltration phyto- and protozooplankton assemblages in the annual sea ice of Disko Island, West Greenland, spring 1996. *Polar Biology, 20*, 377–381. https://doi.org/10.1007/s003000050317.

Cota, G. F., & Horne, E. P. W. (1989). Physical control of Arctic ice algal production. *Marine Ecology Progress Series, 52*, 111–121. https://doi.org/10.3354/meps052111.

David, C., Lange, B., Krumpen, T., Schaafsma, F., Franeker, J. A. V., & Flores, H. (2016). Under-ice distribution of polar cod *Boreogadus saida* in the central Arctic Ocean and their asso-

ciation with sea-ice habitat properties. *Polar Biology, 39*, 981–994. https://doi.org/10.1007/s00300-015-1774-0.

Deming, J. W., & Collins, R. E. (2017). Sea ice as a habitat for Bacteria, Archaea and viruses. In D. N. Thomas (Ed.), *Sea ice* (3rd ed., pp. 326–351, 652 pp). Oxford: Wiley Blackwell.

Espinasse, M., Halsband, C., Varpe, Ø., Gislason, A., Gudmundsson, K., Falk-Petersen, S., & Eiane, K. (2017). The role of local and regional environmental factors for *Calanus finmarchicus* and *C. hyperboreus* abundances in the Nordic Seas. *Polar Biology, 40*, 2363–2380. https://doi.org/10.1007/s00300-017-2150-z.

Gradinger, R. (1999). Vertical fine structure of the biomass and composition of algal communities in Arctic pack ice. *Marine Biology, 133*, 745–754. https://doi.org/10.1007/s002270050516.

Gradinger, R. (2009). Sea-ice algae: Major contributors to primary production and algal biomass in the Chukchi and Beaufort Seas during May/June 2002. *Deep Sea Research Part II Topical Studies in Oceanography, 56*, 1201–1212. https://doi.org/10.1016/j.dsr2.2008.10.016.

Grainger, E. H., & Hsiao, S. I. C. (1990). Trophic relationships of the sea ice meiofauna in Frobisher Bay, Arctic Canada. *Polar Biology, 10*, 283–292.

Horvat, C., Jones, D. R., Iams, S., Schroeder, D., Flocco, D., & Feltham, D. (2017). The frequency and extent of sub-ice phytoplankton blooms in the Arctic Ocean. *Science Advances, 3*(3). https://doi.org/10.1126/sciadv.1601191.

Juul-Pedersen, T., Michel, K., Gosselin, M., & Seuthe, L. (2008). Seasonal changes in the sinking export of particulate material under First-year sea ice on the Mackenzie Shelf (western Canadian Arctic). *Marine Ecology Progress Series, 353*, 13–25. https://doi.org/10.3354/meps07165.

Kaartokallio, H. (2004). Food web components, and physical and chemical properties of Baltic Sea ice. *Marine Ecology Progress Series, 273*, 49–63. https://doi.org/10.3354/meps273049.

Kohlbach, D., Lange, B. A., Schaafsma, F. L., David, C., Vortkamp, M., Graeve, M., Franeker, J. A., Krumpen, T., & Flores, H. (2017). Ice algae-produced carbon is critical for overwintering of Antarctic Krill *Euphausia superba*. *Frontiers Marine Science, 4*, 310. https://doi.org/10.3389/fmars.2017.00310.

Kortsch, S., Primicerio, R., Fossheim, M., Dolgov, A. V., & Aschan, M. (2015). Climate change alters the structure of arctic marine food webs due to poleward shifts of boreal generalists. *Proceedings of the Royal Society B: Biological Sciences, 282*. https://doi.org/10.1098/rspb.2015.1546.

Leu, E., Mundy, C. J., Assmy, P., Campbell, K., Gabrielsen, T. M., Gosselin, M., Juul-Pedersen, T., & Gradinger, R. (2015). Arctic spring awakening – Steering principles behind the phenology of vernal ice algal blooms. *Progress in Oceanography, 139*, 151–170. https://doi.org/10.1016/j.pocean.2015.07.012.

Lønne, O. J., & Gulliksen, B. (1991). Source, density and composition of sympagic fauna in the Barents Sea. *Polar Research, 10*, 289–294. https://doi.org/10.3402/polar.v10i1.6747.

Lund-Hansen, L. C., Hawes, I., Nielsen, M. H., Dahllöf, I., & Sorrell, B. K. (2018). Summer meltwater and spring sea ice primary production, light climate and nutrients in an Arctic estuary, Kangerlussuaq, west Greenland. *Arctic, Antarctic and Alpine Research, 50*. https://doi.org/10.1080/15230430.2017.1414468.

Martin, A., & McMinn, A. (2018). Sea ice, extremophiles and life on extra-terrestrial ocean worlds. *International Journal of Astrobiology, 17*, 1–16. https://doi.org/10.1017/S1473550416000483.

McMahon, K. W., Ambrose, W. G., Johnson, B. J., Sun, M.-Y., Lopez, G. R., Clough, L. M., & Carroll, M. L. (2006). Benthic community response to ice algae and phytoplankton in Ny Ålesund, Svalbard. *Marine Ecology Progress Series, 310*, 1–14. https://doi.org/10.3354/meps310001.

Meiners, K. M., & Michel, C. (2017). Dynamics of nutrients, dissolved organic matter and exopolymers in sea ice. In D. N. Thomas (Ed.), *Sea ice* (3rd ed., pp. 415–432, 652 pp). Oxford: Wiley Blackwell. https://doi.org/10.1002/9781118778371.ch17

Mikkelsen, D. M., Rysgaard, S., & Glud, R. N. (2008). Microalgal composition and primary production in Arctic sea ice: A seasonal study from Kobbefjord (Kangerluarsunnguaq), West Greenland. *Marine Ecology Progress Series, 368*, 65–74. https://doi.org/10.3354/meps07627.

Mundy, C. J., Gosselin, M., Ehn, J., Gratton, Y., Rossnagel, A., Barber, D. G., Martin, J., Trembley, J. E., Palmer, M., Aarigo, K. R., Darnis, G., Fortier, L., Else, B., & Papakyriakou, T. (2009). Contribution of under-ice primary production to an ice-edge upwelling phytoplankton bloom in the Canadian Beaufort Sea. *Geophysical Research Letters, 36*, L17601. https://doi.org/10.1029/2009GL038837.

Pineault, S., Tremblay, J.-É., Gosselin, M., Thomas, H., & Shadwick, E. (2013). The isotopic signature of particulate organic C and N in bottom ice: Key influencing factors and applications for tracing the fate of ice-algae in the Arctic Ocean. *Journal of Geophysical Research, 118*, 287–300. https://doi.org/10.1029/2012JC008331.

Reigstad, M., Carroll, J., Slagstad, D., Ellingsen, I., & Wassmann, P. (2011). Intra-regional comparison of productivity, carbon flux and ecosystem composition within the northern Barents Sea. *Progress in Oceanography, 90*, 33–46. https://doi.org/10.1016/j.pocean.2011.02.005.

Rysgaard, S., & Glud, R. N. (Eds.) (2007). *Carbon cycling in Arctic marine ecosystems: Case study Young Sound*. Meddelelser om Grønland. Bioscience 58, 214 pp. DCE Copenhagen, Denmark.

Rysgaard, S., Kühl, M., Glud, R. N., & Hansen, J. W. (2001). Biomass, production and horizontal patchiness of sea ice algae in a high-Arctic fjord (Young Sound, NE Greenland). *Marine Ecology Progress Series, 223*, 15–26. https://doi.org/10.3354/meps223015.

Sakshaug, E. (2004). Primary and secondary production in the Arctic seas. In R. Stein & R. W. MacDonald (Eds.), *The organic carbon cycle in the Arctic Ocean* (pp. 57–81, 363 pp). Berlin Heidelberg: Springer.

Schuback, N., Hoppe, C. J. K., Tremblay, J. E., Maldonado, M. T., & Tortell, P. D. (2017). Primary productivity and the coupling of the photosynthetic electron transport and carbon fixation in the Arctic Ocean. *Limnology and Oceanography, 62*, 898–921. https://doi.org/10.1002/lno.10475.

Scott, C. L., Kwasniewski, S., Falk-Petersen, S., & Sargent, J. R. (2000). Lipids and life strategies of *Calanus finmarchicus, Calanus glacialis* and *Calanus hyperboreus* in late autumn, Kongsfjorden, Svalbard. *Polar Biology, 23*, 510–516. https://doi.org/10.1007/s003000000114.

Selz, V., Saenz, B. T., van Dijken, G. L., & Arrigo, K. R. (2018). Drivers of ice algal bloom variability between 1980 and 2015 in the Chukchi Sea. *Journal of Geophysical Research, 123*, 7037–7052. https://doi.org/10.1029/2018JC014123.

Søgaard, D. H., Kristensen, M., Rysgaard, S., Glud, R. N., Hansen, P. J., & Hilligsøe, K. M. (2010). Autotrophic and heterotrophic activity in Arctic first-year sea ice: Seasonal study from Malene Bight, SW Greenland. *Marine Ecology Progress Series, 419*, 31–45. https://doi.org/10.3354/meps08845.

Søgaard, D. H., Deming, J. W., Meire, L., & Rysgaard, S. (2019). Effects of microbial processes and $CaCO_3$ dynamics on inorganic carbon cycling in snow-covered Arctic winter sea ice. *Marine Ecology Progress Series*. https://doi.org/10.3354/meps12868.

Stiling, P. D. (1996). *Ecology: Theories and applications* (539 pp). Upper Saddle River: Prentice Hall.

Szymanski, A., & Gradinger, R. (2016). The diversity, abundance and fate of ice algae and phytoplankton in the Bering Sea. *Polar Biology, 39*, 309–325. https://doi.org/10.1007/s00300-015-1783-z.

Tamelander, T., Renaud, P. E., Hop, H., Carroll, M. L., Ambrode, W. G., & Hobson, K. A. (2006). Trophic relationships and pelagic-benthic coupling during summer in the Barents Sea Marginal Ice Zone revealed by stable carbon and nitrogen isotope measurements. *Marine Ecology Progress Series, 310*, 33–46. https://doi.org/10.3354/meps310033.

Chapter 2
Autumn, Development and Consolidation of Sea Ice

Abstract This chapter describes the period of development of new ice during autumn freeze-up, different ice types, and development of the brine channels (2.1). Optical properties of young and developing sea ice are described in terms of the transition from open water to bare sea ice, that later can be covered by snow (2.2). The incorporation and scavenging of ice algae, bacteria and meiofauna from the water column during ice growth and freeze-up are then described (2.3). Development of platelet ice, a prominent under-ice feature in Antarctica and recently observed in the Arctic, is described (2.4). The final section describes frost flowers and brine skim development, and the dynamics of the bacteria communities in the frost flowers and brine skim on top of newly formed sea ice (2.5).

Keywords Sea ice formation · Development of brine channel · Optical properties · Incorporation of organisms · Frost flowers · Platelet ice

2.1 Sea Ice Formation, Growth and Properties

In autumn and winter, when the ocean surface layer cools to temperatures close to $-1.86\ ^\circ$C (the freezing point of seawater with a salinity of 34), ice crystals start growing on the surface (Weeks 2010) and form a soupy suspension consisting of frazil ice crystals of 3–4 mm in diameter (Fig. 2.1). Organic and inorganic particles in the water are centres for ice condensation, called nucleation. Under calm conditions, the ice crystals freeze together to form a sheet of new ice called nilas, which forms a sea ice crust up to 10 cm thick with randomly oriented ice crystals termed granular ice texture (Timco and Weeks 2010) (Fig. 2.2a) that can cover dozens of km² of sea surface during calm weather conditions. At this point frost flowers may form from the brine skim on the ice surface (Sect. 2.5). The transitional granular/columnar ice layer forms as the sheet ice thickens through congelation, called thermodynamic ice growth, at the ice-water interface (Eicken and Lange 1989). This
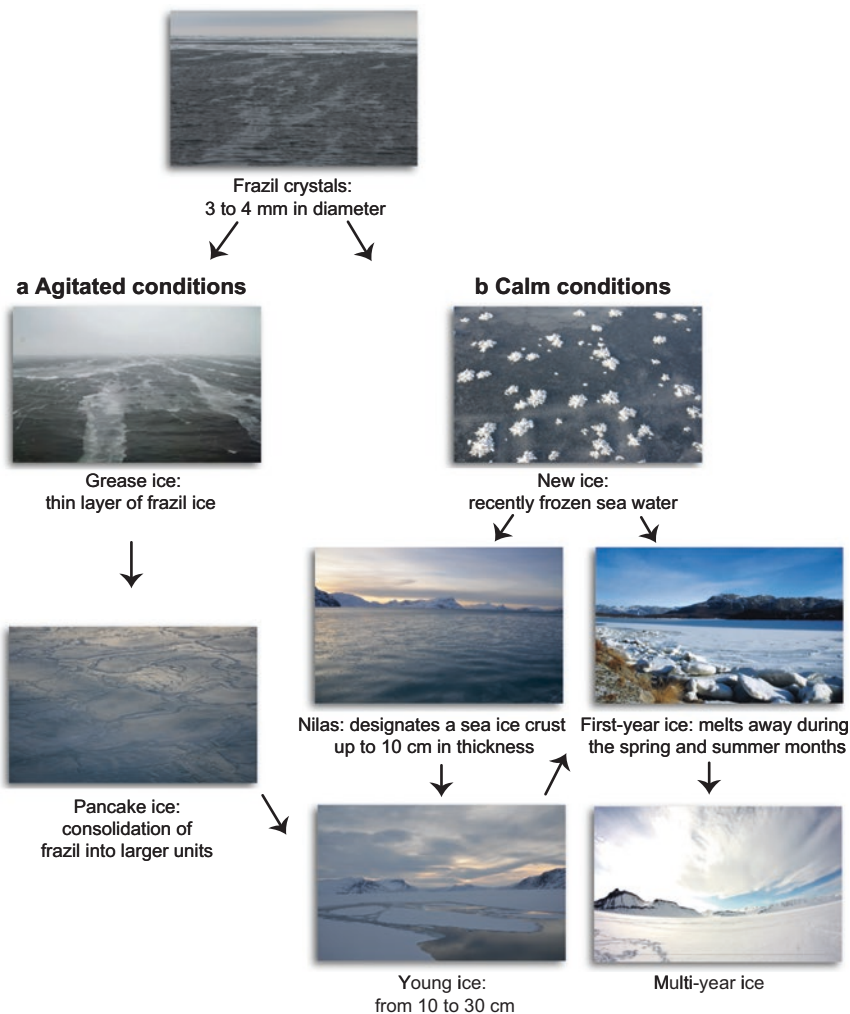
Fig. 2.1 Sea ice development stages – agitated conditions with ice growth in wave fields (**a**), and calm conditions with ice growth through quiescent bottom freezing (**b**). (Photographs by: Authors)

layer is a transition zone a few cm thick that is characterized mainly by elongated grains (Fig. 2.2a). Below the transitional granular/columnar layer, the sea ice consists of columnar ice, characterised by vertically elongated ice crystals, where individual ice crystals can have lengths of several mm to cm (Fig. 2.3). A skeletal layer is found at the bottom of the growing sea ice with ice crystals and relatively large brine-filled gaps in-between the lamellae (Fig. 2.2b). The thickness of the skeletal layer varies from 1 to 3 cm and with a distance of 0.5–1.0 mm between the tips of the lamellae. Sea ice is classified as young ice when the ice sheet becomes thicker
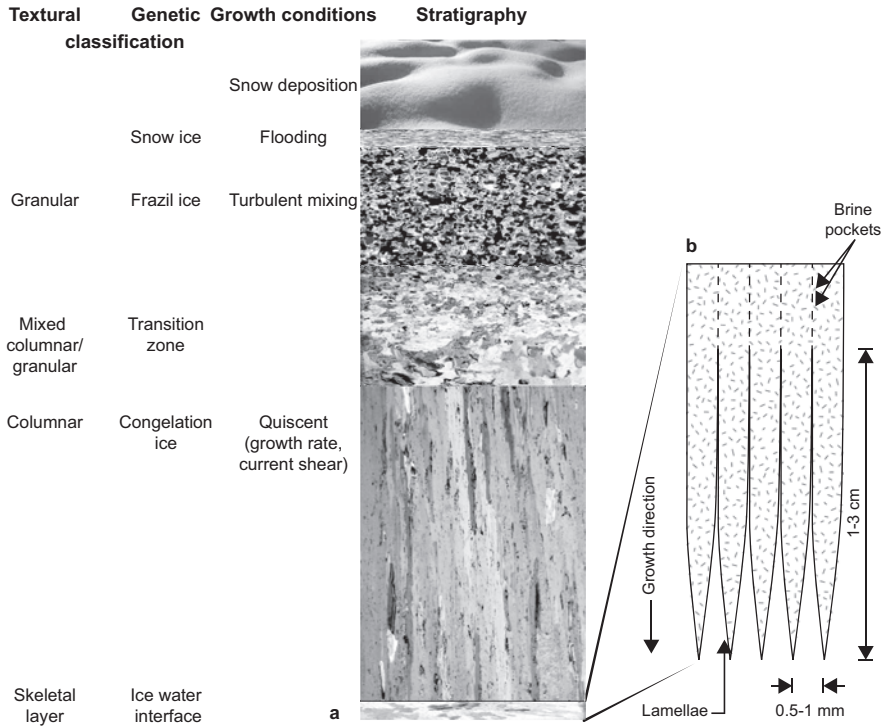
Fig. 2.2 Schematic representation of the main ice growth conditions and resulting textures in first-year sea ice (**a**), and the structure and dimensions of the skeletal layer with lamellae of ice at the bottom of the sea ice (**b**). (Modified from: Eicken 2003 and Søgaard 2014)

Fig. 2.3 Thin section of first-year sea ice with ice lamellae (**a**), and brine pockets along the grain boundaries (**b**). (Photographs by: M. Pucko)
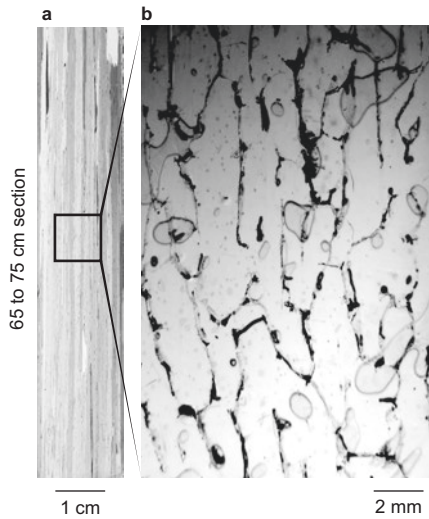
than 10 cm and as first-year sea ice when the ice sheet becomes thicker than 30 cm (Weeks 2010). If the first-year ice survives at least one melting season, which is one summer, it is termed multi-year ice (or second year ice after the first summer). Multi-year ice can reach ages of typically 4–5 years or more (Weeks 2010). In more dynamic conditions with ice growing in wave-fields, frazil crystals consolidate into grease. The grease ice layer can consolidate into ice discs known as pancakes (Fig. 2.1a). As they grow from a few cm to a few metres across, they solidify and thicken by mechanically rafting on top of each other. Pancakes freeze together to form ice cakes and floes, which contain a large amount of ice with a granular texture. With ongoing freezing, the pancakes adhere into a continuous ice sheet by bottom freezing at the ice-water interface. The frazil–congelation process described above is the most frequent, but other sea ice types exist, e.g. snow-ice and superimposed ice formation. Snow-ice forms by surface freezing after surface flooding of ice floes due to snow loading that submerges the ice below freeboard levels and an infiltration layer is developed (Fig. 2.2a, Eicken 2003; Fritsen et al. 1998; Rysgaard et al. 2012). Superimposed ice develops during spring and summer when the snow melts internally and melt water refreezes either in the snow or at the snow-ice interface, e.g. when the temperature gradients within snow and ice are reversed (Haas et al. 2008; Nicolaus et al. 2010). When sea water solidifies, some of the salts and solutes including inorganic and organic nutrients and gases present in the seawater are rejected into the water column below, whereas the rest is trapped within the brine pockets, channels and tubes (Fig. 2.3b) (Weeks and Ackley 1982; Petrich and Eicken 2017). Thus, the initial concentrations of solutes in sea ice are mainly controlled by the composition of the seawater from which the sea ice is formed and by the freezing process itself. Recent studies indicate a preferential incorporation of dissolved organic carbon (DOC) and extracellular polymeric substances (EPS) into sea ice compared to other substances (Meiners and Michel 2017). This suggests that the classical concept of conservative incorporation of substances (e.g., salt, gases, and dissolved nutrients) into sea ice needs further investigation. Once the ice has formed, a reduction in sea ice temperature decreases the brine volume with a concurrent increase in brine salinity (Cox and Weeks 1983; Papadimitriou et al. 2004) (Fig. 2.4). Dissolved inorganic and organic nutrient pools will be further modified within the sea ice and may be enriched (Fig. 2.5) or depleted (Fig. 4.3) due to biological activity by the bacteria and ice algae. Bulk salinity is the salinity of a sample of melted sea ice and is generally around 2–10 depending on type and age of the ice (Cox and Weeks 1983). Bulk inorganic nutrient concentrations in newly formed sea ice are equivalent to bulk salinity and concentrations are normally lower than in the underlying seawater column (Vancoppenolle et al. 2013). Their concentrations in the sea ice are proportional to the bulk salinity following a theoretical dilution line, provided that there is no biological accumulation or depletion of nutrients in the sea ice. In a recent study of newly formed sea ice, plots of concentrations of phosphate (PO_4^{3-}), silicic acid ($Si(OH)_4$), nitrate (NO_3^-) and nitrite (NO_2^-), dissolved organic carbon (DOC) and dissolved organic nitrogen (DON) concentrations versus bulk salinity were generally all above the dilution line (Fig. 2.5). This implies that there

Fig. 2.4 Illustration of the fate of the brine and brine solute concentrations when sea ice temperatures decrease, and accordingly the brine volume

must have been a production and accumulation of these nutrients in the ice by heterotrophic bacteria, being the most active components of the biological community in this newly formed sea ice (Fig. 2.5). Sea ice DOC and DON concentrations are also generally enriched in newly formed sea ice when compared with the seawater from which the sea ice has formed, and the high concentrations in sea ice indicate biological production (Fig. 2.5d, e). DOC and DON comprise a diverse pool of complex organic compounds that are defined as smaller than 0.2 μm. In practice, dissolved organic matter (DOM) is often operationally defined as material that passes through glass-fibre filters with a nominal pore size of 0.7 μm (Meiners and Michel 2017). The sea ice DOC and DON pool consists of carbohydrates, amino acids as well as more complex substances such as humic acids. The DOC and DON pools remain poorly characterized at the molecular level and can range in size from monomers to large polymers. Molecular size can indicate the bioavailability of compounds and the pools are often grouped into bioavailable (biolabile) and non-bioavailable (refractory) fractions. Sea ice DOC and DON includes material that has been produced *in situ* through biological release from organisms living in the sea ice, which is termed autochthonous (Underwood et al. 2010; Aslam et al. 2012).
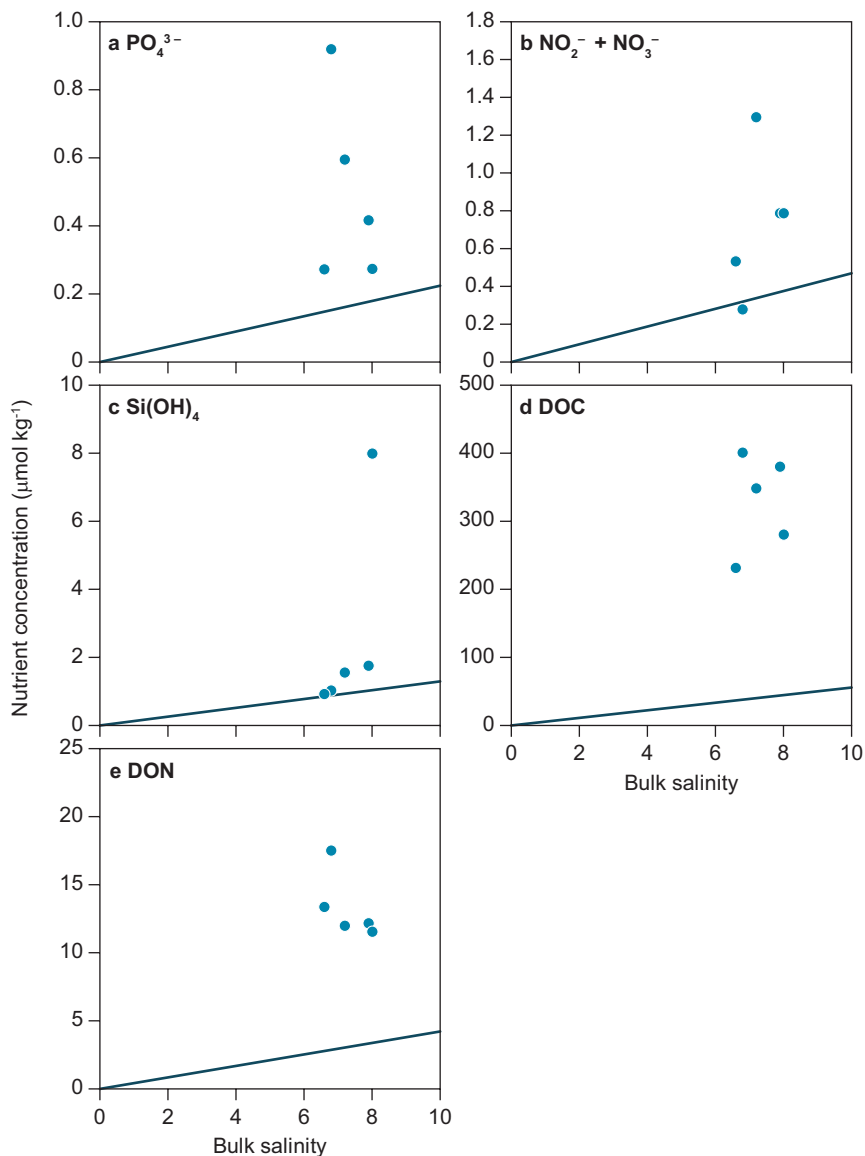
Fig. 2.5 Concentrations of dissolved nutrients, DOC, and DON versus ice bulk salinity in newly formed sea ice (<5 days old). The solid line indicates the expected dilution line predicted from salinity and nutrient concentrations in seawater. If values are below the dilution line, depletion of the solute has taken place, and if above the dilution line, production, or net deposition, of the solute has occurred. (**a**) Phosphate (PO_4^{3-}), (**b**) Nitrite (NO_2^-) + Nitrate (NO_3^-), (**c**) Silicate ($Si(OH)_4$, (**d**) DOC, and (**e**) DON. (Modified from: Søgaard et al. 2019)

This is opposite to material trapped during the sea ice formation, which is termed allochthonous (Stedmon et al. 2007). The former can be orders of magnitude higher than the latter and can reach concentrations of up to 2.5 mmol L^{-1} (Thomas et al. 2001; Riedel et al. 2007). High DOC/DON ratios, increasing with total DOC concentration, have been reported from Arctic sea ice (Thomas et al. 2001) and are probably a result of DOC-rich riverine supply. The high carbon content of sea ice DOM has also been attributed to high concentrations of biologically produced sea ice carbohydrates, which may be a result of high concentrations of sea ice Extracellular Polymeric Substances (EPS) (Juhl et al. 2011; Underwood et al. 2010). EPS can contribute a significant fraction of the total sea ice carbon pool (Meiners et al. 2008; Riedel et al. 2007) and are thought to be extracellular cryoprotectants and likely osmoprotectants for bacteria surviving in the sea ice (Ewert and Deming 2013). This was observed at extremely low temperatures around $-27\ °C$ and corresponding high brine salinities of 220 (Collins et al. 2008). Importantly, DOC and DON can be chromophoric, and this coloured dissolved organic matter (CDOM) has a strong absorption in the ultraviolet (UVR) (280–400 nm) and blue part of the visible (400–700 nm) PAR spectrum. This absorption affects the energy budget of the sea ice as well as the exposure of ice-associated organisms to UVR and PAR (Belzile et al. 2000). Photochemical degradation of DOM can lead to direct remineralization of DOM, but also to the formation of biolabile organic compounds that can fuel sea ice microbial food webs (Thomas et al. 2001; Norman et al. 2011).

2.2   Optics of Young and Newly Formed Sea Ice

The occurrence and formation of ice on an ocean water surface causes dramatic changes in the ocean's optical properties, shifting from a highly transparent element (water) with a very low albedo (the ratio between reflected and incident irradiance) to a low transparency element (ice) with a high albedo and attenuation, with or without a snow cover. This proceeds from autumn towards winter, but the changes are likewise established when moving from open sea and towards an ice-covered fjord, for instance. Changes in optical properties over time from open water to a state with a cover of sea ice were studied by Perovich (1991) in a two-stream multi-layer model. Two-stream refers to modelling of downwelling irradiance (first-stream) where absorption and scattering of the irradiance in the layers of snow, ice and water (multi-layer) are quantified along with the upwelling irradiance (second-stream) from the water through the same layers. The model was run between 16 October and 5 November when ice thickness increased from 0.0 to about 25 cm with a snow cover of 4.0 cm from about the middle of the period (Fig. 2.6). Transmittance, the ratio between under the ice PAR and surface PAR, decreased from 0.95 to 0.30 with a connected increase in ice thickness. Transmittance decreased further to 0.1 with a snow cover established on top of the ice around 25 October. Under-ice light availability was reduced from 67 to *ca.* 3 μmol photons m^{-2} s^{-1} through the same time and remained low. During the period of ice growth,
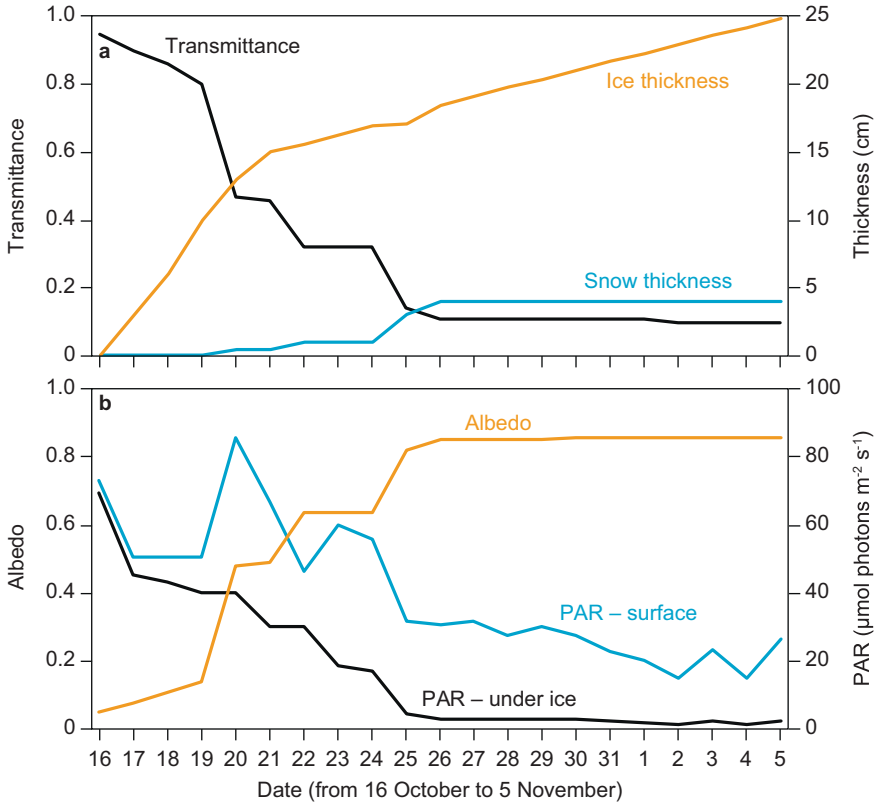
Fig. 2.6 Ice and snow thickness (cm) and transmittance (**a**), albedo, surface and under ice PAR (**b**) between 16 October and 5 November. (Modified from: Perovich 1991)

there was a strong increase in albedo from 0.05 to about 0.64, which increased further to 0.85 with the snow cover. The transition from open water to ice with snow strongly resulted in a decrease in irradiance at the bottom of the ice, though in combination with a seasonally related decrease in surface irradiance during autumn. The modelling demonstrates that significant changes in optical properties can occur within a relatively short time of ice formation, here about 10 days.

2.3   Scavenging of Bacteria and Algae in Developing Sea Ice

In autumn the water column still contains quantities of microscopic algae, heterotrophic protists, bacteria, and small metazoans and these are incorporated into the ice during freeze-up and ice growth. The incorporation is facilitated by different processes including scavenging, e.g. harvesting of organisms by ice crystals rising through the water column as well as wave-field pumping, i.e., accumulation of

organisms that get trapped into an existing ice cover by wave action (Spindler 1994). Garrison et al. (1983) pointed out that algae and bacteria adhere to the surfaces of the frazil ice particles and are incorporated into the ice when the ice is developing. Gradinger and Ikävalko (1998) developed an enrichment index, which expresses the concentrations of Chl *a*, nutrients or an organism in the ice relative to the concentration in the water column below at the time of ice development. Water concentrations of Chl *a* were around 1.0 μg L^{-1} but high concentrations of 19.8 μg L^{-1} were measured in newly formed pancake ice during the autumn freeze-up, proportionate to an enrichment index of 20. Enrichment factors varied between groups and significantly with ice type, with an enrichment index for diatoms of 10 in grease ice, 200 in nilas and minor pancake ice, and increasing to 20,000 in large pancake ice (Gradinger and Ikävalko (1998). Enrichment factors for bacteria during ice formation and incorporation varied between 5 and 10; even higher factors up to 54 have been reported (Deming and Collins 2017). Incorporation processes and sources for sea ice meiofauna taxa are not well understood, but in nearshore waters sediment with benthic micro- and meiofauna can be incorporated into the sea ice with strong mixing and high current speeds (Carey and Montagna 1982; Reimnitz et al. 1993). In offshore deep water regions, multi-year ice floes or zooplankton can act as seed stocks (Bluhm et al. 2010) for incorporation in the sea ice. Once ice algae are incorporated into the ice they are dormant or almost inactive throughout the cold and dark winter and start growing at first light in spring (Leu et al. 2015). Little is known about how the cells, often forming spores and cysts, actually survive the winter in the ice, but they are there and become viable around first light. A seasonal study showed a gradual increase in Chl *a* in the entire ice from around March (Fig. 2.7), presumably related to spring awakening of the cysts and spores (Søgaard et al. 2010). The ice interior remains cold in February–March with a low brine volume, so that inflow of seawater into the brine channels and thereby seeding of the channels is limited. The Chl *a* increase co-occurs with increased
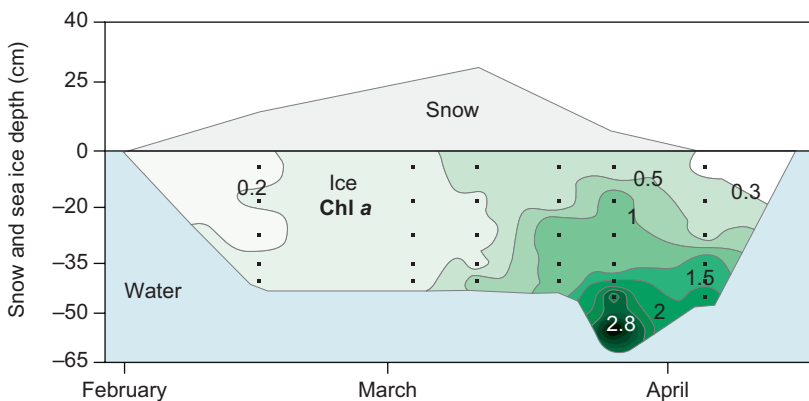
Fig. 2.7 Seasonal development of Chl *a* (mg m-3) in the sea ice, Malene Bight, SW Greenland. (Modified from: Søgaard et al. 2010)

irradiance levels in the ice. In contrast, the heterotrophic microbial community in newly formed sea ice is able to establish an ice-adapted and active bacterial biomass within a week of ice formation. The productivity of the microorganisms inhabiting sea ice during the first stages of ice formation is poorly understood, but recent studies have shown that the ice-associated biological community in newly formed sea ice is net heterotrophic with very high ratios (average of 14) of bacterial production to primary production (Søgaard et al. 2019).

2.4 Platelet Ice

Platelets are crystal discs of about 5–30 cm in diameter and a few mm thickness and are found below the sea ice in ice shelf areas (Fig. 2.8a). They are formed by super-cooling of the water below the ice shelf and can form an up to a 10 m thick layer of platelets accumulating under sea ice after they rise from depth. Platelet ice is a common phenomenon of Antarctic land-fast sea ice that abuts an ice shelf (Langhorne et al. 2015), and has just recently been observed at sites in Greenland (Kirillov et al. 2018). A video from below the ice at Cape Evans, Antarctica, shows the three dimensional structure at the bottom of the ice established by the platelets (Fig. 2.9). There are green and brownish aggregations of ice algae on the bottom of the sea ice with the platelets sticking out of the bottom of the ice (Fig. 2.8b–d). The occurrence of the platelets establishes a complex three-dimensional structure with algae growing on the platelets and a significant increase of the sea ice surface area. Brown colours at the bottom of the cores are related to the presence of ice algae. Figure 2.8e shows an upward directed photo perpendicular to the bottom of the sea ice. An under-ice video from Station Nord, NE Greenland also shows some clear platelets frozen into the bottom of the ice (Fig. 2.10).

2.5 Frost Flowers

During the initial phase (hours) of sea ice formation, a highly saline layer of brine skim is often observed on the surface of newly forming ice (e.g. Isleifson et al. 2014) (Fig. 2.11). The skim layer is typically 1–2 mm thick and is highly saline, with salinities up to 120 (Barber et al. 2014). This skim layer is formed by brine expulsion towards the surface in the brine channels as these constrict during sea ice growth (Martin et al. 1995). Highly saline water or brine leaves the ice not only through brine channels at the bottom of the ice, but can also be expelled to the surface of the sea ice. Frost flowers will develop on top of the brine skim if the air is cold enough and there is a strong temperature gradient between ice and air (Fig. 2.12). The skeleton of the frost flowers is pure ice but later the brine skim will move up and cover the skeleton with brine. Formation of frost flowers requires low (< 5 m s^{-1}) wind speeds and calm conditions, as the structures are very fragile (Style
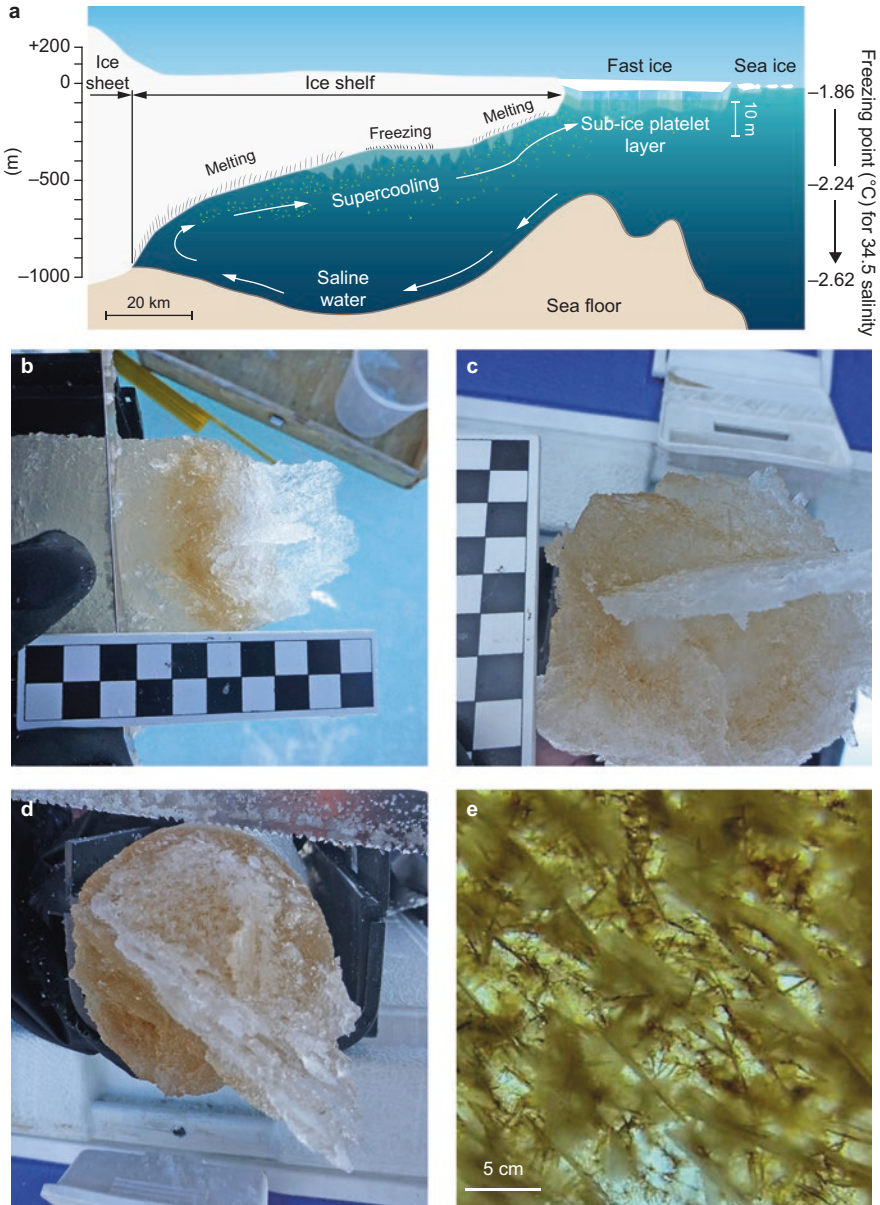
Fig. 2.8 Illustration showing the formation of platelet ice around an Antarctic ice shelf (**a**) (Courtesy: AWI, Bremerhafen, Germany), pictures of three cores with ice algae (brown colouring) and platelets frozen into the bottom of the ice (**b–d**), and under ice picture showing platelets sticking out of the ice partly covered with greenish and brown ice algae (**e**). (Photographs by: Authors)
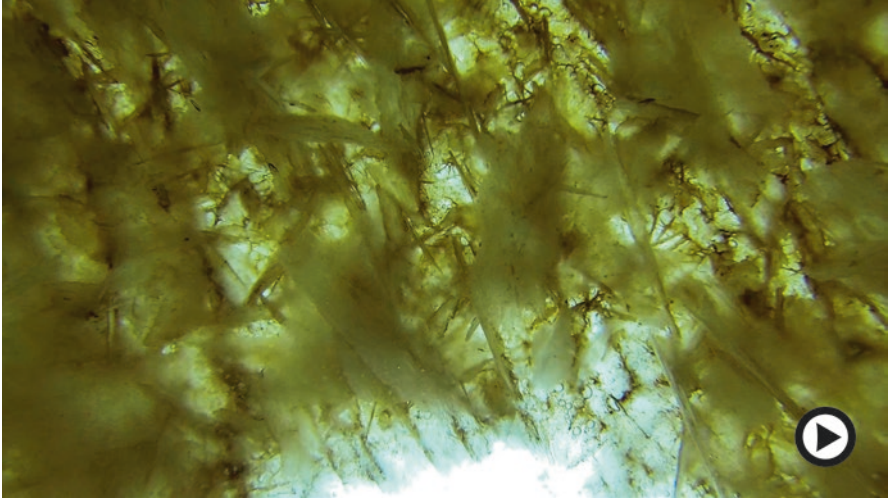
Fig. 2.9 A video from below the ice at Cape Evans, Antarctica, shows the three dimensional struc-
ture at the bottom of the ice established by the platelets. Video: V. Lucieer (https://doi.org/10.100
7/000-05g)

Fig. 2.10 An under-ice video from St. Nord NE Greenland also shows some clear platelets frozen
into the bottom of the ice. Video: K. Hancke (https://doi.org/10.1007/000-05f)

Fig. 2.11 Illustration
showing the development
of frost flowers and brine
skim on top of the sea ice
over time. The brine skim
is also called slush layer or
skim layer
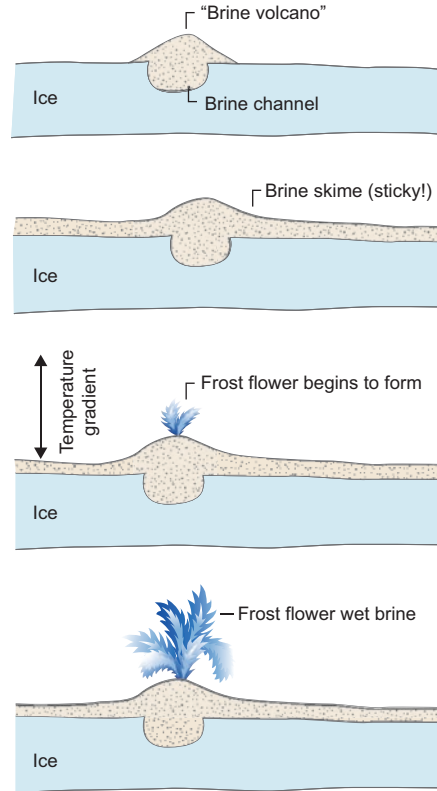
and Worster 2009; Barber et al. 2014). There is still an ongoing debate regarding
whether frost flowers form due to sublimation or evaporation from the sea ice sur-
face or from deposition from the atmosphere (Domine et al. 2005). The initial $\delta^{18}O$
values in frost flowers are close to 0‰, which is similar to the signature of the sur-
face brine skim layer, suggesting that newly formed frost flowers are composed
primarily of the surface brine skim (Barber et al. 2014). Frost flowers become sig-
nificantly modified within a few days since they are extremely effective collectors
of drifting snow on the ice, which suggests an increase over time in their atmo-
spheric fraction (Barber et al. 2014). As a consequence, they are integrated into the
snow layer on top of the sea ice (Perovich and Richter-Menge 1994). Ice crystals
with brine will be detached from the frost flowers at higher wind speeds and trans-
ported up into the atmosphere as marine aerosols containing a variety of elements
such as Na^+, Cl^-, Mg^+, Br^-, and others. These elements are enriched 1.4–3.7 times
in concentration compared to seawater as they originate from the concentrated
brine. Frost flowers provide a significant source of atmospheric Br^-, which reacts
with other elements and is an efficient depleter of the ozone layer (Kaleschke et al.
2004). The flowers also play a key role in the dynamics and exchange of Hg_2^{2+}
between sea ice, snow, and atmosphere (Douglas et al. 2005, 2012). Although the

Fig. 2.12 Frost flowers on sea ice. (Photographs by: D. Barber, S. Rysgaard, and authors)

mechanisms behind frost flower formation are relatively well-described, the bio-logical components in frost flowers are poorly known. Recent studies have shown that bacterial concentrations generally increase with salinity in frost flowers, and that bacteria in frost flowers survive the challenging conditions encountered as the frost flowers age (Fig. 2.13). In frost flowers as noted in Sect 2.1 for sea ice, bacteria produce EPS which serve as extracellular cryoprotectants and osmoprotectants. The only combined study of the bacterial community and EPS production in frost flow-ers shows that EPS values increase over time in both frost flowers and the surface brine skim layer (Fig. 2.13). This suggests that the bacteria are struggling to survive when they are transported upward from sea ice into the even more extreme condi-tions in the surface brine skim layer and frost flowers. This is supported by the higher EPS values in frost flowers and brine skim layer as compared to EPS values reported for Arctic sea ice (Barber et al. 2014; Underwood et al. 2010).
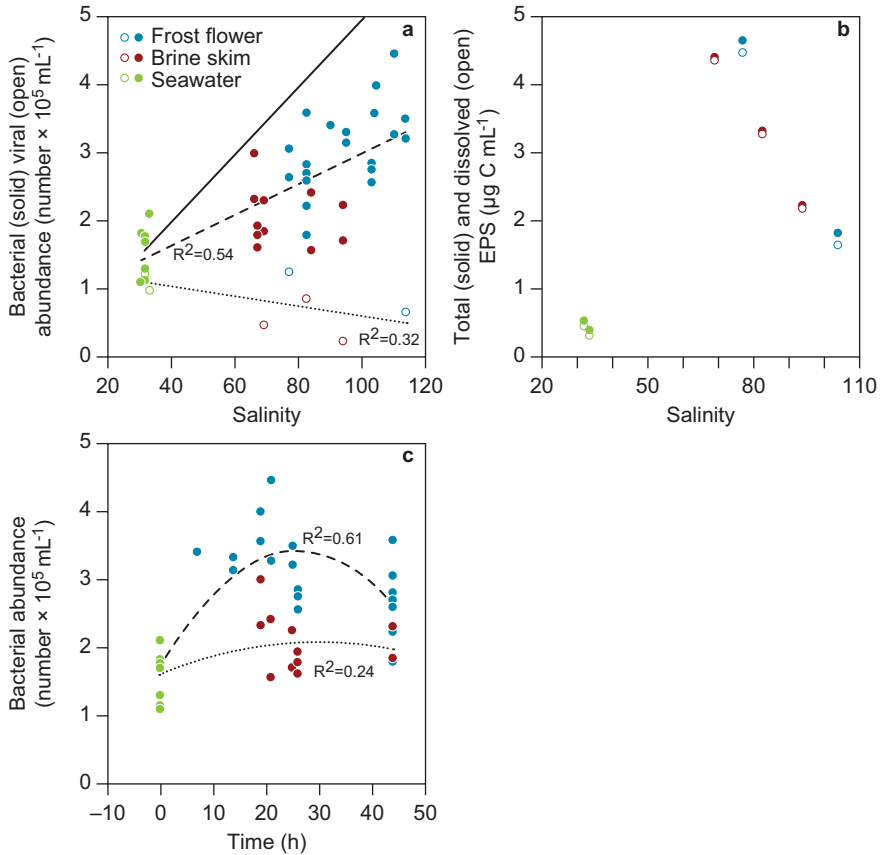
Fig. 2.13 Abundance of bacteria (solid symbols) and viral-like particles (open symbols) in frost flowers (blue circles), brine skim (red circles) and in seawater (green circles) as a function of salinity (**a**), concentration of total EPS (solid) and dissolved EPS (dEPS, open) in frost flowers (blue circles), brine skim (red circles) and in seawater (green circles) as a function of salinity. The saltiest samples are the youngest samples (19 h for frost flowers and 25 h for brine skim) and the freshest samples are the oldest samples (44 h); i.e. EPS values in these samples are not only higher than in seawater but also appear to have increased over time (**b**), and bacterial abundance in frost flowers (blue circles), brine skim (red circles) and in sea water (green circles) as a function of time (**c**). (Modified from: Barber et al. 2014)

References

Aslam, S. N., Graham, J., Underwood, C., Kaartokallio, H., Norman, L., Autio, R., Fischer, M., Kousa, H., Dieckmann, G. S., & Thomas, D. N. (2012). Dissolved extracellular polymeric substances (dEPS) dynamics and bacterial growth during sea ice formation in an ice tank study. *Polar Biology, 35*, 661–676. https://doi.org/10.1007/s00300-011-1112-0.

Barber, D. G., Ehn, J. K., Pucko, M., Rysgaard, S., Deming, J. W., Bowman, J. S., Papakyriakou, T., Galley, R. J., & Søgaard, D. H. (2014). Frost flowers on young Arctic sea ice: The cli-

matic, chemical, and microbial significance of an emerging ice type. *Journal of Geophysical Research, Atmospheres, 119*, 11593–11612. https://doi.org/10.1002/2014JD021736.

Belzile, C. L., Johannesen, S. C., Gosselin, M., Demers, S., & Miller, W. L. (2000). Ultraviolet attenuation by dissolved and particulate constituents of first-year ice during late spring in an Arctic polynya. *Limnology and Oceanography, 45*, 1265–1273. https://doi.org/10.4319/lo.2000.45.6.1265.

Bluhm, B. A., Gradinger, R. R., & Schnack-Schiel, S. B. (2010). Sea ice meio- and macrofauna. In D. Thomas & G. Dieckmann (Eds.), *Sea ice* (pp. 357–394). Oxford: Wiley-Blackwell.

Carey, A. G. J., & Montagna, P. A. (1982). Arctic sea ice faunal assemblage: First approach to description and source of the underice meiofauna. *Marine Ecology Progress Series, 8*, 1–8. https://doi.org/10.3354/meps008001.

Collins, R. E., Carpenter, S. D., & Deming, J. W. (2008). Spatial heterogeneity and temporal dynamics of particles and pEPS in arctic winter sea ice. *Journal of Marine Systems, 74*, 902–917. https://doi.org/10.1016/j.jmarsys.2007.09.005.

Cox, G. F. N., & Weeks, W. F. (1983). Equations for determining the gas and brine volumes in sea-ice samples. *Journal of Glaciology, 29*, 306–316. https://doi.org/10.3189/S0022143000008364.

Deming, J. W., & Collins, R. E. (2017). Sea ice as a habitat for Bacteria, Archaea and viruses. In: D. N. Thomas (Ed.), *Sea ice* (3rd ed., pp. 326–351). Oxford: Wiley Blackwell, 652 pp.

Domine, F., Taillandier, A. S., Simpson, W. R., & Severin, K. (2005). Specific surface area, density and microstructure of frost flowers. *Geophysical Research Letters, 32*, L13502. https://doi.org/10.1029/2005GL023245.

Douglas, T. A., Sturm, M., Simpson, W. R., Brooks, S., Lindberg, S. E., & Perovich, D. K. (2005). Elevated mercury measured in snow and frost flowers near Arctic sea ice leads. *Geophysical Research Letters, 32*. https://doi.org/10.1029/2004GL022132.

Douglas, T. A., Domine, F., Barret, M., Anastasio, C., Beine, H. J., Bottenheim, J., Grannas, A., Houdier, S., Netcheva, S., Rowland, G., Staebler, R., & Steffen, A. (2012). Frost flowers growing in the Arctic ocean-atmosphere-sea ice-snow interface: 1. Chemical composition. *Journal of Geophysical Research, 117*. https://doi.org/10.1029/2011JD016460.

Eicken, H. (2003). From the microscopic to the macroscopic to the regional scale, growth, microstructure and properties of sea ice. In D. N. Thomas & G. S. Dieckmann (Eds.), *Sea Ice: An introduction to its physics, chemistry, biology and geology* (1st ed., pp. 22–181). Oxford: Wiley Blackwell.

Eicken, H., & Lange, M. A. (1989). Development and properties of sea ice in the coastal regime of the southeastern Weddell Sea. *Journal of Geophysical Research-Ocean, 94*, 8193–8206. https://doi.org/10.1029/JC094iC06p08193.

Ewert, M., & Deming, J. W. (2013). Sea ice microorganisms: Environmental constraints and extracellular responses. *Biology, 2*, 603–628. https://doi.org/10.3390/biology2020603.

Fritsen, C. H., Ackley, S. F., Kremer, J. N., & Sullivan, C. W. (1998). Flood-freeze cycles and microalgal dynamics in Antarctic pack ice. In M. P. Lizotte & K. R. Arrigo (Eds.), *Antarctic sea ice: Biological processes, interactions and variability* (Antarctic research series) (Vol. 73, pp. 1–21). Washington, DC: AGU. https://doi.org/10.1029/AR073.

Garrison, D. L., Ackley, S. F., & Buck, K. R. (1983). A physical mechanism for establishing algal populations in frazil ice. *Nature, 306*, 363–365. https://doi.org/10.1038/306363a0.

Gradinger, R., & Ikävalko, J. (1998). Organism incorporation into newly forming Arctic sea ice in the Greenland Sea. *Journal of Plankton Research, 20*, 871–886. https://doi.org/10.1093/plankt/20.5.871.

Haas, C., Pfaffling, A., Hendricks, S., Rabenstein, L., Etienne, J.-L., & Rigor, I. (2008). Reduced ice thickness in Arctic Transpolar Drift favors rapid ice retreat. *Geophysical Research Letters, 35*, L17501. https://doi.org/10.1029/2008GL034457.

Isleifson, D., Galley, R. J., Barber, D. G., Landy, J. C., Komarov, A. S., & Shafai, L. (2014). A study on the C-band polarimetric scattering and physical characteristics of frost flowers on experimental sea ice. *IEEE Transactions on Geoscience and Remote Sensing, 52*, 1787–1798. https://doi.org/10.1109/TGRS.2013.2255060.

Juhl, A. R., Krembs, C., & Meiners, K. M. (2011). Seasonal development and differential retention of ice algae and other organic fractions in first-year Arctic sea ice. *Marine Ecology Progress Series, 436*, 1–16. https://doi.org/10.3354/meps09277.

Kaleschke, L., Richter, A., Burrows, J., Afe, O., Heygster, G., Notholt, J., Rankin, A. M., Roscoe, H. K., Hollwedel, J., Wagner, T., & Jacobi, H.-W. (2004). Frost flowers on sea ice as a source of sea salt and their influence on tropospheric halogen chemistry. *Geophysical Research Letters, 31*. https://doi.org/10.1029/2004GL020655.

Kirillov, S., Dmitrenko, I., Rysgaard, S., Babb, D., Ehn, J., Bendtsen, J., Boone, W., Barber, D., & Geilfus, N. (2018). The inferred formation of a subice platelet layer below the multiyear landfast sea ice in the Wandel Sea (NE Greenland) induced by meltwater drainage. *Journal of Geophysical Research, 123*, 3489–3506. https://doi.org/10.1029/2017JC013672.

Langhorne, P. J., Hughes, K. G., Gough, A. J., Smith, I. J., Williams, M. J. M., Robinson, N. J., Stevens, C. L., Rack, W., Price, D., Leonard, G. H., Mahoney, A. R., & Haskell, T. G. (2015). Observed platelet ice distributions in Antarctic sea ice: An index for ocean-ice heat flux. *Geophysical Research Letters, 42*, 5442–5451. https://doi.org/10.1002/2015GL064508.

Leu, E., Mundy, C. J., Assmy, P., Campbell, K., Gabrielsen, T. M., Gosselin, M., Juul-Pedersen, T., & Gradinger, R. (2015). Arctic spring awakening – Steering principles behind the phenology of vernal ice algal blooms. *Progress in Oceanography, 139*, 151–170. https://doi.org/10.1016/j.pocean.2015.07.012.

Martin, S., Drucker, R., & Fort, M. (1995). A laboratory study of frost flower growth on the surface of young sea ice. *Journal of Geophysical Research, 100*, 7027–7036. https://doi.org/10.1029/94JC03243.

Meiners, K. M., & Michel, C. (2017). Dynamics of nutrients, dissolved organic matter and exopolymers in sea ice. In D. N. Thomas (Ed.), *Sea ice* (3rd ed., pp. 415–432). Oxford: Wiley Blackwell, 652 pp. https://doi.org/10.1002/9781118778371.ch17

Meiners, K. M., Krembs, C., & Gradinger, R. (2008). Exopolymer particles: Microbial hotspots of enhanced bacterial activity in Arctic fast ice (Chukchi Sea). *Aquatic Microbial Ecology, 52*, 195–207. https://doi.org/10.3354/ame01214.

Nicolaus, M., Gerland, S., Hudson, S. R., Hanson, S., Haapala, J., & Perovich, D. K. (2010). Seasonality of spectral albedo and transmittance as observed in the Arctic Transpolar Drift in 2007. *Journal of Geophysical Research, 115*. https://doi.org/10.1029/2009JC006074.

Norman, L., Thomas, D. N., Stedmon, C. A., Granskog, M. A., Papadimitriou, Krapp, R. H., Meiners, K. M., Lannuzel, D., Merwe, P. D., & Dieckmann, G. S. (2011). The characteristics of dissolved organic matter (DOM) and chromophoric dissolved organic matter (CDOM) in Antarctic sea ice. *Deep Sea Research Part II: Topical Studies in Oceanography, 58*, 1075–1092. https://doi.org/10.1016/j.dsr2.2010.10.030.

Papadimitriou, S., Kennedy, H., Kattner, G., Dieckmann, G. S., & Thomas, D. N. (2004). Experimental evidence for carbonate precipitation and CO_2 degassing during sea ice formation. *Geochimica et Cosmochimica Acta, 68*, 1749–1761. https://doi.org/10.1016/j.gca.2003.07.004.

Perovich, D. K. (1991). Seasonal changes in sea ice optical properties during fall freeze-up. *Cold Regions Science and Technology, 18*, 261–273. https://doi.org/10.1016/0165-232x(91)90041-E.

Perovich, D. K., & Richter-Menge, J. A. (1994). Surface characteristics of lead ice. *Journal of Geophysical Research, 99*, 16341–16350. https://doi.org/10.1029/94JC01194.

Petrich, C., & Eicken, H. (2017). Overview of sea ice growth and properties. In D. N. Thomas (Ed.), *Sea ice* (3rd ed., pp. 1–41). Oxford: Wiley Blackwell, 652 pp. https://doi.org/10.1002/9781118778371.ch1.

Reimnitz, E., McCormick, M., McDougall, K., & Brouwers, E. (1993). Sediment export by ice rafting from a coastal polynya, Arctic Alaska, U.S. *Arctic Alpine Research, 25*, 83–98. https://doi.org/10.2307/1551544.

Riedel, A., Michel, C., Gosselin, M., & LeBlanc, B. (2007). Enrichment of nutrients, exopolymeric substances and microorganisms in newly formed sea ice on the Mackenzie Shelf. *Marine Ecology Progress Series, 342*, 55–67. https://doi.org/10.3354/meps342055.

Rysgaard, S., Glud, R. N., Lennert, K., Cooper, M., Halden, N., Leakey, R. J. G., Hawthorne, F. C., & Barber, D. (2012). Ikaite crystals in melting sea ice – Implications for pCO$_2$ and pH levels in Arctic surface waters. *The Cryosphere, 6*, 901–908. https://doi.org/10.5194/tc-6-901-2012.

Søgaard, D. H., Kristensen, M., Rysgaard, S., Glud, R. N., Hansen, P. J., & Hilligsøe, K. M. (2010). Autotrophic and heterotrophic activity in Arctic first-year sea ice: Seasonal study from Malene Bight, SW Greenland. *Marine Ecology Progress Series, 419*, 31–45. https://doi.org/10.3354/meps08845.

Søgaard, D. H. (2014). Biological activity and calcium carbonate dynamics in Greenland sea ice – Implication for the inorganic carbon cycle. PhD thesis. Greenland Climate Research Centre and Department of Biology. University of Southern Denmark, Greenland Institute of Natural Resources, 148p

Søgaard, D. H., Deming, J. W., Meire, L., & Rysgaard, S. (2019). Effects of microbial processes and CaCO$_3$ dynamics on inorganic carbon cycling in snow-covered Arctic winter sea ice. *Marine Ecology Progress Series*. https://doi.org/10.3354/meps12868.

Spindler, M. (1994). Notes on the biology of sea ice in the Arctic and Antarctic. *Polar Biology, 14*, 319–324. https://doi.org/10.1007/BF00238447.

Stedmon, C. A., Thomas, D. N., Granskog, M., Kaartokallio, H., Papadimitriou, S., & Kousa, H. (2007). Characteristics of dissolved organic matter in Baltic coastal sea ice: Allochthonous or autochthonous origins? *Environmental Science and Technology, 41*, 7273–7279. https://doi.org/10.1021/es071210f.

Style, R. W., & Worster, M. G. (2009). Frost flower formation on sea ice and lake ice. *Geophysical Research Letters, 36*. https://doi.org/10.1029/2009GL037304.

Thomas, D. N., Kattner, G., Engbrodt, R., Gianelli, V., Kennedy, H., Haas, C., & Dieckmann, G. (2001). Dissolved organic matter in Antarctic sea ice. *Annals of Glaciology, 33*, 297–303. https://doi.org/10.3189/172756401781818338.

Timco, G. W., & Weeks, W. F. (2010). A review of the engineering properties of sea ice. *Cold Regions Science and Technology, 60*, 107–129. https://doi.org/10.1016/j.coldregions.2009.10.003.

Underwood, G. J. C., Fietz, S., Papadimitriou, S., Thomas, D. N., & Dieckmann, G. S. (2010). Distribution and composition of dissolved extracellular polymeric substances (EPS) in Antarctic sea ice. *Marine Ecology Progress Series, 404*, 1–19. https://doi.org/10.3354/meps08557.

Vancoppenolle, M., Meiners, K. M., Michel, C., Bopp, L., Brabant, F., Carnat, G., Delille, B., Lannuzel, D., Madec, G., Moreau, S., Tison, J.-L., & Merwe, P. V. D. (2013). Role of sea ice in global biogeochemical cycles: Emerging views and challenges. *Quaternary Science Reviews, 79*, 207–230. https://doi.org/10.1016/j.quascirev.2013.04.011.

Weeks, W. F. (2010). *On sea ice*. Fairbanks: University of Alaska Press, 664 pp.

Weeks, W. F., & Ackley, S. F. (1982). *The growth, structure and properties of sea ice, CRREL monograph*. 117 pp.

Chapter 3
Winter, Cold and Mature Sea Ice

Abstract This chapter describes a period of low air temperatures, darkness or very little light, cold ice, minimum brine volumes, and strongly reduced ice permeability. The first section provides an overview of the physical and optical conditions of this winter ice (3.1). Both snowfall and snowdrift are frequent during winter and an overview of the effects of a thick snow cover on sea ice is provided (3.2). Increased colonization of the sea ice bottom by bacteria and ice algae is initiated in late winter around first light, and an example is given (3.3). Once these microorganisms have colonized the ice the important growth limitations of bacteria and algae are considered (3.4), along with how they are able to adapt to these extreme conditions, and their seasonal species succession (3.5). The purposes of EPS and the functioning of different pigments found in ice algae are described (3.6). This is combined with a description of low light conditions and related photosynthesis (3.7), and exemplified with a case study from Station North, NE Greenland (3.8).

Keywords Cold ice · Snow · Low light · Colonization

3.1 Physics and Optics of Winter Sea Ice

The polar winter provides very low air temperatures and cold sea ice, very little to no surface light depending on latitude, and a snow layer of varying thickness that covers the ice surface. Ice reaches its maximum thickness and there is very little or no under-ice light. In spite of this, there is still a desalination of the ice by which the ice is losing salt. This is an ongoing process though at different rates, depending on the permeability of the ice. There are three types of desalination mechanisms: **(1)** brine expulsion, **(2)** gravity drainage, and **(3)** brine pocket migration, but only brine expulsion and gravity drainage are of quantitative importance (Eicken 2003). Brine expulsion is the flow of liquid brine driven by the freezing of the sea ice, which results in pressure buildup in the brine pockets. This mechanism forces the brine to escape from the brine pocket and migrate towards the warmer end, which is the bottom of the sea ice (Weeks 2010). Brine drainage (under the influence of gravity) includes all processes in which the brine drains out of the sea ice into the underlying seawater column (Cox and Weeks 1974). A brine channel opening at the bottom of
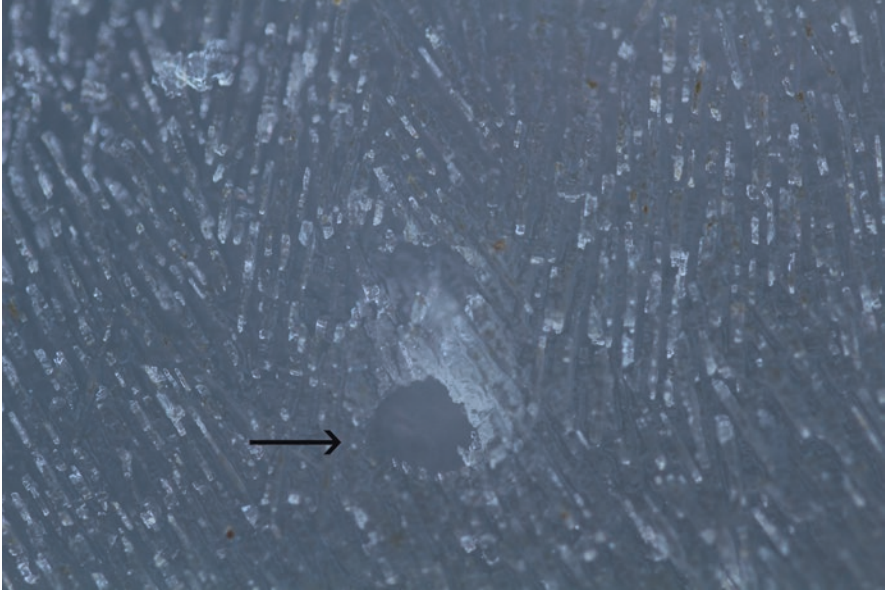
Fig. 3.1 Image of the bottom section of an ice core with a brine channel in lower center, from where brine is released to the underlying water. Diameter of the brine channel is about 1 cm. Ice lamella with ice algae (brown spots) are clearly visible. (Photograph by: Authors)

an ice core is shown in Fig. 3.1. The two desalination mechanisms explain the typical "C-shape" of the bulk salinity profiles, which evolves into the "L-shape" during the melting season in spring and summer (Eicken 2003). Furthermore, these two mechanisms result in the rejection of gases and other impurities to the underlying water column along with the expelled brine during sea ice growth. In the cold winter ice, brine volumes are low and generally below 5%, and the permeability of the ice is strongly reduced. The permeability of sea ice increases significantly at a brine volume > 5%, which is reached at a temperature of −5 °C for a typical bulk salinity (salinity of a melted sea ice sample) of 5, which is termed the "rule of five" (Golden et al. 1998). A brine volume of 5% is generally considered as the threshold at which the sea ice matrix becomes impermeable, minimizing brine and gas transport in the ice. An example of seasonal ice and snow conditions from Kobbefjord, SW Greenland shows that the ice cooled to −3.7 °C in the interior of the ice in February–March, during which brine volume decreased to 5% or below for about 1 month (Fig. 3.2b). At this point the brine channel system is not fully interconnected, resulting in no or only very little exchange of water and nutrients from below the ice (Golden et al. 2007). Accordingly, brine volume can be calculated depending on ice temperature, bulk salinity, and density of the ice (Sect. 6.2). Optical properties are independent of season *per se*, but some properties are more prevalent in winter compared to summer, as winter ice is often covered with a snow layer of specific optical properties. Irradiance intensity and its spectral composition below the ice
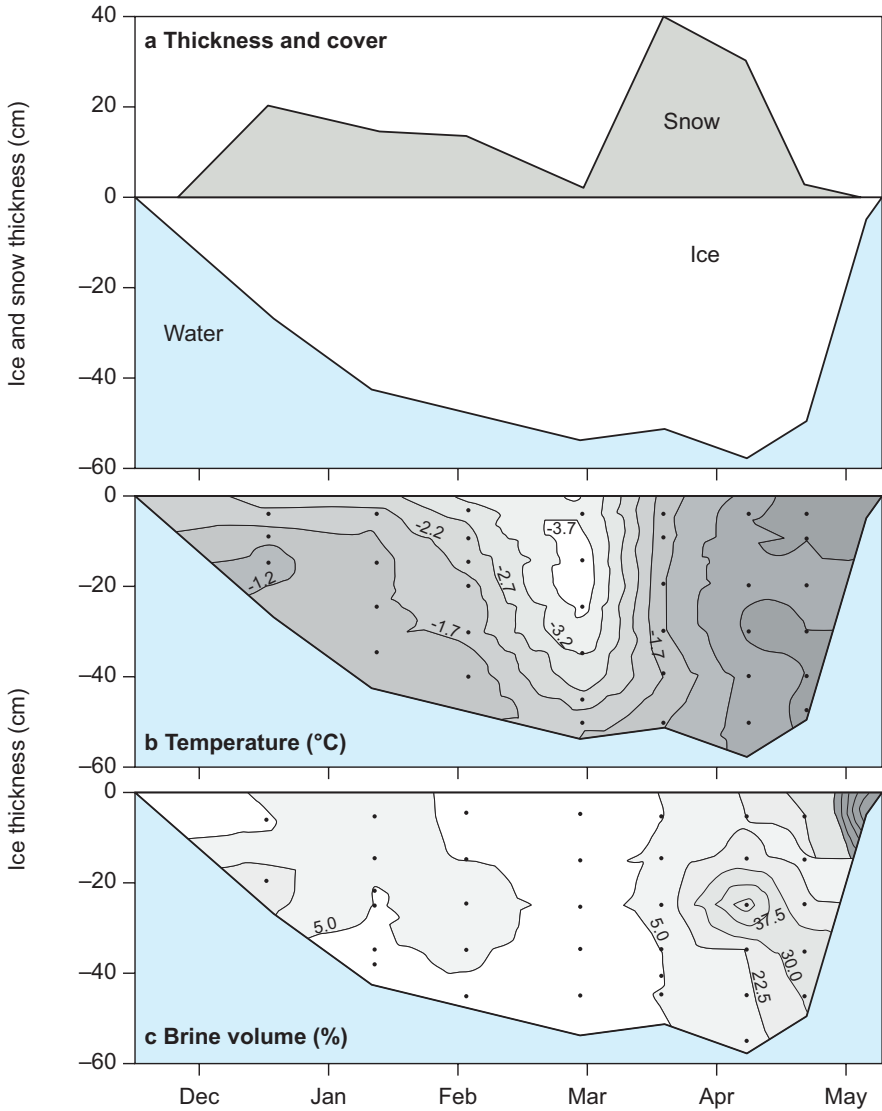
Fig. 3.2 Sea ice and snow thickness (cm) from December until May (**a**), contour plots of ice temperature (**b**), and brine volume (**c**), in Kobbefjord, SW Greenland. (Modified from: Mikkelsen et al. 2008)

depends on the albedo of the snow and ice surface, as well as absorption and scattering of the irradiance on its way through the column of snow and ice (Perovich 2017). Dry cold snow has a very high albedo (0.8–0.9) compared to bare ice (0.5–0.6) and the presence of a snow cover changes optical properties significantly. Transmittance is related to both absorption and scattering, with absorption in the

snow and ice, in the brine (and solutes therein), in solid salts, biota, sediments, and by dust particles, and the energy of the light photons is generally transformed into heat (Kirk 1994). Scattering in the ice and snow occurs at boundaries between substances with different refractive indexes, e.g., air bubbles, brine inclusions and sediment grains. Scattering in sea ice is complex and difficult to measure directly, but can be modelled. Hamre et al. (2004) produced scattering coefficients of around 1100 m^{-1} for brine channels and around 25 m^{-1} for air bubbles in typical first-year landfast ice, with air and brine volumes of 3% and 12%, respectively. Absorption is likewise expressed through an absorption coefficient (m^{-1}) as how much light is absorbed per metre in the substance, and can be quantified for the substances involved (Light et al. 2008). Absorption by snow, sea ice and its constituents including algal pigments such as Chl a can strongly alter the spectral composition of light transmitted through the ice. There is in ice a relatively stronger absorption in the red part of the spectrum compared to the blue part, whereas scattering is independent of wavelength. Ice algal derived changes in spectral composition are taken advantage of in remote sensing, applied for mapping of ice algae and dealt with in detail later (Sect. 6.5).

3.2 Effects of a Snow Cover on Sea Ice

During ice growth and when a solid ice surface develops, snow can accumulate on the ice and is redistributed by winds (snow drift) and melts at increasing air temperatures and during rain-on-snow events (Fig. 3.1 in Sturm and Massom 2017). There are three major ways by which snow on sea ice can affect or influence ice algae and bacteria inside or at the bottom of the sea ice. First, a snow layer will significantly decrease light available for photosynthesis in the sea ice and at the bottom. Scattering of light inside the snowpack dominates light attenuation compared to absorption, and snow has a very high albedo of 0.7–0.9 (Perovich 2017). Examples of time series of under-ice PAR in snow-cleared and snow-covered areas of ice, clearly demonstrate that the snow cover governs light transmittance in sea ice (Fig. 3.3). In this example, snow thickness during 12–18 March was about 5 cm in the snow-covered area but a snowfall event between 18 and 19 March reduced transmittance from about 0.3 to 0.1 by the increase in snow thickness to 8 cm. The new snow further increased albedo from 0.82 to 0.91. The reverse situation where snow on sea ice melts and thereby increases under-ice irradiance is very common and especially at increased air temperatures and melt during spring (Perovich 2017). This all demonstrates very clearly the strong variability in under-ice irradiance that ice algae and other biota must cope with, and ice algae have developed a range of coping strategies. Ice algae respond closely in all seasons to changes in under-ice irradiance in different ways: **(1)** by increasing intracellular Chl a concentrations, **(2)** by developing photoprotective "sunscreen" pigments and amino acids, and **(3)** by downregulation of the photosynthetic apparatus in high light (Kono and Terashima 2014). Snow not only changes the amount of light but also its spectral composition,
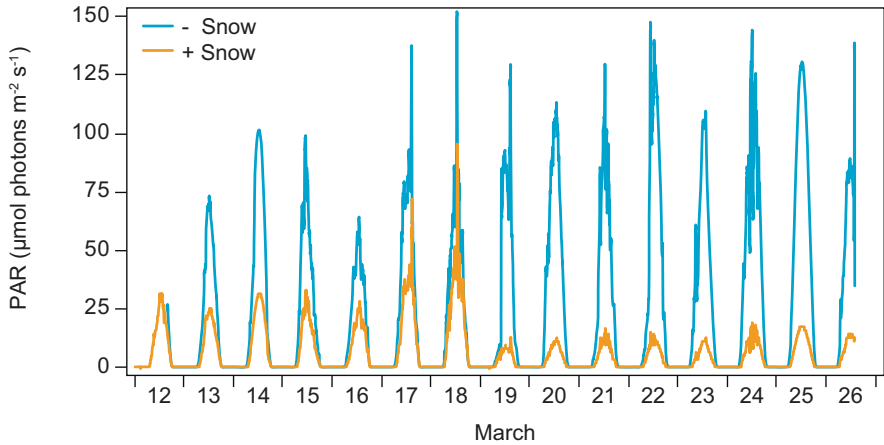
Fig. 3.3 PAR time series below the ice with snow (+Snow) and no snow (−Snow) areas from 12 to 26 March 2016, Kangerlussuaq, W Greenland. (Modified from: Lund-Hansen et al. 2020)
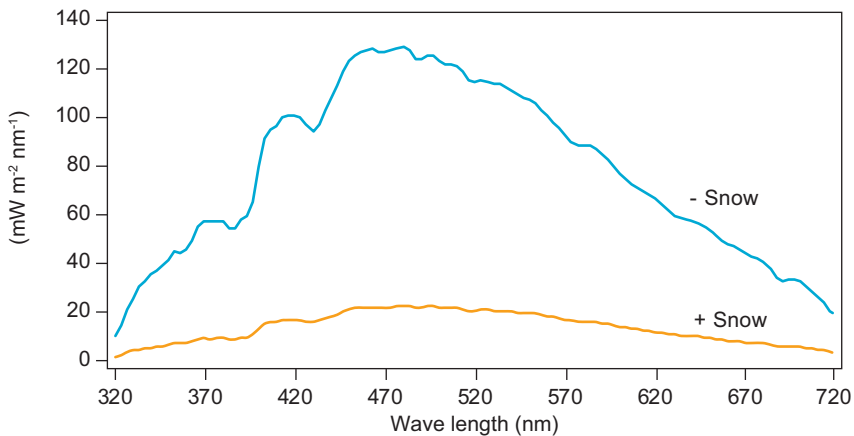
Fig. 3.4 Spectral distribution of under-ice irradiance with snow (+Snow) and with no snow (−Snow), March 2016, Kangerlussuaq, W Greenland. (Modified from: Lund-Hansen et al. 2020)

compared to ice without a snow cover. Figure 3.4 shows two under-ice light spectra from sites with an ice thickness of 79 cm with and without a snow cover of about 2 cm thickness. Ultraviolet light, and here UV-A (315–400 nm) below the ice increased from 0.4 Wm^{-2} with snow to 0.7 Wm^{-2} without snow. The effect of the snow cover layer on the under-ice irradiance is so significant due to the high albedo and the strong scattering and absorption causing high light attenuation coefficients $K_d(PAR)$ of ~11.9 m^{-1} in the snow, compared to ~0.84 m^{-1} of the ice below (Sect. 6.3). Apart from the thickness of the snow, there are several other variables that affect the optical properties of the snow, including its grain size, water content,

Fig. 3.5 Chl *a*
concentrations in a
multi-year ice (MYI) core
in August from Amundsen
Basin in the Arctic Ocean
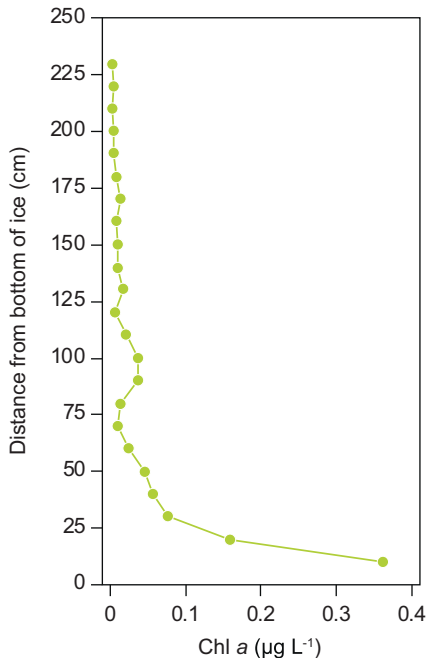
moisture, packing of the snow grains, and age of the snow (Perovich 2017; Hamre
et al. 2004). Snow metamorphosis at higher air temperatures increases the transmit-
tance, and thereby the irradiance reaching the bottom of the sea ice, as shown in
Case study I (Sect. 3.8). The second way snow on ice can affect ice algae and bac-
teria is by development of an infiltration layer. This layer comprises seawater that
floods the ice when the weight of the snowpack on top of the ice is higher than the
buoyancy forces acting on the ice. The thickness ratio between snow and sea ice is
approximately 1:3 before the ice is flooded, exemplified by 50 cm of ice where only
15 cm of snow is required before the ice is flooded (Sturm and Massom 2017).
Infiltration layers are generally located near the surface where the increased Chl *a*
around 100 cm is more likely an ice bottom from a previous year that has been
trapped in the ice (Fig. 3.5). Infiltration layers have historically not been prominent
features in the Arctic, but recent studies suggest these layers may be more common
in the future with an ongoing thinning of the sea ice (Kwok and Rothrock 2009;
Kwok 2018) as supported by current observations (Fernández-Méndez et al. 2015).
The third way in which snow on sea ice can affect ice algae and bacteria inside the
ice is related to the low thermal conductivity of snow, whereby heat loss from the
ice to the atmosphere is strongly reduced with a snow cover. The snow insulates the
ice from the cold air, and temperatures in sea ice with a snow cover will be relatively
higher, which affects living conditions of ice algae and bacteria as brine volume and
brine salinity strongly depend on temperature. The colder the ice the smaller the
brine volume and the higher the brine salinity (Cox and Weeks 1983) (Sect. 6.2).
Snow is a matrix of solid ice crystals and air (Sturm and Massom 2017), and its low
thermal conductivity was observed during an experiment where ice cores were
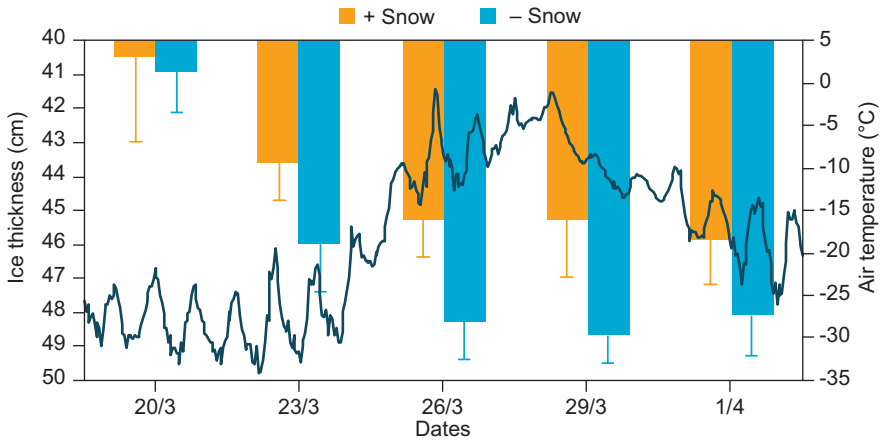
Fig. 3.6 Air temperatures and ice thickness with snow (+Snow) and without snow (−Snow) from 18 March to 4 April 2011, Kangerlussuaq, W Greenland. (Modified from: Lund-Hansen et al. 2013)

collected from an area with a 10 cm snow cover and an area with no snow (Fig. 3.6). Ice cores were about 40–41 cm thick at first sampling on 20 March, followed by a clear growth of the ice in both areas but significantly higher in the snow-cleared area, reaching a thickness of 48.5 cm. Without a snow cover the heat loss was higher here which enhanced ice growth rates. Air temperatures were down to −35 °C at the beginning of the experiment and later increased to nearly 0 °C and the ice stopped growing with the onset of the warm period (Fig. 3.6). The low thermal conductivity of snow and its insulating properties also affect the brine volumes and brine salinities of the ice, as mentioned above, and is demonstrated for two ice cores with and without snow cover in Fig. 3.7. The sea ice without snow cover was relatively cold down to −7 °C at the surface compared to about −5 °C with snow, and brine salinities were also higher around 110 without snow and 80 with snow. Calculated mean brine volumes were 3.6% with no snow and 5.1% with snow which are small differences, but brine channels become interconnected at brine volumes >5% (Golden et al. 2007; Morawetz et al. 2017). Thus, the snow-covered ice in this experiment is permeable, and nutrients from the water below the ice have access to the network of brine channels to sustain ice algae growth inside the ice in the snow-covered ice (Legendre et al. 1991). The insulating effects of the snow can accordingly stimulate the microbial life in the brine channels due to more favourable growth conditions such as higher temperatures, lower brine salinities and increased nutrient availability in snow-covered ice. Arctic snow cover and snow thickness can now be measured using satellite remote sensing combined with ground truth data where satellite signals are compared to actual measured snow depths (Sturm and Massom 2017). The mean snow depth on sea ice in the Arctic Ocean has reportedly decreased from about 28 cm in 1980 to 26 cm in 2015 (Blanchard-Wrigglesworth et al. 2018). Figure 3.8 shows how to clear a snow patch for experiments in Kangerlussuaq in West Greenland. Figure 3.9 shows how to work in a snow pit on sea ice at Station Nord in North East Greenland.
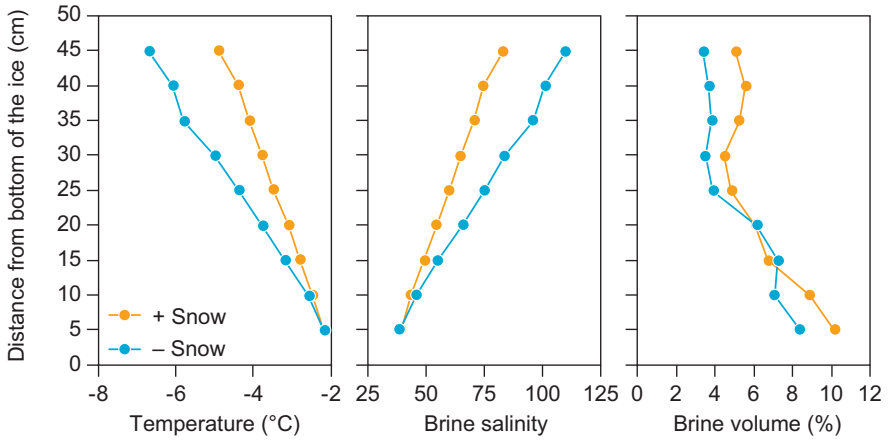
Fig. 3.7 Ice core temperatures, brine salinity, and brine volume with (+Snow) and without (−Snow) snow, March 2011, Kangerlussuaq, W Greenland. (Modified from: Lund-Hansen et al. 2013)

Fig. 3.8 Clearing of a snow patch for experiments, March 2013, Kangerlussuaq, W Greenland. (Photographs by: Authors)

Fig. 3.9 Working in a
snow pit on the sea ice,
May 2017, Station Nord,
NE Greenland.
(Photograph by:
K. Hancke)
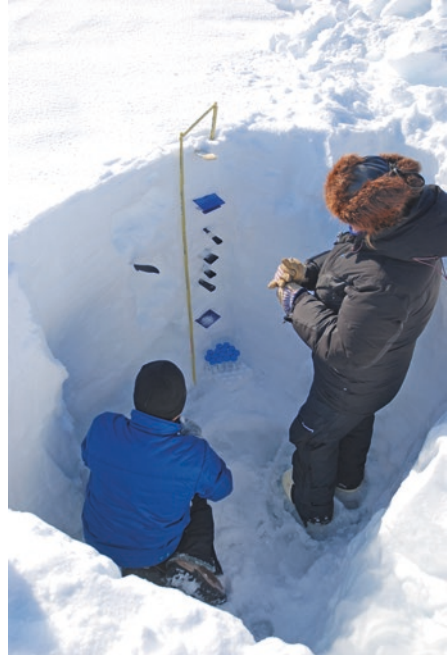
3.3 Colonization of Sea Ice by Ice Algae

Ice algae are algae which use the sea ice as a habitat, both inside the brine channels
and attached to ice surfaces, and described here are different mechanisms by which
algae get into the ice and attached to the ice (Fig. 3.10). The examples illustrate two
notably different ice algae distributions (Chl *a*), with a nearly even vertical distribu-
tion in the Godthåbsfjord, compared to Kangerlussuaq with most of the Chl *a*
located at the bottom of the ice. Why are distributions so different in two first-year
ice cores, and what mechanisms can explain the distributions? Besides the develop-
ment of interstitial layers related to flooding of the ice as mentioned earlier, there
are four main mechanisms to explain vertical distributions of ice algae in sea ice.
Note that most of the algae in sea ice are taxa such as diatoms and dinoflagellates
that are able to form cysts, an inactive stage of the microorganism that can become
active when requirements such as light or nutrients improve (Enberg et al. 2018).
Accordingly, the first mechanism is conservative incorporation, where the cysts are
passively frozen into the ice during autumn freeze-up as the sea ice develops. The
second is inflow of seawater containing algae into the brine channels and thereby
seeding the channels (Stoecker et al. 1997). The μm-sized algae can easily pass into
the mm-sized brine channels, though the dominant flow direction of the high-den-
sity brine is from the channels to the ocean, at least when the ice is growing (Petrich
and Eicken 2017). The third mechanism is freeze-in, where active viable algae from
the water below are captured in the growing ice and continue to photosynthesize in
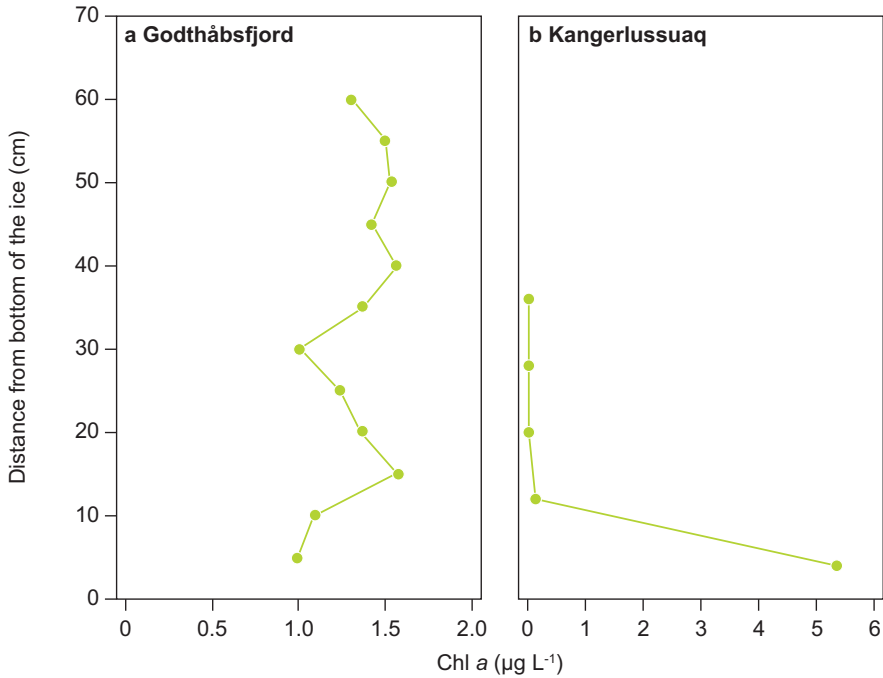
Fig. 3.10 Chl *a* distribution in two cores, February 2017, Nuuk Fjord, SW Greenland (**a**), and in March, 2011, Kangerlussuaq, W Greenland (**b**)

the brine channels inside the ice (Syvertsen 1991). Continued growth requires that algal freeze-in occurs at a time of sufficient light and nutrients. The nearly constant Chl *a* in the Godthåbsfjord ice core (Fig. 3.10) is presumably a result of freeze-in, as the sea ice developed rapidly during a short and cold period in late January and February with a surface light level of about 250 µmol photons $m^{-2} s^{-1}$ (Fig. 1.5). The fourth mechanism is actual colonization, by which algae from the water column adhere to the bottom of the ice either by a physical process or in combination with the development of biofilms at the bottom of the ice. Bacteria develop the biofilm, being the first organisms to colonize a new surface, followed by attachment to the biofilm by larger organisms such as algae, which is the dominant succession observed at exposed marine surfaces (Köhler et al. 1999). The potential role and development of sea ice biofilms is an understudied topic, but it has been observed that ice algae apply EPS to attach to ice surfaces (Meiners and Michel 2017). A field-based time series experiment showed that the colonization expressed as a significant increase in Chl *a* concentrations at the ice bottom was amplified by the development of a skeletal layer (Fig. 2.2b) during a period of ice growth (Fig. 3.11). The figure is analogous to Fig. 3.6 but includes Chl *a* and Chl *a*-specific primary production (mg C m^{-2} day^{-1}/mg Chl *a* m^{-2}) in addition to ice thickness. Chl *a* increased from 0.3 to 1.0 mg Chl *a* m^{-2} between 20 and 26 March, in parallel with an increase in Chl *a*-specific primary production from 0.09 to about 0.6 mg C m^{-2}
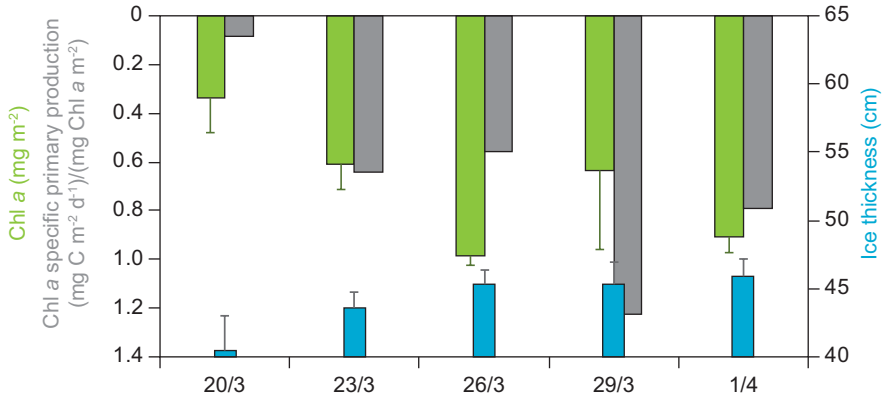
Fig. 3.11 Ice thickness (blue bars), Chl *a* (green bars), and Chl *a*-specific primary production (grey bars and divided by 20 for scaling) with a 10 cm snow cover from 20 March to 1 April 2011, Kangerlussuaq, W Greenland. (Modified from: Lund-Hansen et al. 2016)

day^{-1}/mg Chl *a* m^{-2} (Fig. 3.11). The biomass specific production (Fig. 3.11) of the sea ice algae increased during the study period, suggesting that the algae in the ice became more efficient. Chl a specific primary production takes into account the changes in the biomass of the algae. Chlorophyll fluorescence-based images of the ice bottom sampled at 20 March show only traces of active algae (small green spots) and no specific structure of the ice (Fig. 3.12a), as compared to 26 March with larger green areas of active algae which are clearly organized in elongated structures (Fig. 3.12b). A macro-photo (RGB) of the bottom ice shows that clumps of algae (brown) are located and concentrated at the tip of the ice crystals in the skeletal layer (Fig. 3.12c). The skeletal layer developed at the bottom of the ice during ice growth from 20 to 26 March (Fig. 3.11) and ice algae became attached to the tip of the ice crystals, where the algae started to colonize the bottom of the ice (Fig. 3.12). Analogous colonizations of tips or protrusions have been observed in other marine studies (Köhler et al. 1999; Krembs et al. 2002). A 1-month long study of colonization of newly formed sea ice north of Svalbard showed a significant increase in Chl *a* and carbon biomass, and also that species composition became more dominated by a typical ice algae *Nitzschia frigida* (Kauko et al. 2018). Colonization of the young ice was facilitated by algae from the water column, but seemingly also from older multi-year sea ice that acted as a repository (Olsen et al. 2017). Once incorporated into the sea ice, the microorganisms are challenged by changes in space, temperature, light availability, salinity, nutrients, TCO$_2$, grazing, and O$_2$ concentrations.

Fig. 3.12 Imaging-PAM
minimum chlorophyll
fluorescence images (F_0) of
the bottom section of an
ice core on 20 March (**a**),
and on 26 March (**b**), and
an image (RGB) of the sea
ice underside 26 March
2011 with clumps of algae
on tip of the ice lamellae in
the skeletal layer (**c**),
Kangerlussuaq, W
Greenland. (Modified
from: Lund-Hansen
et al. 2016)
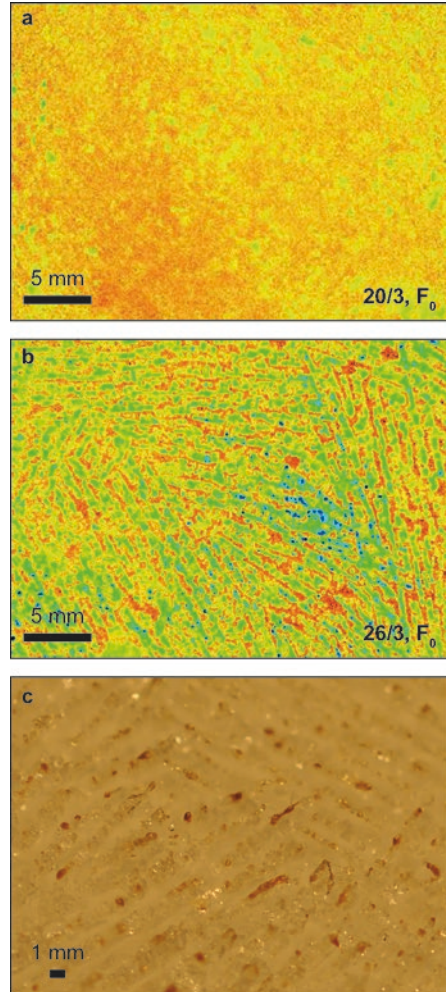
3.4   Growth Limitations of Sea Ice Bacteria and Algae

The seasonal variation in light availability in polar regions is primarily a function
of latitude (Figs. 1.5; 3.13). Sea ice further reduces the amount of light available,
particularly in areas with heavy snow cover or heavy incorporated sediment loads
that attenuate incoming light. Therefore, the light availability will be different in
various regions of the Arctic, even during the darkest phase of the polar night. In
winter, light availability in polar sea ice is insufficient for algal bloom development,
so the sympagic communities remain net heterotrophic with a high bacterial carbon
demand which varies between 0.80 mg C m^{-2} day^{-1} and 26 mg C m^{-2} day^{-1} (Søgaard
et al. 2019; Glud et al. 2014; Long et al. 2012). Regardless of location and bacterial
carbon demand, minima in bacterial abundances are also observed in the sea ice

Fig. 3.13 Differences in light climate according to the angle of the sun with civil twilight between the polar circle and 72°N (**a**), civil polar night between 72°N and 78°N (**b**), and nautical polar night at latitudes above 78°N (**c**). (Modified from: Berge et al. 2015)
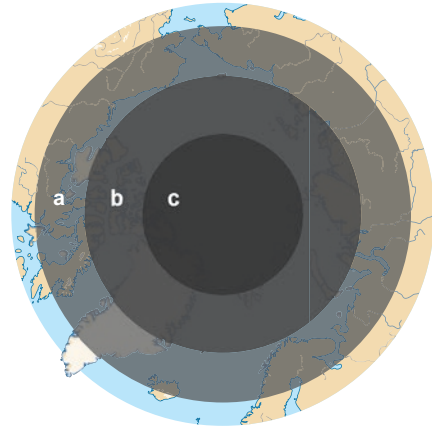
during winter, ranging from $4.0 \cdot 10^3$ to $1.5 \cdot 10^5$ mL^{-1} in cold winter ice (Søgaard et al. 2019). The low bacterial abundance in sea ice during winter (compared to ice bottom summer abundances) might be due to virally-mediated cell death (Collins et al. 2008) or grazing by bacterivorous protists (Rózanska et al. 2008). Other reasons could be low organic substrate availability, reduction in habitable space, or the formation of intracellular ice crystals and puncturing of cells by ice crystals (Collins and Deming 2011). High brine salinity is the key parameter influencing the constitution and activity of the bacterial community in winter sea ice, influencing bacteria directly and indirectly the rest of the sea ice-based food web (Kaartokallio et al. 2013). Bacterial adaptation to sea ice conditions may involve intracellular processes such as production of osmolytes and membrane proteins, release of antifreeze proteins, or the release of extracellular polymeric substances (EPS). Sea ice interstitial habitats resemble a biofilm-like system rather than being analogous to mixed open–water systems, which may help protect the heterotrophic community in this hostile environment (Kaartokallio et al. 2013). It is not surprising that early season sea ice is taxonomically diverse, given the wide range of colonization mechanisms for the winter sea ice discussed previously, with several different large and small algae groups being able to incorporate from a variety of sources. The overall progression during the season is one of a steadily decreasing species and taxonomic group diversity, with the characteristic sea ice specialists, especially diatoms, gradually increasing in number and replacing other groups as the biomass increases. Identifying single driving factors during this early growth phase is difficult given that light, salinity and nutrients are changing simultaneously in the ice matrix. There is, however, much evidence linking early increases in biomass to increasing irradiance at the ice-water interface, and recent data suggest that this can be triggered even at extreme low irradiances (Hancke et al. 2018). There are also other interactions taking place within the community that are not light-dependent, but important in determining species composition and biomass.

3.5   Ice Algae, Photosynthesis, and Their Species Succession

The different mechanisms discussed above can contribute different taxa in different locations and this can differ from year to year. Before the first photon hits an algal cell in spring, the mix of taxa reflects the species present in the under-ice water, how close the ice is to benthic sources or any multi-year ice, and to open water where phytoplankton cells may have survived into autumn. Even before any light-driven productivity, the community is therefore already starting stochastically. As the first photosynthesis begins, allowing new cell division to occur, all these taxa can in principle respond (Kauko et al. 2018). However, it appears that none of the normal abiotic factors that algae respond to control the species composition at this stage. There is no apparent correlation between irradiance, nutrients, salinity or tempera- ture with the changes in species composition that occur during the winter to spring transition, or during the early bloom phase. Nor is grazing by zooplankton or sea ice meiofauna an important factor controlling species diversity, but biotic competition between algal taxa appears to be the important process driving succession (Kauko et al. 2018). Some types of algae are simply more suited to growth in sea ice, and these will displace the other early colonizers with time. Light controls biomass, but interspecific competition controls species composition. At the end of the winter, the community that is about to undergo this competition is typically dominated by flag- ellates and dinoflagellates, with relatively few diatoms. The succession during the bloom is then from flagellate-dinoflagellate dominance to diatom dominance, and within the diatoms from centric to pennate diatoms, provided irradiance remains low. This succession is largely a matter of characteristics of these different groups. Flagellates and dinoflagellates are present in the winter ice mainly as cysts, and cysts may remain the dominant biomass for several weeks early in the season. Resting cysts are characteristic of these species, but less so for diatoms (McMinn and Martin 2012). The dominance of flagellates in early season ice therefore reflects their abundance in the water as ice freezes, and the greater likelihood of their per- sistence without light. There is then a selection process as diatoms, which are better adapted for life in ice, replace the flagellates. Some pennate diatoms are motile, can attach to and move along the ice surface, and are also tolerant of the high salinity there. *Nitzschia frigida*, the species most characteristic of sea ice communities in the Arctic, forms large colonies as shown with a microscope image and a chlorophyll fluorescence-based image (Fig. 3.14). This species can penetrate brine channels and is also salinity-tolerant, as are *Fragilariopsis* species (Petrou et al. 2011). Throughout the spring as light increases, the growth rate of the diatoms greatly exceeds that of the other taxa, due to the ability of species such as *N. frigida* to maintain very high growth rates at low temperatures. That diatoms do not dominate earlier is simply because they are starting from a low abundance and need time to catch up and over- take the other groups. The specialist ice algae are present in extremely low numbers in the water or at the sediment surface during winter, and their colonizing cells in offshore areas are now generally agreed to be derived solely from other ice, either adjacent multi-year ice, or wind-blown fragments of ice that fall into the water and

Fig. 3.14 Microscope image of the sea ice alga *Nitzschia frigida*, and a fluorescence image (32 × 24 mm) of sea ice with visible colonies of *Nitzschia frigida*, August 2012, Amundsen Basin, Arctic Ocean. (Photograps by: Authors)
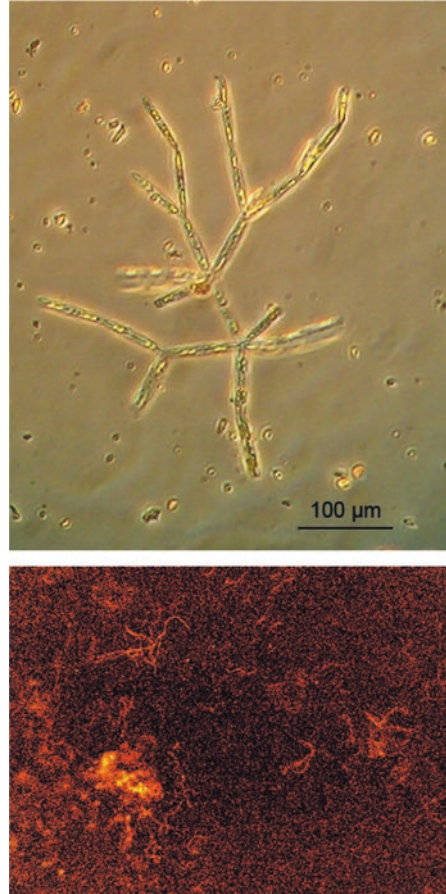
are trapped in the newly forming ice. Another implication of this is that relatively few of the species present in the water column are adapted for life in ice, and those species well-adapted for the sea ice habitat are only ever present in small numbers in the water. This is a largely universal pattern: the species composition of the sea ice community and the seawater community is usually different, and this reflects the limited ability and lack of adaptations to the sea ice habitat in most Arctic marine microalgae. Only in the very newest winter ice (usually <30 cm thick) does the species composition of the ice reflect that of the underlying water, before any selection can take place (Rózanska et al. 2009).

3.6   Extracellular Polymeric Substances, Algal Pigments for Identification, and Seasonal Species Composition

As the season progresses, there are further traits of the sea ice specialists that lead to their dominance. The production of EPS by some sea ice diatoms changes the microstructure of growing sea ice (Krembs et al. 2001), further enhancing their habitat suitability at the expense of other taxa. Taxa that produce EPS become progressively more dominant during the season over non-EPS taxa, apparently being selectively incorporated in growing early season ice (Rózanska et al. 2008). Other possible biotic interactions that may be important include allelopathy and parasitism, neither of which have been studied in any great detail. Following and documenting these changes in species composition requires multiple sources of evidence, especially as cysts are so prevalent. Cysts have little or no chlorophyll content, and their large contribution to the biomass is therefore not reflected if biomass is measured as Chl *a* alone. Studying the early bloom therefore relies heavily on cell counts and microscopic identification of algal groups, and can be greatly enhanced by documenting pigment composition, which is a key method for determining microalgal species composition, especially as not all taxa are easily identified in the microscope e.g., when the community is dominated by very small picoplankton (Hancke et al. 2018). However, some pigments are shared across groups and so the best data are produced by combining pigment and microscope data. The taxonomic distribution of pigments is an especially important tool during this early bloom when the species diversity is high and many of the taxa are small. The key pigments are alloxanthin for cryptophytes, gyroxanthin for dinoflagellates and the coccolithophore *Emiliana huxleyi*, and occasionally some cryptophytes, peridinin in dinoflagellates, and fucoxanthin in diatoms. Chlorophylls c_1 and c_2 are also pigments associated with diatoms and dinoflagellates, and Chl *b* is only found in green algae. Note that it is the ratio of concentrations of these pigments to Chl *a* that is used for identification and description of relative abundance, as Chl *a* is present in all taxa and provides a useful total pigment indicator to normalize against. Pigment analysis has become a highly sophisticated tool for identification and quantitative analysis of algal species composition at the class level, and the CHEMTAX program for calculating abundances at the class level (Mackey et al. 1996) is now an almost universal tool for taxonomic analysis of HPLC data. Note that pigments become less useful at lower taxonomic levels as they cannot, for example, usefully distinguish between centric and pennate diatoms.

The convergence of species composition to a pennate diatom community as the season progresses is typical for the Arctic (Leu et al. 2015) given that taxa such as *N. frigida* are cryophilic. Their ability to dominate is only limited by the distance to a colonization source at the start of the season. Multi-year ice is an essential seeding stock (Olsen et al. 2017), such that the loss of multi-year ice with climate change is a concern for the future persistence of this community. Higher light transmittance due to reduced snow cover with climate change is likely to favour centric diatoms over pennate diatoms. Dominance of centric over pennate
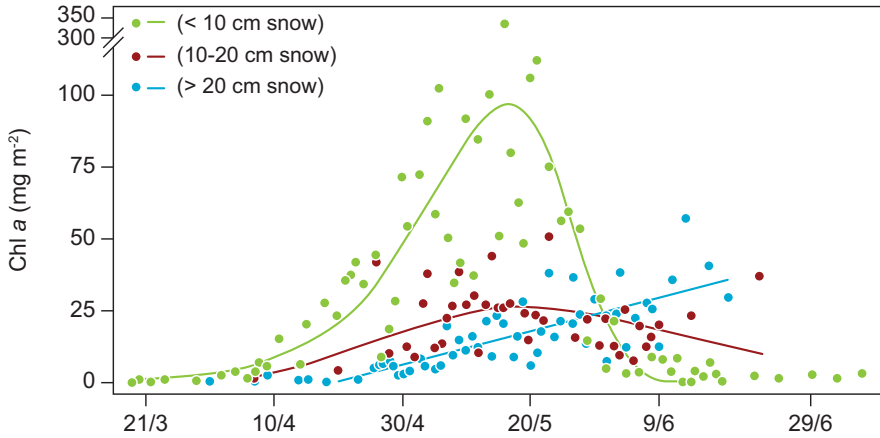
Fig. 3.15 Development of ice algal (Chl *a*) biomass at Resolute Bay Canada between end of March and end of June under different snow depths. Snow cover has been divided into three classes: low (<10 cm), medium (10–20 cm) and high (>20 cm). (Modified from: Leu et al. 2015)

diatoms is common in thin ice or ice with a thin snow cover (Rózanska et al. 2008) and they may also be very common within pressure ridges. Across the Arctic, the process of diatom biomass increase in sea ice bottom layers seems very consistent during this early light-limited phase. Leu et al. (2015) have documented a wide range in Chl *a* biomass between different sites in the Arctic. Values <1 mg Chl *a* m^{-2} have been noted in Greenland Fjords with first-year ice (Søgaard et al. 2010). Slightly higher values occur in the Central Arctic (< 2 mg Chl *a* m^{-2}), increasing to 20 mg Chl *a* m^{-2} over much of the Arctic, with some of the highest values (up to 120 mg Chl *a* m^{-2}) in Resolute Bay, Canada (Fig. 1.4). Time-series analysis from a single study site shows that snow cover, compared to other factors such as local weather and daylength, is responsible for most of the variation in ice algae biomass, and in particular snow thickness (Fig. 3.15). There is a clear difference in maximum ice algae biomass between areas, which is reached with a snow cover <10 cm and thus highest transmittance. It would have been interesting if this study had data from areas with no snow, but it is a solid verification of the strong link between ice algae biomass, irradiance, and transmittance. Despite sea ice algae being extreme shade-adapted organisms, they remain strongly light-limited during the early growth phase. Rapid changes in snow cover and sudden increases in irradiance might inhibit photosynthetic processes due to photoinhibition, but the overall pattern at this time of year is acclimation to the prevailing low irradiance and light being a limiting resource rather than a stress factor. Much of our current understanding of the development of the sea ice algal community is based on such biomass data, but less is known about the productivity in the ice and when the community is heterotrophic or autotrophic. At some point in winter there is a shift from net heterotrophy to net autotrophy (Fig. 1.1). Development of new productivity methods such as eddy covariance (Long et al. 2012), which measures net rather than gross photosynthesis, offers new insights into these seasonal changes in productivity. Net productivity

methods have the advantage of providing a combined measurement of respiration as well as photosynthesis, allowing better identification of when the community, and hence the sea ice, shifts from net heterotrophic to net autotrophic. Respiration in darkness (dark respiration) rates of algae can be 10–30% of their photosynthetic rates, and there is also the heterotrophic bacterial and eukaryotic respiration as an additional load on net heterotrophy of the community (Holtappels et al. 2015). Eddy covariance methods are revealing that net daily heterotrophy does occur, and is probably widespread during winter and in the early mixed community phase in spring. This net heterotrophy is likely driven by large bacterial populations still present, and with a respiratory demand that exceeds the inorganic carbon assimilation of the algae (Rysgaard et al. 2008; Søgaard et al. 2019). At this time, even though Chl *a* and algal cell numbers are increasing during the winter to spring transition period, the community remains a net carbon source during the early bloom. There is no clear indication of a consistent point in different communities when the switch from net heterotrophic to net autotrophic occurs, but these studies are showing that respiration has been greatly neglected and is quantitatively significant.

3.7   Photosynthesis Under Very Low Light

The extreme shade adaptation of ice algae is their most widely recognised and discussed attribute. They are able to photosynthesise at a fraction of the irradiances required by pelagic phytoplankton despite having similar photosynthetic processes. Sea ice algae have chloroplasts with a photosynthetic machinery that includes a biophysical light harvesting component and biochemical carbon fixation, with the enzyme Rubisco used for fixing CO_2 into sugars as in all photosynthetic organisms. The pH (approximately 8.2) of seawater and the brine in the brine channels is too high for there to be any appreciable availability of free CO_2 for photosynthesis. All of the algal groups found in sea ice communities have bicarbonate usage, a CO_2-concentrating mechanism for photosynthesis, which allows them to exploit bicarbonate ions (HCO_3^-) as an inorganic carbon source (Falkowski and Raven 2007).

The usage of HCO_3^- is almost universal in diatoms – the most important microalgae group in sea ice (Matsuda et al. 2001). HCO_3^- use is an active process that requires energy, which puts an additional demand on the energy produced in photosynthesis. A basic question is how do ice algae manage to capture sufficient photons to fix carbon and produce new cell growth at these extremely low under-ice irradiances? To answer this we must consider the light reactions of photosynthesis and the machinery that autotrophs use to capture light, but we also need a mechanism that can adjust the machinery to changes in irradiance. The amount of carbon that ice algae can assimilate at any given irradiance can be assessed from the photosynthesis-irradiance (P-*E*) curve where *E* is the energy in the photons used in photosynthesis (P). An example of P-*E* curves for ice algae is shown in Fig. 3.16. The photosynthetic carbon assimilation is represented as gross photosynthesis, a measure that is quantified by the most common methods for algal photosynthesis, here as ^{14}C uptake.
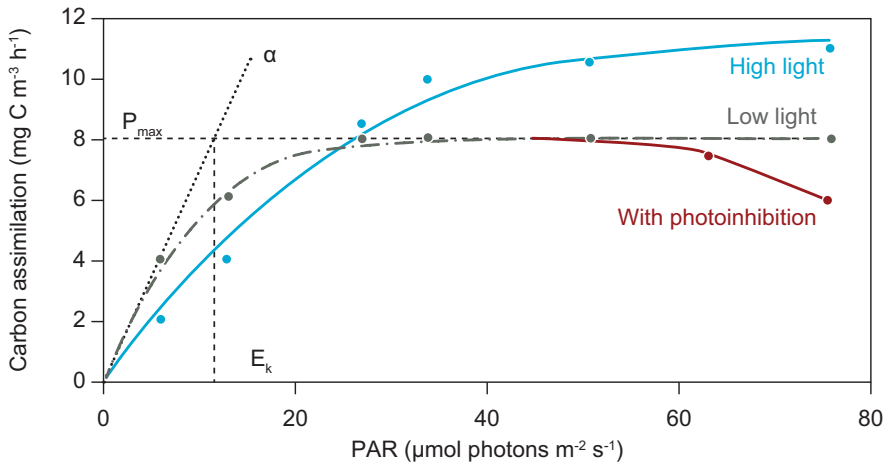
Fig. 3.16 Examples of photosynthesis-irradiance (P-*E*) curves for a hypothetical high-light (blue solid line and blue dots)), and low light (black dashed line)-acclimated ice algal community during the spring bloom. The fitted curves are based on the formula of Jassby and Platt (1976); and photosynthetic parameters (P_{max}, E_k, and α) are shown for the low-light (black dashed line) and with photoinhibition (red solid line). If the low-light acclimated community suffers photoinhibition, it will lose activity and a reduction in P at high irradiances as shown by the red symbols

A net photosynthesis P-*E* curve would have a negative y-axis intercept rather than passing through the origin, representing cellular mitochondrial respiration in the dark. Methods that measure net photosynthesis include dissolved oxygen methods or the eddy covariance technique (Holtappels et al. 2015). Modelling the P-*E* response involves fitting an appropriate curve to the discrete data points produced in an experiment as shown in Fig. 3.16. The Jassby and Platt (1976) equation has been the most widely applied and is suitable for sea ice algae. It describes the P-*E* response as: $P = P_{max} \times \tanh(\alpha \times E_{PAR}/P_{max})$ where P is the photosynthetic rate (mg C m^{-3} h^{-1}) at a particular irradiance E_{PAR} (µmol m^{-2} s^{-1}), P_{max} is the maximum photosynthetic activity (mg C m^{-3} h^{-1}), and α is the initial slope of the light-limited response (mg C m^{-3} h^{-1}/µmol m^{-2} s^{-1}). The onset of light saturation E_k, the irradiance at which photosynthesis is reaching a maximum and becoming independent of irradiance, is calculated as $E_k = P_{max}/\alpha$. In higher light conditions (high light), the photosynthetic activity is upregulated and P_{max} is higher than in low-light conditions (shade), allowing maximum exploitation of available light. The higher E_k in the high-light vs low light-curve represents the greater light demand of the high-light community. In low-light conditions, there is less investment in photosynthetic capacity as this would be wasteful when light is severely limiting, and more investment in capturing as much light as possible at low photon fluxes. A low-light, or shade-adapted, *P-E* curve will therefore have a lower P_{max} and E_k consistent with reduced demand for light when less is available, and a higher initial slope (higher α), showing that the cells have upregulated their ability to capture light at extreme low irradiances. The ability to acclimate and therefore change the *P-E* response is widespread in aquatic

autotrophs, which reflects the low light intensities and variable light climate of aquatic compared to terrestrial environments (Raven et al. 2000). This applies especially for ice algae where extreme low irradiances are typical, but where also sudden changes in irradiance associated with snowmelt are common. The major challenge for ice algae in relation to light is the need to be an organism that can do much with very little. They should also be able to deal with the fact that irradiance will exceed E_k at some point during the growth season, when they are exposed to too many photons for photosynthesis to handle (Sect. 4.4.) Here we focus on the low-light conditions during the early bloom, and especially how early season algae can enhance their ability to capture photons and maximise α. These early season ice algae need to find ways to enhance the flux of photons into the photosystems, which they do with applying a range of accessory pigments, as they are accessories to the main Chl *a* pigment. The most important of these are termed photosynthetic accessory carotenoid pigments (PSC), and comprise fucoxanthin, peridinin, neoxanthin, and alloxanthin used to increase photon flux to the algae cells (Kirk 1994). Other chlorophylls (Chl *b* and *c* chlorophylls) also enhance light capture. These different pigments absorb photons most effectively at different wavelengths, but they all absorb green light more efficiently than Chl *a*, which absorbs light mostly in the red and blue part of the spectrum. It should be emphasized that it is the ratio of these pigments normalised to Chl *a* that allows comparisons between communities over time for their light acclimation. Ice algae can further adapt to very low light conditions by increasing the numbers of light-harvesting complexes (LHC) in the chloroplast, which are complexes of proteins and chlorophylls in the chloroplast that transport photons to the photosystems. In microalgae including diatoms, a reduction in irradiance triggers the rapid assembly of more LHCs, and this is reversible with LHCs being disassembled or broken down when irradiance suddenly increases (Falkowski and LaRoche 1991). The very low E_k and high α values associated with sea ice algae are therefore a function of these pigment and light-harvesting acclimations. Ice algae are some of the most shade-adapted autotrophs on earth, where E_k values of < 20 μmol photons m^{-2} s^{-1} are common (Selz et al. 2018), and irradiances necessary for growth have often been reported in the range of < 10 μmol photons m^{-2} s^{-1} (Gosselin et al. 1986), and recently < 0.17 μmol photons m^{-2} s^{-1} (Hancke et al. 2018). These values are more than an order of magnitude lower than those of terrestrial autotrophs and also considerably lower than phytoplankton. Ice algae are essentially pushing low-light acclimation in photosynthesis almost as far as theoretically possible, on energetic grounds. As cells usually need about 10 mol of photons to fix 1 mol of C, this is close to the minimum light that allow cells to exist.

3.8   Photosynthesis at Extreme Low Light – Case Study 1

This case study focuses on the very early development of the ice algal community at extremely low irradiances. It will further illustrate the principles of transmittance through snow and ice, and the physical properties of snow that govern when the
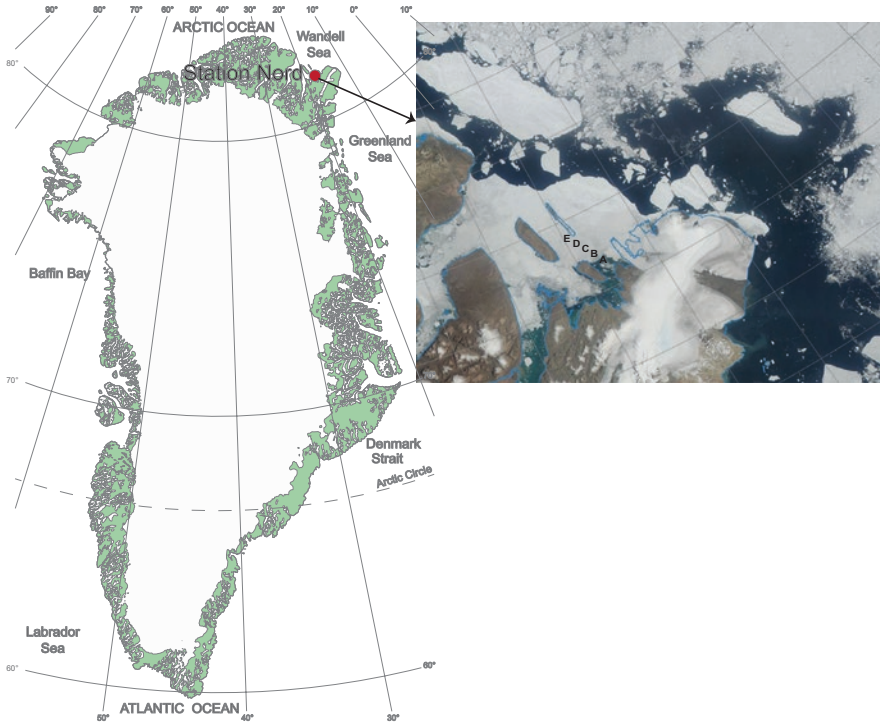
Fig. 3.17 Map of sampling area with five sampling stations (A to E) along a 20 km transect from the shoreline outside the Villum Research Station (VRS) at Station Nord. Main station is at C. (Modified from: Hancke et al. 2018)

earliest productivity can occur. Algal biomass, species composition, and variable chlorophyll fluorescence methods are applied in the case study, which also includes modelling of transmittance through a snow package to evaluate observational data. The study was carried out at 81.3 °N during April–May 2015 in NE Greenland at the Villum Research Station (VRS) and at Station Nord (Fig. 3.17). The study site is located in a glacier-covered fjord with a mixture of first- and multi-year ice. The sun is above the horizon from late March until about 10 October, resulting in 6 months of darkness or very dim light (Fig. 1.5). Sea ice thickness here is generally about 1 m and the ice is covered by a snowpack of 1.0–1.5 m except for a few summer months. The central research question was under which conditions, when, and which ice algae species would start to develop spring growth. We established a 20 km long transect with five sampling stations to resolve any spatial variations and all stations were sampled 5–6 times between mid-April and mid-May to observe this early development (Fig. 3.17). During this period surface light (PAR) increased gradually from an average of 100 μmol photons m^{-2} s^{-1} on 1 April to about 800 μmol photons m^{-2} s^{-1} 1 July (Fig. 3.18a). Chl *a* concentrations at the bottom of the ice were zero at the end of April, but increased gradually to about 0.002 mg Chl *a* m^{-2} between 29 April and 13 May. Although these concentrations are extremely low,
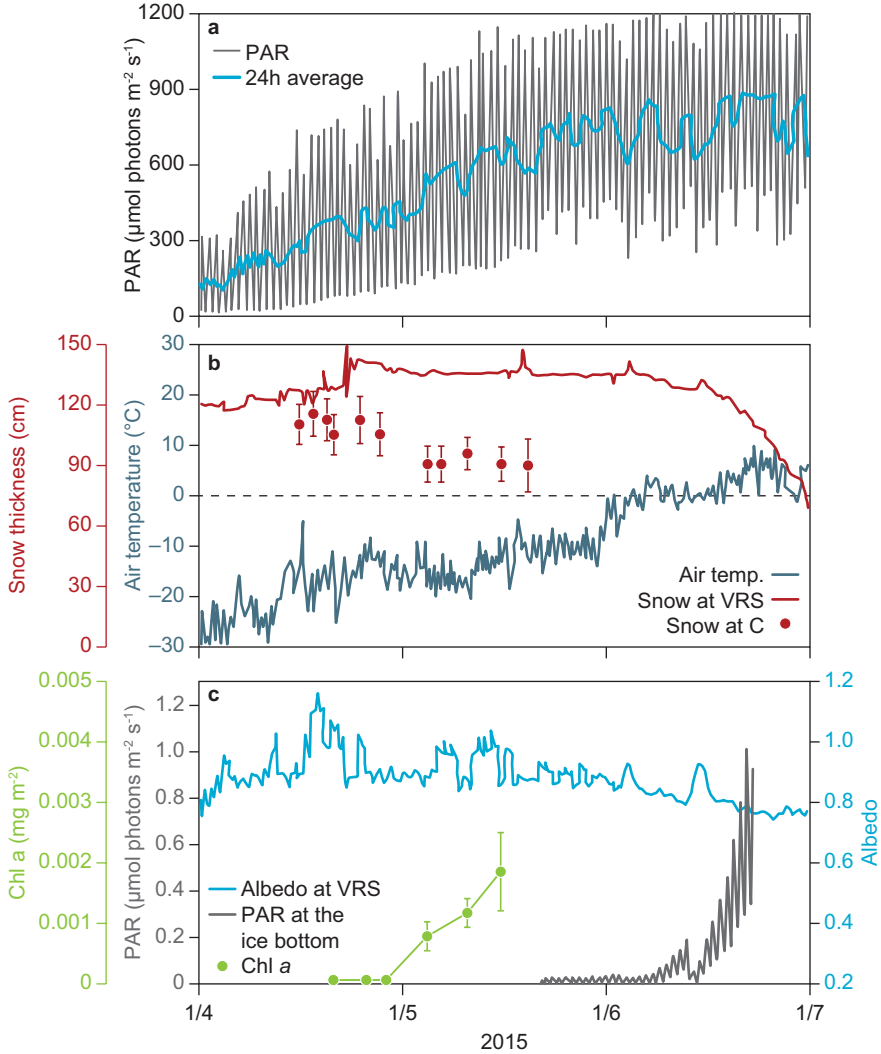
Fig. 3.18 Surface PAR measurements (black line) with daily average (blue line) (**a**), snow thickness at Villum Research Station (VRS; red line), snow thickness (cm) at sampling station C (red dots) and air temperature (blue line) (**b**), and under-ice Chl *a* (green dots), PAR at the sea ice bottom (grey line), and albedo at VRS (blue line) (**c**) between 1 April and 1 July 2015. (Modified from Hancke et al. 2018)

they clearly demonstrate that the spring ice algae development was initiated in early May in near darkness below the ice. On 5 May we measured PAR of 0.17 µmol photons m^{-2} s^{-1} at the ice bottom near noon with a surface PAR of about 750 µmol photons m^{-2} s^{-1}. It was a real surprise that the algae were able to photosynthesize and increase their biomass at such very low PAR levels. The algae were clearly above the light compensation point for positive net primary production, even at this low irradiance. We expected low irradiances under a package of about 1 m snow and
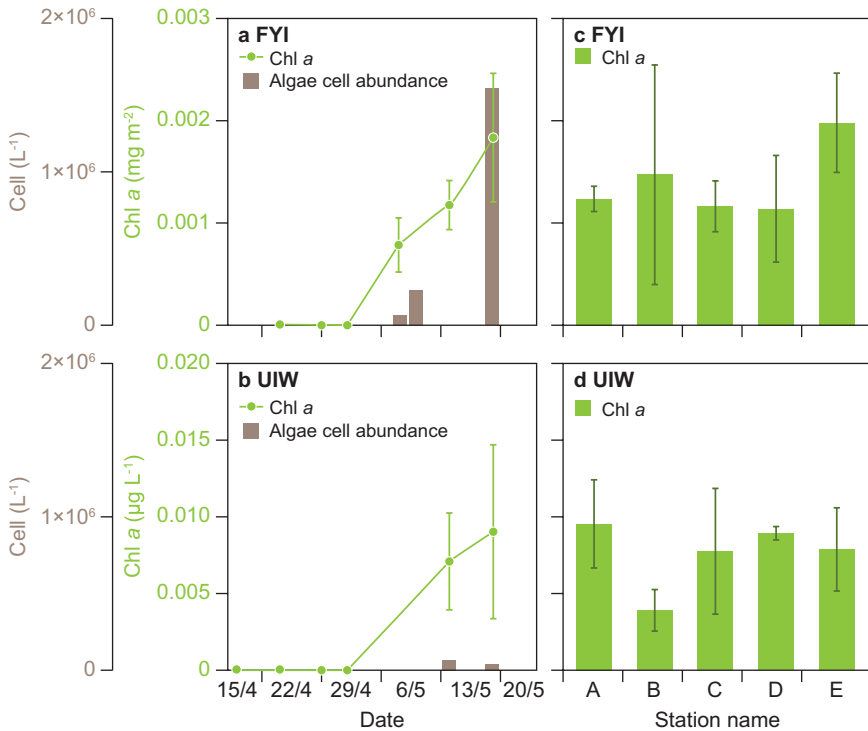
Fig. 3.19 Algal cell abundance (brown bars) and Chl *a* (green lines) in bottom first-year (**FYI**) sea ice at sampling station C between 15 April and 20 May (**a**), algal cell abundance (brown bars) and Chl *a* (green lines) in under-ice seawater (**UIW**) at C (**b**), Chl *a* (green bars) in bottom of first-year sea ice on a transect with sampling station C as centre station (**c**), and Chl *a* (green bars) in under-ice seawater on a transect with sampling station C as centre station (**d**). Note different units for Chl *a* concentrations in bottom sea ice and in under-ice seawater. (Modified from: Hancke et al. 2018)

1.2 m thick sea ice (Fig. 3.18b), but that ice algae were able to photosynthesize at such low irradiance was a new discovery. Ice bottom Chl *a* was measured along the transect with the central station C (Fig. 3.17) and there were no significant differences in concentrations, which demonstrates that the ice algae growth was not only restricted to the central site C (Fig. 3.19c). It could be that what we observed in the ice was just phytoplankton that somehow got attached to the ice, and not algae actually growing there. There were clear differences, however, between the ice bottom and water column as ice algae cell numbers were about 10 times higher in the bottom of the sea ice (maximum $1.5 \cdot 10^6$ cells L^{-1}) compared to the water column (maximum $0.15 \cdot 10^6$ cells L^{-1}). Ice algae were also more viable with maximum quantum yields F$_v$/F$_m$ of 0.31 compared to the phytoplankton below the ice of 0.13. (Fig. 3.20). Algae species composition in the ice was dominated (>70%) by very small unidentified picophytoplankton and flagellates, and a small amount of dinoflagellates and diatoms (e.g., *Nitzschia closterium, Nitzschia longissima*). However, what triggered the increase in under-ice irradiance and bottom-ice productivity? One explanation is that the snow depth at station C reduced by about

Fig. 3.20 Maximum
quantum yield (F_v/F_m) of
ice algae in first-year ice
and in under-ice seawater.
(Modified: from Hancke
et al. 2018)
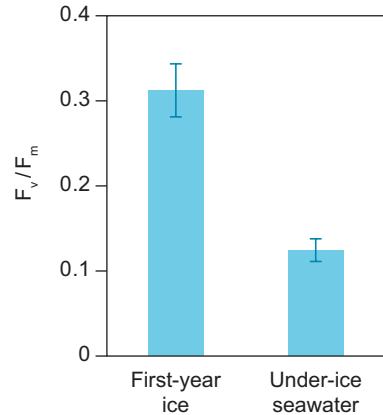
10 cm between the end of April and beginning of May, which could have suffi-
ciently increased ice bottom irradiance (Fig. 3.18b). Based on snow depths and
under ice irradiance data, we estimated the increase in under-ice PAR per cm loss
of snow depth, and showed that PAR increased by 0.44 μmol photons m^{-2} s^{-1} for
a 15 cm decrease in snow depth. Another explanation might be that the optical
properties of the snow changed over time and thereby increased light transmittance
in the snow. Snow and ice temperature data were obtained from a thermistor string
at station C, which measured temperatures in 25 cm of air above the snow, 90 cm of
snow, 115 cm of ice, and 10 cm of water below the ice at high resolution (every
2 cm) (Fig. 3.21). There was a strong diurnal variation in air temperatures with night
temperatures down to −25 °C and noon temperatures of −12 °C with a significant
heat flux into (daytime) and out (nighttime) of the upper 50 cm of the snow in early
May. However, it is the increase in snow temperature over time which is important,
going from −8 °C to −3 °C at 50 cm depth between 8 and 19 May (Fig. 3.21). The
ice was isothermal, meaning that the temperature was vertically constant, and at
−1 °C. The snow temperature increase likely resulted in snow metamorphosis
which increases the grain sizes of the snow, and as scattering of light in the snow
decreases with increasing grain sizes, this could explain the higher irradiance that
reached the bottom of the ice. A model (https://nar.ucar.edu/2016/acom/31-release-
tropospheric-ultraviolet-visible-tuv-model-version-53) was used to quantify the
increase in irradiance at the bottom of the ice during snow heating and snow meta-
morphosis. The purpose was to validate the optical properties of different snow
types in relation to PAR transmittance and to compare modelled under-ice irradi-
ance with our measurements in the field. The model describes PAR transmittance
through the atmosphere, snow, and ice based on measured snow and ice densities,
thickness, albedos, and was run for three types of snow, i.e. cold polar snow, coastal
wind packed snow and melting snow. Model results showed an under-ice PAR of
0.24 μmol m^{-2} s^{-1} for the cold snow and an under-ice PAR of 0.65 μmol m^{-2} s^{-1} for
coastal wind-packed snow, and demonstrate that under-ice PAR actually increased
with the increase in snow temperature. Results also show that the increase in under-
ice PAR was comparable to the 0.17 μmol photons m^{-2} s^{-1} that was measured below
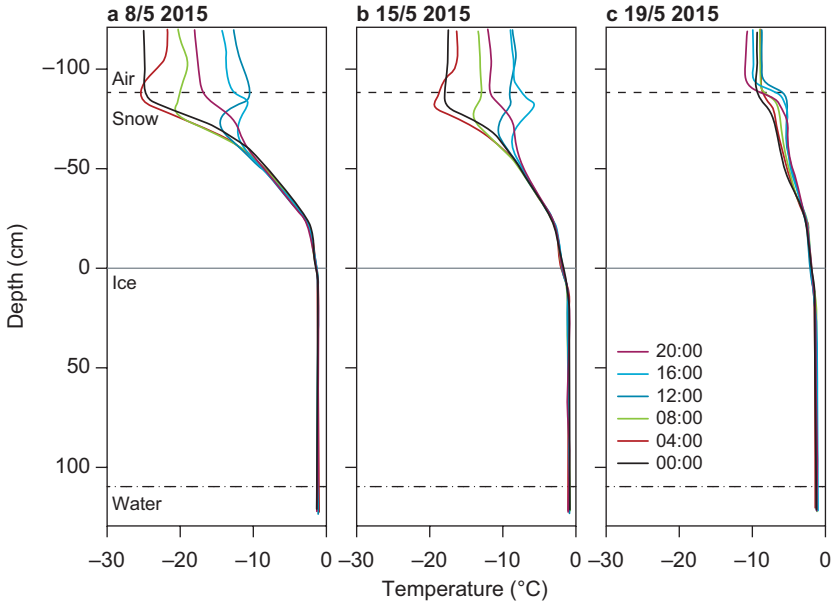
Fig. 3.21 Temperature profiles in air, snow, ice, and water during a 20 h cycle between midnight (00:00) and 20:00 on 8 May 2015 (**a**), 15 May 2015 (**b**), and 19 May 2015 (**c**). (Modified: from Hancke et al. 2018)
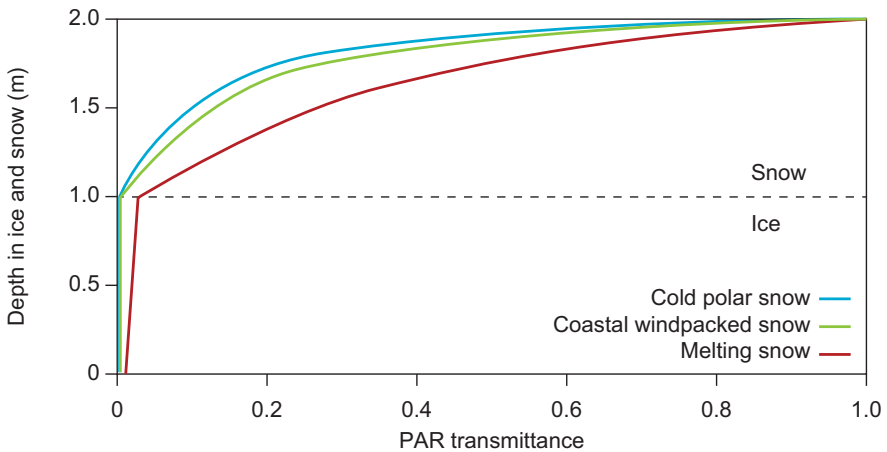
Fig. 3.22 Model results of PAR transmittance through snow and ice package for cold polar snow (blue line), coastal wind packed snow (green line), and melting snow (red line). (Modified: from Hancke et al. 2018)

the ice on 5 May. Irrespective of what actually triggered the bloom, the scientifically most interesting aspect of this study is that sea ice algae were able to start growing at very low PAR levels, and illustrates the extreme shade adaptation of sea ice algae (Fig. 3.22).

References

Berge, J., Renaud, P. E., Darnis, G., Cottier, F., Last, K., Gabrielsen, T. M., Johnsen, G., Seuthe, L., Weslawski, J. M., Leu, E., Moline, M., Nahrgang, J., Søreide, J. E., Varpe, Ø., Lønne, O. J., Daase, M., & Falk-Petersen, S. (2015). In the dark: A review of ecosystem process during the Arctic polar night. *Progress in Oceanography, 139*, 258–271. https://doi.org/10.1016/j.pocean.2015.08.005.

Blanchard-Wrigglesworth, E., Webster, M. A., Farrell, S. L., & Bitz, C. M. (2018). Reconstruction of snow on Arctic Sea Ice. *Journal of Geophysical Research, 123*, 3588–3602. https://doi.org/10.1002/2017JC013364.

Collins, R. E., & Deming, J. W. (2011). Abundant dissolved genetic material in Arctic sea ice Part II: Viral dynamics during autumn freeze-up. *Polar Biology, 34*, 1831–1841. https://doi.org/10.1007/s00300-011-1008-z.

Collins, R. E., Carpenter, S. D., & Deming, J. W. (2008). Spatial heterogeneity and temporal dynamics of particles, bacteria, and pEPS in arctic winter sea ice. *Journal of Marine Systems, 74*, 902–917. https://doi.org/10.1016/j.jmarsys.2007.09.005.

Cox, G. F. N., & Weeks, W. F. (1974). Salinity variations in sea ice. *Journal of Glaciology, 13*, 109–120. https://doi.org/10.3189/S0022143000023418.

Cox, G. F. N., & Weeks, W. F. (1983). Equations for determining the gas and brine volumes in sea-ice samples. *Journal of Glaciology, 29*, 306–316. https://doi.org/10.3189/S0022143000008364.

Eicken, H. (2003). From the microscopic to the macroscopic to the regional scale, growth, microstructure and properties of sea ice. In D. N. Thomas & G. S. Dieckmann (Eds.), *Sea Ice: An introduction to its physics, chemistry, biology and geology* (1st ed., pp. 22–181). Oxford: Wiley Blackwell.

Enberg, S., Majaneva, M., Autio, R., Blomster, J., & Rintala, J. M. (2018). Phases of microalgal succession in sea ice and the water column in the Baltic Sea from autumn to spring. *Marine Ecology Progress Series, 599*, 19–34. https://doi.org/10.3354/meps12645.

Falkowski, P. G., & LaRoche, J. (1991). Acclimation to spectral irradiance in algae. *Journal of Phycology, 27*, 8–14. https://doi.org/10.1111/j.0022-3646.1991.00008.x.

Falkowski, P. G., & Raven, J. A. (2007). *Aquatic photosynthesis* (2nd ed.). Princeton: Princeton University Press.

Fernández-Méndez, M., Katlein, C., Rabe, B., Nicolaus, M., Peeken, I., Bakker, K., Flores, H., & Boetius, A. (2015). Photosynthetic production in the central Arctic Ocean during the record sea-ice minimum in 2012. *Biogeosciences, 12*, 3525–3549. https://doi.org/10.5194/bg-12-3525-2015.

Glud, R. N., Rysgaard, S., Turner, G., McGinnis, D. F., & Leakey, R. J. G. (2014). Biological and physical-induced oxygen dynamics in melting sea ice of the Fram Strait. *Limnology Oceanography, 59*, 1097–1111. https://doi.org/10.4319/lo.2014.59.4.1097.

Golden, K. M., Ackley, S. F., & Lytle, V. I. (1998). The percolation phase transition in sea ice. *Science, 282*, 2238–2241. https://doi.org/10.1126/science.282.5397.2238.

Golden, K. M., Eicken, H., Heaton, A. L., Miner, J., Pringle, D. J., & Zhu, J. (2007). Thermal evolution of permeability and microstructure in sea ice. *Geophysical Research Letters, 34*. https://doi.org/10.1029/2007GL030447.

Gosselin, M., Legendre, L., Therriault, J.-C., Demers, S., & Rochet, M. (1986). Physical control of the horizontal patchiness of sea-ice microalgae. *Marine Ecology Progress Series, 29*, 289–298. https://doi.org/10.3354/meps029289.

Hamre, B., Winther, J. G., Gerland, S., Stamnes, J. J., & Stamnes, K. (2004). Modeled and measured optical transmittance of snow-covered first-year sea ice in Kongsfjorden, Svalbard. *Journal of Geophysical Research, 109*, C10006. https://doi.org/10.1029/2003JC001926.

Hancke, K., Lund-Hansen, L. C., Lamare, M. L., Pedersen, S. H., King, M. D., Andersen, P., & Sorrell, B. K. (2018). Extreme low light requirement for algae growth underneath sea ice: A case study from Station Nord, NE Greenland. *Journal of Geophysical Research, 123*, 985–1000. https://doi.org/10.1002/2017JC013263.

Holtappels, M., Noss, C., Hancke, K., Cathalot, C., McGinnis, D. F., Lorke, A., & Glud, R. N. (2015). Aquatic eddy correlation: Quantifying the artificial flux caused by stirring-sensitive O2 sensors. *PLoS One, 10*, e0121931. https://doi.org/10.1371/journal.pone.0121931.

Jassby, A. D., & Platt, T. (1976). Mathematical formulation of the relationship between photosynthesis and light for phytoplankton. *Limnology and Oceanography, 21*, 540–547. https://doi.org/10.4319/lo.1976.21.4.0540.

Kaartokallio, H., Søgaard, D. H., Norman, L., Rysgaard, S., Tison, J.-L., Delille, B., & Thomas, D. N. (2013). Short-term variability in bacterial abundance, cell properties, and incorporation of leucine and thymidine in subarctic sea ice. *Aquatic Microbial Ecology, 71*, 57–73. https://doi.org/10.3354/ame01667.

Kauko, H. M., Olsen, L. M., Duarte, P., Peeken, I., Granskog, M. A., Johnsen, G., Fernández-Méndez, M., Pavlov, A. K., Mundy, C. J., & Assmy, P. (2018). Algal colonization of young Arctic sea ice in Spring. *Frontiers in Marine Science*. https://doi.org/10.3389/fmars.2018.00199.

Kirk, J. T. O. (1994). *Light and photosynthesis in aquatic ecosystems* (662 pp). Cambridge: Cambridge University Press.

Köhler, J., Hansen, P. D., & Wahl, M. (1999). Colonization patterns at the substratum-water interface: How does surface microtopography influence recruitment patterns of sessile organisms? *The Journal of Bioadhesion and Biofilm Research, 14*, 237–248. https://doi.org/10.1080/08927019909378415.

Kono, M., & Terashima, I. (2014). Long-term and short-term responses of the photosynthetic electron transport to fluctuating light. *Journal of Photochemistry and Photobiology B: Biology, 137*, 89–99. https://doi.org/10.1016/j.jphotobiol.2014.02.016.

Krembs, C., Mock, T., & Gradinger, R. (2001). A mesocosm study of physical-biological interactions in artificial sea ice: Effects of brine channels surface evolution and brine movement on algal biomass. *Polar Biology, 24*, 356–364. https://doi.org/10.1007/s003000000219.

Krembs, C., Tuschling, K., & Juterzenka, K. V. (2002). The topography of the ice-water interface – Its influence on the colonization of sea ice algae. *Polar Biology, 25*, 106–117. https://doi.org/10.1007/s003000100318.

Kwok, R. (2018). Arctic sea ice thickness, volume, and multiyear ice coverage: Losses and coupled variability (1958–2018). *Environmental Research Letters, 13*, 105005. https://doi.org/10.1088/1748-9326/aae3ec.

Kwok, R., & Rothrock, D. A. (2009). Decline in Arctic sea ice thickness from submarine and ICESat records: 1958–2008. *Geophysical Research Letters, 36*. https://doi.org/10.1029/2009GL039035.

Legendre, L., Aota, M., Shirasawa, K., Martineau, M. J., & Ishikawa, M. (1991). Crystallographic structure of sea ice along a salinity gradient and environmental control of microalgae in the brine cells. *Journal of Marine Systems, 2*, 347–357. https://doi.org/10.1016/0924-7963(91)90041-R.

Leu, E., Mundy, C. J., Assmy, P., Campbell, K., Gabrielsen, T. M., Gosselin, M., Juul-Pedersen, T., & Gradinger, R. (2015). Arctic spring awakening – Steering principles behind the phenology of vernal ice algal blooms. *Progress in Oceanography, 139*, 151–170. https://doi.org/10.1016/j.pocean.2015.07.012.

Light, B., Grenfell, T. C., & Perovich, D. K. (2008). Transmission and absorption of solar radiation by Arctic sea ice during the melt season. *Journal of Geophysical Research, 113*. https://doi.org/10.1029/2006JC003977.

Long, M. H., Koopmans, D., Berg, P., Rysgaard, S., Glud, R. N., & Søgaard, D. H. (2012). Oxygen exchange and ice melt measured at the ice-water interface by eddy correlation. *Biogeosciences, 9*, 1957–1967. https://doi.org/10.5194/bg-9-1957-2012.

Lund-Hansen, L. C., Hawes, I., Sorrell, B. K., & Nielsen, M. H. (2013). Removal of snow cover inhibits spring growth of Arctic ice algae through physiological and behavioral effects. *Polar Biology, 37*, 471–481. https://doi.org/10.1007/s00300-013-1444-z.

Lund-Hansen, L. C., Hawes, I., Nielsen, M. H., & Sorrell, B. K. (2016). Is colonization of sea ice by diatoms facilitated by increased surface roughness in growing ice crystals? *Polar Biology, 40*, 593–602. https://doi.org/10.1007/s00300-016-1981-3.

Lund-Hansen, L. C., Hancke, K., Salmansen, N., Balslev, L., Nielsen, J., Hawes, I., & Sorell, B. K. (2020). Effects of snow removal and increased irradiance on biomass, pigments, photobiology and nutritional quality of Arctic sea ice algae during spring growth. *Marine Ecology Progress Series* (In press).

Mackey, M. D., Mackey, D. J., Higgins, H. W., & Wright, S. W. (1996). CHEMTAX – A program for estimating class abundances from chemical markers: Application to HPLC measurements of phytoplankton. *Marine Ecology Progress Series, 144*, 265–283. https://doi.org/10.3354/meps144265.

Matsuda, Y., Hara, T., & Colman, B. (2001). Regulation of the induction of bicarbonate uptake by dissolved CO_2 in the marine diatom, *Phaeodactylum tricornutum*. *Plant, Cell and Environment, 24*, 611–624. https://doi.org/10.1046/j.1365-3040.2001.00702.x.

McMinn, A., & Martin, A. (2012). Dark survival in a warming world. *Proceedings of the Royal Society Series B, 280*, 20122909. https://doi.org/10.1098/rspb.2012.2909.

Meiners, K. M., & Michel, C. (2017). Dynamics of nutrients, dissolved organic matter and exopolymers in sea ice. In: D. N. Thomas (Ed.), *Sea ice* (3rd ed., pp. 415–432). Oxford: Wiley Blackwell, 652 pp. https://doi.org/10.1002/9781118778371.ch17.

Mikkelsen, D. M., Rysgaard, S., & Glud, R. N. (2008). Microalgal composition and primary production in Arctic sea ice: A seasonal study from Kobbefjord (Kangerluarsunnguaq), West Greenland. *Marine Ecology Progress Series, 368*, 65–74. https://doi.org/10.3354/meps07627.

Morawetz, K., Thoms, S., & Kutschan, B. (2017). Formation of brine channels in sea ice. *The European Physical Journal E, 40*, 25. https://doi.org/10.1140/epje/i2017-11512-x.

Olsen, L. M., Laney, S. M., Duarte, P., Kauko, H. M., Fernández-Méndez, M., Mundy, C. J., Rösel, A., Meyer, A., Itkin, P., Cohen, L., Peeken, I., Tatarek, A., Różańska-Pluta, M., Wiktor, J., Taskjelle, T., Pavlov, A. K., Hudson, S. R., Granskog, M. A., Hop, H., & Assmy, P. (2017). The seeding of ice algal blooms in Arctic pack ice: The multiyear ice seed repository hypothesis. *Journal of Geophysical Research, 122*, 1529–1548. https://doi.org/10.1002/2016JG003668.

Perovich, D. K. (2017). Sea ice and sunlight. In D. N. Thomas (Ed.), *Sea ice* (3rd ed., pp. 110–137, 652 pp). Oxford: Wiley Blackwell. https://doi.org/10.1002/9781118778371.ch4.

Petrich, C., & Eicken, H. (2017). Overview of sea ice growth and properties. In D. N. Thomas (Ed.), *Sea ice* (3rd ed., pp. 1–41, 652 pp). Oxford: Wiley Blackwell. https://doi.org/10.1002/9781118778371.ch1.

Petrou, K., Doblin, M. A., & Ralph, P. J. (2011). Heterogeneity in the photoprotective capacity of three Antarctic diatoms during short-term changes in salinity and temperature. *Marine Biology, 158*, 1029–1041. https://doi.org/10.1007/s00227-011-1628-4.

Raven, J. A., Kübler, J. E., & Beardell, J. (2000). Put out the light, and then put out the light. *Journal of the Marine Biological Association of the United Kingdom, 80*, 1–25. https://doi.org/10.1017/S0025315499001526.

Rózańska, M., Poulin, M., & Gosselin, M. (2008). Protist entrapment in newly formed sea ice in the coastal Arctic Ocean. *Journal of Marine Systems, 74*, 887–901. https://doi.org/10.1016/j.jmarsys.2007.11.009.

Rózanska, M., Gosselin, M., Poulin, M., Wiktor, J. M., & Michel, C. (2009). Influence of environmental factors on the development of bottom ice protest communities during the winter-spring transition. *Marine Ecology Progress Series, 386*, 43–59. https://doi.org/10.3354/meps08092.

Rysgaard, S., Glud, R. N., Sejr, M. K., Blichner, M. E., & Stahl, H. J. (2008). Denitrification activity and oxygen dynamics in Arctic sea ice. *Polar Biology, 31*, 527–537. https://doi.org/10.1007/s00300-007-0384-x.

Selz, V., Saenz, B. T., van Dijken, G. L., & Arrigo, K. R. (2018). Drivers of ice algal bloom variability between 1980 and 2015 in the Chukchi Sea. *Journal of Geophysical Research, 123*, 7037–7052. https://doi.org/10.1029/2018JC014123.

Søgaard, D. H., Kristensen, M., Rysgaard, S., Glud, R. N., Hansen, P. J., & Hilligsøe, K. M. (2010). Autotrophic and heterotrophic activity in Arctic first-year sea ice: Seasonal study from Malene Bight, SW Greenland. *Marine Ecology Progress Series, 419*, 31–45. https://doi.org/10.3354/meps08845.

Søgaard, D. H., Deming, J. W., Meire, L., & Rysgaard, S. (2019). Effects of microbial processes and CaCO$_3$ dynamics on inorganic carbon cycling in snow-covered Arctic winter sea ice. *Marine Ecology Progress Series*. https://doi.org/10.3354/meps12868.

Stoecker, D. K., Gustafson, D. E., Merrell, J. R., Black, M. M. D., & Baier, C. T. (1997). Excystment and growth of chrysophytes and dinoflagellates at low temperatures and high salinities in Antarctic sea-ice. *Journal of Phycology, 33*, 585–595. https://doi.org/10.1111/j.0022-3646.1997.00585.x.

Sturm, M., & Massom, R. A. (2017). Snow in the sea ice system: Friend or foe? In D. N. Thomas (Ed.), *Sea ice* (3rd ed., pp. 65–109, 653 pp). Oxford: Wiley Blackwell. https://doi.org/10.1002/9781118778371.ch3.

Syvertsen, E. E. (1991). Ice algae in the Barents Sea: Types of assemblages, origin, fate and role in the ice-edge phytoplankton bloom. *Polar Research, 10*, 277–288. https://doi.org/10.3402/polar.v10i1.6746.

Weeks, W. F. (2010). *On sea ice* (664 pp). Fairbanks: University of Alaska Press.

Chapter 4
Spring, Summer and Melting Sea Ice

Abstract This chapter describes one of the most dynamic and ecological important seasons. The onset of ice melt initiates significant changes in the physical properties of the ice (4.1), and the related biotic processes in the spring/summer sea ice are addressed (4.2). Ice algal spring blooms are described and exemplified with two studies from contrasting Arctic sites (4.3). A Case Study 2 has a focus on effects and consequences for ice algae of increased irradiances at the ice bottom in terms of pigments, fatty acids, and MAAs (4.4). Ice algae bloom dynamics are investigated in a combined model and field study (4.5). Melt ponds termed "windows to the ocean" develop on the surface of the ice with increased light transmittance (4.6). Seeding of the ice or water column below with viable ice algae can initiate ice algae or pelagic blooms, and mechanisms are explored in model and field studies (4.7). Case study 3 show that species of meiofauna graze directly on the ice algae, and that the meiofauna establishes an important ecological component in the sea ice (4.8).

Keywords Spring bloom · High PAR · Melt ponds · Meiofauna

4.1 The Melting Sea Ice

The spring warming of sea ice is accompanied by a reduction in ice salinity resulting in characteristic "L-shaped" profiles, because of internal ice melt and the flushing of the brine channels due to the draining of meltwater from surface melt ponds (Cox and Weeks 1974; Fetterer and Untersteiner 1998). Brine inclusions and channels enlarge upon warming and form new pathways for brine and melt water. Generally, brine channels and pockets become interconnected at brine volumes above 5% allowing fluid transport (Golden et al. 2007). These new pathways form longer and wider channels than the original pathways. The melt water percolates downwards through the ice, flushing out salts and nutrients into the ocean below the ice (Petrich and Eicken 2017). In spring, air temperatures increase with increased solar zenith angle and snow on sea ice will start to melt, and the insulating effects of the snow disappear and the sea ice is directly exposed to higher air temperatures,
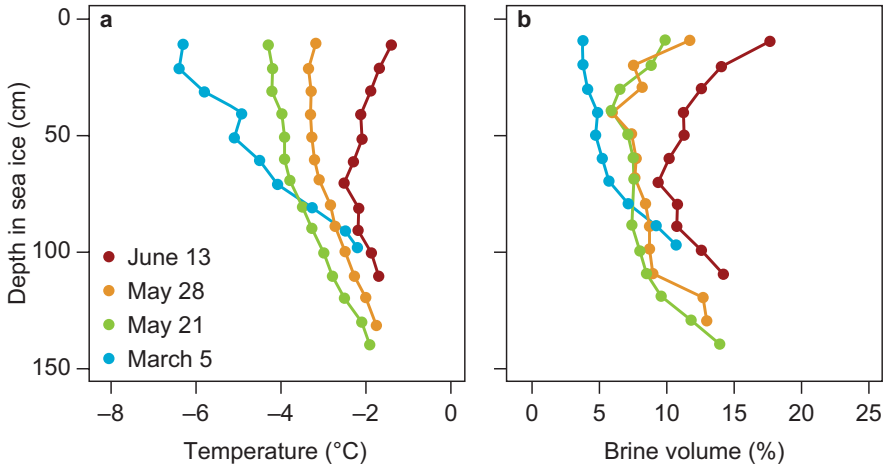
Fig. 4.1 Sea ice temperatures (°C) (**a**) and brine volume (%) (**b**) during a spring period at 84°N of Svalbard. (Modified from: Olsen et al. 2017)

which again increases the temperature of the ice. A time series of sea ice temperatures and related brine volumes from north of Svalbard (~84 °N) between March and June provides an example of the progression from a cold (−6.5 °C) to a warmer (−1.5 °C) ice surface (Fig. 4.1a). In this example there was some ice growth between March and May by about 40 cm and melting of the ice during May and June, but temperatures of the upper part of the ice increased with time, with only minor temperature changes deeper in the ice. Brine volume increased similarly over time, reflecting that brine volume is mainly governed by the temperature of the ice, as the warmer the ice the higher the brine volume (Sect. 6.2). Ice algae and bacteria residing inside the brine channels or attached to the bottom of the ice are released from the ice and can seed the water column below. Thereby they contribute to pelagic algal and bacterial production, a theory or concept termed seeding (Olsen et al. 2017). Seeding presupposes that the ice algae seeding the water are viable and that conditions in the water column are beneficial for algal growth. Alternatively, the ice algae can be rapidly exported to the deep ocean where they can fuel benthic food webs (Boetius et al. 2013).

4.2   Biotic Processes in Spring/Summer Sea Ice

It is the ice algae bloom that marks the transition from winter to spring/summer in ice–covered waters. Ice algae typically start blooming after light levels in the sea ice have passed a critical level ranging from 0.17 to 20 μmol m^{-2} s^{-1} (Gradinger and Ikävalko 1998; Mock and Gradinger 1999; Campbell et al. 2014; Hancke et al.

2018). Light has previously been identified as the major limiting factor for algal productivity, with snowpack depth largely controlling light transmittance in snow and sea ice during winter and early spring. Hence, the snow depth influences the transition from winter to spring, and the thicker the snow cover, the more the transition is delayed. The spring/summer period can roughly be divided into four main phases based on rates of ice algal growth and photosynthesis in relation to light and nutrients: (**1**) Early season and light limitation; (**2**) Transition period of light and nutrient limitation; (**3**) Late season of nutrient limitation and excess light; (**4**) Late summer with ice bottom ablation.

Early Season   During this stage the ice algal community is generally light-limited. Nutrient concentrations in the ice are replete, either due to nutrient incorporation during initial ice formation, increased exchange with the underlying water due to increasing brine volumes, as well as bacterial nutrient remineralisation in the ice (nutrient production). At the beginning of this phase the ice will be transitioning from a net heterotrophic into a net autotrophic system when primary production increases, draws down nutrients, and strongly influences their concentrations, and nutrients can be depleted in the ice.

Transitional   The algal bloom in the Arctic is usually initiated at the ice-water interface, in the lamellar bottom skeletal layer (Fig. 2.2b) that harbours one of the highest algal concentrations in the world's oceans (Arrigo et al. 2014). It is dominated by pennate diatoms often accounting for >90% of the total biomass (Rózanska et al. 2008) and is generally highly productive. Seasonal studies have shown that at this time of year the integrated vertical biomass in the ice is often ten times higher than in the water column, and in some locations ice algae can contribute up to 50–60% of the total primary production (Gosselin et al. 1986; Fernandez-Mendez et al. 2015). The biomass evolution of the bloom is closely related to the increase in spring irradiance. By the time the bloom is accelerating towards maximum growth rates, the transition to diatoms is already underway and the diatoms are already beginning to acclimate their photosynthetic activity to higher irradiances, while other algal classes progressively disappear or become a quantitatively insignificant part of the community. This temporal change in pigment composition is summarised in Fig. 4.2 for newly formed spring ice where the pigment peridinin is especially utilised by dinoflagellates, whereas the pigment fucoxanthin is typical of diatoms. In this transitional phase the sea ice algae community sustains itself as long as sufficient amounts of nutrients remain, however dissolved inorganic and organic nutrients may become depleted. The temporal development of inorganic nutrient levels in sea ice is summarized in Fig. 4.3. This study indicated that the algal community in the sea ice is nitrate and phosphate limited. In other studies silicic acid limitations have also been observed, which strongly affects the growth of the sea ice diatoms. Another potential factor limiting sea ice algal growth and photosynthesis is high pH levels. The pH in sea ice follows a C–shape profile i.e., high pH (> 9) in the surface and bottom sea ice and slightly lower pH (8.5) in the internal sea ice layers (Fig. 4.4a) (Hare et al. 2013). There is little information about how high pH affects growth rates
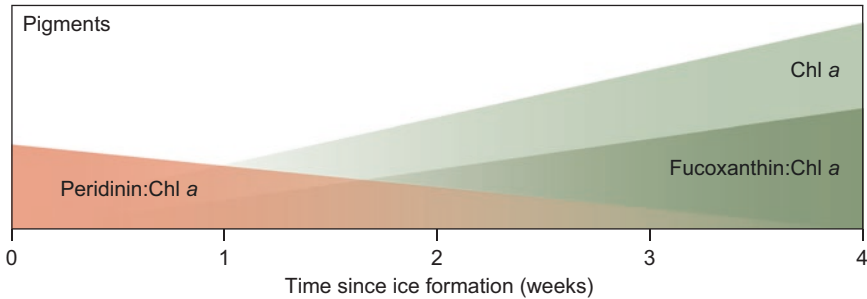
Fig. 4.2 Development of Chl *a* biomass in the ice over time with a decrease in the peridinin:Chl *a* ratio and an increase in the fucoxanthin:Chl *a* ratio. A progression from diverse flagellates to a *Nitzschia*-dominated ice algal community is reflected in the higher fucoxanthin concentrations. (Modified from: Kauko et al. 2018)

of Arctic ice algae and bacteria. However, high extracellular pH is known to cause gross alterations in membrane transport processes and metabolic functions involved in internal pH regulation (Raven 1993), and alters cellular content of amino acids and their composition, which might affect cellular growth (Taraldsvik and Myklestad 2000). Changes in pH also influence the speciation of inorganic carbon (CO_2 (aq), HCO_3^-, CO_3^{2-}). At pH 8.2 in seawater (TCO_2 is approximately 2.000 µmol L^{-1} in ocean water), approximately 1% of TCO_2 is present as CO_2 while at pH 9, only 0.1% of TCO_2 is present in this form (Hinga 2002). The limited CO_2 supply due to elevated pH may restrict photosynthesis and growth of algae in the brine channels (Hansen 2002). However, most ice algae species have active ion transport across the plasmalemma allowing them to use HCO_3^- in photosynthesis and thereby avoid inorganic carbon limitation at elevated pH (Korb et al. 1997; Huertas et al. 2000; Hansen 2002). Nevertheless, the growth rates of some sea ice diatoms species (e.g., *Fragilariosis nana* and *Fragilariopsis* sp.) are affected by increasing pH levels and they stop growing altogether at pH = 9.5 irrespective of TCO_2, indicating that pH directly affects their growth (Fig. 4.4b) (Søgaard et al. 2011). In contrast, *Chlamydomonas* sp., a chlorophyte genus commonly encountered in sea ice has extreme pH–tolerance as there is only a small reduction in its growth rate above pH = 9.5, but it is sensitive to low TCO_2 concentrations suggesting that elevated pH may be involved in the seasonal succession of Arctic sea ice algae (Fig. 4.4b). Extremely high pH (i.e. pH as high as 10.0) has been observed in sea ice with high primary production (Gleitz et al. 1995; Thomas et al. 2001) and, thus, prevails during spring when the irradiance increases (Cota and Horne 1989; Kühl et al. 2001). An interesting feature of the succession is that the communities higher up in the sea ice, within the brine channels, remain more similar to the early season composition and essentially fail to achieve the pennate diatom climax community that forms in the skeletal layer. Whereas the bottom climax community is largely similar irrespective of the type of ice, the community that persists in the interior of the ice differs between ice types, with pennate diatoms for example being far more numerous in first-year sea ice than in multi-year ice. If the interior community in the brine chan-
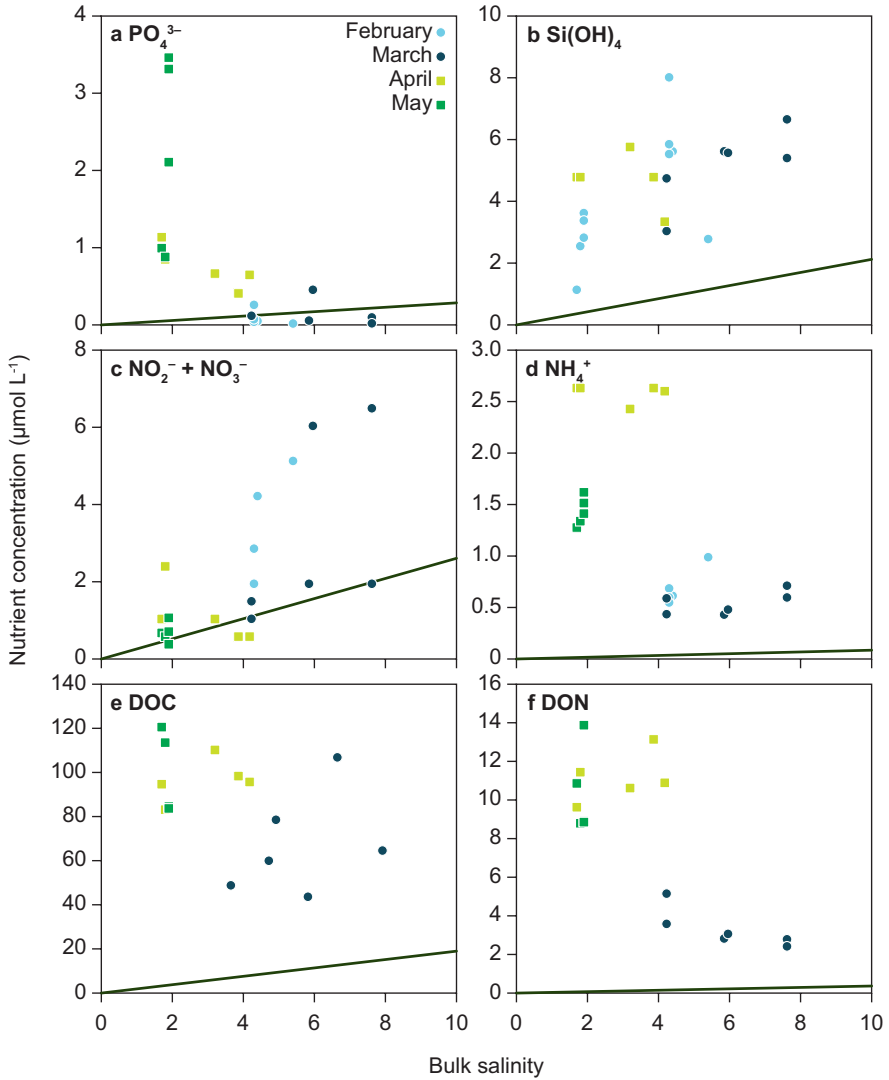
Fig. 4.3 Concentrations of dissolved nutrients, DOC, and DON versus bulk ice salinity in land-fast first-year ice between February and May, Godthåbsfjord, SW Greenland. The solid line indicates the expected dilution line predicted from salinity and nutrient concentrations in seawater. If values are below the dilution line, depletion of the solute has taken place, and if above the dilution line production, or net deposition, of the solute has occurred. (**a**) Phosphate (PO_4^{3-}), (**b**) Silicate ($Si(OH)_4$, (**c**) Nitrite (NO_2^-) + Nitrate (NO_3^-), (**d**) Ammonium (NH_4^+), (**e**) DOC, and (**f**) DON. (Modified from: Søgaard et al. 2013)

nels is truncated in its development and prevented from reaching the pennate diatom dominance, this is presumably related to the harsher conditions in the channels. The smaller brine volume in the semi-enclosed sea ice interior likely leads to earlier nutrient limitation and thus limits succession towards a diatom-dominated community as well as overall biomass accumulation. As mentioned above, the bottom ice
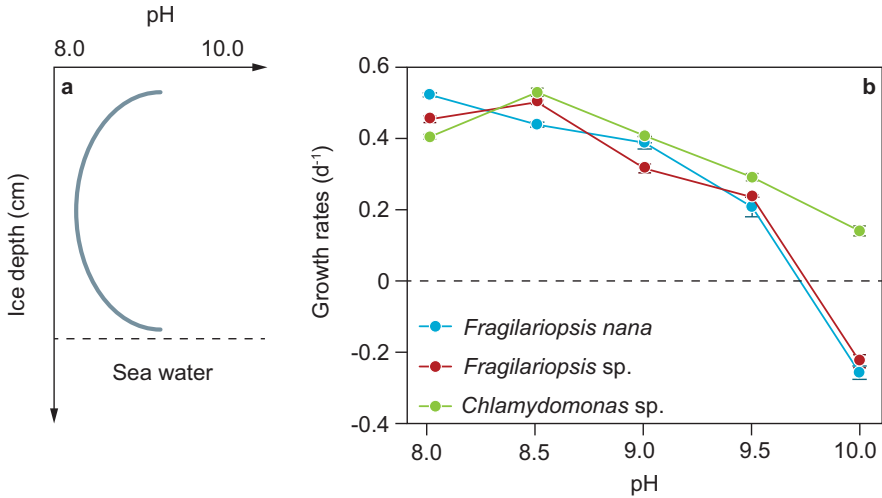
Fig. 4.4 Variation of pH with depth in the sea ice (**a**), and growth rates of three different sea ice algae species as a function of pH (**b**). (Modified: from Hare et al. 2013 (**a**), and modified: from Søgaard et al. 2011 (**b**))

in this period is dominated by pennate diatoms, and an explanation for the dominance of diatoms in spring and summer ice is that diatom species are only slightly affected by decreasing salinities, whereas the decreasing salinity may result in substantial losses of species such as ciliates and flagellates (Garrison and Buck 1986; Ryan et al. 2004; Ralph et al. 2007; Mikkelsen and Witkowski 2010). Thus, sea ice diatoms may have a competitive advantage during spring and summer thaw when sea ice salinity becomes low (Søgaard et al. 2011).

Excess Light Period The extent to which ice algae suffer photoinhibition and become chronically photodamaged in this late season period deserves further study. One important issue is the length of exposure to the excess irradiance, compared against the nocturnal period when photosystems can relax and photorepair mechanisms can operate. The long day lengths and absence of sufficient night periods in the polar summer for relaxation and repair of photosystems suggest that chronic photoinhibition is likely to be increasing for ice algae with latitude. Unlike phytoplankton, which are periodically mixed into deeper water and escape high irradiance, ice algae are fixed in position and unable to escape, and hence may be subject to photo-damaging irradiance for days or weeks without any opportunity for repair (Falkowski and Raven 2007). Photoinhibition occurs in ice algae when the photon flux exceeds photosynthetic capacity (Fig. 3.16). The excess energy generated by the photosystems needs to be managed to avoid damaging proteins in the chloroplasts, especially the highly sensitive D1 proteins in the machinery of Photosystem II. In normal daily cycles of illumination, irradiances in excess of E_K are managed by the carotenoid pigments in the cellular xanthophyll cycle; in diatoms these are

diadinoxanthin (Ddx) and diatoxanthin (Dtx). These two pigments rapidly interconvert, and the energy-demanding reaction of Ddx to Dtx allows cells to avoid damage from excess light (photodamage) as the excess photons are converted to and lost as heat, and are therefore not allowed to strike the sensitive photosystem proteins (Goss and Jacob 2010). At the same time, photorepair mechanisms become active to repair any proteins that have become denatured by energy not managed by the Ddx-Dtx system. This normal, daily photoinhibition is termed dynamic photoinhibition and is a routine feature already early in the season, and is more or less harmless. As the algae are exposed to greater irradiances during the season, the cellular contents of Ddx and Dtx increase, and synthesis of new xanthophylls can occur within a few hours of sudden increases in irradiance. Increases in the ratio of (Dtx + Ddx):Chl a are frequently observed as photoinhibition becomes more prolonged (Kauko et al. 2018). Longer exposures to excess light that cannot be managed by the xanthophyll cycle and reduced photosynthetic capacity of the cells, as quantified by decreases in the maximum quantum yield in photosynthetic activity (F_v/F_m), are termed chronic photoinhibition. This type of inhibition can be countered by production of photo-protective pigments that absorb light not only in the photosynthetically active spectrum, but also other harmful radiation such as UV light (Marcoval et al. 2007). In recent years, other non-photosynthetic compounds that strongly absorb UV wavelengths have been identified. Prime among these are mycosporine-like amino acids (MAAs) (Piiparinen et al. 2015). These are a family of amino acids with peak absorbance in slightly different ranges of the UV spectrum, and increase in sea ice algae as snow melts during the season and algae are exposed to longer periods of higher light intensities (Ha et al. 2018). Recently, more attention has been paid to ice-associated algae in higher-light environments such as the surface of ice floes, fractured pressure ridges, and refrozen leads (Kauko et al. 2018; Assmy et al. 2017). These types of environments are likely to become more widespread and frequent in the Arctic with the ongoing trend from multi-year ice to first-year ice (Fig. 5.4). Unsurprisingly, such communities are acclimating to higher-light environments with higher E_k values and preferred irradiance ranges, often showing little sign of photoinhibition at irradiances up to 250 μmol photons m^{-2} s^{-1}. Ridges and lead habitats can have very high algal biomass by Arctic standards (> 70 mg Chl a m^{-2}) and could support some 30–70% of all Arctic algal biomass (Lange et al. 2015; Assmy et al. 2017). Nutrient limitation becomes increasingly important in these habitats, limiting activity and productivity as the season progresses (Fig. 4.3). This is particularly so for nitrogen, as its main function is in photosynthetic enzymes and nitrogen deficiencies will both limit carbon uptake and enhance photoinhibition. Normally sea ice bacteria follow the progress of the ice algal bloom near the seawater interface, which is attributed to the ice algal release of new DOM (Deming and Collins 2017). However, bacterial density and production is also increasing in upper regions of the ice where the ice algae are not blooming, which is attributed to the consumption of old DOC and possibly EPS. This old DOC and EPS is concentrated in the sea ice during autumn or produced during autumn and winter for cryoprotection. High bacterial production with rates in the order of 3.80–290 mg C m^{-2} day^{-1} have been measured in spring sea ice (Glud et al. 2007, 2014). Although these rates

are much higher than reported in autumn and winter, bacterial production rates typically represent less than 10% of primary production rates during spring and summer, and often peak during post–bloom condition in spring/summer ice. However, integrated measurements from sea ice in Young Sound, NE Greenland (Glud et al. 2007) and in melting sea ice in the Fram Strait (Glud et al. 2014), revealed that the sea ice was net heterotrophic during summer in these areas. In some areas with high enough net heterotrophic activity the oxygen is fully consumed in the sea ice, leaving pockets of anoxia in the sea ice that support both denitrification and anaerobic ammonia oxidation in the ice (Rysgaard et al. 2008). An example from NE Greenland shows that oxygen concentrations in the ice are low, but remain nearly constant in the water below (Fig. 4.5). These processes might influence nutrient availability for the ice algae and therefore impact the total primary productivity in these areas.

Late Summer When the sea ice begins melting, the dissolved inorganic and organic nutrients are released into the seawater column where they can influence pelagic microbial processes, or contribute to particle export (Meiners and Michel 2017). Differential retention of different classes of organic matter have been described for coastal Arctic fast ice (Juhl et al. 2011). This indicates that the type and quality of the dissolved substances exported from the ice will change as the melt season progresses. Ice algae can contribute a large proportion of the total algal carbon export from ice-covered waters, with the timing of snowmelt likely affecting the timing of ice algae release and total carbon export (Lalande et al. 2009). Overall, algal development is controlled mainly by the physical, optical, and chemical environment within the ice – a process called bottom-up control. Alternatively, their development could be controlled by food web interactions, mainly grazing by herbivores (ie., top-down control). Many herbivores are found within the ice throughout the growth season, including rotifers, polychaetes, and nematodes (e.g., Gradinger 1999). Their abundance and biomass follows closely the seasonal cycle
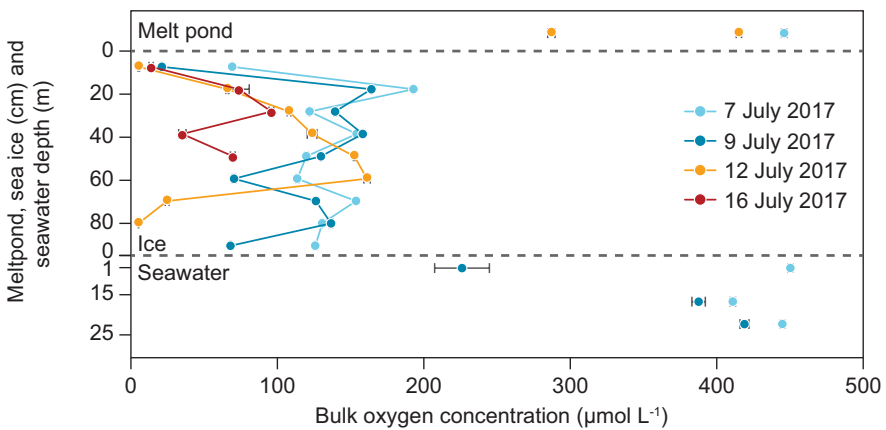
Fig. 4.5 Comparison of vertical bulk oxygen concentration in a melt pond, sea ice and underlying seawater from 7 to 16 July in Young Sound, NE Greenland (unpublished data)

of the ice algae, but is never large enough to cause a major loss of algal biomass – current estimates are all below 10% of daily ingestion related to the algal standing stock.

4.3 The Sea Ice Algal Spring Bloom

Classically the term "spring bloom" refers to a situation where pelagic phytoplankton develop high concentrations due to high primary production rates at a specific time during spring when irradiances and water temperatures increase, and when nutrients are still available in stratified surface waters (Falkowski and Raven 2007). For sea ice algae, the term 'spring bloom' refers to the bloom of ice algae inside or at the bottom of the ice, which also occurs during spring and summer when the reducing snow cover results in higher light levels in the sea ice. The ice algal spring bloom is likewise controlled by nutrient availability in the brine channels and at the bottom of the ice (Gradinger 2009; Søreide et al. 2010; Leu et al. 2015; Leeuwe et al. 2018). The ice algae bloom can then seed the water column with viable algal cells that can then fuel the pelagic production following the ice melt. There are several time-series studies of the development of ice algae during spring blooms, but few covering several months such as those described here. Time-series are established by sampling at the same site, sampling for a specific or several parameters over a specified period of time, and with a specified frequency of sampling. To illustrate how different the sea ice algae spring bloom development is between sea ice sites we compare two time-series: one from Arctic Canada (70°N) (Horner and Schrader 1982), and one from Kobbefjord, SW Greenland (64°N) (Mikkelsen et al. 2008). In Arctic Canada, there is a gradual increase in sea ice algal productivity from late April until the end of May with a maximum of 63 mg C m^{-2} day^{-1} and a similar peak in the beginning of June (Fig. 4.6a). The SW Greenland time series covers about 6 months but sampling frequency is lower. Here, ice algal production reaches a maximum of 21 mg C m^{-2} day^{-1} at the beginning of March and there is a second peak of 15 mg C m^{-2} day^{-1} at the end of April (Fig. 4.6b). At this location, the primary productivity increases to maximum when snow cover is thin but decreases again when new snow (up to 40 cm) accumulated on top of the ice in March–April. The blooming period is initiated about 2 months earlier in Kobbefjord at 64°N compared to the Canada site at 70°N. Considerable snowfall is typical of the Arctic Canada site and there is no sunlight during December and January. Nevertheless, maximum primary productivity and Chl *a* concentrations at the Arctic Canada site are about three times higher compared to the Kobbefjord site. The ^{14}C incubation method was applied in both studies to measure primary production, with incubation of samples in the ice (Canada) and in the laboratory (Kobbefjord). Therefore, despite possible minor methodological variations, the results are comparable. Recent studies have pointed towards the effects of nutrient availability, differences in water column stratification and period of melting of the sea ice from below but the reason for the very low productivity in sea ice in Greenland is still unknown.
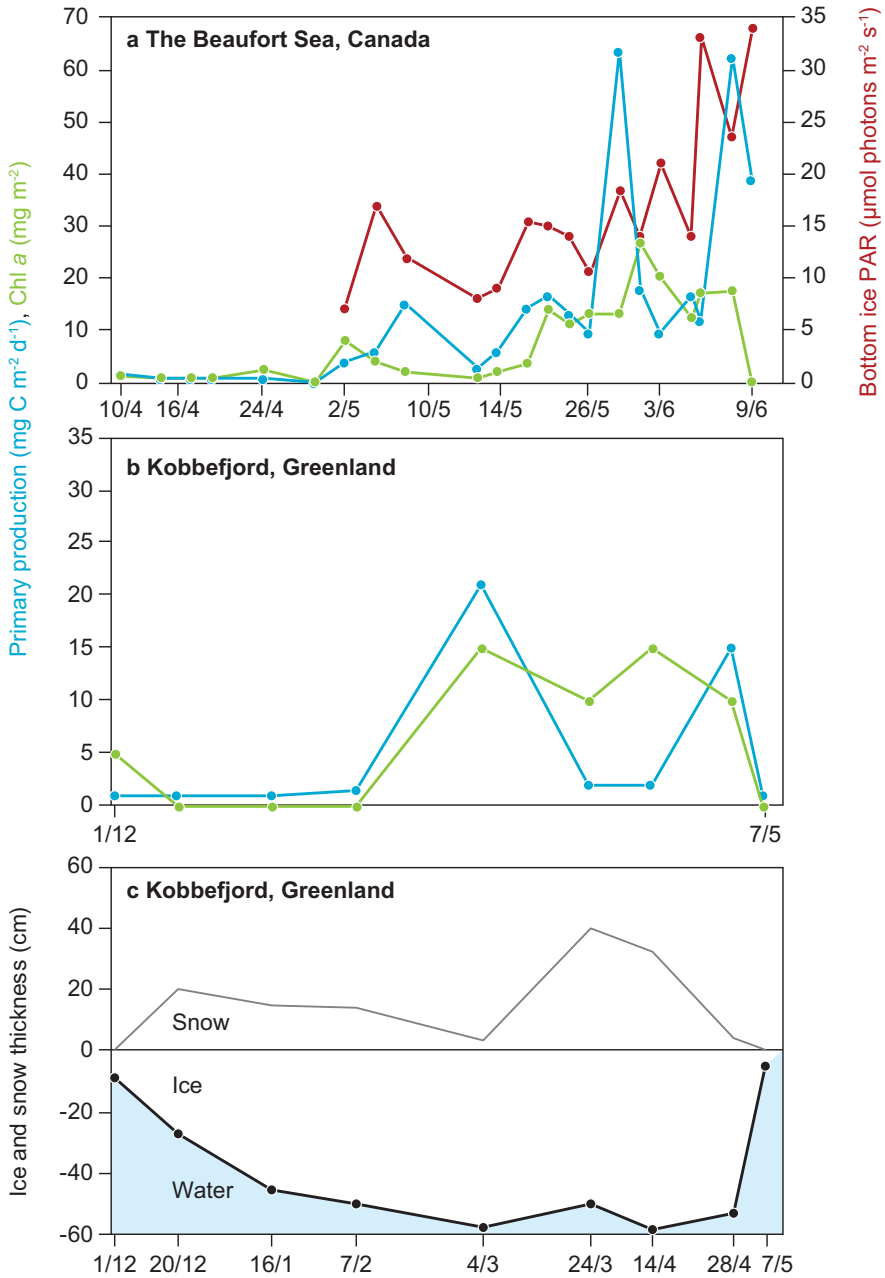
Fig. 4.6 Time series of primary production (blue line), Chl *a* (green line) and bottom ice PAR (red line) in the Beaufort Sea, Canadian Arctic (**a**), primary production (blue line) and Chl *a* (green line) in Kobbefjord, SW Greenland (**b**), and snow and sea ice thickness in Kobbefjord, SW Greenland (**c**). (Modified from: Horner and Schrader 1982 (**a**), and modified from: Mikkelsen et al. 2008 (**b** + **c**))

Ice algae species composition was dominated (about 50%) by small flagellates and about 50% pennate diatoms at the Arctic Canada site with no significant changes in this ratio during the 2-month study period. In contrast, in the 6-month long Kobbefjord study, there was a clear succession from flagellates in December and January, to a bloom of a centric diatoms in March, which were replaced by pennate diatoms in the April–May bloom.

4.4   Sea Ice Algae and Effects of Increased Under-Ice PAR and UV – Case Study 2

We have carried out several sea ice research experiments in Kangerlussuaq Fjord, W Greenland (Fig. 4.7). This case study illustrates the principles governing the critical importance of snow depth on irradiance in the spring as one of the driving factors of the spring bloom. The stochastic variability between seasons due to different preceding light history is noteworthy, and the dramatic changes that can occur when irradiance suddenly increases after loss of snow cover. The two experiments in this case study involve snow-clearing experiments and application of ice coring, biomass and species composition, and primary productivity, including variable chlorophyll fluorescence methods (Sect. 6.8).

4.4.1   Experiment I

The sea ice here is land-fast first-year ice, which starts to develop in late November and breaks up in late May. Kangerlussuaq is only about 25 km from the Greenland Inland Ice cap, where a persistent high air pressure secures a climate with very low winter temperatures down to −35 °C, generally low wind speeds and low annual snowfall (10–40 cm). The sea ice at Kangerlussuaq varies from 50–80 cm in
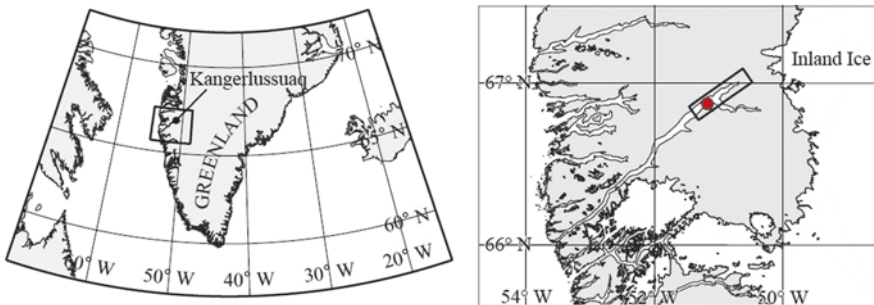
Fig. 4.7 Map of Greenland with location of Kangerlussuaq field site. (Modified from: Lund-Hansen et al. 2013)
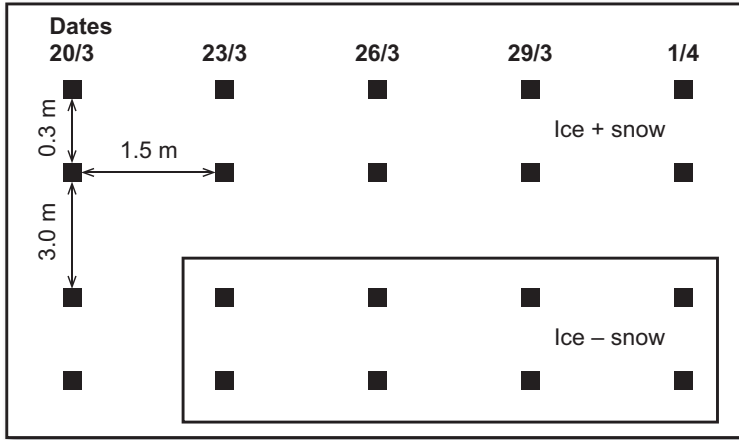
Fig. 4.8 Experimental design of the snow clearing experiment, with sampling dates. (Modified from: Lund-Hansen et al. 2013)
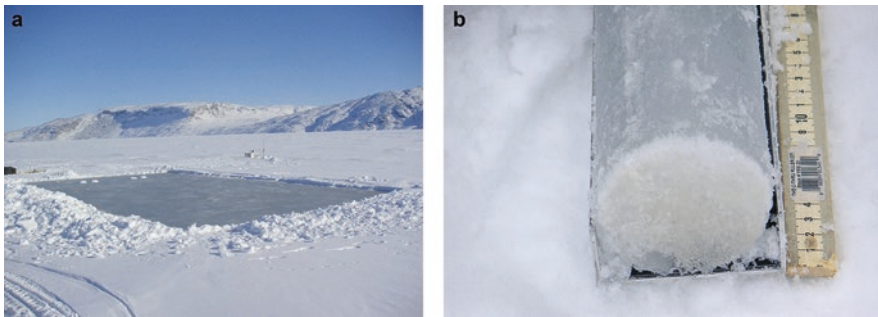
Fig. 4.9 Snow-cleared area (**a**), and a typical ice core with a clear white skeletal layer at the bottom of the ice core, and brownish colouring due to the presence of ice algae (**b**) Kangerlussuaq, March 2011, W Greenland. (Photographs by: Authors)

thickness depending on winter air temperatures and snow cover. We artificially removed the snow cover and followed over time the development and changes in sea ice Chl *a*, algal physiological parameters, their absorption properties, and species composition induced by increased PAR at the bottom of the ice, and changes in spectral composition. Our design was a control area with an intact snow cover and an area where the snow cover of 10 cm was artificially removed (Fig. 4.8). Ice cores were collected every three days between 20 March and 1 April in the control area with intact snow cover (+Snow) and no snow cover (-Snow). Photos of the snow-cleared area and a sea ice core with brown colouring by ice algae in the skeletal layer are shown in Fig. 4.9. The main purpose of this snow clearing experiment was to test the hypothesis that ice algae photosynthesis is light-limited, and snow removal should then increase photosynthesis and thus enhance primary production.

Fig. 4.10 Albedo, K_d(PAR) attenuation coefficients for snow (thickness 0.1 m), ice (thickness 0.5 m), and water, and range (minimum – maximum during a day) in bottom ice PAR for a situation with snow (**a**), and without a snow cover (**b**). (Modified from: Lund-Hansen et al. 2018)

We measured some significantly different optical properties between the snow-cleared and uncleared areas, with an albedo of 0.8 in the +snow area, and an albedo of 0.25 for the bare ice in the – snow area. The change in albedo increased the PAR transmittance from 0.05 to 0.36, equivalent to an increase from 32.4 to 293.1 μmol photons m^{-2} s^{-1} at the bottom of the ice at a surface PAR of 648 μmol photons m^{-2} s^{-1} (Fig. 4.10). The ice thickness at the -snow area was 50 cm with a PAR sea ice attenuation coefficient K_d(PAR) = 0.84 m^{-1}, as compared to the +snow area with a snow attenuation coefficient K_d(PAR) = 11.9 m^{-1}, which clearly demonstrates that snow is far more effective in irradiance attenuation than ice. There were some significant differences and changes in parameters over time between the two areas e.g., for Chl a, which decreased exponentially in the -snow area from 0.77 to 0.04 mg Chl a m^{-2}. There was, in comparison, a gradual increase in Chl a from 0.34 mg Chl a m^{-2} on 20 March to a stable level of about 0.95 mg Chl a m^{-2} during the last three samplings in +snow area (Fig. 4.11a). The maximum quantum yield parameter (F_v/F_m), a measure of how viable and photosynthetically active the algae are, increased both in the -snow and + snow areas, but was below zero in the -snow area on 1 April. The ^{14}C-based primary production showed a pattern comparable to the quantum yield with an increase in production in the +snow area, but a significantly lower in the -snow area, and only 0.5 mg C m^{-3} h^{-1} during the last sampling on 1 April (Fig. 4.11c). Ice algae species composition showed that total number of cells mL^{-1} decreased significantly in the -snow area, especially the diatoms *Fragilariopsis oceanica* and *Navicula vanhoeffni*, but increased in the +snow area along with a third diatom, *Achnantes taeniata*. Chlorophyll fluorescence images obtained on 26 March by the Imaging-PAM fluorometer (Sect. 6.8) clearly demonstrate that values for the minimum fluorescence F_o are relatively high in the +snow area (Fig. 4.12a) where also F_v/F_m is higher (Fig. 4.12b) compared to the -snow area with reduced F_o (Fig. 4.12c) and F_v/F_m (Fig. 4.12d). Our initial hypothesis was that even though ice algae are strongly adapted to low light conditions below the ice and snow, giving them more light by removing a snow cover would boost and increase the primary

Fig. 4.11 Chl *a* concentrations in bottom ice with snow (orange bars) and without snow (blue bars) (**a**), maximum quantum yield (F_v/F_m) in bottom ice with snow (orange bars) and without snow (blue bars) (**b**), and primary production in bottom ice with snow (orange bars) and without snow (blue bars) (**c**), between 20 March and 1 April, Kangerlussuaq, W Greenland. (Modified from: Lund-Hansen et al. 2013)
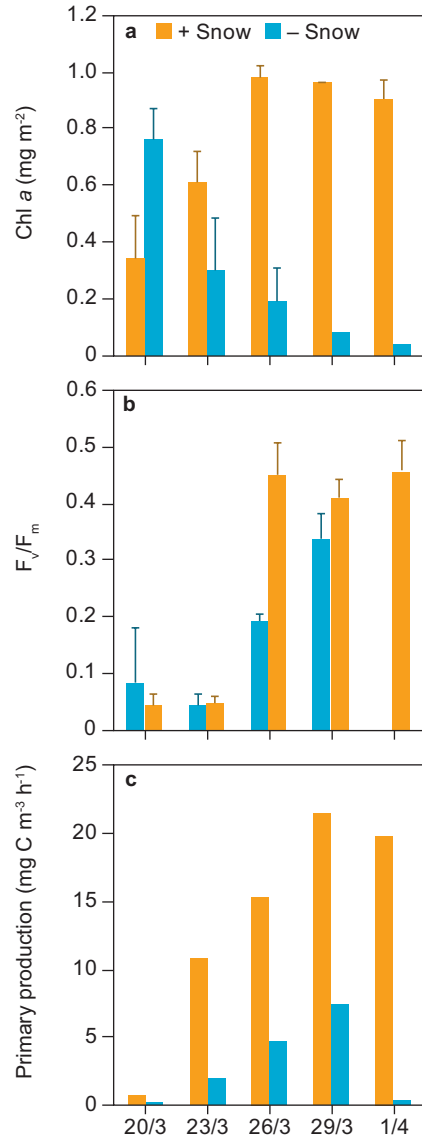
production. Surprisingly, the algae biomass and production was lower at the -snow compared to the +snow areas indicating that the ice algae at the -snow area were suffering from photoinhibition. Some algae at the -snow area might have actively abandoned the ice in favour of the water column, as pennate diatoms are motile. Other algae might not have been able to survive the sudden increase in UV-A which increased from 1% with a snow cover to about 17% of surface radiation in the cleared area. Under-ice PAR levels increased 9-fold by the snow clearing and the
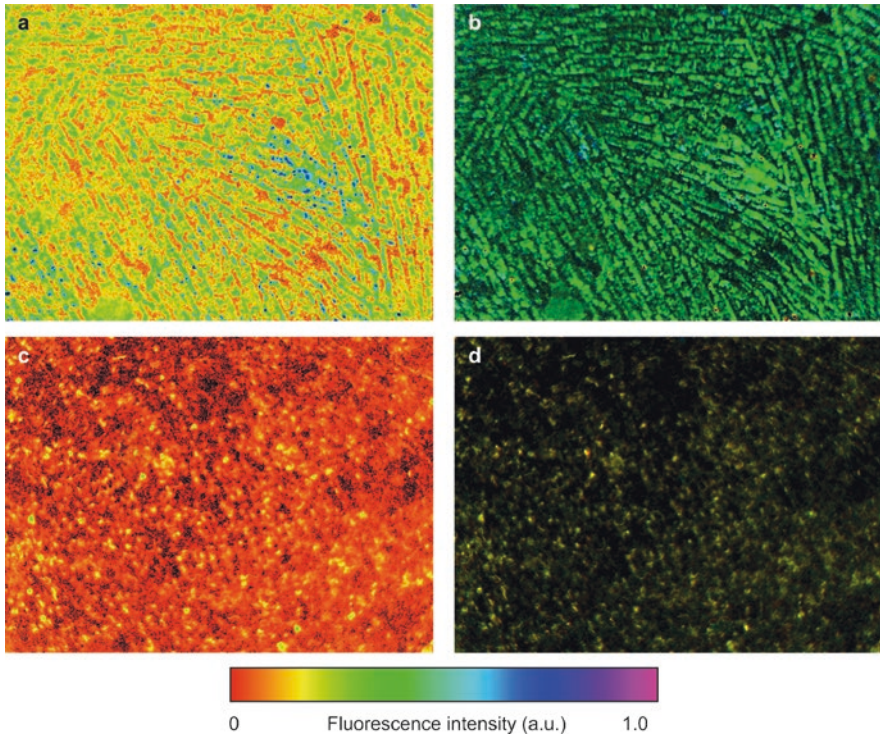
Fig. 4.12 Fluorescence images of the base of ice cores on 26 March, Kangerlussuaq, W Greenland. F_o for ice with snow (**a**), F_v/F_m for ice with snow (**b**), F_o for ice without snow (**c**), and F_v/F_m for ice without snow (**d**). All images are 30×23 mm. (Modified from: Lund-Hansen et al. 2013)

experiment mimics a sudden snow melt/disappearance at increased air temperatures, which would expose the ice algae to similar conditions and with similar effects for the ice algae community as described.

4.4.2   Experiment II

Ice algae have several strategies for protection of the photosynthetic apparatus against a sudden increase in irradiance and UV radiation, which we studied in a follow-up project also in Kangerlussuaq. Three separate rectangular areas of 15 · 10 m were established on the ice in March 2016. These areas established a gradient of PAR treatments: high light, intermediate light, and low light, where we measured a selection of optical and algal parameters over time. A snow layer (5–10 cm) was removed from high and intermediate light areas and left undisturbed in the low light, and the intermediate light area was then covered with a white semi-transparent tarpaulin that reduced bottom-ice irradiance to 50% of the high light area. High
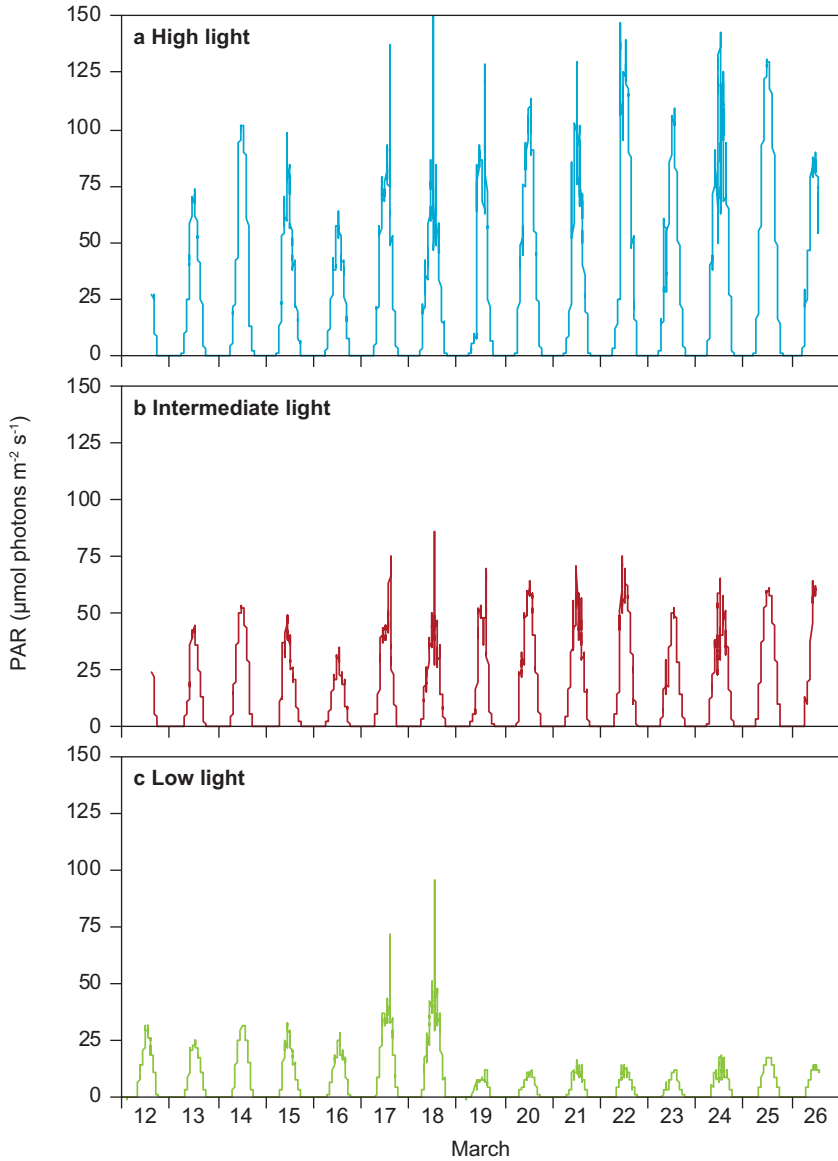
Fig. 4.13 Under-ice PAR time series without snow (High light) (**a**), ice with shade (Intermediate light) (**b**), and under ice with snow (Low light) (**c**) between 12 and 26 March 2016, Kangerlussuaq, W Greenland. (Modified from: Lund-Hansen et al. 2020)

and intermediate areas were cleared of any small snow patches each day of the experiment but not in the low light area, and a snowfall between 18 and 19 March reduced the initial 25% light levels of the high light area to just 10% (Fig. 4.13). Irradiance was strongly attenuated at intermediate and low light compared to high
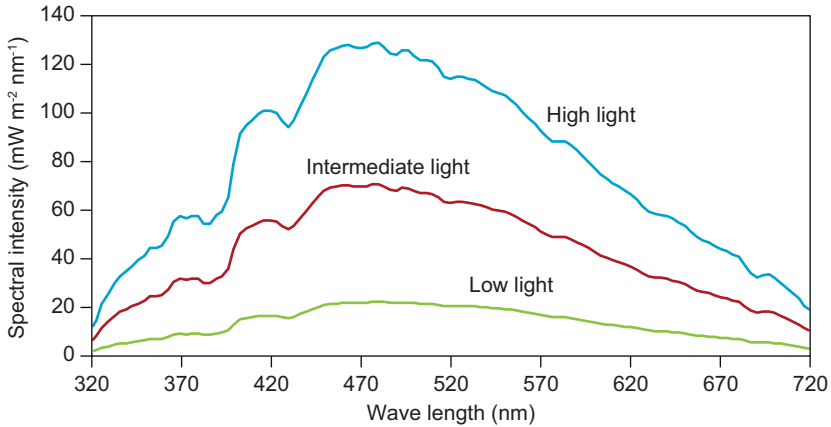
Fig. 4.14 Spectral composition of under-ice irradiance without snow (High light), ice with shade (Intermediate light), and with snow (Low light), March 2016, Kangerlussuaq, W Greenland. (Modified from: Lund-Hansen et al. 2020)

light, but with blue light around 480 nm being least attenuated (Fig. 4.14). UV-A levels were 0.4 W m^{-2} in the low light area, and 2.0 W m^{-2} and 3.7 W m^{-2} in the intermediate and high light areas, respectively. Ice algae were initially adapted to low light, but exposed to both higher PAR and UV-A levels with the snow clearing. Selected pigments were measured in the ice algae, including fucoxanthin, a light harvesting pigment (photosynthetic carotenoid), and diatoxanthin+diadinoxanthin (Dtx + Ddx, photoprotective carotenoids), so-called 'sunscreen' pigments. As mentioned previously, ice algae can regulate the concentrations of these pigments inside the cells relative to light conditions, increasing fucoxanthin at low light and increasing (Dtx + Ddx) at high light and UV to protect the photosynthetic system (Sect. 4.2). The experiment showed that the fucoxanthin:Chl *a* ratio increased at the last sampling in the low light treatment compared to the intermediate and high light treatments (Fig. 4.15a). This is likely a response to the snowfall that reduced low light even further. Note that pigment concentrations are shown as ratios to the concentrations of the main light harvesting pigment Chl *a*, to take into account any possible variation in this pigment during the experiment. There was, in comparison, a clear increase in the Dtx + Ddx:Chl *a* ratio, especially in the high and intermediate light areas, which demonstrates that the algae developed sunscreen pigments as a response to the increased light here (Fig. 4.15b). When ice algae are exposed to increased irradiance and accordingly also high UV levels, they can also develop mycosporine-like amino acids (MAAs). These compounds have strong absorption properties in the UV-A band to protect the cells from photodamage, and each MAA has specific wavelengths of maximum absorption. The procedure is to measure the spectral absorption of the ice algae on a filter, i.e. how much of the irradiance at a specific wavelength is absorbed by the algae (Fig. 4.16a).
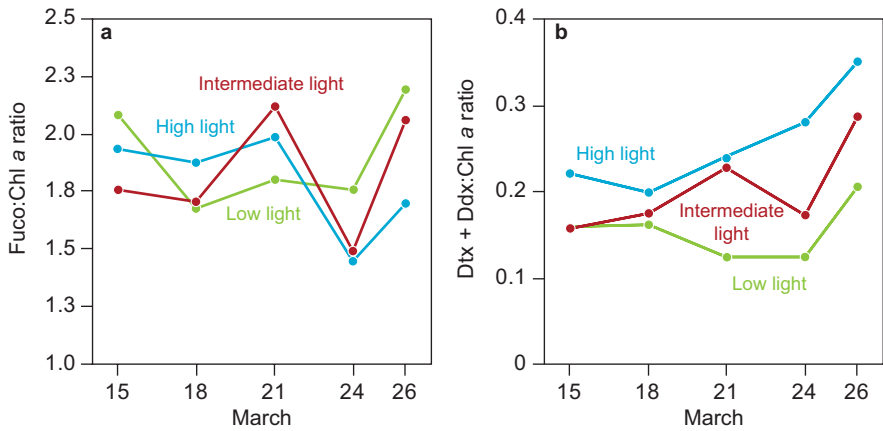
Fig. 4.15 Fucoxanthin:Chl *a* ratios (**a**), and (Diatoxanthin (Dtx) + Diadinoxanthin (Ddx)):Chl *a* ratios (**b**) in ice without snow (High light), ice with shade (Intermediate light), and ice with snow (Low light) between 15 and 26 March 2016, Kangerlussuaq, W Greenland. (Modified from: Lund-Hansen et al. 2020)
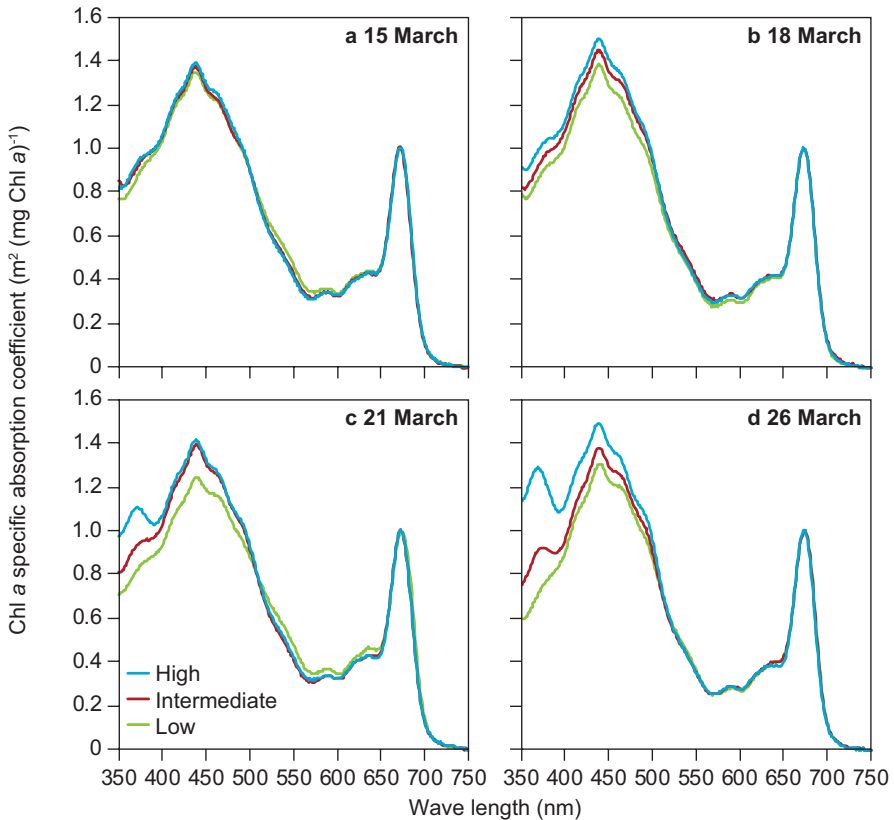
Fig. 4.16 Chl *a* - specific absorption coefficient between 350 and 750 nm on 15 March 2016 (**a**), 18 March 2016 (**b**), 21 March 2016 (**c**), and 26 March 2016 (**d**) in ice without snow (High light), ice with shade (Intermediate light) and ice with snow (Low light), Kangerlussauq, W Greenland. (Modified from: Lund-Hansen et al. 2020)

The ordinate is the Chl *a* specific absorption coefficient as the absorption is normalized to Chl *a* concentration to take into account any variations in Chl *a* and thus biomass concentrations between samples. The unit of the Chl *a*- specific absorption coefficient is m^2 (mg Chl a)$^{-1}$. Besides the two significant and strong absorption peaks at 440 nm and 670 nm related to Chl *a* for all light treatments, there is a gradual development over time of a strong peak at 360 nm and particularly at high light, and also at intermediate, but not at low light (Fig. 4.16b–d). The absorption peak centered at 360 nm is related to a specific compound (palythene), which the algae develop as protection against the UV-A at the bottom of the ice (Fig. 4.16). There are about 18 identified MAAs, and nearly all have maximum absorption peaks in the UV-A band (400–320 nm), and only a few in the UV-B band. It is unknown which MAAs ice algae develop in which conditions, but this might be related to spectral composition, intensity, and algae species composition. A third objective of the study was to detect any possible changes in the composition of the algal fatty acids in relation to increased PAR and UV. Only ice algae and phytoplankton species can synthesize the marine based essential fatty acids such as Omega-3, which is up-concentrated in the food chain via ice algae grazed by zooplankton, that are eaten by fish. Omega-3 belongs to the group of polyunsaturated fatty acids (PUFA), but not to the monounsaturated (MUFA) fatty acids group. We actually observed an increase in the MUFA:PUFA ratio over time in all three treatments, but most significantly in the high light treatment. The ratio was around 0.5 at first sampling in all treatments, and increased to about 1.3 in the high light treatment (Fig. 4.17). It illustrates that an increase in UV irradiance at the ice bottom can change the fatty acid composition, and that especially the Omega-3 fatty acid concentration will decrease and accordingly the nutritional value of the ice algae.
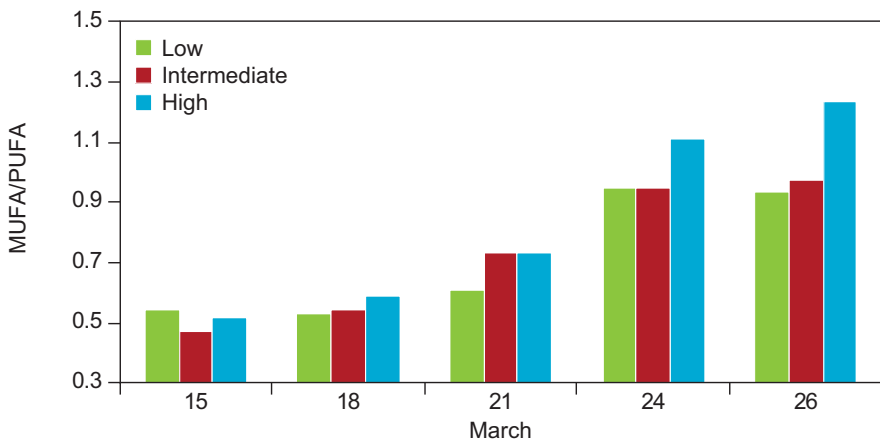
Fig. 4.17 The ratio of MUFA (monounsaturated fatty acids) to PUFA (polyunsaturated fatty acids) content in sea ice algae in ice without snow (High light), ice with shade (Intermediate light) and ice with snow (Low light) between 15 and 26 March 2016, Kangerlussuaq, W Greenland. (Modified from: Lund-Hansen et al. 2020)

Thus, bottom-ice irradiance and UV will inevitably increase with the ongoing thin-
ning of the sea ice (Sect. 5.1), and this change in sea ice irradiance and UV will
most likely affect also the Omega-3 content of the algae. At the end of our sam-
pling we conducted an experiment to examine the extent of any photodamage in
the ice algae when suddenly exposed to increased irradiances and UV in the inter-
mediate and high light treatments. Ice samples were collected every three hours
from each of the treatment areas between sunrise and sunset. We measured effec-
tive quantum yield Y(II), which is the quantum yield of photosynthesis of a sample
exposed to light and measured directly after sampling (see Sect. 6.6). Y(II) is high-
est in the low light treatment (0.41) and lowest in the high light treatment (0.34)
before sunrise, which indicates some degree of photodamage in both the medium
and high light areas (Fig. 4.18). Y(II) decreased gradually during the day until
around midday, after which it again increased in response to the decreasing bot-
tom-ice irradiance. This diurnal decrease of Y(II) with increasing irradiance is the
excess energy dissipation associated with the diadinoxanthin cycle, as described
earlier. This means that the algae can protect the cells from excessive and damag-
ing light. The experiment was continued in the laboratory where samples collected
at 17.00 h were kept in the dark to measure how long it would take for the algae to
recover back to the initial Y(II) levels, which occurred after 3–4 h (Fig. 4.18). This
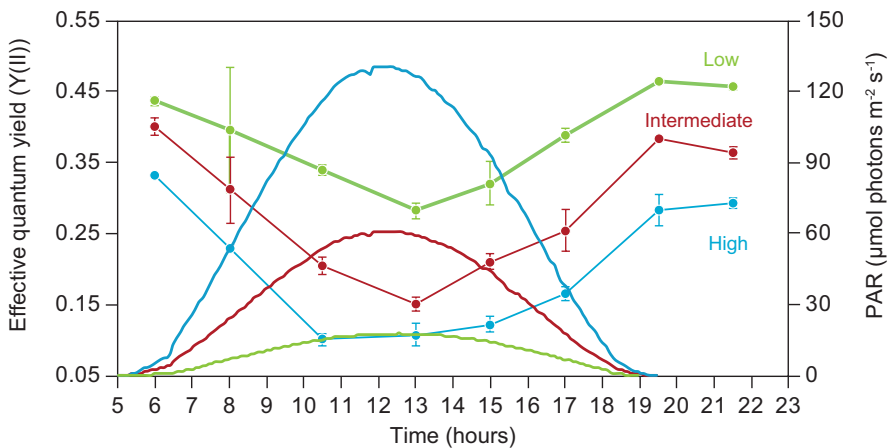experiment demonstrated that the sea ice algal communities were photodamaged to
some degree, but that they were still able to react to increased irradiances by energy
dissipation mechanisms (Fig. 4.18).

Fig. 4.18 Diurnal effective quantum yield Y(II) in ice without snow (High light), ice with shade
(Intermediate light) and ice with snow (Low light) and under ice PAR between sunrise at 5:00 and
21:30, March 2016, Kangerlussuaq, W Greenland. (Modified from: Lund-Hansen et al. 2020)

Fig. 4.19 Experimental site with transparent tarpaulin and shaded ice (Intermediate light) (**a**), work on the sea ice with the Imaging-PAM fluorometer in a tent (**b**), and cutting a sea ice core on the ice (**c**) Note the black cloth to protect the ice core from sunlight. (Photographs by: Authors)

4.5   A Numerical Model and Observations of Ice Algal Dynamics

A model is a set of differential equations that describe the state or the change of something over time in relation to input variables. For example, the equation:

$$\frac{d(C)}{d(t)} = \text{Production of carbon} - \text{Loss of carbon} \qquad (4.1)$$

comprises the terms that govern the production of carbon as irradiance, nutrients etc., and the terms that govern the loss of produced carbon as grazing, sinking etc. to list the most basic terms. When production is higher there is a surplus of carbon produced and vice versa. All equations describing governing parameters as PAR, water temperature, meteorological parameters, nutrient concentrations, species compositions, grazing etc. and how they influence carbon production or loss are then combined into a model. Input data to the model are the above-mentioned and the model is now able to calculate carbon production or loss for a specific site and specific time. The final model is validated in a comparison with field measurements of actual carbon production or loss. With a high correlation between model and observations, the model can then be applied to answer questions such as how will carbon production change with a reduced and thinner sea ice cover? There will be a higher irradiance, but are there still nutrients available? A high correlation between model output data and measurements shows that all general governing equations and process rates of the system are known and included. There might be small differences but this shows in principle that the right terms were selected in the equation, and that we know the variables that govern carbon production. Lavoie et al. (2005) developed a model that comprised modules of sea ice growth or melt, snow dynamics, distribution of light in snow and ice, and an ice algae module. This module described ice algae growth or loss based on input of nutrients and the amount of light at the ice bottom available for photosynthesis, and grazing (loss) by large protozoa such as flagellates and ciliates. Input parameters to force or run the model were incoming light, air and water temperatures, current speeds, and water level measured at the study site. The model was run for 1.5 months between 10 May and 29 June during
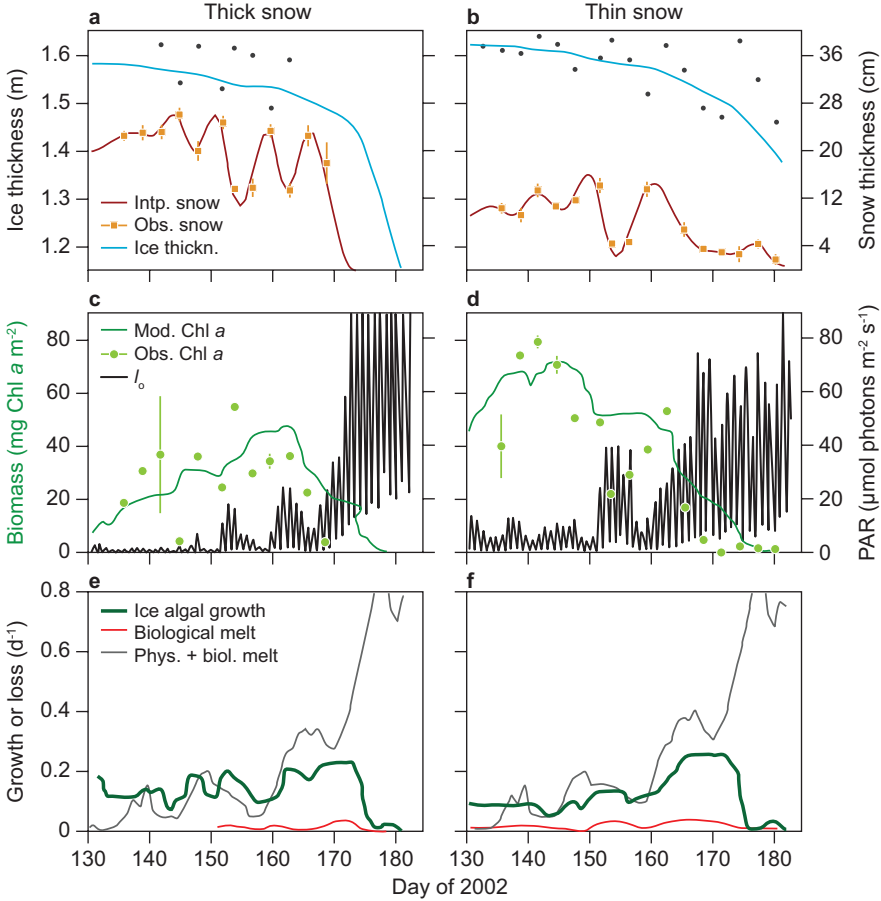
Fig. 4.20 Time-series of PAR, snow cover and ice thickness, Chl *a*, algal growth, and ice melt in areas with thick (0.25 cm) and thin snow (0.08) between 9 May and 28 June, Resolute Passage, Canadian Arctic. Blue line is modelled ice thickness (m), dots are observations, and orange dots are snow thickness with interpolated line (**a–b**), green dots are measured Chl *a*, line is modelled Chl *a*, and full black line is PAR (**c–d**), and green line is ice algal growth, red line is biological melt loss of algae, and thin black line is the combined physical and biological related melt loss of algae (**e–f**). (Modified from: Lavoie et al. 2005)

the snow and ice melting season for two areas with different snow thicknesses of 20 and 10 cm and compared with observations. Snow disappeared earlier in the thick snow area, and the gradual decrease in ice thickness was accelerated with the disappearance of the snow and the area was ice-free by day 180 (29 June) (Fig. 4.20). Model output and observations compare quite well for ice thickness, both with a thin and a thick snow cover (Fig. 4.20a, b). Note that snow cover was not modelled but based on interpolations of observations. There is a good agreement between modelled and the ice with observed ice algae biomass (Chl *a*) with maximums of about 80 mg Chl *a* m^{-2} in thin snow cover and about 50 mg Chl *a* m^{-2} in the ice with thick

snow cover (Fig. 4.12c, d), with integrated biomasses of 2150 and 1310 mg Chl *a* m^{-2}, respectively. Higher biomass in sea ice with thin snow cover was attributed to the higher under ice PAR levels here. Algal growth rates were quite stable until day 173 after which they declined at both high and low snow thickness sites. There is a loss of algae biomass related to increased air temperatures, changes in ice thickness and melting of the ice at the bottom whereby ice algae are lost, which is the physical melt loss (Fig. 4.20e, f). Biological melt loss is loss of biomass due to absorption of solar energy and melting of the ice whereby ice algae are lost. Ice algal growth decreases around day 170 when the combined physical and biological melt loss is increasing, e.g., where the loss of ice algae and biomass exceeds the growth. Based on a set of equations similar to Eq. (4.1) the model was able to describe the seasonal development and Chl *a* concentrations in the ice. This demonstrates that we know which parameters govern Chl *a* growth and lost, and that the model can predict Chl *a* based on input data as irradiance, nutrients, etc. The model shows further that biological melt loss related to heat absorption is very low compared to the physical melt loss. This exemplifies how a numerical model can give answers based on parameters that are difficult/impossible to measure directly, such as how big is the physical melt loss of algae relative to the biological melt loss?

4.6   Melt Ponds – Windows of Light

Melt ponds develop on the surface of the sea ice during early and late summer, depending on latitude, and comprise accumulations of freshwater from the melted snow and surface ice (Fig. 4.21). Using ship-based observations Lüthje et al. (2006) estimated an 80% total melt pond coverage by area for the entire Arctic Ocean. More detailed satellite image based studies have shown that up to 50% of a first-year sea ice area in the Arctic Ocean can be covered by melt ponds at their maximum (Webster et al. 2015). Coverage varies with season with a maximum in July in the Arctic Ocean (Fetterer and Untersteiner 1998). The coverage is lower at about 38% in multi-year ice, as the surface of this ice type is more hummocky, which prevents the spread of the melt water on the surface (Polashenski et al. 2012). First-year ice surfaces are generally more flat and melt water will cover a relatively larger area. It has been estimated that Arctic Ocean sea ice in 2006 consisted of about 50% first-year ice and 50% multi-year ice (Maslanik et al. 2011) but there is a clear tendency of multi-year ice being replaced by thinner first-year ice (Fig. 5.4) (Comiso 2012). The albedo in a first-year ice area is 0.37 compared to 0.62 in a multi-year ice area with transmittances of 0.11 and 0.04, respectively (Nicolaus et al. 2012). Thus, the decrease in multi-year ice coverage will raise the absorption of heat and irradiance in the water column below.

   Melt ponds occur in a variety of sizes from as low as 1–2 m^2 and up to several hundred m^2 (Fetterer and Untersteiner 1998). The melt ponds are shallow with water depths between a few cm and up to 0.5 m and rarely more, depending on the amount of snow and ice that have melted, and the surface topography of the ice. Melt ponds

Fig. 4.21 Sea ice with a high density of melt ponds as viewed from a helicopter and a close-up photo taken from the bridge of an icebreaker, August 2012, Amundsen Basin, Arctic Ocean. Note the Polar Bear footprint in lower right corner. (Photographs by: Authors)

Fig. 4.22 Structure of closed (top) and open (bottom) melt ponds
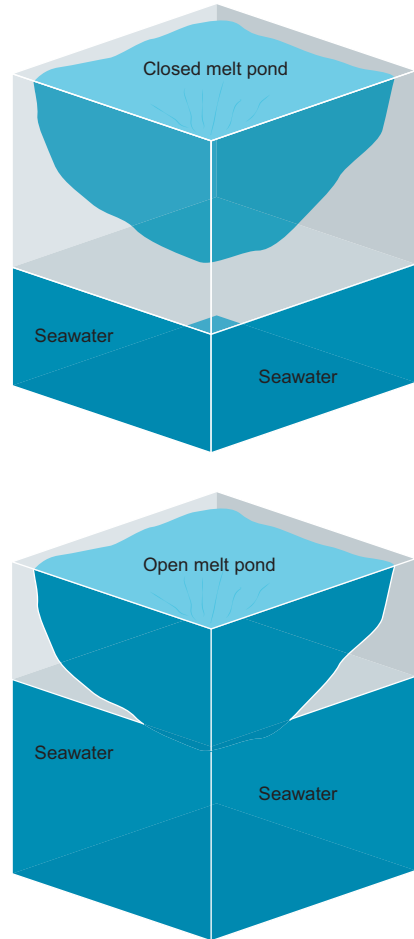
can be open at the bottom and in direct contact with ocean water, and salinities in the melt ponds are then similar to those of the water below. A closed melt pond is in contrast not open at the bottom and salinities in the melt pond are very low with salinities of <1–2 or lower (Fig. 4.22). Closed melt ponds are more frequent in multi-year ice, which is generally thicker compared to first-year ice. The multi-year ice melt ponds appear more bluish in colour as they are closed at the bottom, compared to the more dark-appearing melt ponds in first-year ice. The differences in melt pond colours can be seen in the upper photo in Fig. 4.21. An example of why melt ponds are called "windows to the ocean" is from the Canadian Arctic where light transmittance was determined below two closed melt ponds in relatively thinner (0.6 m) and thicker (1.2 m) ice (Fig. 4.23). Light transmittance is about 0.1 below the thin ice but increases significantly to about 0.6 at the edges of the melt pond with a maximum of 0.65 in the center. There is a similar pattern for the thick ice but with significantly lower maximum transmittance (0.38), which demonstrates
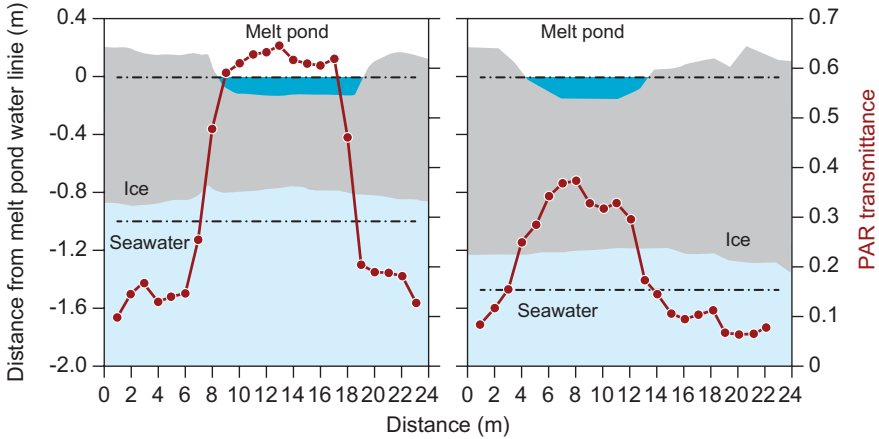
Fig. 4.23 PAR transmittance (red line) below melt ponds at two locations in summer 2016 in Canadian Arctic. Upper horizontal dashed line with dots is water level in the pond and lower is depth of the rope pulling the unit mounted with PAR sensor. (Modified from: Ehn et al. 2011)

that ice thickness strongly regulates the light windows (Ehn et al. 2011). The absorption and scattering in the section of water between the PAR sensor head and sea ice bottom is accounted for in the transmittance calculations. An under-ice video (Fig. 4.24) from near the North Pole in August 2012 shows strong light in the background related to the high transmittance of nearby melt ponds. The very sculptured, eroded bottom of the ice is related to melting of the ice from below, and the brown spots in some places are remnant patches of ice algae attached to the ice bottom (Figs. 4.25 and 4.26).

The few studies of melt pond ecology have shown that primary production in the ponds is low (Mundy et al. 2011) and lower than primary production rates within sea ice. For instance, melt pond production rates were 0.04–0.4 mg C m^{-2} day^{-1} and sea ice rates were 3.7–5.7 mg C m^{-2} day^{-1}, i.e. rates in ponds were about 45–100 times lower than in thawed sea ice as demonstrated in a study from Young Sound, NE Greenland (Søgaard et al. unpubl.). The bacterial production is also low in melt ponds and about 5–6 times lower than algal primary production (Sørensen et al. 2014). Meiofauna abundances are also low in melt ponds but increase slightly with increasing salinity (Gradinger unpubl.). There are observations of very high algal blooms of a green algae (*Carteria lunzensis*) in some melt ponds in the Arctic Ocean with Chl *a* concentrations up to 15.2 μg L^{-1} (Lin et al. 2016). Such blooms are considered to be rare and Lee et al. (2012) estimated that melt ponds (2005–2008) contributed less than 1% of the total carbon production in the Arctic Ocean. Fig. 4.27 shows a variety of melt ponds from Young Sound (upper left) and from the Arctic Ocean.

Fig. 4.24 An under-ice video from near the North Pole in August 2012 shows strong light in the background related to the high transmittance of nearby melt ponds. (https://doi.org/10.1007/000-05j)

Fig. 4.25 Melt ponds on land-fast first-year sea ice in Young Sound and Arctic Ocean. Mixture of open and closed melt ponds. (Photographs by: Authors)
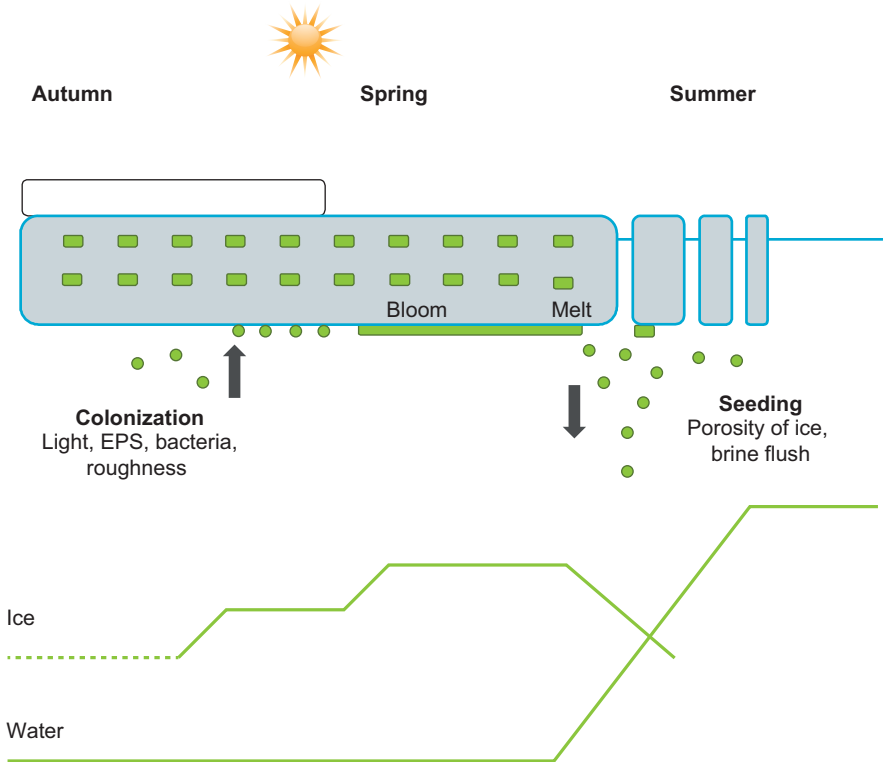
Fig. 4.26 Conceptual model showing ice algae dynamics with colonization of the sea ice and governing parameters (light, EPS, surface roughness, and bacteria) in early spring and development of a bottom ice algae community of high biomass. Seeding of the water column can take place when the ice algae melt out at increased porosity where brine is flushed containing ice algae that can initiate or enhance the pelagic phytoplankton bloom. Ice algae inside the ice column were supposedly scavenged into the ice when it developed in autumn. Green lines below are relative Chl a concentrations in the ice and water column

4.7   Seeding of the Water Column and the Ice

Ice algae can colonize the sea ice around early spring at sufficient light, followed by a bloom at the bottom of the ice around spring-summer, and they again leave the ice during summer and ice melt. Ice algae released from the ice can then seed the water column and thereby initiate or enhance the pelagic primary production. In Fig. 4.26 the green rectangles symbolize cysts or viable ice algae that were incorporated during autumn freeze-up, which will add to the seeding. In the figure the green lines are relative Chl a concentrations in the ice and water column over time (Fig. 4.26). Higher pelagic water column Chl a concentrations in summer reflect that pelagic production generally exceeds the sympagic production, as demonstrated in a SW Greenland study (Mikkelsen et al. 2008). Seeding is the transfer or

Fig. 4.27 Model showing the Chl a concentrations in the sea ice and in the pelagic zone for an entire year where both sea ice and pelagic diatoms have low light utilization coefficients ($\alpha^0_{chla} = 4.6 \cdot 10^{-6}$) (**a**), both ice and pelagic diatoms are adapted to high light utilization coefficients ($\alpha^0_{chla} = 1.8 \cdot 10^{-3}$) (**b**), and pelagic diatoms are adapted to low light and ice diatoms to high light (**c**). (Modified from: Tedesco et al. 2012)
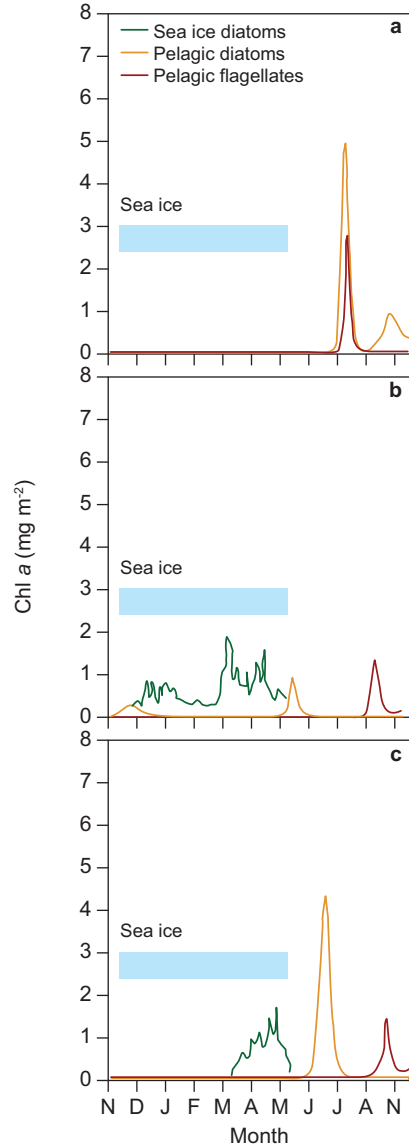
transport of viable ice algae from the ice to the water column during melt of the ice at higher tempertatures and thereby larger brine volumes, and flushing of brine channels. That ice algae leave the ice during melt is obvious and can be quantified using traps below the ice (Riebesell 1991), but it has been a challenge to actually measure and quantify the effects of seeding (Szymanski and Gradinger 2016). Tedesco et al. (2012) has analyzed the seeding process in a biogeochemical flux model for sea ice and water column based on governing variables such as algal

viability, light acclimation, PAR, nutrients, and formation of aggregates. This combined biogeochemical flux model for sea ice and the water column was run for different scenarios of the governing variables to analyze precisely where the bloom took place (sea ice or water column), dominant algae species of the bloom, and specifically the effects of adaptation and acclimation to different light levels. Both ice and pelagic algae (phytoplankton) are adapted to high light in the first scenario (Fig. 4.28a), and the model show that there is only a pelagic bloom of diatoms and
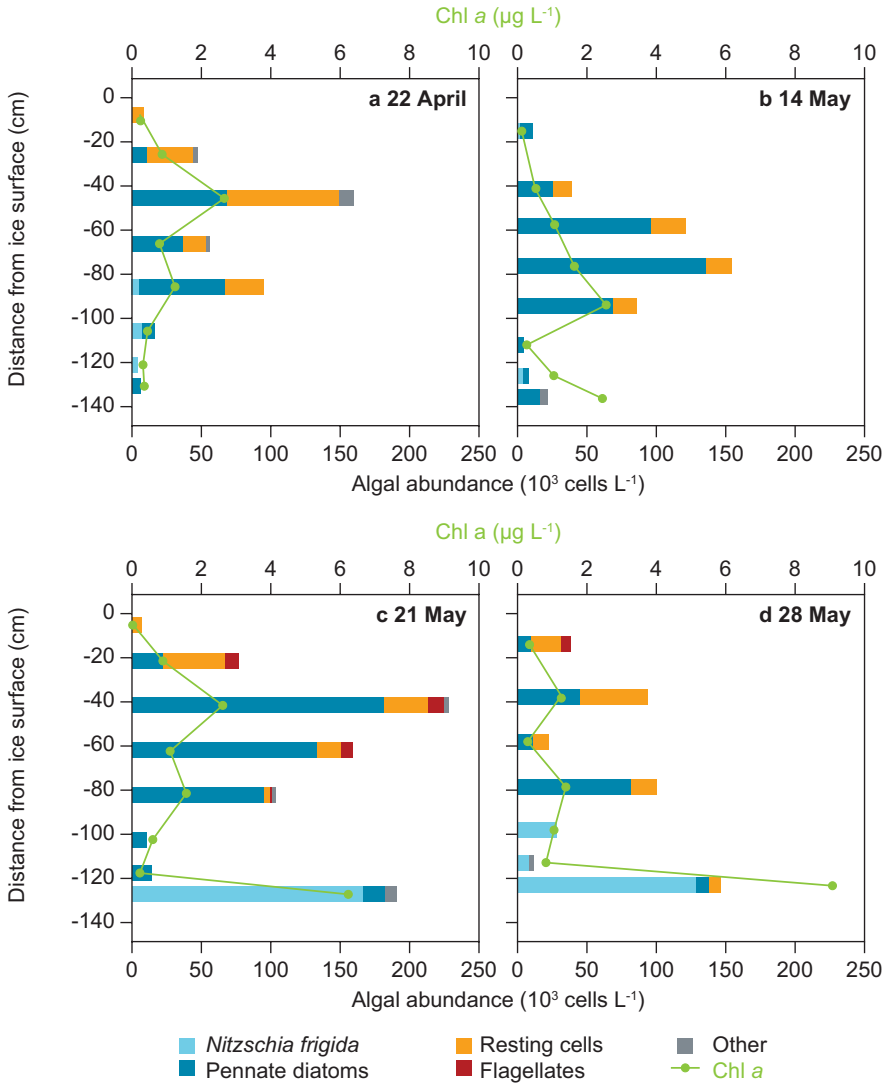
Fig. 4.28 Time series of algal abundance, algae species groups, and Chl *a* in multi-year ice in April to May 2015, 84° N of Svalbard. Time series - (**a**) 22 April, (**b**) 14 May, (**c**) 21 May, (**d**) 28 May - of algal. (Modified from: Olsen et al. 2017)

flagellates at increased light in the water column. In the second scenario both ice algae and pelagic diatoms are low light-adapted, and there is a significant bloom in the sea ice followed by minor pelagic blooms of diatoms and flagellates (Fig. 4.28b). Ice algae are adapted to high light in the third scenario, and pelagic diatoms are adapted to low light. The model shows a small bloom of ice algae at the end of the season where there is also more light and a significant bloom of pelagic diatoms (Fig. 4.27c). The light utilization parameter $\alpha^0_{chl\ a}$ (mg C (mg Chl a)$^{-1}$ (µmol photons m^{-2} s^{-1})$^{-1}$) was applied in the model, and is the carbon content per unit Chl a and irradiance. A low number such as $\alpha^0_{Chl\ a} = 4.6 \times 10^{-6}$ mg C (mg Chl a)$^{-1}$ (µmol photons m^{-2} s^{-1})$^{-1}$ indicates that the algae are adapted to high light, as $\alpha^0_{chl\ a}$ is inverse proportional to the irradiance. Conversely, a high number as $\alpha^0_{chl\ a} = 1.8 \times 10^{-3}$ mg C (mg Chl a)$^{-1}$ (µmol photons m^{-2} s^{-1})$^{-1}$ indicates that the algae are adapted to low light conditions. As mentioned previously, the algae will tend to increase the amount of light harvesting pigments at low light, which is still an effect in the model, though the changes in irradiance are more dominant regarding the light utilization parameter $\alpha^0_{chl\ a}$. The effects of aggregation, e.g. when both ice and pelagic algae tend to stick together and form larger mm-sized aggregates, is also a significant parameter in the seeding process. The sinking velocity of aggregates in the water column depends mainly on aggregate size (Riebesell 1991) and with aggregation of ice algae diatoms, the bloom in the water column was mainly driven by flagellates (Tedesco et al. 2012). In summary: the model shows that seeding of the water column is governed by a composite of parameters as photosynthetic activity of the ice algae, time of year, productivity, and especially the aggregation of algae and whether they sink out of the water column. In this scenario the ice algae formed large aggregates with high sinking rates, and they sank out of the water column towards the seabed before the pelagic bloom was initiated. A seeding field study north of Svalbard tested the hypothesis that multi-year sea ice can act as a depository of seeds that seed the bottom of the ice, which promotes or enhances an ice algal bloom (Olsen et al. 2017). A time-series of depth profiles in ice cores, which comprise Chl a, ice algae species, and number of cells shows a relatively high concentration of pennate diatoms and resting cells in the central part of the ice (Fig. 4.28). The ice is second-year ice and the algal resting cells might be ice algae that formed the bottom layer last summer, and new algae that were frozen into the ice during freezing and new ice growth. There was a tendency for cell numbers and Chl a in the centre of the ice to increase until 21 May, and concurrently a significant bloom of the diatom *Nitzschia frigida* at the bottom of the ice where Chl a increased from about 2 µg Chl a L^{-1} on 14 May to about 6 µg Chl a L^{-1} on 21 May (Fig. 4.28c, d). The number of pennate diatoms inside the ice decreased between 21 and 28 May, concurrent with an increase in ice core temperatures and an increase in brine volume especially at the bottom of the ice (Fig. 4.1b). It is highly likely that the ice algal bloom of *Nitzschia frigida* was promoted by seeds from the upper part of the ice column, but also likely that the water column below was seeded with the increased brine volumes and flushing, but there are no data available to clarify this. The study pointed out that the gradual loss of multi-year ice will reduce this seeding mechanism and thereby probably also the size of ice algal blooms. There is clearly still much work needed to quantify the importance of the seeding process, whether seeding of the ice and or water column.

4.8   Sea Ice Meiofauna: Unknown Diversity and Food Web Interactions – Case Study 3

This case study addresses the importance of meiofauna in the sea ice through the sea ice season with a focus on their changing composition and food web contribution during the ice algal bloom season. The small animal fauna within sea ice (Fig. 1.2) are often overlooked, potentially due to methodological challenges. Sea ice algae can relatively easily be quantified by bulk parameters like Chl *a* or particulate organic carbon. No such bulk variable is available for meiofauna. They are microscopically small, occur often in low abundances and their taxonomy is challenging. It requires therefore the sampling of many ice cores at the same site and skilled biologists to estimate their abundance and composition in the field, often entangled and hidden between hundreds of small ice algal cells and aggregates (Fig. 4.29a).
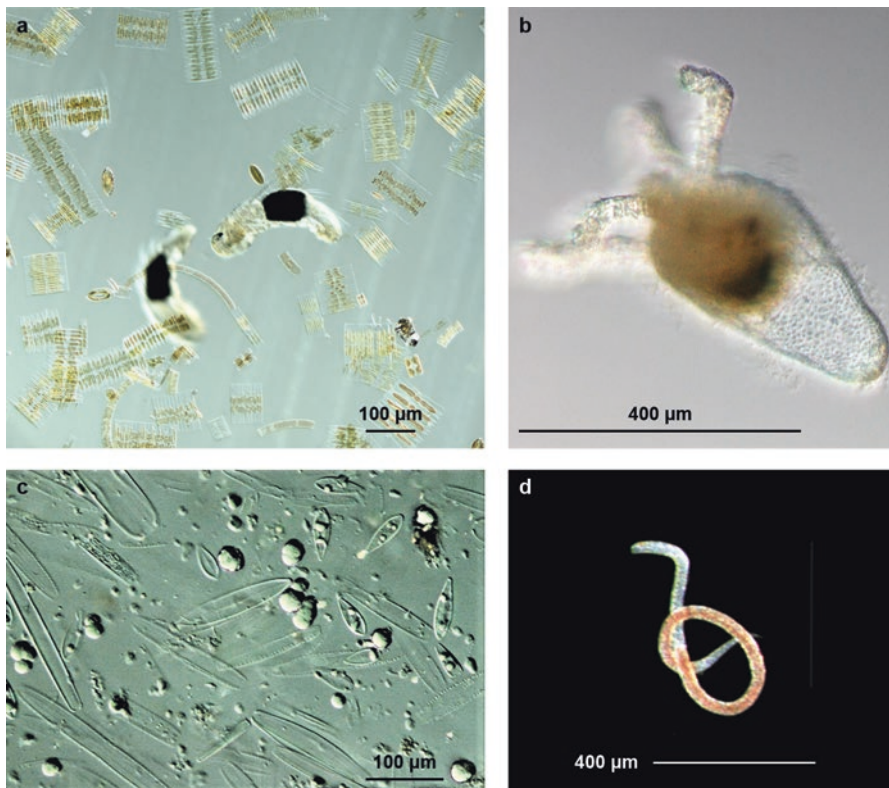
Fig. 4.29 Pictures of living sea ice meiofauna from Alaskan nearshore fast ice from the bottom 10 cm of sea ice, showing ice algae and polychaete juveniles (**a**), *Sympagohydra tuuli* (Gradinger and Bluhm 2010) (**b**), gut content of the nearshore Arctic amphipod *Onisimus litoralis* showing high abundances of empty frustules of sea ice diatoms (Gradinger and Bluhm 2010) (**c**), and a sea ice nematode (**d**)

We conducted several studies on meiofauna abundance in the nearshore Alaskan Arctic and contrasted those results with data from expeditions into the central Arctic Ocean (e.g. Gradinger et al. 2009). All these efforts combined with work from other colleagues led to the recent and first ever synopsis of meiofauna occurrences on a pan-Arctic scale (Bluhm et al. 2017). These studies demonstrated the complexity in the composition and seasonal changes of the ice meiofauna communities and provided new insights into their role in the food web dynamics. The following paragraphs highlight some of the challenges and advances made but also the many open questions still remaining in terms of basic biology and climate change challenges. One of the most basic questions addressed by field biologists is: Who lives where? To approach this question, sea ice biologists have to deal with methodological challenges, as melting of ice causes sudden changes in environmental properties that some taxa might not survive, or may cause shifts in their physiology (relevant for experimental work). Current standard approaches for sea ice meiofauna (Gradinger and Bluhm 2009) include melting of the ice in sea water to reduce salinity effects such as osmotic stress. As most sea ice meiofauna taxa are found in the bottom 10 cm of the sea ice, most of our studies focused on this small part of the ice column. This can underestimate the true meiofauna abundance, especially in summer in the central Arctic (Friedrich 1997), when meiofauna (and algae) are found throughout the entire ice thickness. Given the complexity of collecting ice, melting it in buffered sea water, concentrating the animals over a 20 μm sieve and counting them alive or fixed in a microscope, it does not really come as a surprise that the current inventory of species is far from complete and new additions have occurred and will occur in the future. The following short examples illustrate the exciting discoveries and ongoing research questions related to the existence of meiofauna in Arctic sea ice. The focus will be on studies in the nearshore Alaskan Arctic, where coastal fast ice occurs over shallow water depths of less than 20 m.

4.8.1 The Incomplete Inventory

A by now well-studied example of incomplete inventory taxa has been the discovery of a new species and genus of a small hydrozoan living with Arctic within sea ice (Piraino et al. 2008). When analysing ice core meiofauna samples from the nearshore Alaskan Arctic, we (Bodil Bluhm and Rolf Gradinger) suddenly discovered an animal within the ice samples that we had not seen before. It looked like a microscopically small jellyfish with small arms, very transparent and slowly gliding across the petri dish bottom we used to look at the sample under the microscope (Fig. 4.29b). Was it a pelagic jellyfish freshly frozen into the ice? Was it a juvenile stage of a benthic or pelagic cnidarian? Our certainty that we had discovered a new ice related species increased, when – looking through more samples – other specimens also in other samples were found. Together with Italian jellyfish taxonomists, we described the new species *Sympagohydra tuuli*, which has now also been found in many other areas of the Arctic sea ice (Marquard et al. 2018). It seems likely that

studies in the past have overlooked this jellyfish due its transparency and small size. What makes *S. tuuli* unique is its position within the food web. While traditionally the polar bear has been considered the top predator in Arctic marine systems, this is not the case within the ice brine channel network. Here *S. tuuli* is at the end of the food web, preying on many other sea ice meiofauna taxa including rotifers and jellyfish (Siebert et al. 2009). Although we now have a concept of its basic occurrence, taxonomy, and ecology, many questions remain unresolved regarding the reproductive cycle and its occurrence in other pelagic or benthic habitats. So far, *S. tuuli* is considered ice endemic (only occurring within sea ice), but maybe it has been overlooked in other habitats as we had done in the past for *S. tuuli*.

4.8.2   The Unknown Food Web Interactions and Life Cycles

S. tuuli is only one example of the many species of meiofauna existing within the sea ice. The following is an example for a major taxonomic group found in Arctic sea ice that has a complex life cycle involving sea ice, namely Polychaeta. For Polychaeta and similarly for Nematoda, our time series analyses in Alaskan sea ice demonstrated changes in occurrences and abundances closely related to the seasonal cycle of the sea ice itself and the sea ice algal spring blooms. Although similar, they have also distinctive different ecological niches and life cycles. Both taxa together contribute the highest abundances to total ice metazoans. We observed a seasonal increase from 17,700 in February to 276,200 animals m^{-2} sea ice in May, with the largest fractions contributed by nematodes and ice-associated polychaete juveniles (Gradinger et al. 2009). Abundances within the ice far exceeded their abundances in the water column. In addition to Nematoda and Polychaeta, also copepods (calanoid, cyclopoid and harpacticoid), copepod nauplii and *Acoela* were observed within the ice. One common feature for most of these taxa is their herbivory – grazing on sea ice algae. Unfortunately, no direct grazing measurements can be conducted with sea ice communities as for example with serial dilution experiments in pelagic environments. Here, our current knowledge is based on gut contents analysis and/or use of allometric equations. Gut contents analysis which involved squeezing meiofauna on microscope slides revealed that nearly all meiofauna taxa are able to ingest sea ice algae (Grainger and Hsiao 1990). Interestingly sea ice algae are also found in the guts of under-ice and benthic amphipods in the nearshore waters, indicating close benthic-sea ice coupling in these shallow waters (Fig. 4.29c) (Gradinger and Bluhm 2010). The use of allometric equations is an alternative approach that allows the potential carbon ingestion of a species to be estimated based on the biomass of each individual using the following equation:

$$I_{max} = 63.0 \cdot M^{-0.25} \cdot 0.2177 \cdot B \qquad (4.2)$$

where I_{max} is the potential maximum ingestion rate (μg C L^{-1} day^{-1}), 63.0 the biomass specific ingestion (pg C day^{-1}), M the body mass of one individual (pg C), B is the

carbon biomass of the taxon in the sea ice sample (μg C L^{-1}), and 0.2177 is a Q_{10} factor, which varies with the temperature of the environment. This approach does not require any experimental work and only needs estimates of the body mass of individuals that can be found tabulated in several publications (e.g. Gradinger 1999). The resulting ingestion rates only need to be multiplied with the organism abundances to estimate community ingestion. This approach has been used several times for different parts of the Arctic with the outcome that the potential carbon ingestion of the meiofauna was nearly always below 10% of the algal standing stock (e.g. Gradinger 1999; Michel et al. 2002). While this approach provided an estimate of the potential grazing, it does not provide the real grazing rates, as it is currently unknown how high the feeding rates are under *in situ* conditions within the ice. Nevertheless the allometric approach at least provides guidance regarding the order of magnitude of the meiofauna grazing. Now, how could we get more insights into the grazing by individual taxa, and – more specifically – why do we find juveniles of polychaetes (benthic living worms as adults) within the ice? And how important is the ice algal spring bloom in the growth of these juveniles? Here experimental studies using different food concentrations helped to solve this puzzle further (McConnell et al. 2012). High abundances of Polychaeta are easy to reach in coastal fast ice in Alaska which allowed for the collection of large numbers of similarly-sized polychaete juveniles within a few days. These specimens were split into different food treatments to simulate ice and pelagic feeding environments and incubated in the laboratory over several weeks (up to 80 days), monitoring their growth several times over the entire feeding period. At the start of one of the experiments the polychaete juveniles had a mean length of ca. 0.9 mm. Over time we determined that the change in length or growth (y) in μm day^{-1} was significantly related to the available food (x) in μg Chl *a* L^{-1} with y = 0.90 · x + 12.57 (r^2 = 0.81; p < 0.001; n = 20), and animals in the sea ice-simulating food treatment grew significantly faster than in the water treatment. We concluded from this experiment, combined with field observations, that polychaete juveniles are swimming from the water column into the sea ice to feed on the early spring high biomass enabling their very fast growth rates. Once big enough (or even getting too big for the brine channels) they leave the ice system and settle at the sea floor for further maturation, which provides an example of sympagic – benthic coupling through organism life cycles. It should be evident from these two examples that meiofauna taxa are an interesting component of the sea ice biota, with particularly high abundances and life cycle couplings linking ice and seafloor. In more shallow water the distance between seafloor and ice is obviously shorter and the existence of a sympagic-benthic coupling is a possibility. An under-ice video from a fjord in Greenland shows a distance between sea ice and sea floor of about 2 m (Fig. 4.30). The diverse meiofauna communities respond strongly to the seasonal formation of the ice algal blooms and utilize it for fast growth. It should also be clear from these examples that any climate change-driven change in ice biota characteristics will have impacts on life in other Arctic habitats. Earlier ice melt, different snow accumulations, and changes in current systems all have the potential to interrupt the currently tight coupling between systems and the processes within the sea ice itself. Although we have by now a

Fig. 4.30 An under-ice video from a fjord in Greenland shows a distance between sea ice and sea floor of about 2 m (https://doi.org/10.1007/000-05h) (Photograph by: Christof Pearce)

principal understanding of the major players within the ice, there is still a lot of work to be conducted to understand the individual life cycles and adaptations, and to realistically incorporate the ice meiofauna in ecosystem models for sea ice in general.

References

Arrigo, K. R., Perovich, D., Pickart, R. R., Brown, Z. W., Dijken, G. L., Lowry, K. E., Mills, M. M., Palmer, M. A., Balch, W. M., Bates, N. R., Benitez-Nelson, C. R., Brownlee, E., Frey, K. E., Laney, S. R., Mathis, J., Matsouka, A., Mitchell, B. G., Moore, G. W. K., Reynolds, R. A., Sosik, H. M., & Swift, J. H. (2014). Phytoplankton blooms beneath at the sea ice in the Chukchi Sea. *Deep-Sea Research II, 105*, 1–16. https://doi.org/10.1016/j.dsr2.2014.03.018.
Assmy, P., Fernández-Méndez, M., Duarte, P., Meyer, A., Randelhoff, A., Mundy, C. J., Olsen, L. M., Kauko, H. M., Bailey, A., Chierici, M., Cohen, L., Doulgeris, A. P., Ehn, J. K., Fransson, A., Gerland, S., Hop, H., Hudsonm, S. R., Hughes, N., Itkin, P., Johnsen, G. M., King, J. A., Koch, B. P., Koening, Z., Kwasniewski, S., Laney, S. R., Nicolaus, M., Pavlov, A. K., Polashenski, C. M., Provost, C., Rösel, A., Sandbu, M., Spreen, G., Smedsrud, L. H., Sundfjord, A., Taskjelle, T., Tatarek, A., Wiktor, J., & Wagner, P. M. (2017). Leads in Arctic pack ice enable early phytoplankton blooms below snow-covered sea ice. *Scientific Reports, 7*. https://doi.org/10.1038/srep40850.
Bluhm, B. A., Swadling, K. M., & Gradinger, R. (2017). Sea ice as a habitat for macrograzers. In D. N. Thomas (Ed.), *Sea Ice* (3rd ed., pp. 394–414). Chichester: Wiley Blackwell, 652 pp.
Boetius, A., Albrecht, S., Bakker, K., Beinhold, C., Felden, J., Fernández-Méndez, M., Hendricks, S., Katlein, C., Lalande, C., Krumpen, T., Nicolaus, M., Peeken, I., Rabe, B., Rogacheva, A., Rybakova, E., Somavilla, R., & Wenzhöfer, F. (2013). Export of algal biomass from the melting Arctic sea ice. *Science, 339*. https://doi.org/10.1126/science.1231346.

Campbell, K., Mundy, C. J., Barner, D. G., & Gosselin, M. (2014). Characterizing the sea ice algae chlorophyll a-snow depth relationship over Arctic spring melt using transmitted irradiance. *Journal of Marine Systems, 147*, 76–84. https://doi.org/10.1016/j.jmarsys.2014.01.008.

Comiso, J. C. (2012). Large decadal decline of the Arctic multiyear ice cover. *Journal of Climate, 25*, 1176–1193. https://doi.org/10.1175/JCLI-D-11-00113.1.

Cota, G. F., & Horne, E. P. W. (1989). Physical control of Arctic ice algal production. *Marine Ecology Progress Series, 52*, 111–121. https://doi.org/10.3354/meps052111.

Cox, G. F. N., & Weeks, W. F. (1974). Salinity variations in sea ice. *Journal of Glaciology, 13*, 109–120. https://doi.org/10.3189/S0022143000023418.

Deming, J. W., & Collins, R. E. (2017). Sea ice as a habitat for Bacteria, Archaea and viruses. In D. N. Thomas (Ed.), *Sea Ice* (3rd ed., pp. 326–351). Chichester: Wiley Blackwell, 652 pp.

Ehn, J. K., Mundy, C. J., Barber, D. G., Hop, H., Rossnagel, A., & Stewart, J. (2011). Impact of horizontal spreading on light propagation in melt pond covered seasonal sea ice in the Canadian Arctic. *Journal of Geophysical Research, 116*. https://doi.org/10.1029/2010JC006908.

Falkowski, P. G., & Raven, J. A. (2007). *Aquatic photosynthesis* (2nd ed.). Princeton: Princeton University Press, 488 pp.

Fernández-Méndez, M., Katlein, C., Rabe, B., Nicolaus, M., Peeken, I., Bakker, K., Flores, H., & Boetius, A. (2015). Photosynthetic production in the Central Arctic Ocean during the record sea-ice minimum in 2012. *Biogeosciences, 12*, 3525–3549. https://doi.org/10.5194/bg-12-3525-2015.

Fetterer, F., & Untersteiner, N. (1998). Observations of melt ponds on Arctic Sea ice. *Journal of Geophysical Research, 103*, 24.821–24.835. https://doi.org/10.1029/98JC02034.

Friedrich, C. (1997). Ecological investigations on the fauna of the Arctic Sea-ice. *Reports on Polar and Marine Research, 246*, 1–211.

Garrison, D. L., & Buck, K. R. (1986). Organism losses during ice melting: A serious bias in sea ice community studies. *Polar Biology, 6*, 237–239. https://doi.org/10.1007/BF00443401.

Gleitz, M., Rutgers, V. D., Thomas, D. N., Dieckmann, G. S., & Millero, F. J. (1995). Comparison of summer and winter inorganic carbon, oxygen and nutrient concentrations in Antarctic Sea ice brine. *Marine Chemistry, 51*, 81–91. https://doi.org/10.1016/0304-4203(95)00053-T.

Glud, R. N., Rysgaard, S., Kühl, M., & Hansen, J. W. (2007). The sea ice in Young Sound: Implications for carbon cycling. In S. Rysgaard & R. N. Glud (Eds.), *Carbon cycling in Arctic marine Ecosystems – Case study Young Sound* (Meddelelser om Grønland, Bioscience, Vol. 58) (pp. 62–85). Copenhagen: Copenhagen the Commission for Scientific Research in Greenland.

Glud, R. N., Rysgaard, S., Turner, G., McGinnis, D. F., & Leakey, R. J. G. (2014). Biological and physical-induced oxygen dynamics in melting sea ice of the Fram Strait. *Limnology Oceanography, 59*, 1097–1111. https://doi.org/10.4319/lo.2014.59.4.1097.

Golden, K. M., Eicken, H., Heaton, A. L., Miner, J., Pringle, D. J., & Zhu, J. (2007). Thermal evolution of permeability and microstructure in sea ice. *Geophysical Research Letters, 34*. https://doi.org/10.1029/2007GL030447.

Goss, R., & Jacob, T. (2010). Regulation and function of xanthophyll cycle-dependent photoprotection in algae. *Photosynthesis Research, 106*, 103–122. https://doi.org/10.1007/s11120-010-9536-x.

Gosselin, M., Legendre, L., Therriault, J.-C., Demers, S., & Rochet, M. (1986). Physical control of the horizontal patchiness of sea-ice microalgae. *Marine Ecology Progress Series, 29*, 289–298. https://doi.org/10.3354/meps029289.

Gradinger, R., & Ikävalko, J. (1998). Organism incorporation into newly forming Arctic Sea ice in the Greenland Sea. *Journal of Plankton Research, 20*, 871–886. https://doi.org/10.1093/plankt/20.5.871.

Gradinger, R. (1999). Integrated abundances and biomass of sympagic meiofauna from Arctic and Antarctic pack ice. *Polar Biology, 22*, 169–177.

Gradinger, R. (2009). Sea-ice algae: Major contributors to primary production and algal biomass in the Chukchi and Beaufort Seas during May/June 2002. *Deep Sea Research Part II Topical Studies in Oceanography, 56*, 1201–1212. https://doi.org/10.1016/j.dsr2.2008.10.016.

Gradinger, R., and Bluhm, B. (2009). Assessment of the abundance and diversity of sea ice biota. *In* Sea ice field research techniques, pp. 283-300. Ed. by Eicken H, R. Gradinger, M. Salganek, K. Shirasawa, D. K. Perovich, and Leppäranta, M. University of Alaska Press, Fairbanks.

Gradinger, R., & Bluhm, B. (2010). Timing of ice algal grazing by the arctic nearshore benthic amphipod *Onisimus litoralis*. *Arctic, 63*, 355–358. https://doi.org/10.14430/arctic1498.

Gradinger, R. R., Kaufman, M. R., & Bluhm, B. A. (2009). Pivotal role of sea ice sediments in the seasonal development of near-shore Arctic fast ice biota. *Marine Ecology Progress Series, 394*, 49–63. https://doi.org/10.3354/meps08320.

Grainger, E. H., & Hsiao, S. I. C. (1990). Trophic relationships of the sea ice meiofauna in Frobisher Bay, Arctic Canada. *Polar Biology, 10*, 283–292.

Ha, S.-Y., Min, J.-O., Joo, H., Kim, M.-S., Kang, S.-H., & Shin, K.-H. (2018). Synthesis of mycosporine-like amino acids by a size-fractionated marine phytoplankton community of the arctic Beaufort Sea. *Journal of Photochemistry and Photobiology B: Biology, 188*, 87–94. https://doi.org/10.1016/j.jphotobiol.2018.09.008.

Hancke, K., Lund-Hansen, L. C., Lamare, M. L., Pedersen, S. H., King, M. D., Andersen, P., & Sorrell, B. K. (2018). Extreme low light requirement for algae growth underneath sea ice: A case study from station Nord, NE Greenland. *Journal of Geophysical Research, 123*, 985–1000. https://doi.org/10.1002/2017JC013263.

Hansen, P. J. (2002). Effect of high pH on the growth and survival of marine phytoplankton: Implications for species succession. *Aquatic Microbial Ecology, 28*, 279–288. https://doi.org/10.3354/ame028279.

Hare, K. R., Wang, F., Barber, D., Geilfus, N.-X., Galley, R. J., & Rysgaard, S. (2013). pH evolution in sea ice grown at an outdoor experimental facility. *Marine Chemistry, 154*, 46–54. https://doi.org/10.1016/j.marchem.2013.04.007.

Hinga, K. R. (2002). Effect of pH on coastal marine phytoplankton. *Marine Ecology Progress Series, 238*, 281–300. https://doi.org/10.3354/meps238281.

Horner, R. A., & Schrader, G. C. (1982). Relative contributions of ice algae, phytoplankton, and benthic microalgae to primary production in nearshore regions of the Beaufort Sea. *Arctic, 35*, 485–503.

Huertas, I. E., Colman, B., Espie, G. S., & Lubian, L. M. (2000). Active transport of CO_2 by the three species of marine microalgae. *Journal of Phycology, 36*, 314–320. https://doi.org/10.1046/j.1529-8817.2000.99142.x.

Juhl, A. R., Krembs, C., & Meiners, K. M. (2011). Seasonal development and differential retention of ice algae and other organic fractions in first-year Arctic Sea ice. *Marine Ecology Progress Series, 436*, 1–16. https://doi.org/10.3354/meps09277.

Kauko, H. M., Olsen, L. M., Duarte, P., Peeken, I., Granskog, M. A., Johnsen, G., Fernández-Méndez, M., Pavlov, A. K., Mundy, C. J., & Assmy, P. (2018). Algal colonization of young Arctic Sea ice in spring. *Frontiers in Marine Science, 5*. https://doi.org/10.3389/fmars.2018.00199.

Korb, R. E., Saville, P. J., Johnston, A. M., & Raven, J. A. (1997). Sources of inorganic carbon for photosynthesis by three species of marine diatoms. *Journal of Phycology, 33*, 433–440. https://doi.org/10.1111/j.0022-3646.1997.00433.x.

Kühl, M., Glud, R. N., Borum, J., Roberts, R., & Rygaard, S. (2001). Photosynthetic performance of surface-associated algae below sea ice as measured with a pulse-amplitude-modulated (PAM) fluorometer and O_2 microsensors. *Marine Ecology Progress Series, 223*, 1–114. https://doi.org/10.3354/meps223001.

Lalande, C., Bélanger, S., & Fortier, L. (2009). Impact of a decreasing sea ice cover on the vertical export of particulate organic carbon in the northern Laptev Sea, Siberian Arctic Ocean. *Geophysical Research Letters, 36*, L21604. https://doi.org/10.1029/2009GL040570.

Lange, B. A., Michel, C., Beckers, J. F., Casey, J. A., Flores, H., Hatam, I., & Haas, C. (2015). Comparing spring time ice-algal chlorophyll a and physical properties of multi-year and first-year sea ice from the Lincoln Sea. *PlosOne, 10*, 34–41. https://doi.org/10.1371/journal.pone.0122418.

Lavoie, D., Denman, K., & Michel, C. (2005). Modeling ice algal growth and decline in a season-ally ice-covered region of the Arctic (Resolute Passage, Canadian Archipelago). *Journal of Geophysical Research, 110*, C11009. https://doi.org/10.1029/2005JC002922.

Lee, S. H., Stockwell, D. A., Joo, H.-M., Son, Y. B., Kang, C.-K., & Whitledge, T. E. (2012). Phytoplankton production from melting ponds on Arctic Sea ice. *Journal of Geophysical Research, 117*, C04030. https://doi.org/10.1029/2011JC007717.

Leu, E., Mundy, C. J., Assmy, P., Campbell, K., Gabrielsen, T. M., Gosselin, M., Juul-Pedersen, T., & Gradinger, R. (2015). Arctic spring awakening – Steering principles behind the phenology of vernal ice algal blooms. *Progress in Oceanography, 139*, 151–170. https://doi.org/10.1016/j.pocean.2015.07.012.

Leeuwe, M. A., Tedesco, L., Arrigo, K. R., Assmy, P., Campbell, K., Meiners, K. M., Rintala, J.-M., Thomas, D. N., & Stefels, J. (2018). Microalgal community structure and primary pro-duction in Arctic and Antarctic Sea ice: A synthesis. Elementa: Science of the. *Anthropocene, 6*, 1–25. https://doi.org/10.1525/elementa.267.

Lin, L., He, J., Zhang, F., Cao, S., & Zhang, C. (2016). Algal bloom in a melt pond on Canada Basin pack ice. *Polar Record, 52*, 114–117. https://doi.org/10.1017/S0032247415000510.

Lund-Hansen, L.C., Hawes, I., Sorrell, B.K and Nielsen, M.H. (2013). Removal of snow cover inhibits spring growth of Arctic ice algae through physiological and behavioral effects. Polar Biology, https://doi.org/10.1007/s00300-013-1444-z

Lund-Hansen, L. C., Hawes, I., Nielsen, M. H., Dahllöf, I., & Sorrell, B. K. (2018). Summer melt-water and spring sea ice primary production, light climate and nutrients in an Arctic estuary, Kangerlussuaq, West Greenland. *Arctic, Antarctic and Alpine Research, 50*. https://doi.org/10.1080/15230430.2017.1414468.

Lund-Hansen, L. C., Hancke, K., Salmansen, N., Balslev, L., Nielsen, J., Hawes, I. and Sorell, B. K. (2020). Effects of snow removal and increased irradiance on biomass, pigments, photo-biology and nutritional quality of Arctic sea ice algae during spring growth. Marine Ecology Progress Series (In press).

Lüthje, M., Feltham, D. L., Taylor, P. D., & Worster, M. G. (2006). Modeling the summer-time evolution of sea-ice melt ponds. *Journal of Geophysical Research, 111*. https://doi.org/10.1029/2004JC002818.

Maslanik, J., Stroeve, J., Fowler, C., & Emery, W. (2011). Distribution and trends in Arctic Sea ice age through spring 2011. *Geophysical Research Letters, 38*. https://doi.org/10.1029/2011GL047735.

Marcoval, M. A., Villafane, V. E., & Helbling, E. W. (2007). Interactive effects of ultraviolet radia-tion and nutrient addition on growth and photosynthesis performance of four species of marine phytoplankton. *Journal of Photochemistry and Photobiology B: Biology, 89*, 78–87. https://doi.org/10.1016/j.jphotobiol.2007.09.004.

Marquard, M., Majaneva, S., Pitusi, V., & Søreide, J. E. (2018). Pan-Arctic distribution of the hydrozoan *Sympagohydra tuuli*? First record in sea ice from Svalbard (European Arctic). *Polar Biology, 41*, 583–588.

McConnell, B., Gradinger, R., Iken, K., & Bluhm, B. (2012). Growth rates of arctic juvenile *Scolelepis squamata* (Polychaeta: Spionidae) isolated from Chukchi Sea fast ice. *Polar Biology, 35*, 1487–1494.

Meiners, K. M., & Michel, C. (2017). Dynamics of nutrients, dissolved organic matter and exo-polymers in sea ice. In D. N. Thomas (Ed.), *Sea Ice* (3rd ed., pp. 415–432). Chichester, 652 pp: Wiley Blackwell. https://doi.org/10.1002/9781118778371.ch17.

Michel, C., Nielsen, T. G., Nozais, C., & Gosselin, M. (2002). Significance of sedimentation and grazing by ice micro- and meiofauna for carbon cycling in annual sea ice (northern Baffin Bay). *Aquatic Microbial Ecology, 30*, 57–68.

Mikkelsen, D. M., Rysgaard, S., & Glud, R. N. (2008). Microalgal composition and primary production in Arctic Sea ice: A seasonal study from Kobbefjord (Kangerluarsunnguaq), West Greenland. *Marine Ecology Progress Series, 368*, 65–74. https://doi.org/10.3354/meps07627.

Mikkelsen, D. M., & Witkowski, A. (2010). Melting Sea ice for taxonomic analysis: A comparison of four melting procedures. *Polar Research, 29*, 451–454. https://doi.org/10.1111/j.1751-8369.2010.00162.x.

Mock, T., & Gradinger, R. (1999). Determination of Arctic algal production with a new in situ incubation technique. *Marine Ecology Progress Series, 177*, 15–26. https://doi.org/10.3354/meps177015.

Mundy, C. J., Gosselin, M., Ehn, J. K., Belzile, C. M., Poulin, M., Alou, E., Roy, S., Hop, H., Lessard, S., Papakyriakou, T. N., Barber, D. G., & Stewart, J. (2011). Characteristics of two distinct high-light acclimated algal communities during advanced stages of sea ice melt. *Polar Biology, 34*, 1869–1886. https://doi.org/10.1007/s00300-011-0998-x.

Nicolaus, M., Katlein, C., Maslanik, J., & Hendricks, S. (2012). Changes in Arctic Sea ice result in increasing light transmittance. *Geophysical Research Letters, 39*. https://doi.org/10.1029/2012GL053738.

Olsen, L. M., Laney, S. M., Duarte, P., Kauko, H. M., Fernández-Méndez, M., Mundy, C. J., Rösel, A., Meyer, A., Itkin, P., Cohen, L., Peeken, I., Tatarek, A., Różańska-Pluta, M., Wiktor, J., Taskjelle, T., Pavlov, A. K., Hudson, S. R., Granskog, M. A., Hop, H., & Assmy, P. (2017). The seeding of ice algal blooms in Arctic pack ice: The multiyear ice seed repository hypothesis. *Journal of Geophysical Research, 122*, 1529–1548. https://doi.org/10.1002/2016JG003668.

Piiparinen, J., Enberg, S., Rintala, J.-M., Sommaruga, R., Majaneva, M., Autio, R., & Vähätalo, A. V. (2015). The contribution of mycosporine-like amino acids, chromophoric dissived organic matter and particles to the UV protection of sea-ice organisms in the Balt Sea. *Photochemical and Photobiological Sciences, 14*, 1025–1038. https://doi.org/10.1039/c4pp00342j.

Petrich, C., & Eicken, H. (2017). Overview of sea ice growth and properties, 1-41. In D. N. Thomas (Ed.), *Sea Ice* (3rd ed., p. 652). Chichester: Wiley Blackwell. https://doi.org/10.1002/9781118778371.ch1.

Piraino, S., Bluhm, B. A., Gradinger, R., & Boero, F. (2008). *Sympagohydra tuuli* gen. nov. and sp. nov.. (Cnidaria: Hydrozoa) a cool hydroid from the Arctic Sea ice. *Journal of the Marine Biological Association of the United Kingdom, 88*, 1637–1642. https://doi.org/10.1017/s0025315408002166.

Polashenski, C., Perovich, D., & Courville, Z. (2012). The mechanisms of sea ice melt pond formation and evolution. *Journal of Geophysical Research, 117*. https://doi.org/10.1029/2011JC007231.

Ralph, P. J., Ryan, K. G., Martin, A., & Fenton, G. (2007). Melting out of sea ice causes greater photosynthetic stress in algae than freezing in. *Journal of Phycology, 43*, 948–956. https://doi.org/10.1111/j.1529-8817.2007.00382.x.

Raven, J. (1993). Limits on growth rate. *Nature, 361*, 209–210.

Riebesell, U. (1991). Particle aggregation during a diatom bloom. I. Physical aspects. *Marine Ecology Progress Series, 69*, 273–280. https://doi.org/10.3354/meps069273.

Rózańska, M., Poulin, M., & Gosselin, M. (2008). Protist entrapment in newly formed sea ice in the coastal Arctic Ocean. *Journal of Marine Systems, 74*, 887–901. https://doi.org/10.1016/j.jmarsys.2007.11.009.

Ryan, K. G., Ralph, P. J., & McMinn, A. (2004). Acclimation of Antarctic bottom-ice algal communities to lowered salinities during melting. *Polar Biology, 27*, 679–686. https://doi.org/10.1007/s00300-004-0636-y.

Rysgaard, S., Glud, R. N., Sejr, M. K., Blichner, M. E., & Stahl, H. J. (2008). Denitrification activity and oxygen dynamics in Arctic Sea ice. *Polar Biology, 31*, 527–537. https://doi.org/10.1007/s00300-007-0384-x.

Siebert, S., Anton-Erxleben, F., Kiko, R., & Kramer, M. (2009). *Sympagohydra tuuli* (Cnidaria, hydrozoa): First report from sea ice of the Central Arctic Ocean and insights into histology, reproduction and locomotion. *Marine Biology, 156*, 541–554. https://doi.org/10.1007/s00227-008-1106-9.

Søgaard, D. H., Hansen, P. J., Rysgaard, S., & Glud, R. N. (2011). Growth limitation of three Arctic Sea ice algal species: Effects of salinity, pH, and inorganic carbon availability. *Polar Biology, 34*, 1157–1165. https://doi.org/10.1007/s00300-011-0976-3.

Søgaard, D. H., Thomas, D. N., Rysgaard, S., Glud, R. N., Norman, L., Kaartokallio, H., Juul-Pedersen, T., & Geilfus, N.-X. (2013). The relative contributions of biological and abiotic process to carbon dynamics in subarctic sea ice. *Polar Biology, 36*, 1761–1777. https://doi.org/10.1007/s00300-013-1396-3.

Søreide, J. E., Leu, E., Berge, J., Graeve, M., & Falk-Petersen, S. (2010). Timing of blooms, algal food quality and Calanus glacialis reproduction and growth in a changing Arctic. *Global Change Biology, 6*, 3154–3163. https://doi.org/10.1111/j.1365-2486.2010.02175.x.

Sørensen, L. L., Jensen, B., Glud, R. N., McGinnis, D. F., Sejr, M. K., Sievers, J., Søgaard, D. H., Tison, J. L., & Rysgaard, S. (2014). Parameterization of atmospheric-surface exchange of CO_2 over sea ice. *The Cryosphere, 8*, 853–866. https://doi.org/10.5194/tc-8-853-2014.

Szymanski, A., & Gradinger, R. (2016). The diversity, abundance and fate of ice algae and phytoplankton in the Bering Sea. *Polar Biology, 39*, 309–325. https://doi.org/10.1007/s00300-015-1783-z.

Taraldsvik, M., & Myklestad, S. M. (2000). The effect of pH on the growth rate, biochemical composition and extracellular carbohydrate production of the marine diatom *Skeletonema costatum. European Journal of Phycology, 35*, 189–194. https://doi.org/10.1080/09670260010001735781.

Tedesco, L., Vichi, M., & Thomas, D. N. (2012). Process studies on the ecological coupling between sea ice algae and phytoplankton. *Ecological Modelling, 226*, 120–138. https://doi.org/10.1016/j.ecolmodel.2011.11.011.

Thomas, D. N., Kattner, G., Engbrodt, R., & Gianelli, V. (2001). Dissolved organic matter in Antarctic Sea ice. *Annals of Glaciology, 33*, 297–303. https://doi.org/10.3189/172756401781818338.

Webster, M. A., Rigor, I. G., Perovich, D. K., Richter-Menge, J. A., Polashenski, C. M., & Light, B. (2015). Seasonal evolution of melt ponds on Arctic Sea ice. *Journal of Geophysical Research, 120*, 5968–5982. https://doi.org/10.1002/2015JC011030.

Chapter 5
Sea Ice in a Climate Change Context

Abstract This chapter is a description of the role and importance of sea ice and sea ice biota on large scales and in relation to the effects of climate change. The decrease in summer sea ice extent and thickness are evident and described in (5.1). A Case Study 4 based on our observations in the Fram Strait and the Arctic Ocean illustrates some of the consequences and effects of increased inflow of warm Atlantic water (5.2). The question whether more light in an ice-free water column will increase pelagic primary production in the Arctic Ocean, is addressed with a model (5.3). Sea ice plays an important role in the exchange of CO_2 between ocean and atmosphere and the sea ice CO_2 pump is described in (5.4).

Keywords Effects of climate change · Ice extent · Atlantification · Primary production · CO_2

5.1 The Decrease in Arctic Sea Ice Extent and Thickness

Data on sea ice extent covering the entire Arctic Ocean first became available in 1979 when passive microwave remote sensing by satellites was developed (Wang and Overland 2009; Serreze et al. 2007). The Arctic sea ice extent varies annually between a maximum range of 14.3–16.3 million km² in March and a minimum range of 7.7–4.7 million km² in September, showing that about 8 million km² of sea ice melts every summer and develops again during autumn and winter. This is close to the area of Australia (7.7 million km²). Figure 5.1a–b shows the maximum and minimum sea-ice extent on 18 March and 16 September 2012. The sea ice extent recorded in September 2012 was the lowest seasonal minimum extent ever recorded with satelites (Fig 5.1). Comparison of the September minimum sea ice extent and the bathymetry of the Arctic Ocean shows that it is the more shallow water (<200 m) shelf areas that are ice-free in summer. The large and extensive shelf areas are characteristic features of the Arctic Ocean where about half of the ocean seabed consists of shelf areas (Jakobsson 2016), potentially rich in oil and gas (Gautier et al. 2009). Sea ice extent varies annually and gradually between a maximum and minimum extent, as shown in a plot of year versus sea ice extent with maximum in March and minimum in September for the period 1979–2018 (Fig. 5.2a). Trend lines of annual maximum (March) and minimum (September) sea ice extent between 1979 and
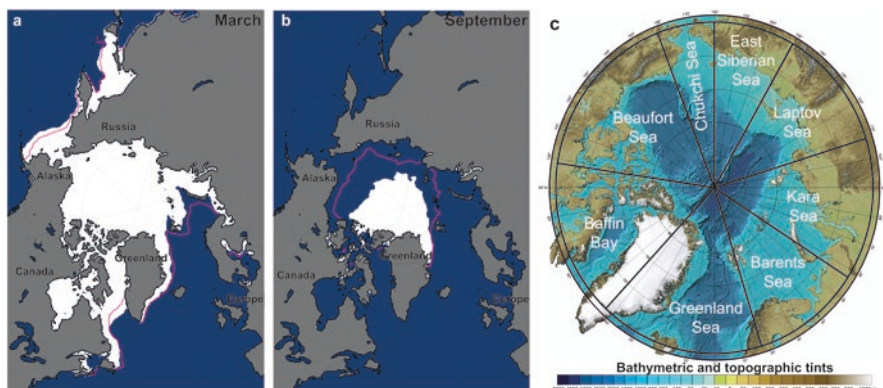
Fig. 5.1 Sea ice extent on 18 March 2012 (**a**), and 16 September 2012 (**b**), where the magenta line is the median (1979–2000) sea ice extent (Courtesy: National Snow and Ice Data Center, Boulder, Colorado, USA http://nsidc.org/arcticseaicenews/2012/09/), and bathymetric map of the Arctic Ocean and the different sections referred to in the text (**c**)

2018 demonstrate a clear decrease during September of about 0.082 million km^2 per year or 3.2 million km^2 between 1979 and 2018 (Fig. 5.2b). The loss in March sea ice extent was half that, about 0.042 million km^2 per year equal to 1.6 million km^2, and demonstrates that the loss in sea ice extent is highest in September. The trend line for the September extent is: y = − 0.082 · x + 170.5 (Fig. 5.2a), which gives an ice-free Arctic Ocean in about 2080 if the decrease continues unabated. Longer time-series (1950–2015) from a high Arctic fjord, Young Sound in NE Greenland also show a significantly decreasing trend in the number of days with sea ice and thus, a corresponding longer open-water period is observed (Fig. 5.3). The loss in number of days with sea ice in this Young Sound area appears to be related to increased summer temperatures (Glud et al. 2007), which implies that the seasonal length of the ice–free period of this Arctic site has increased due to later freeze-up (Fig. 5.3). This also agrees with observations of later freeze-up from other Arctic sites (Parkinson 2014). A longer open-water period also results in an increasing potential for pelagic primary production, which agrees with estimates from remote sensing analysis of ocean colour that indicate a 30% increase in pelagic primary production between 1998–2009 in the Arctic Ocean (Arrigo and Dijken 2011). However, these trends vary between regions and the differences in increased pelagic production largely depend on the balance between the effects of sea ice decline, surface stratification, mixing and upwelling, and light conditions (Barber et al. 2015). Concomitant with a decrease in sea ice extent and ice cover duration in the Arctic, there has been a decrease in the thickness of the sea ice from an average of 3.5 m in November 1980 to about 2 m in November 2005 (Kwok and Rothrock 2009) and a parallel decrease in the age of the sea ice. The extent of multi-year ice defined as ice that survives one or more summer melts, was reduced by nearly 50% between 1999 and 2017 (Kwok 2018) with a decrease in coverage from about 22% in 1983 to about 5% in 2014 for multiyear ice >4 years. For multiyear ice >1 year
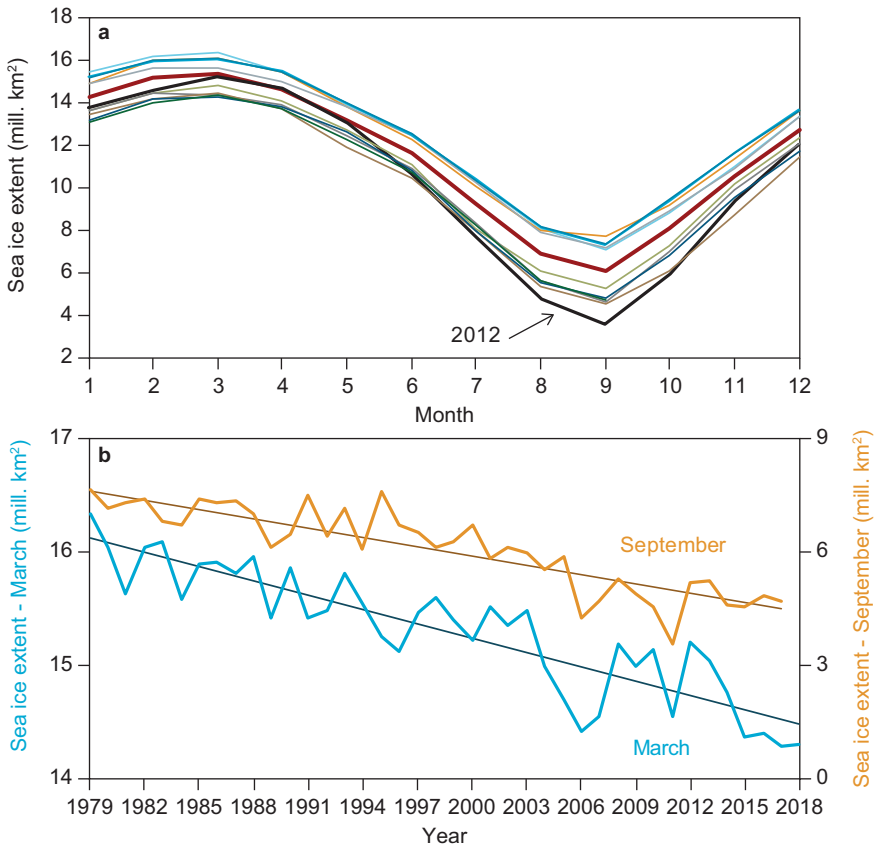
Fig. 5.2 Annual variation between maximum sea ice extent in March and minimum in September comprising the period 1979–2018 where the year 2012 with the lowest minimum is marked, and bold red line represents the average for the period (**a**), and the minimum sea ice extent in September and maximum sea ice extent in March for each of the years 1979-2018 with trend lines. Note different ordinate scales for the maximum (blue) and minimum (orange) sea ice extent (**b**). (Data available at: https://nsidc.org/arcticseaicenews/sea-ice-tools/)

the coverage decreased from about 60% in 1983 to about 40% in 2014 (Fig. 5.4). The air temperature is increasing in the Arctic, and the increase is higher here than for the global average. The Arctic here refers to the area between latitudes 60 and 90°N, and the temperature anomaly, defined as the deviation from an average, is much higher in the Arctic than the global average (Fig. 5.5). The increase in air temperature reduces the growth of the sea ice, reinforcing the later autumn freeze-up, and enhances its melting. The significant decrease in summer sea ice extent and ice thickness are generally linked to the increase in air temperatures and secondly the increase in upper water column temperatures (Lindsay and Zhang 2005). There are, however, additional factors that also explain the decrease in summer sea ice extent. The lowest minimum extent observed until now was in September 2012
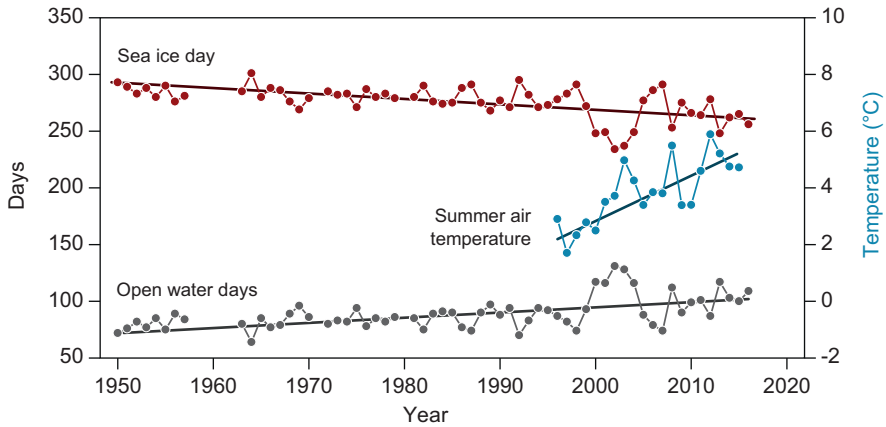
Fig. 5.3 The average sea ice days (red dots) and open water days (black dots) (1950-2015) and average summer air temperatures (blue dots) (1997-2015) in Young Sound, NW Greenland. (Modified from: Rysgaard and Glud 2007)
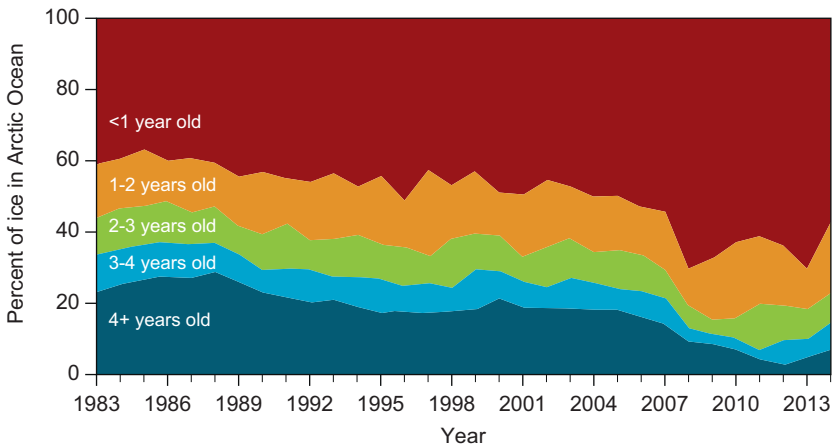
Fig. 5.4 The extent of sea ice as age groups: <1y, 1-2y, 2-3y, 3-4y, +4y at the end of summer between 1983 and 2014 in the Arctic Ocean. (Courtesy: Tschudi M. and Stewart S., University of Colorado, Boulder; Meiner W. and Stroeve J., NSIDC, http://nsidc.org/arcticseaicenews/2014/04/arctic-sea-ice-at-fifth-lowest-annual-maximum/)

(Fig. 5.2) and was related to extraordinary strong Arctic winds which transported large amounts of sea ice out of the Arctic Ocean through the Fram Strait (Zhang et al. 2013), eventually melting in the Fram Strait on its path south with the East Greenland current (Smedsrud et al. 2017). The general circulation of the Arctic Ocean comprises of a circular wind-driven current over the Canada Basin, termed the Beaufort Gyre, and a transpolar drift of ice and water from the Laptev and Kara Seas across the North Pole towards the Fram Strait (Fig. 5.6). The surface currents in the Arctic Ocean are colder and less saline, compared to the warm and saline
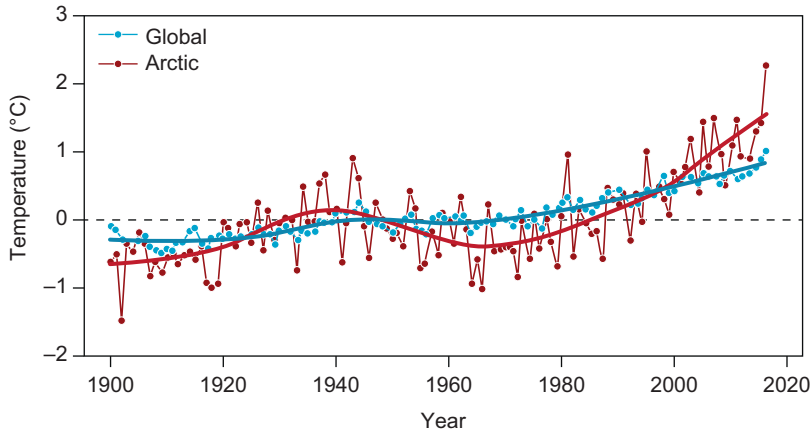
Fig. 5.5 Annual temperature anomaly in the Arctic (red dots with thin line) and average (red solid line), annual temperature anomaly in global temperatures (blue dots with thin line), and average (blue solid line) between 1900 and 2017. Data available at https://data.giss.nasa.gov/gistemp/

Atlantic water that flows into the Arctic Ocean, where it sinks beneath the polar surface waters (Jakobsson et al. 2004) but is still a surface current in the Fram Strait. There has been an increase in the volume inflow of warm Atlantic water to the Arctic Ocean which is termed "Atlantification" (Polyakov et al. 2017; Randelhoff et al. 2016), and it was demonstrated that the increased inflow limits the southward expansion of winter sea ice in the Barents Sea (Barton et al. 2018). Larger areas in the Barents Sea are then ice-free during winter driven by the increased inflow of Atlantic water, and demonstrated by a comparison of March and median 1979–2000 sea ice extent where the Barents Sea winter ice edge has moved north-east (Fig. 5.1a). The water budget for the Arctic Ocean shows a discharge of warm saline Atlantic water into the Arctic Ocean and the pathways of colder, and less saline waters, which leave the Arctic Ocean through the Fram Strait, Narres Strait, and Canadian Archipelago (Fig. 5.6). It is also foreseen that precipitation and thus freshwater discharges into the Arctic Ocean will increase in the future (Carmack et al. 2015), which will enhance stratification of the water column and inhibit the vertical exchange of nutrients (Sect. 5.3).

5.2   A Glimpse into a Future Arctic Ocean - Case Study 4

The summer season offers research possibilities in the Arctic, as the thawing ice allows icebreakers access to areas that are largely inaccessible in winter. Here, two icebreaker cruises highlight the conditions and abiotic stressors that the sea ice community experiences during summer in the Fram Strait, and early autumn in the central Arctic Ocean.

Fig. 5.6 Circulation and transport pathways of water masses in the Arctic Ocean, where red arrows signify warm and saline water from the Atlantic Ocean. This water sinks below the less saline surface waters influenced by freshwater outflow from large Russian rivers, and inflow through the Bering Strait. The Transpolar Drift (TD) transports ice and water from Laptev and Kara Sea towards the Fram Strait. *BC* Baffin Bay Current, *EGC* East Greenland current, *WGC* West Greenland Current, and *IrC* Irminger Current. (Modified from https://www.whoi.edu/main/topic/arctic-ocean-circulation)

5.2.1   Melting Sea Ice in the Fram Strait

Both the Fram Strait campaign and the Central Arctic Ocean campaign demonstrated the ecological consequences of melting of the sea ice and gave us a glimpse of what a future Arctic Ocean might look like. The purpose of the Fram Strait case study is also to highlight the strong west-east gradient (Randelhoff et al. 2018) in sea ice and ice algae conditions with the western section in the cold and low saline East Greenland Current, and eastern section in the warm saline Atlantic water (Fig. 5.6). As can be envisioned from the satellite image, there is a transport of ice out of the Arctic Ocean with the southward East Greenland current (Fig. 5.7). The annual amount of ice transported equals an area of about 500,000 km^2 and is
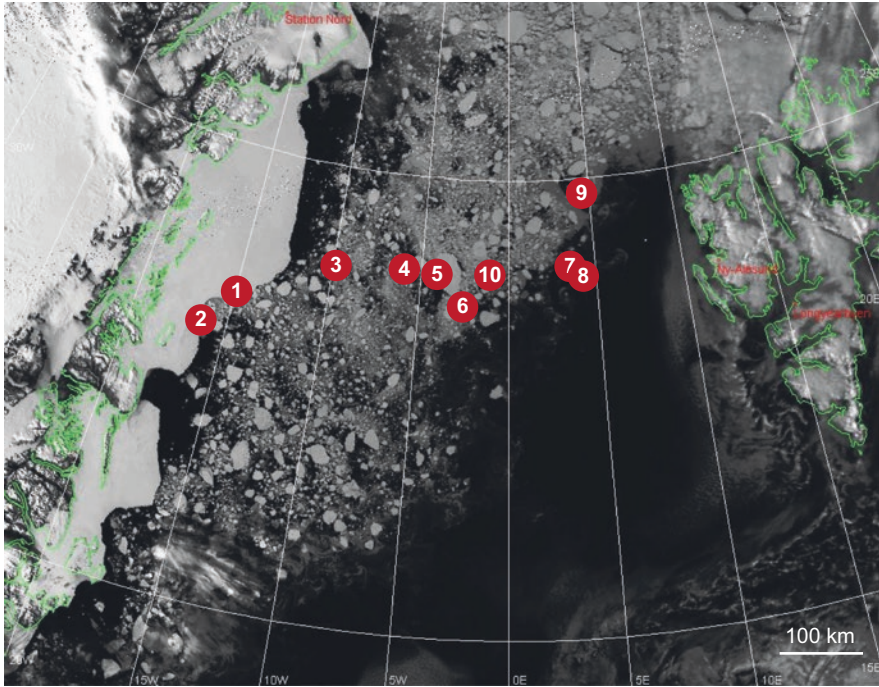
Fig. 5.7 Satellite image of sea ice conditions in the Fram Strait on 10 June 2014 with drifting pack ice, large ice-floes and land-fast ice at the east Greenland coast. The numbers refer to station numbers in the Fram Strait sea ice campaign. (Courtesy: NOAA/National Oceanic and Atmospheric Administration)

equivalent to 10% of the summer sea ice in the Arctic Ocean (Comiso et al. 2008). We sampled a transect of stations between East Greenland and Svalbard in June 2014 with stations 1 and 2 at land-fast ice stations, meaning that the ice was fixed in position and attached to land (Fig. 5.7), and stations 3–10 in the pack ice, which is free-floating floes of different sizes from km to m (Figs. 5.7 and 5.11). The floes can be packed together due to wind and currents and large ridges can develop (Fig. 5.11), and the mixture of land-fast and pack-ice floes are clearly reflected in the different ice thicknesses (2.80–0.65 m) with thin ice stations to the east (Fig. 5.8a). Transmittance was high at the thinner ice at stations 7 and 8, and also low in Chl a, and lower (< 0.25) in maximum quantum yield (F_v/F_m) compared to western stations (~ 0.5) (Figs. 5.8b–c and 5.9). Ice algae at the bottom of the two stations had, in comparison, the highest concentrations of Diadinoxanthin and Diatoxanthin (Dtx + Ddx) relative to Chl a at all stations. This demonstrates, that the ice algae at these stations started to adapt to the increased transmittance and higher light by developing sunscreen pigments (Dtx + Ddx) in the thinner ice as a response to melting from below in the warmer Atlantic water, with surface water temperatures of 1–2 °C compared to minus 1–2 °C at the western station 3 (Fig. 5.10b). With the increased inflow of warm Atlantic water (Polyakov et al. 2017) larger areas with ice in the Fram Strait would then be affected by warming and melting as observed here at stations 7 and 8, with significantly reduced ice algae biomass and low viability.
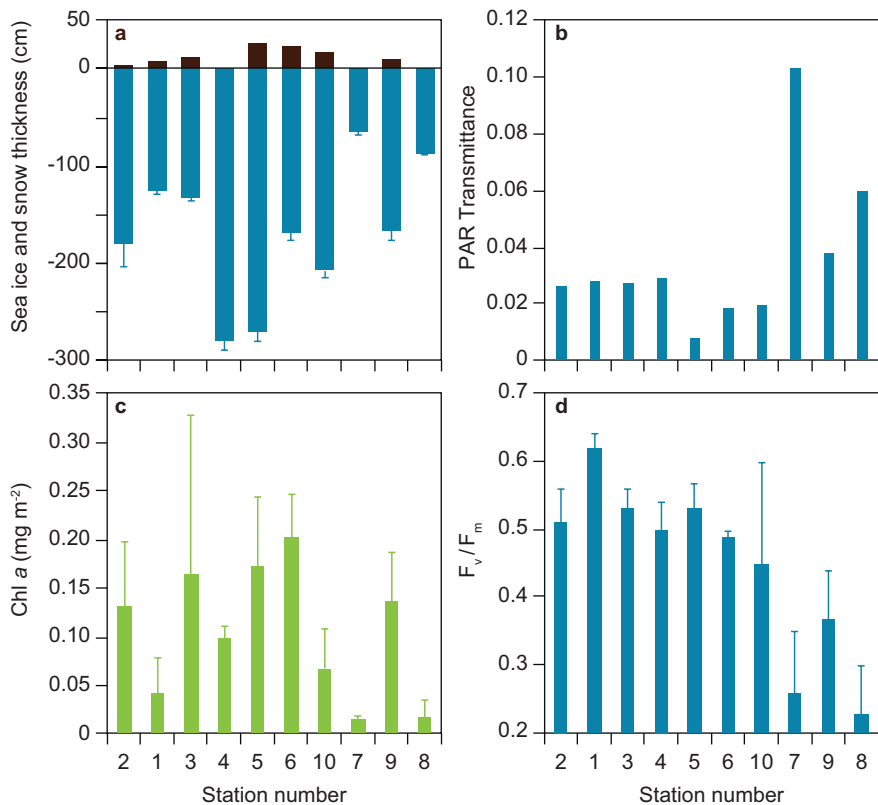
Fig. 5.8 Snow thickness (black bars) and sea ice thickness (blue bars) (**a**), PAR transmittance (**b**), Chl *a* concentration (**c**), and maximum quantum yield (F_v/F_m) (**d**) at stations 1 to 10 in June 2014 in the Fram Strait. Values are means with standard deviations

Fig. 5.9 Station 3 in the cold and low saline water originating from the Arctic Ocean and station 8 in the warm and high saline water flowing into the Arctic Ocean
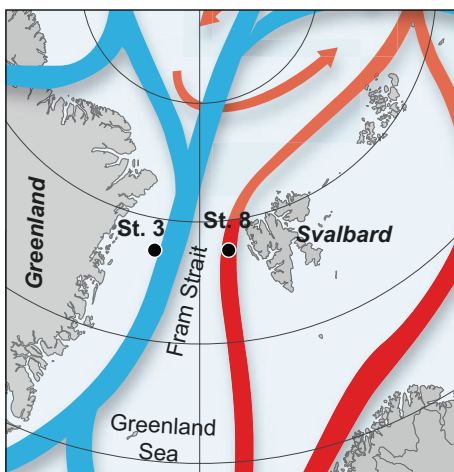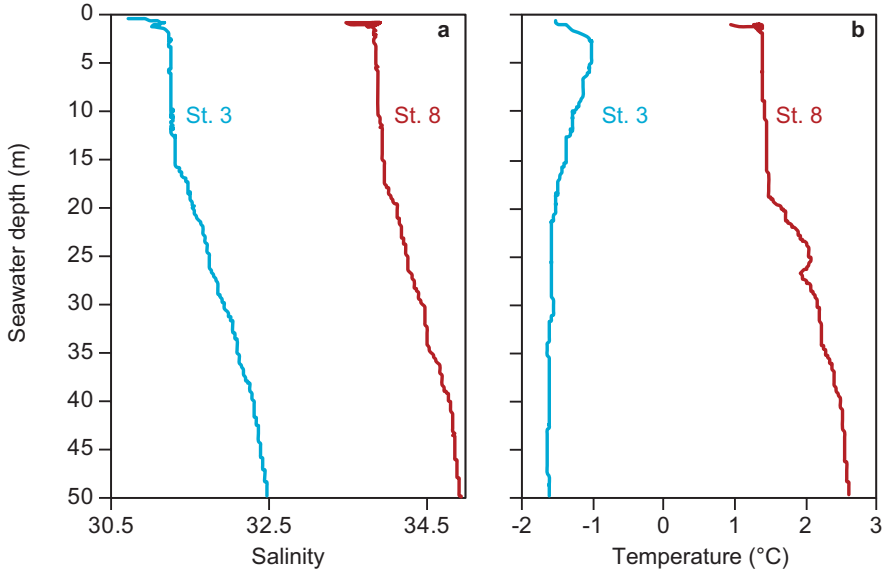
Fig. 5.10 Profiles of salinity (**a**), and temperature (**b**) with depth at stations 3 (blue line) and 8 (red line) in June 2014 in the Fram Strait

The west-east transect can be considered as a "space for time" concept where going from west to east (space) demonstrates the ecological consequences of melting of the sea ice with higher transmittances, and reduced biomass and viability. This will become the conditions at more sea ice sites in a future Arctic Ocean. Field work on the ice in the Fram Strait (Fig. 5.11).

5.2.2   Late and Future Arctic Ocean

There has been a gradual decrease in summer sea ice extent in the Arctic Ocean with a significant minimum in 2012 (Fig. 5.12a), where we participated in a research cruise in the Arctic Ocean on board the Swedish icebreaker *Oden*. A video shows *Oden* breaking heavy pack ice in the Amundsen Basin, Arctic Ocean. The purposes of this case study are to show and discuss the specific physiological conditions in the central of ice algae and related physical and optical properties at the end of summer in central Arctic Ocean. The ice algae was in very bad condition with low average maximum quantum yield *(F_v/F_m* = 0.33)* (Fig. 5.13a), but what was to reason for this? Is transmittance increasing in a thinner ice and are the algae photo-damaged, and how low are nutrient conditions? Sampling was focused on the western part of the Amundsen Basin in central Arctic Ocean >86°N (Fig. 5.12), where station numbers are Julian day, i.e. station 226 was sampled on 13 August. Ice types were a mixture of first-year and multi-year ice with an average thickness of 152 cm (Fig. 5.13a), and identified based on bulk salinity of the ice.

Fig. 5.11 Pressure ridges, sampling from ice floes and first-year ice, June 2014, Fram Strait. (Photographs by: Authors)

Lower salinities around 2–3 showed that the desalination processes of the ice had been active for a longer time period and indicative of a multi-year sea ice compared to first-year sea ice salinities around 5–7 (Warner et al. 2013; Lund-Hansen et al. 2015), and about 33% of the ice at stations were multi-year ice. Snow cover was absent in August/September, but transmittance in the ice was still comparatively low (0.05) (Fig. 5.13b), and with no difference in transmittance between first- or multi-year ice opposite to findings by Nicolaus et al. (2012). Ice algae occurred in very low (Chl $a < 0.05$ mg m^{-2}) concentrations at most stations (Figs. 5.13c–d and 5.14) and were strongly dominated by diatoms (~80%) half of which was *Nitzschia frigida*, a very common Arctic diatom (Fig. 5.15a). Our August/September sampling was the end of season, and it is likely that ice algae were photodamaged after being exposed to 24 h of sunlight during summer months, but nutrient concentrations in the water were also low, e.g. nitrate (< 0.5 NO$_3^-$ μmol L^{-1}) (Fig. 5.15a), which might have affected conditions of the algae. Accordingly, a higher maximum quantum yield of the phytoplankton of 0.58 in the water below the ice compared to the ice algae (0.33) could reflect that phytoplankton is mixed up and down along light gradients and not fixed in position below the ice and exposed to perpetual light all through the summer. Ice thickness in the Arctic Ocean, north of Svalbard, has decreased about 0.5 m over the last 10 years (Kwok 2018) driven by the observed increase in Arctic air temperatures (Kurtz et al. 2014). A thinner ice with no snow cover will increase transmittance as observed in the Fram Strait which, in the future could have further negative consequences for the low light adapted ice algae in an environment of perpetual summer light as the Arctic Ocean.
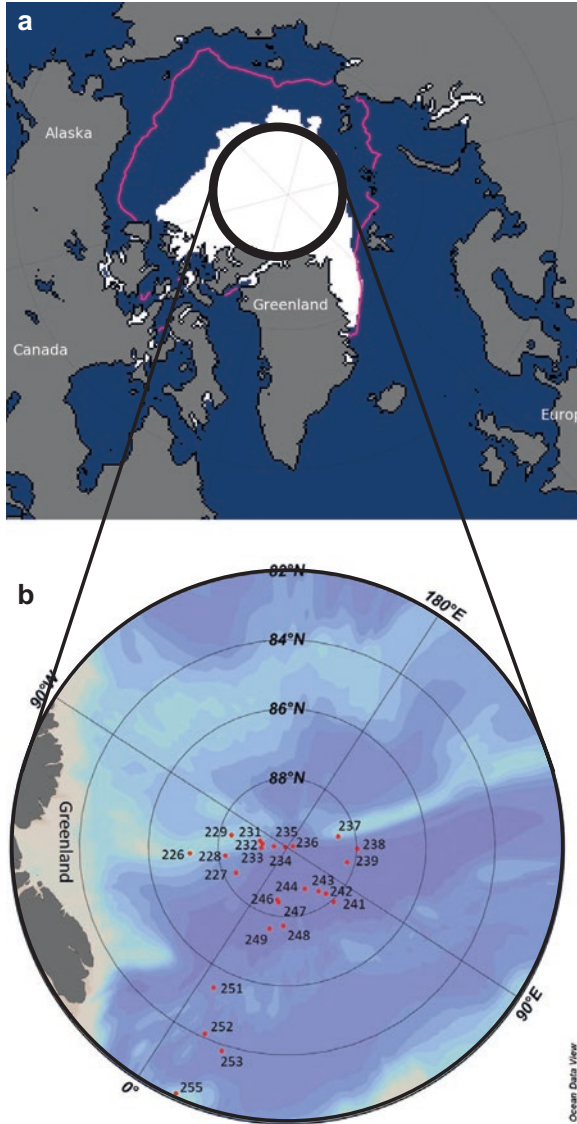
Fig. 5.12 Sea ice extent on 16 September 2012 (**a**), where the magenta line is the median (1979-2000) sea ice extent. (Courtesy: National Snow and Ice Data Center, Boulder, Colorado, USA http://nsidc.org/arcticseaicenews/2012/09/), and bathymetric map of the Arctic Ocean with LOMROG III sea ice stations (**b**). (Modified from: Lund-Hansen et al. 2015)

5.3   Pelagic Primary Production Increase in Future Ice-Free Central Arctic Ocean?

Sea ice extent in the Arctic Ocean has decreased significantly during nearly four decades and is predicted to decrease as described above. The transition from a state with ice cover to a state of open water and its governing parameters is
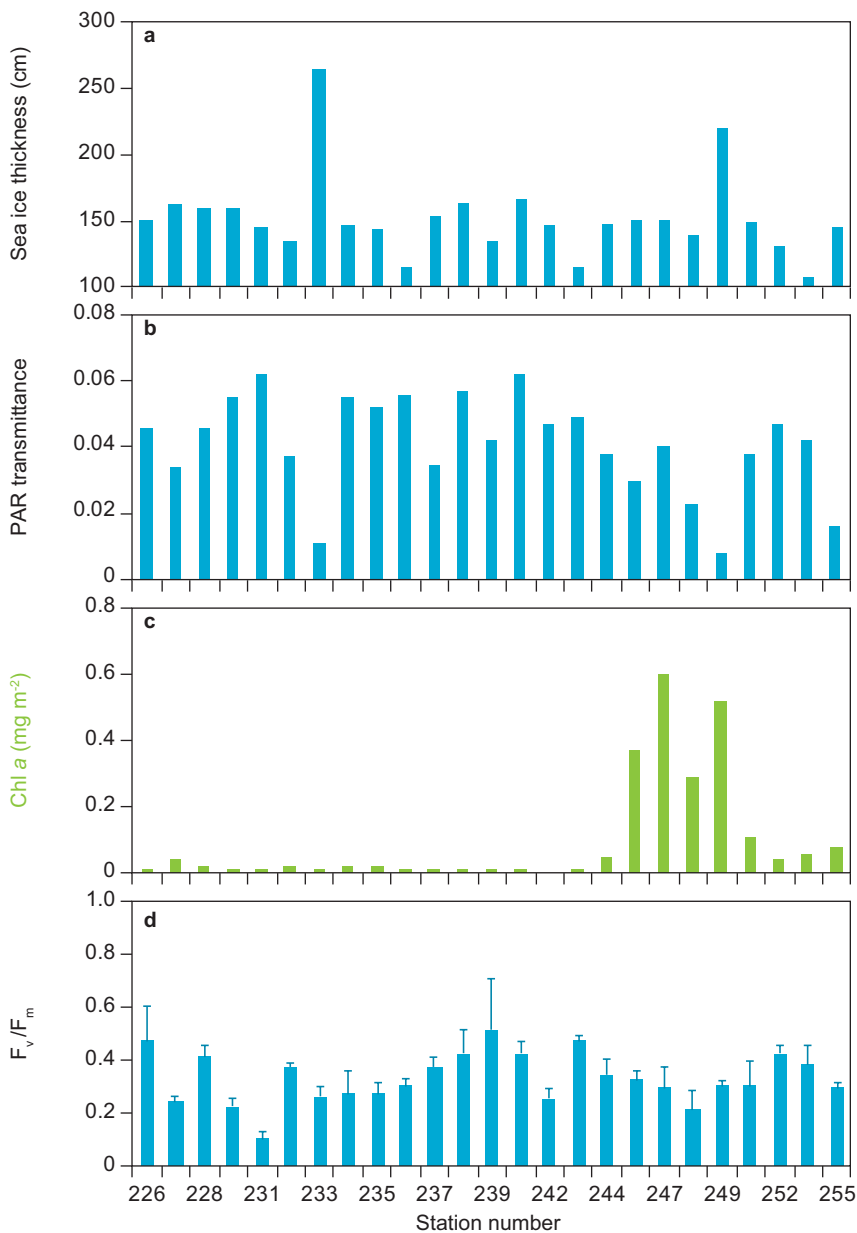
Fig. 5.13 Sea ice thickness (cm) (**a**), PAR transmittance (**b**), Chl *a* concentration (**c**), and maximum quantum yield (F_v/F_m) (**d**) at sea ice stations in August-September 2012, LOMROG III stations. Station numbers refer to Julian day. (Modified from: Lund-Hansen et al. 2015)

Fig. 5.14 Maximum quantum yield (F_v/F_m) in sea ice and seawater just below the ice, August-September 2012 at LOMROG III stations. (Modified from: Lund-Hansen et al. 2015)
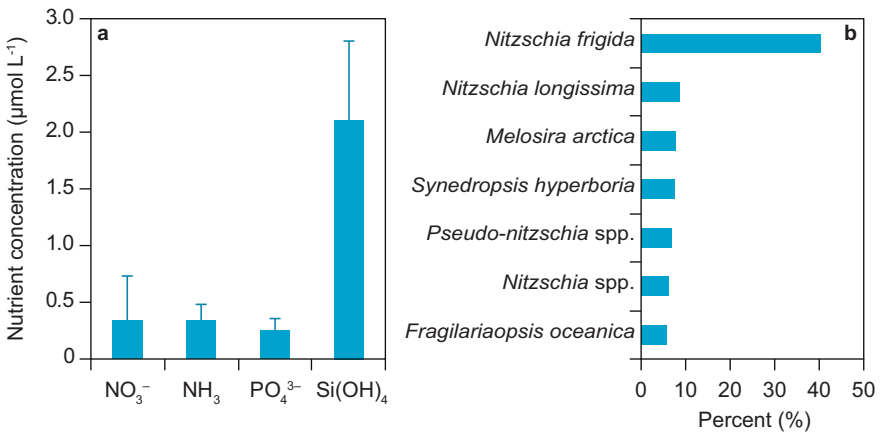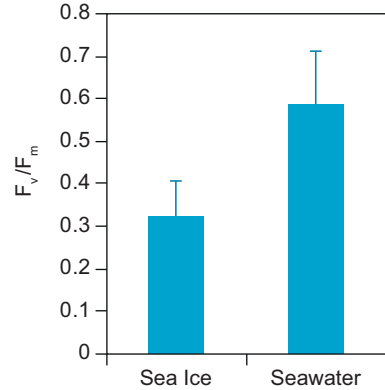
Fig. 5.15 Average concentrations of nitrate, ammonium, phosphate and silicic acid in seawater just below ice (**a**), and abundances of dominant ice algae in ice bottom, August-September 2012, LOMROG III stations (**b**). (Modified from: Lund-Hansen et al. 2015)

conceptualized in Fig. 5.16. The ice-free water column will be exposed to winds and significantly higher irradiances with a water albedo of 0.1 compared to 0.6 for ice, and up to 0.8 if the ice is snow-covered. Wind exposure will induce mixing of the water column, whereby nutrients deeper in the water column can reach the surface and become available in the light-exposed surface waters. A question of high interest from a biological point of view is how the decrease in sea ice extent will affect the pelagic primary production in the Arctic Ocean? This is a question also of economic interest, as a higher primary production will result in higher secondary production and ultimately larger fish stocks and greater fisheries. Note that the conceptualization is simplified, as sea ice cover varies locally with larger and smaller leads (Fig. 5.17) (Assmy et al. 2017). Anyway, rates of primary production can be measured directly by applying the ^{14}C method (Sect. 6.6), but satellite-based remote sensing techniques are often applied to estimate primary production rates for extensive areas that are difficult to access. Basically, the techniques rely on the
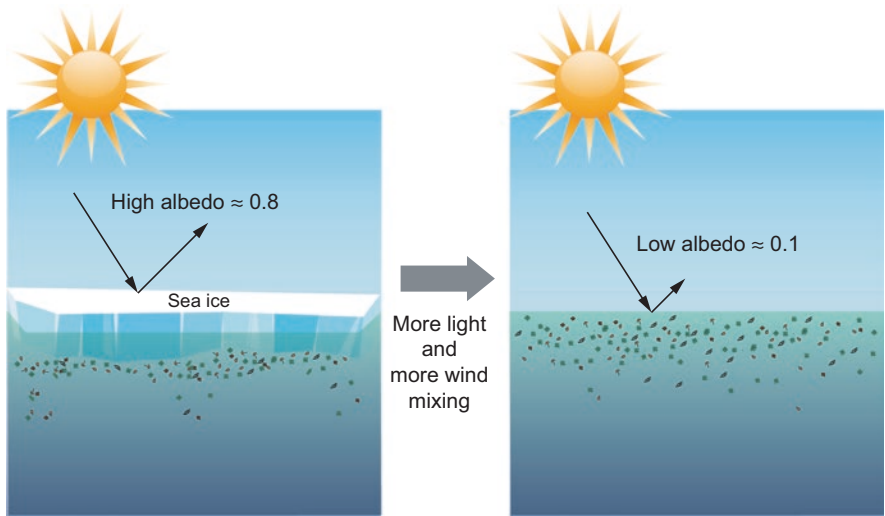
Fig. 5.16 Change of Arctic Ocean marine conditions with and without a sea ice cover – increased light in the water column and increased wind mixing

Fig. 5.17 Photo of sea ice, leads, and melt ponds near the North Pole, August 2012 from a helicopter. (Photograph by: Authors)
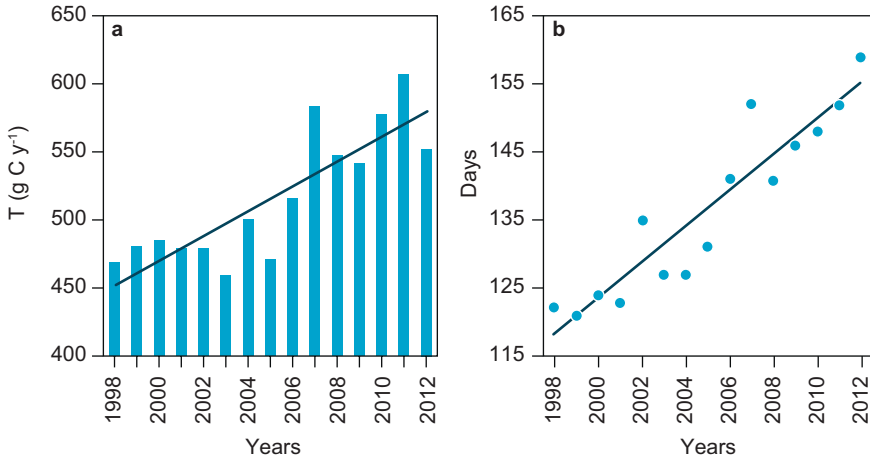
Fig. 5.18 Annual net primary production (**a**), and length of open water period (**b**) between 1998 and 2012 in the Arctic Ocean. (Modified from: Arrigo and Dijken 2015)

assumption that a high Chl *a* concentration in the water presupposes a high primary production (Pabi et al. 2008). An equation is subsequently developed based on *in situ* measured primary production and Chl *a* concentrations, and the satellite-measured Chl *a* signal is then converted into a primary production (Arrigo et al. 2008; Arrigo and Dijken 2015). Application of this method has demonstrated that net primary production (NPP), i.e., gross primary production minus respiration, has increased significantly from 460 Tg C year^{-1} to 560 Tg C year^{-1} between 1998 and 2012 in the Arctic Ocean (Fig. 5.18a). Satellite-based primary production rates are then scaled up with the size of the area and production time, as for areas with several months in darkness. Apart from irradiance there are additional parameters that influence primary production such as nutrients, grazing, and stratification (Popova et al. 2012), but it appeared that a longer period of higher irradiance could explain the observed increases in NPP in the Arctic Ocean (Arrigo and Dijken 2015). The 21% increase in NPP correlates with a longer open water period, which has increased by more than a month from about 120 days (4 months) to 160 days (5.3 months) between 1998 and 2012 (Fig. 5.18b). The increase of about 100 Tg C year^{-1} compares to the entire carbon production of the Barents Sea of 129 Tg C year^{-1} in 2012 as the most productive shelf in the study (Arrigo and Dijken 2011). An average NPP increase of 21% conceals some significant regional differences between the shelves, ranging from 8.3% in Baffin Bay to 112.4% in the Laptev Sea. The Greenland Sea experienced, in comparison, a significant decrease in NPP (Arrigo and Dijken 2011), see Fig. 5.1c for locations. The study of Arrigo and Dijken (2015) was focused on the now summer ice-free shelf areas, but how will primary production change in the central Arctic Ocean when this area becomes ice-free in the near future (Fig. 5.2)? To answer the question we need a more detailed look of the Arctic Ocean. It is surrounded by large continents with limited exchange of water through

the Bering and Fram Straits, and the Barents Sea (Fig. 5.1). It receives a large and increasing amount of freshwater from Russian and Canadian rivers (Peterson et al. 2002), where the freshwater and melting of ice establish the surface Polar Mixed Layer, a cold (*ca.* -1.6 °C) and low saline (30–33) layer up to 40 m thick. A strong halocline separates the Polar Mixed Layer from the deeper lying warm and saline water of Atlantic origin (Fig. 5.19). The central Arctic Ocean is different to the shelves with deeper waters, generally low wind speeds due to the atmospheric high pressure covering the central Arctic (Overland et al. 2012), no supply of nutrients from surrounding rivers (Blais et al. 2017) and an extensive sea ice cover. Current primary production rates below the ice in the central Arctic Ocean in August–September are about 20 mg C m^{-2} day^{-1} (Fernández-Méndez et al. 2015), but will rates here increase with an ice-free water column and higher irradiances as observed on the shelf areas? In spite of low wind speeds there will be an increased mixing of the water column. But will the mixing bring nutrients to the sun-lit surface waters (Lincoln et al. 2016; Randelhoff et al. 2016) to fuel primary production? To address these questions in detail and more thoroughly, Lund-Hansen et al. (2019) applied a physical numerical 1-D model for the central Arctic Ocean with an added model describing primary production driven by wind speed, irradiance, nutrients, and Chl *a* concentrations as initial conditions. The model calculated primary production rates below the sea ice and for an ice-free period where the ice was removed in the

Fig. 5.19 Vertical distribution of salinity (blue), Chl *a* (green), NO$_3^-$ (red), and PAR (red) below the ice in August 2012, Amundsen Basin, Arctic Ocean. (Modified from: Lund-Hansen et al. 2019)
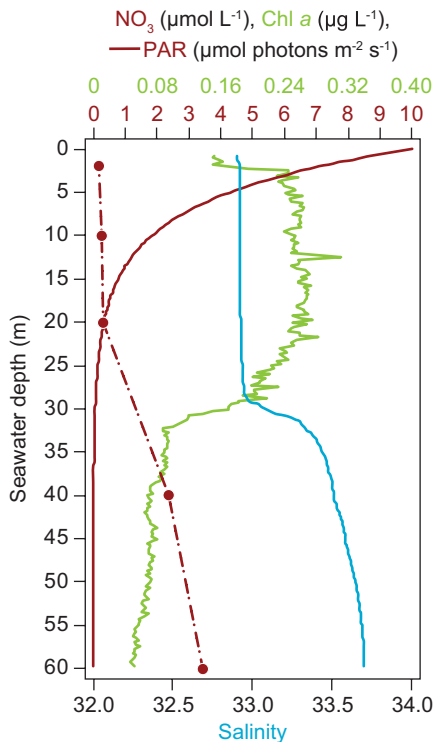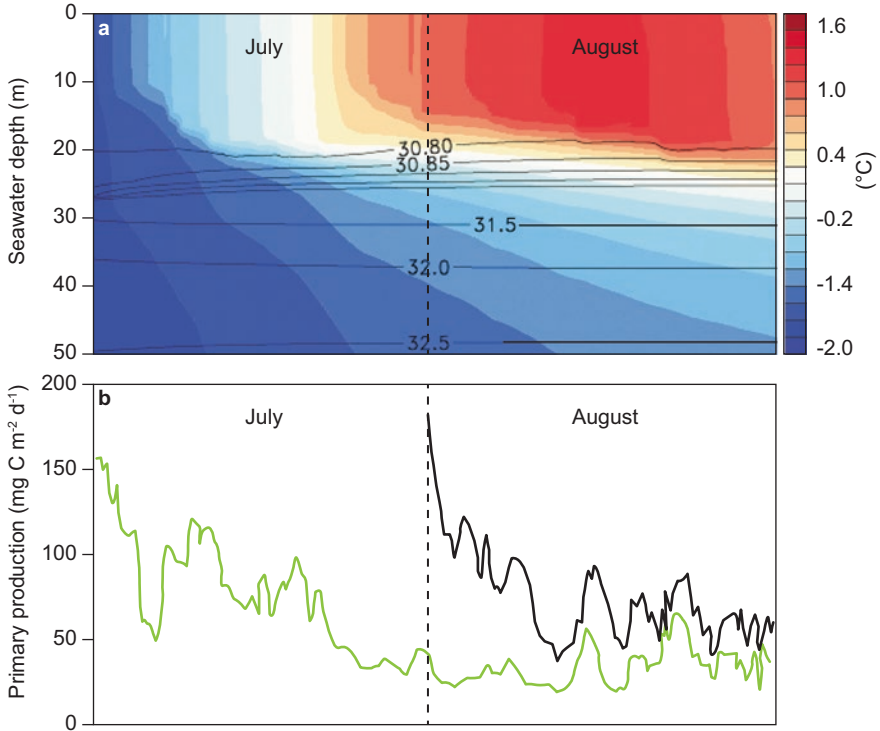
Fig. 5.20 Model results with depth vs temperature for the water column (0-50 m), with isohalines (salinity) during ice-free July and August (**a**), and primary production during July and August (green line) and only August (black line) (**b**). (Modified from: Lund-Hansen et al. 2019)

model. A typical under-ice CTD profile near the North Pole shows a strongly stratified water column with a low (33) surface layer salinity, which increases to 33.7 at 60 m depth. Irradiance is low (10.0 μmol photons m^{-2} s^{-1}) at the bottom of the ice, but there is still some (~0.3 μmol L^{-1}) nitrate (NO_3) in the surface layer where Chl *a* is also higher (0.24 mg Chl *a* m^{-3}) (Fig. 5.19). Primary production in the water column with ice was 3.9 mg C m^{-2} day^{-1}. The surface layer is close to being depleted of nitrate and production is mainly sustained by regenerated nutrients in the surface layer. The limiting factor for the primary production is here nutrients, but mixing of the water was strongly limited by the ice, and transport of nutrients as nitrate towards the surface layer was low. Model results showed that the temperature of the surface water increased by 3–4 °C when ice-free and exposed to more light, but salinity stratification was still maintained (Fig. 5.20a). This implies that open water and wind mixing was too weak to fully break down stratification, but wind mixing events transported some nutrients to the surface waters, as shown by the peaks in primary production in early and late July (Lund-Hansen et al. 2019) (Fig. 5.20b). The model shows that primary production is initially high after the ice melts but decreases over time. Total integrated primary production reached 37.4 mg C m^{-2}

day^{-1} in August and 55.2 mg C m^{-2} day^{-1} for July–August, which is higher, but still comparatively low. The 55.2 mg C m^{-2} day^{-1} equals 3.3 g C m^{-2} year^{-1} for a two-month period compared to the Barents Sea shelf production of 90 g C m^{-2} year^{-1} (Sakshaug 2004). The below-ice production of 3.9 mg C m^{-2} day^{-1} in the model is lower than the average 20.0 mg C m^{-2} day^{-1} measured in the same area (Fernandez-Méndez et al. 2015). However, productions of 37.4 mg C m^{-2} day^{-1} in August and 55.2 mg C m^{-2} day^{-1} for July-August are still higher. Primary production in the sea ice reached an average of 2.2 mg C m^{-2} day^{-1} in August–September (Fernández-Méndez et al. 2015), lower than the pelagic primary production. The model results demonstrate that an ice-free Arctic Ocean at latitudes >85°N will therefore not add significantly to overall Arctic marine primary production, predominantly due to the strong stratification of the water column. This stratification will only increase with higher precipitation and riverine discharges. The observed higher shelf production is because of a longer open water period at lower latitutes (Fig. 5.1), and therefore a stronger wind mixing in these areas transporting nutrients to the sun-lit surface waters (Randelhoff et al. 2016).

5.4   Sea Ice Driven CO_2 Uptake

This section briefly describes the drivers of inorganic carbon dynamics in sea ice and illustrates that sea ice can function as a CO_2 pump that draws CO_2 from the atmosphere into the ocean. The main driver of climate warming is the accumulation of CO_2 and other greenhouse gases in the atmosphere. The atmospheric concentration of CO_2 has increased from a preindustrial value of about 280 ppm to about 410 ppm (August 2019). Fortunately, the global oceans play an important role in buffering the effects of CO_2 emissions to the atmosphere by absorbing large amounts of the emitted CO_2 (approximately 30%; Sabine et al. 2012). Until recently, the role of sea ice-covered regions in ocean-atmosphere CO_2 exchange was assumed to be insignificant, because sea ice has been treated as an impermeable barrier to the exchange of CO_2 (Tison et al. 2002). However, scientists now know that sea ice can affect the capacity of the polar oceans for taking up atmospheric CO_2. One of the first descriptions of the transport of CO_2 across the sea ice-ocean interface (i.e., the sea ice CO_2 pump) was by Jones and Coote (1981). Now, 39 years later, understanding the seasonal events controlling the inorganic carbon dynamics, including both abiotic and biotic processes in sea ice-covered regions, is still a challenging subject. An important question to address within this field of research is: what is the relative impact of abiotic and biotic processes on carbon cycling in sea ice and what is the effect of these sea ice processes on the ocean carbon system? During winter, as sea ice grows, some of the salts and gases present in the seawater are rejected, whereas the rest are trapped within the brine pockets, channels and tubes (Petrich and Eicken 2017) (Fig. 5.21). A reduction in sea ice temperature decreases the brine volume (Fig. 5.22) with a concurrent increase in brine salinity and concentrations of solutes and gases in the brine (Cox and Weeks 1983; Papadimitriou et al. 2004). In addition,
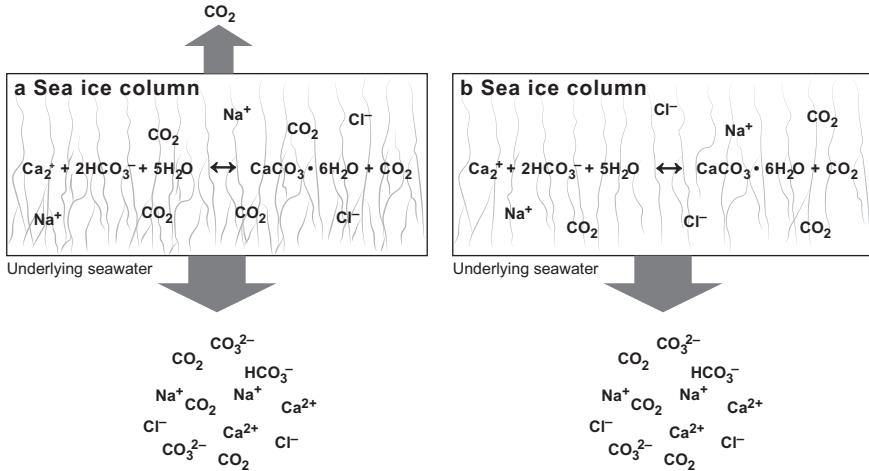
Fig. 5.21 Conceptual model of the fate of CO_2 in growing permeable sea ice (**a**), and cold impermeable sea ice (**b**)

Fig. 5.22 Thermal related evolution of the brine pore space as percent volume (P) at a set of temperatures (T). (Modified from: Pringle et al. 2009)
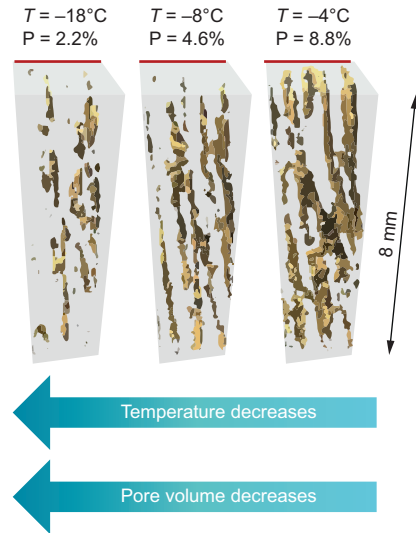
calcium carbonate ($CaCO_3$) can precipitate as brine temperatures decrease and solute concentrations increase. On the basis of thermodynamic equilibrium calculations, $CaCO_3$ precipitation was predicted to occur during natural sea ice formation (Assur 1960), which was later confirmed by observations: first in freezing seawater by Richardson (1976), then in artificial sea ice (Tison et al. 2002) and then finally observed in Antarctic and Arctic sea ice as ikaite crystals (Dieckmann et al. 2008, 2010). The precipitated ikaite crystals increase the amount of CO_2 in the brine beyond that attributed solely to the solubility effect. The ikaite crystals are trapped
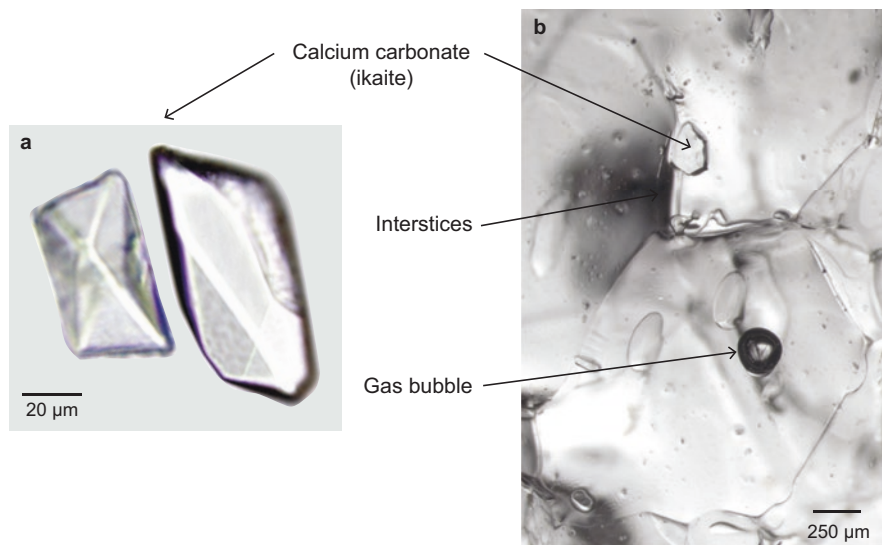
Fig. 5.23 Microscopic image of ikaite crystals at high magnification (**a**), and microscopic image of sea ice showing ice crystal borders, brine pockets, air bubbles and ikaite crystals (**b**). (Modified from: Rysgaard et al. 2013)

within the interstices between the ice crystals (Rysgaard et al. 2013; Fig. 5.23), whereas the CO_2 released through the ikaite production within the brine can be lost from the sea ice to both the atmosphere and the underlying water (Fig. 5.21). However, when the sea ice temperature reaches -5 °C and the ice becomes less permeable for fluid transport, sea ice-air gas exchanges are also reduced, and CO_2 is mainly lost from the sea ice to the underlying water column (Fig. 5.21). Therefore, as sea ice grows, brine drainage can lead to an export of gases from the sea ice, leaving sea ice depleted in CO_2 compared to ambient seawater (Rysgaard et al. 2009). Brine drainage from sea ice causes the formation of cold, highly saline and dense water that sinks to deeper ocean layers. Observations in the Arctic also suggest that CO_2 by brine drainage can be transported below the pycnocline and, subsequently, be incorporated into intermediate and deep–water masses (Rysgaard et al. 2011). However, the fate of the rejected CO_2 in the water column is still poorly understood. Another important process during winter is the formation of frost flowers. As described in Sect. 2.5, frost flowers and brine skim can develop on the surface of newly formed mm-thick sea ice in cold air temperatures and at low wind speeds. Very high ikaite concentrations have been observed in this high-salinity brine skim and frost flowers within an hour of formation (Barber et al. 2014). Frost flowers are extremely effective collectors of drifting snow on sea ice and, with time, can be integrated into the snow layer on top of the sea ice. Recent studies have indicated that the incorporation of ikaite from frost flowers into the snow cover, together with the CO_2 that is released during ikaite precipitation, may result in snow-driven CO_2 outgassing under high wind speeds above winter sea ice (Sievers et al. 2015). The

overall outcome of this process is a closed CO_2 loop, with snow-driven CO_2 release above the ice in winter and CO_2 uptake during spring due to undersaturation in CO_2 after ikaite dissolution (Rysgaard et al. 2013; Søgaard et al. 2019). Due to their unique growth processes, chemical composition and later integration into the snow layer on top of sea ice, frost flowers and brine skim provide an important link for ocean-ice-atmosphere interactions in the Arctic. Furthermore, these cold and salty structures can support an ecosystem with millions of microbes inside (Barber et al. 2014). The question is: are the bacteria inside these structures active, and are cold-loving algae also living in frost flowers? What is the relative impact of these microbial processes on the net CO_2 exchange? All these questions remain unclear. However, the areal extent and periodicity of frost flowers and brine skim are expected to increase due to later autumn freeze-up, and a higher prevalence of thin and more fragile first-year sea ice with more leads where frost flowers can develop after refreezing (Isleifson et al. 2014). This will have significant implications for the CO_2 exchange and biogeochemical processes operating between the ocean-ice-atmosphere interfaces in the Arctic Ocean.

In spring, the warming of sea ice is accompanied by reduced ice salinity, approaching zero salinity, because of internal ice melt and brine flushing due to the brine draining of meltwater from surface melt ponds. As the sea ice warms, dissolution of ikaite (ikaite dissolves at temperatures above 4 °C), autotrophic assimilation of CO_2 through ice algal photosynthesis, and dilution of brine by melting sea ice are all processes that decrease the pCO_2 of the brines. At this point, the sea ice is depleted in TCO_2 and potentially enriched in TA due to dissolution of ikaite, which will result in a decrease in pCO_2 of the under-ice water (Else et al. 2011). Once the sea ice has melted totally, the surface seawater is highly undersaturated with CO_2, which will lead to an increase in the ocean uptake of atmospheric CO_2 (e.g. Miller et al. 2011). As mentioned above, microbial processes in sea ice can also change the pCO_2 of the brine and ultimately of the surface waters. In general, sea ice algae take up CO_2 and nutrients during the spring bloom, whereas sea ice bacteria may release CO_2 throughout the entire sea ice season. It is very important to understand the significance of these sympagic processes and their effects on net CO_2 exchange. However, few combined measurements of bacterial and primary productivity exist for Arctic sea ice, making it very difficult to assess the spatial and temporal impacts and effects of these processes (Fig. 5.24). Typically, the annual succession of the sea ice organisms seems to follow a distinctive pattern, with a winter stage characterized by a low but net heterotrophic activity (Fig. 5.25). This shift in the balance towards a net heterotrophic community is also consistent with the high concentrations of DOC and DON in sea ice, and the observed accumulation of macronutrients in winter sea ice (Fig. 4.3). Several studies have observed that DOM and EPS can be enriched in sea ice and that active phosphate (Helmke and Weyland 1995) and nitrogen (Baer et al. 2015) remineralization by sea ice bacteria actually occurs. The observed accumulation of algal nutrients indicates not only low ice algal productivity (allowing nutrients to accumulate) but also that heterotrophic bacteria are the main source of biogenic CO_2 in winter sea ice. The autotrophic activity exceeds the heterotrophic activity (Fig. 5.25) once light levels in the sea ice pass a critical level

Chukchi Seas (land-fast ice)

Study	Bacterial production (µg C L^{-1} d^{-1})	Primary production (µg C L^{-1} d^{-1})
Baer et al. (2015)	0.33 ± 0.50	15.90 ± 36.50

Canadian Arctic (land-fast ice)

Study	Bacterial production (µg C L^{-1} d^{-1})	Primary production (µg C L^{-1} d^{-1})
Smith and Clement (1990)	1.65 ± 0.70	–

Central Canadian Arctic (land-fast ice)

Study	Bacterial production (µg C L^{-1} d^{-1})	Primary production (µg C L^{-1} d^{-1})
Nguyen and Maranger(2011)	10.25 ± 6.50	–

The Baltic Sea (land-fast ice)

Study	Bacterial production (µg C L^{-1} d^{-1})	Primary production (µg C L^{-1} d^{-1})
Kaartokallio et al. (2008)	4.08 ± 2.50	–
Kuosa and Kaartokallio (2006)	5.24 ± 3.30	78.50 ± 36.50
Mock et al. (1997)	5.60 ± 1.40	–

North East Greenland

Study	Bacterial production (µg C L^{-1} d^{-1})	Primary production (µg C L^{-1} d^{-1})
Søgaard et al. (2019)	1.95 ± 1.60	0.07 ± 0.09

South West Greenland (land-fast ice)

Study	Bacterial production (µg C L^{-1} d^{-1})	Primary production (µg C L^{-1} d^{-1})
Søgaard et al. (2010)	0.28 ± 0.15	0.30 ± 0.10
Søgaard et al. (2013)	1.80 ± 1.60	3.40 ± 5.80
Kaartokallio et al. (2013)	8.70 ± 12.20	–

Fig. 5.24 Sea ice bacterial and algal productivity compiled for different Arctic sea ice locations
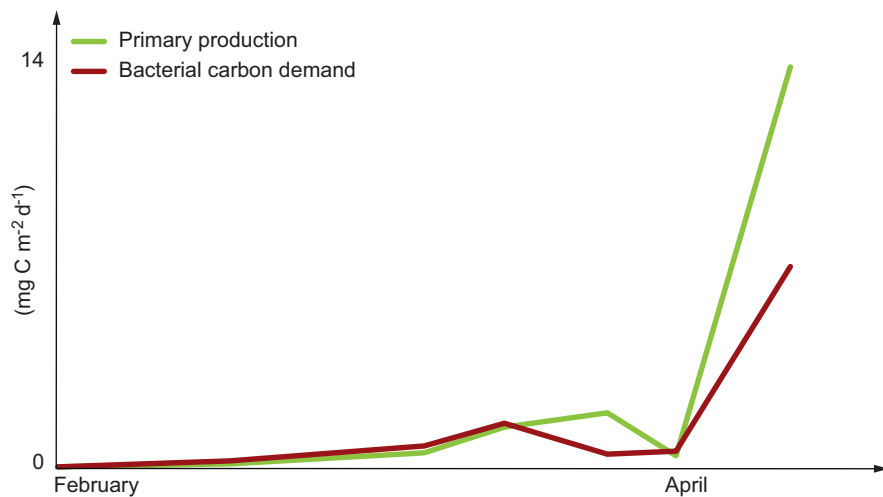
Fig. 5.25 Bacterial carbon demand and primary production between February and April, SW Greenland. (Modified from: Søgaard et al. 2010)
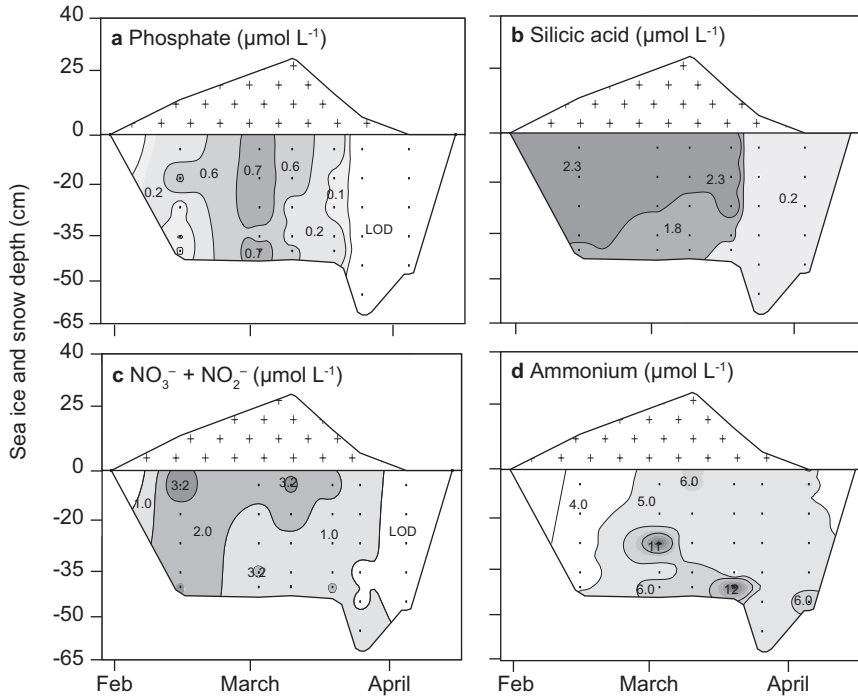
Fig. 5.26 Seasonal development in Phosphate (**a**), silicic acid (**b**), nitrate and nitrite (**c**), and ammonium (**d**) concentrations in sea ice, in Malene Bight, SW Greenland. LOD is lower than detection limit. (Modified from: Søgaard et al. 2010)

(Fig. 1.1), resulting in rapid uptake of nutrients. A recent study has shown that the ice algal biomass was nutrient-limited in the late part of the sea ice season and that the nutrient concentrations in the ice fell to near zero, except ammonium concentrations that increased from winter to spring in the sea ice, indicating exchange and heterotrophic regeneration (Fig. 5.26) (Søgaard et al. 2010). Spring and summer is the season for increased ice algal activity, but even though the sea ice is net autotrophic, the ice bacterial activity is typically also highest in sea ice during spring and summer (Fig. 5.25). Although summer ice bacterial production rates are higher than reported winter rates, the bacterial production only represents 10% of primary production rates during summer. Therefore, at this spring/summer stage, the autotrophic assimilation of CO$_2$ depletes the pCO$_2$ but also the macronutrients of the brine.

One estimate indicates that the sea ice-driven CO$_2$ pump (i.e. including both abiotic and biotic processes in sea ice covered waters) is equivalent to 17–42% of the annual air-sea CO$_2$ flux in open ocean waters at high latitudes (Rysgaard et al. 2011). This estimate strongly contradicts the perception that sea ice acts only as a barrier, sealing off air-sea CO$_2$ fluxes in the Arctic Ocean, and emphasises that sea ice should be considered an essential part of the global carbon cycle. However, when considering the recent and ongoing changes in sea ice extent, age, thickness

and transmittance, a question arises: how will these changes affect the CO_2 uptake in a future Arctic Ocean? Recent estimates have ranged from a decrease to an increase in the net CO_2 uptake by the future Arctic Ocean (Mortenson et al. 2018). Therefore, there are still a lot of important future research questions to answer to better understand the importance of the sea ice driven CO_2 pump.

References

Arrigo, K. R., Dijken, G. V., & Pabi, S. (2008). Impact of a shrinking Arctic ice cover on marine primary production. *Geophysical Research Letters, 35*, L19603. https://doi.org/10.1029/2008GL035028.

Arrigo, K. R., & Dijken, G. L. (2011). Secular trends in Arctic Ocean net primary production. *Journal of Geophysical Research, 116*. https://doi.org/10.1029/2011JC007151.

Arrigo, K. R., & Dijken, G. L. (2015). Continued increases in Arctic Ocean primary production. *Progress in Oceanography, 136*, 60–70. https://doi.org/10.1016/J.POCEAN.2015.05.002.

Assmy, P., Fernández-Méndez, M., Duarte, P., Meyer, A., Randelhoff, A., Mundy, C. J., Olsen, L. M., Kauko, H. M., Bailey, A., Chierici, M., Cohen, L., Doulgeris, A. P., Ehn, J. K., Fransson, A., Gerland, S., Hop, H., Hudsonm, S. R., Hughes, N., Itkin, P., Johnsen, G. M., King, J. A., Koch, B. P., Koening, Z., Kwaśniewski, S., Laney, S. R., Nicolaus, M., Pavlov, A. K., Polashenski, C. M., Provost, C., Rösel, A., Sandbu, M., Spreen, G., Smedsrud, L. H., Sundfjord, A., Taskjelle, T., Tatarek, A., Wiktor, J., & Wagner, P. M. (2017). Leads in Arctic pack ice enable early phytoplankton blooms below snow-covered sea ice. *Scientific Reports, 7*. https://doi.org/10.1038/srep40850.

Assur, A. (1960). *Composition of sea ice and its tensile strength*. U.S. Snow, Ice and Permafrost Establishment Research Report 44. https://hdl.handle.net/2027/uc1.31822020697603

Baer, S., Connelly, T. L., & Bronk, D. A. (2015). Nitrogen uptake dynamics in landfast sea ice of the Chukchi Sea. *Polar Biology, 38*, 781–797. https://doi.org/10.1007/s00300-014-1639-y.

Barber, D. G., Ehn, J. K., Pucko, M., Rysgaard, S., Deming, J. W., Bowman, J. S., Papakyriakou, T., Galley, R. J., & Søgaard, D. H. (2014). Frost flowers on young Arctic Sea ice: The climatic, chemical, and microbial significance of an emerging ice type. *Journal of Geophysical Research, Atmospheres, 119*, 11593–11612. https://doi.org/10.1002/2014JD021736.

Barber, D. G., Hop, H., Mundy, C. J., Else, B., Dmitrenko, I. A., Tremblay, J. E., Ehn, J. K., Assmy, P., Daase, M., Candlish, L. M., & Rysgaard, S. (2015). Selected physical, biological and biogeochemical implications of a rapidly changing Arctic Marginal Ice Zone. *Progress in Oceanography, 139*, 122–150. https://doi.org/10.1016/j.pocean.2015.09.003.

Barton, B., Lenn, Y.-D., & Lique, C. (2018). Observed atlantification of the Barents Sea causes the Polar front to limit the expansion of winter sea ice. *Journal of Physical Oceanography, 34*. https://doi.org/10.1175/JPO-D-18-0003.1.

Blais, M., Ardyna, M., Gosselin, M., Dumont, D., Bélanger, S., Tremblay, J. E., Gratton, Y., Marchesem, C., & Poulin, M. (2017). Contrasting interannual changes in phytoplankton productivity and community structure in the coastal Canadian Arctic Ocean. *Limnology and Oceanography, 62*, 2480–2497. https://doi.org/10.1002/lno.10581.

Carmack, E. C., Yamamoto-Kawai, M., Haine, T. W. N., Bacon, S., Bluhm, B. A., Lique, C., Melling, H., Polyakov, I. V., Straneo, F., Timmermans, M.-L., & Williams, W. J. (2015). Freshwater and its role in the Arctic marine system: Sources disposition, storage, export, and physical and biogeochemical consequences in the Arctic and global oceans. *Journal of Geophysical Research, 121*, 675–717. https://doi.org/10.1002/2015JG003140.

Comiso, J. C., Parkinson, C. L., Gersten, R., & Stock, L. (2008). Accelerated decline in the Arctic Sea ice cover. *Geophysical Research Letters, 35*, L01703. https://doi.org/10.1029/2007GL031972.

Cox, G. F. N., & Weeks, W. F. (1983). Equations for determining the gas and brine volumes in sea-ice samples. *Journal of Glaciology, 29*, 306–316. https://doi.org/10.3189/S0022143000008364.

Dieckmann, G. S., Nehrke, G., Papadimitriou, S., Göttlicher, J., Steininger, R., Kennedy, H., Wolf-Gladrow, D., & Thomas, D. N. (2008). Calcium carbonate as ikaite crystals in Antarctic Sea ice. *Geophysical Research Letters, 35*. https://doi.org/10.1029/2008GL033540.

Dieckmann, G. S., Nehrke, G., Uhlig, C., Göttlicher, J., Gerland, S., Granskog, M. A., & Thomas, D. N. (2010). Brief communication: Ikaite ($CaCO_3.6H_2O$) discovered in Arctic Sea ice. *The Cryosphere, 4*, 227–230. https://doi.org/10.5194/tc-4-227-2010.

Else, B. G. T., Papakyriakou, T. N., Galley, R. J., Drennan, W. M., Miller, A., & Thomas, H. (2011). Wintertime CO_2 fluxes in an Arctic polynya using eddy covariance: Evidence for enhanced air-sea gas transfer during ice formation. *Journal of Geophysical Research, 116*, C00G03. https://doi.org/10.1029/2010JC006760.

Fernández-Méndez, M., Katlein, C., Rabe, B., Nicolaus, M., Peeken, I., Bakker, K., Flores, H., & Boetius, A. (2015). Photosynthetic production in the Central Arctic Ocean during the record sea-ice minimum in 2012. *Biogeosciences, 12*, 3525–3549. https://doi.org/10.5194/bg-12-3525-2015.

Gautier, D. L., Bird, K. J., Charpentier, R. R., Grantz, H. D. W., Klett, T. R., Moore, T. E., Pitman, J. K., Schenk, C. J., Schuenemeyer, J. H., Sørensen, K., Tennyson, M. E., Valin, Z. C., & Wandreay, C. J. (2009). Assessment of undiscovered oil and and gas in the Arctic. *Science, 324*, 1175–1179. https://doi.org/10.1126/science.1169467.

Glud, R. N., Rysgaard, S., Kühl, M., & Hansen, J. W. (2007). The sea ice in young sound: Implications for carbon cycling. In S. Rysgaard & R. N. Glud (Eds.), *Carbon cycling in Arctic marine Ecosystems – Case study Young Sound* (Meddelelser om Grønland, Bioscience, Vol. 58) (pp. 62–85). Copenhagen: Copenhagen the Commission for Scientific Research in Greenland.

Helmke, E., & Weyland, H. (1995). Bacteria in sea ice and underlying water of the Eastern Weddell Sea in midwinter. *Marine Ecology Progress Series, 117*, 269–287.

Isleifson, D., Galley, R. J., Barber, D. G., Landy, J. C., Komarov, A. S., & Shafai, L. (2014). A study on the C-band polarimetric scattering and physical characteristics of frost flowers on experimental sea ice. *IEEE Transactions on Geoscience and Remote Sensing, 52*, 1787–1798. https://doi.org/10.1109/TGRS.2013.2255060.

Jakobsson, M., Grantz, A., Kristoffersen, Y., & Macnab, R. (2004). Bathymetry and physiography of the Arctic Ocean and its constituent seas. In R. Stein & R. W. MacDonald (Eds.), *The organic carbon cycle in the Arctic Ocean* (pp. 1–16). Berlin/Heidelberg/New York: Springer, 363 pp.

Jakobsson, M. (2016). Submarine glacial landform distribution in the Central Arctic Ocean shelf-slope-basin system. *Geological Society, London, Memoirs, 46*, 469–476. https://doi.org/10.1144/M46.179.

Jones, E. P., & Coote, E. R. (1981). Oceanic CO_2 produced by precipitation of $CaCO_3$ from brines in sea ice. *Journal of Geophysical Research, 86*, 11041–11043. https://doi.org/10.1029/JC086iC11p11041.

Kaartokallio, H., Tuomainen, J., Kuosa, H., Kuparinen, J., Martikainen, P. J., & Servomaa, K. (2008). Succession of sea-ice bacterial communities in the Baltic Sea fast ice. *Polar Biology, 31*, 783–793. https://doi.org/10.1007/s00300-008-0416-1.

Kaartokallio, H., Søgaard, D. H., Norman, L., Rysgaard, S., Tison, J.-L., Delille, B., & Thomas, D. N. (2013). Short-term variability in bacterial abundance, cell properties, and incorporation of leucine and thymidine in subarctic sea ice. *Aquatic Microbial Ecology, 71*, 57–73. https://doi.org/10.3354/ame01667.

Kuosa, H., & Kaartokallio, H. (2006). Experimental evidence on nutrient and substrate limitation of Baltic Sea sea-ice algae and bacteria. *Hydrobiologia, 554*, 1–10. https://doi.org/10.1007/s10750-005-1001-z.

Kurtz, N. T., Galin, N., & Studinger, M. (2014). An improved Cryosat-2 sea ice freeboard retrieval algorithm through the use of waveform fitting. *The Cryosphere, 8*, 1217–1237. https://doi.org/10.5194/tc-8-1217-2014.

Kwok, R., & Rothrock, D. A. (2009). Decline in Arctic Sea ice thickness from submarine and ICESat records: 1958-2008. *Geophysical Research Letters, 36*. https://doi.org/10.1029/2009GL039035.

Kwok, R. (2018). Arctic Sea ice thickness, volume, and multiyear ice coverage: Losses and coupled variability (1958–2018). *Environmental Research Letters, 13*, 105005. https://doi.org/10.1088/1748-9326/aae3ec.

Lincoln, B. J., Rippeth, T. P., Lenn, Y.-D., Timmermanns, M. L., Williams, W. J., & Bacon, S. (2016). Wind-driven mixing at intermediate depths in an ice-free Arctic Ocean. *Geophysical Research Letters, 43*, 9749–9756. https://doi.org/10.1002/2016GL070454.

Lindsay, R. W., & Zhang, J. (2005). Arctic Ocean ice thickness: Modes of variability and the best locations from which to monitor them. *Journal of Physical Oceanography, 36*, 496–506. https://doi.org/10.1175/JPO2861.1.

Lund-Hansen, L. C., Markager, S., Hancke, K., Stratmann, T., Rysgaard, S., Ramløv, H., & Sorell, B. (2015). Effects of sea-ice light attenuation and CDOM absorption in the water below the Eurasian sector of the Central Arctic Ocean. *Polar Research, 34*, 23978. https://doi.org/10.3402/polar.v34.23978.

Lund-Hansen, L.C., Bendtsen, J., Stratmann, T., Tonboe, R., Olsen, S., Markager, S. and Sorrell, B. (2019). Will primary production rates in the Amundsen Basin (Arctic Ocean) remain low in a future ice-free setting? *Journal of Marine Systems* (Accepted).

Miller, L. A., Papakyriakou, T. N., Collins, R. E., Deming, J. W., Ehn, J. K., Macdonald, R. W., Mucci, A., Owens, O., Raudsepp, M., & Sutherland, N. (2011). Carbon dynamics in sea ice: A winter flux time series. *Journal of Geophysical Research, 116*. https://doi.org/10.1029/2009JC006058.

Mock, T., Meiners, K. M., & Giesenhagen, H. C. (1997). Bacteria in sea ice and underlying brackish water at 54" 26' 50'' N (Baltic Sea, Kiel Bight). *Marine Ecology Progress Series, 158*, 23–40. https://doi.org/10.3354/meps158023.

Mortenson, E., Steiner, N., Monahan, A. H., Miller, L. A., Geilfus, N.-X., & Brown, K. (2018). A model-based analysis of physical and biogeochemical controls on carbon exchange in the upper water column, sea ice, and atmosphere in a seasonally ice-covered Arctic strait. *Journal of Geophysical Research: Oceans, 123*, 7529–7549. https://doi.org/10.1029/2018JC014376.

Nguyen, D. & Maranger, R. (2011) Respiration and bacterial carbon dynamics in Arctic sea ice. *Polar Biology, 34*, 1843–1855. https://doi.org/10.1007/s00300-011-1040-z.

Nicolaus, M., Katlein, C., Maslanik, J., & Hendricks, S. (2012). Changes in Arctic Sea ice result in increasing light transmittance and absorption. *Geophysical Research Letters, 39*. https://doi.org/10.1029/2012GL053738.

Overland, J. E., Francis, J. A., Hanna, E., & Wang, M. (2012). The recent shift in early summer Arctic atmospheric circulation. *Geophysical Research Letters, 39*. https://doi.org/10.1029/2012GL053268.

Pabi, S., Dijken, G. L., & Arrigo, K. R. (2008). Primary production in the Arctic Ocean, 1998–2006. *Geophysical Research Letters, 113*. https://doi.org/10.1029/2007JC004578.

Papadimitriou, S., Kennedy, H., Kattner, G., Dieckmann, G. S., & Thomas, D. N. (2004). Experimental evidence for carbonate precipitation and CO_2 degassing during sea ice formation. *Geochimica et Cosmochimica Acta, 68*, 1749–1761. https://doi.org/10.1016/j.gca.2003.07.004.

Parkinson, C. L. (2014). Spatially mapped reductions in the length of the Arctic Sea ice season. *Geophysical Research Letters, 41*, 4316–4322. https://doi.org/10.1002/2014GL060434.

Peterson, B. J., Holmes, R. N., McClelland, J. W., Vörösmarty, C. J., Lammers, R. B., Shiklomanov, A. I., Shiklomanov, I. A., & Rahmstorf, S. (2002). Increasing river discharge to the Arctic Ocean. *Science, 298*, 2171–2173. https://doi.org/10.1126/science.1077445.

Petrich, C., & Eicken, H. (2017). Overview of sea ice growth and properties. In D. N. Thomas (Ed.), *Sea Ice* (3rd ed., pp. 1–41). Chichester, 652 pp: Wiley Blackwell. https://doi.org/10.1002/9781118778371.ch1.

Popova, E. E., Yool, A., Coward, A. C., Dupont, F., Deal, C., Elliott, S., Hunke, E., Jin, M., Steele, M., & Zhang, J. (2012). What controls primary production in the Arctic Ocean? Results from an intercomparison of five general circulation models with biogeochemistry. *Journal of Geophysical Research, 117*. https://doi.org/10.1029/2011JC007112.

Polyakov, I. V., Pnyushkov, A. V., Alkire, M. B., Ashik, I. M., Baumann, T. M., Carmack, E. C., Goszczko, I., Guthrie, J., Ivanov, V. V., Kanzow, T., Krishfield, R., Kwok, R., Sundfjord, A., Morison, J., Rember, R., & Yulin, A. (2017). Greater role for Atlantic inflows on sea-ice loss in the Eurasian Basin of the Arctic Ocean. *Science, 356*, 285–291. https://doi.org/10.1126/science.aai8204.

Pringle, D. J., Miner, J. E., Eicken, H., & Golden, K. M. (2009). Pore space percolation in sea ice single crystals. *Journal of Geophysical Research, 114*, C12017. https://doi.org/10.1029/2008JC005145.

Randelhoff, A., Fer, I., Sundfjord, A., Tremblay, J.-É., & Reigstad, M. (2016). Vertical fluxes of nitrate in the seasonal nitracline of the Atlantic sector of the Arctic Ocean. *Journal of Geophysical Research, 121*, 5282–5295. https://doi.org/10.1002/2016JC011779.

Randelhoff, A., Reigstad, M., Chierici, M., Sundfjord, A., Ivanov, V., Cape, M., Vernet, M., Tremblay, J.-E., Bratbak, G., & Kristiansen, S. (2018). Seasonality of the physical and biogeochemical hydrography in the inflow to the Arctic Ocean through the Fram Strait. *Frontiers in Marine Science, 5*, 224. https://doi.org/10.3389/fmars.2018.00224.

Richardson, C. (1976). Phase relationships in sea ice as a function of temperature. *Journal of Glaciology, 17*, 507–519. https://doi.org/10.3189/S0022143000013770.

Rysgaard, S., & Glud, R. N. (Eds.). (2007). *Carbon cycling in Arctic marine ecosystems: Case study Young Sound* (Meddelelser om Grønland. Bioscience 58, 214 pp). Copenhagen: DCE.

Rysgaard, S., Bendtsen, J., Pedersen, L. T., Ramløv, H., & Glud, R. N. (2009). Increased CO_2 uptake due to sea ice growth and decay in the Nordic Seas. *Journal of Geophysical Research, 114*. https://doi.org/10.1029/2008JC005088.

Rysgaard, S., Bendtsen, J., Delille, B., Dieckmann, G. S., Glud, R. N., Kennedy, H., Mortensen, J., Papadimitriou, S., Thomas, D. N., & Tison, J.-L. (2011). Sea ice contribution to the air-sea CO_2 exchange in the Arctic and Southern Oceans. *Tellus B, 63*, 823–830. https://doi.org/10.1111/j.1600-0889.2011.00571.x.

Rysgaard, S., Glud, R. N., Lennert, K., Cooper, M., Halden, N., Leakey, R. J. G., Hawthorne, F. C., & Barber, D. (2012). Ikaite crystals in melting sea ice – Implications for pCO_2 and pH levels in Arctic surface waters. *The Cryosphere, 6*, 901–908. https://doi.org/10.5194/tc-6-901-2012.

Rysgaard, S., Søgaard, D. H., Cooper, M., Pućko, M., Lennert, K., Papakyriakou, T. N., Wang, F., Geilfus, N. X., Glud, R. N., Ehn, J., McGinnis, D. F., Attard, K., Sievers, J., Deming, J. W., & Barber, D. (2013). Ikaite crystal distribution in winter sea ice and implications for CO_2 system dynamics. *The Cryosphere, 7*, 707–718. https://doi.org/10.5194/tc-7-707-2013.

Sabine, C. L., Hankin, S., Koyuk, H., Bakker, D. C. E., Pfeil, B., Olsen, A., Metzl, N., Kozyr, A., Fassbender, A., Manke, A., Malczyk, J., Akl, J., Alin, S. R., Bellerby, R. G. J., Borges, A., Boutin, J., Brown, P. J., Cai, W. J., Chavez, F. P., Chen, A., Cosca, C., Feely, R. A., González-Dávila, M., Goyet, C., Hardman-Mountford, N., Heinze, C., Hoppema, M., Hunt, C. W., Hydes, D., Ishii, M., Johannessen, T., Key, R. M., Körtzinger, A., Landschützer, P., Lauvset, S. K., Lefèvre, N., Lenton, A., Lourantou, A., Merlivat, L., Midorikawa, T., Mintrop, L., Miyazaki, C., Murata, A., Nakadate, A., Nakano, Y., Nakaoka, S., Nojiri, Y., Omar, A. M., Padin, X. A., Park, G. H., Paterson, K., Perez, F. F., Pierrot, D., Poisson, A., Ríos, A. F., Salisbury, J., Santana-Casiano, J. M., Sarma, V. V. S. S., Schlitzer, R., Schneider, B., Schuster, U., Sieger, R., Skjelvan, I., Steinhoff, T., Suzuki, T., Takahashi, T., Tedesco, K., Telszewski, M., Thomas, H., Tilbrook, B., Vandemark, D., Veness, T., Watson, A. J., Weiss, R., Wong, C. S., & Yoshikawa-Inoue, H. (2012). Surface Ocean CO2 atlas (SOCAT) gridded data products. *Earth System Science Data Discussions, 5*, 781–804. https://doi.org/10.5194/essdd-5-781-2012.

Sakshaug, E. (2004). Primary and secondary production in the Arctic seas, 57-81. In R. Stein & R. W. MacDonald (Eds.), *The organic carbon cycle in the Arctic Ocean* (363 pp). Berlin/Heidelberg: Springer.

Serreze, M. C., Holland, M. M., & Stroeve, J. (2007). Perspectives on the Arctic's shrinking sea-ice cover. *Science, 315*, 1533–1536. https://doi.org/10.1126/science.1139426.

Sievers, J., Sørensen, L. L., Papakyriakou, T., Else, B., Sejr, M. K., Haubjerg Søgaard, D., Barber, D., & Rysgaard, S. (2015). Winter observations of CO_2 exchange between sea ice and the atmo-

sphere in a coastal fjord environment. *The Cryosphere, 9*, 1701–1713. https://doi.org/10.5194/tc-9-1701-2015.

Smedsrud, L. H., Halvorsen, M. H., Stroeve, J. C., Zhang, R., & Kloster, K. (2017). Fram Strait sea ice export variability and September Arctic Sea ice extent over the last 80 years. *The Cryosphere, 11*, 65–79. https://doi.org/10.5194/tc-11-65-2017.

Smith, R. E. H., & Clement, P. (1990). Heterotrophic activity and bacterial productivity in assemblages of microbes from sea ice in the high Arctic. *Polar Biology, 10*, 351–357. https://doi.org/10.1007/BF00237822.

Søgaard, D. H., Kristensen, M., Rysgaard, S., Glud, R. N., Hansen, P. J., & Hilligsøe, K. M. (2010). Autotrophic and heterotrophic activity in Arctic first-year sea ice: Seasonal study from Malene bight, SW Greenland. *Marine Ecology Progress Series, 419*, 31–45. https://doi.org/10.3354/meps08845.

Søgaard, D. H., Thomas, D. N., Rysgaard, S., Glud, R. N., Norman, L., Kaartokallio, H., Juul-Pedersen, T., & Geilfus, N.-X. (2013). The relative contributions of biological and abiotic process to carbon dynamics in subarctic sea ice. *Polar Biology, 36*, 1761–1777. https://doi.org/10.1007/s00300-013-1396-3.

Søgaard, D. H., Deming, J. W., Meire, L., & Rysgaard, S. (2019). Effects of microbial processes and CaCO$_3$ dynamics on inorganic carbon cycling in snow-covered Arctic winter sea ice. *Marine Ecology Progress Series*. https://doi.org/10.3354/meps12868.

Tison, J.-L., Haas, C., Gowing, M. M., & Sleewaegen, S. (2002). Tank study of physico-chemical controls on gas content and composition during growth of young sea ice. *Journal of Glaciology, 48*, 177–191. https://doi.org/10.3189/172756502781831377.

Wang, M., & Overland, J. E. (2009). A sea ice free summer Arctic within 30 years? *Geophysical Research Letters, 36*. https://doi.org/10.1029/2009GL037820.

Warner, K., Iacozza, J., Scharien, R., & Barber, D. (2013). On the classification of melt season first-year and multi-year sea ice in the Beaufort Sea using Radarsat-2 data. *International Journal of Remote Sensing, 34*, 3760–3774. https://doi.org/10.1080/01431161.2012.760855.

Zhang, J., Lindsay, R., Schweiger, A., & Steele, M. (2013). The impact of an intense summer cyclone on 2012 Arctic Sea ice retreat. *Geophysical Research Letters, 40*, 720–726. https://doi.org/10.1002/grl.50190.

Chapter 6
Methods and Techniques in Sea Ice Ecology

Abstract This chapter is a description of the field and laboratory methods that are generally applied in sea ice ecological research. The first section describes sampling techniques and handling of sea ice samples (6.1). Calculations of brine and gas volumes are dealt with in (6.2), and how to measure and calculate optical parameters (6.3). Sampling, handling, and calculation of ice bacterial production are described (6.4), and methods for ice algae biomass spatial distributions are dealt with in (6.5). Measuring photosynthesis and ice algae primary production are described (6.6), and the determination of Chl *a* content is explained (6.7). The recently developed fluorescence imaging of ice algae distributions and derived photosynthetic parameters are described (6.8). This is followed by a description of the IP_{25}, a substance synthesized by ice algae and applied for mapping sea ice and food web studies (6.9).

Keywords Sampling · Brine volume · Sea ice methods · Algal and bacterial production · Normalized Difference Index · AUV · PAM

6.1 Sample Techniques

The standard procedure used to collect sea ice physical, biological and biogeochemical parameters is briefly described. For further details see Eicken et al. (2009) as well as Miller et al. (2015). Once a sampling site is selected, basic information is recorded including the GPS position along with time of day (local or UTC), meteorological conditions such as wind speed, wind direction, cloud cover in 1/8, air temperature, downwelling irradiance (PAR) as well as snow and surface conditions. The sampling begins with measuring snow depths (to the nearest 0.5 cm) and, if needed, snow temperatures (to the nearest 0.1 °C). An average of 10 measurements is a working standard for such measurements. Snow if needed for analyses is collected by scooping it into sample containers using clean buckets or a shovel. Sea ice cores are collected using a pre-cleaned ice corer such as a KOVACS Mark II corer

and the ice core is placed onto a cradle on the ice for handling and sectioning. The ice core can be cored manually or by mounting an electric drill on the ice corer. When the core is retrieved and out of the water, it is very important to protect it from sunlight with a black cloth to avoid photodamage of ice algae and their pigments due to the much higher light intensities above than below the ice. The ice core length is measured to the nearest 0.5 cm. Measure also freeboard in the hole, which is the vertical distance between the surface of the ice and the water level in the hole. Note that this is negative when the sea ice is flooded due to snow loading. The temperature of the ice core is measured by drilling holes (4–5 mm diameter) into the middle of the core (perpendicular to the main coring direction) and inserting a high precision, calibrated digital thermometer every 5 cm along the core. The temperature is measured to the nearest 0.1 °C and has to be determined immediately after collecting the core. Ambient air temperatures are always either lower or higher than the ice, so the ice will immediately start melting or freezing. The sea ice core is then divided into sections (to the nearest 0.1 cm) using a pre-cleaned stainless steel saw. Thickness of the sections varies according to the sample volumes required to address specific research questions and is usually between 5 and 10 cm. It is important that the ice cores are sectioned from the bottom end (ice-water interface) upwards to minimize brine loss from the cores. Each ice core section is placed into polyethylene containers or Zip-lock bags and transported back to the laboratory in a dark and thermally insulated box. If required, light transmittance and albedo can be measured (Sect. 6.3). A video showing the preparations before a sea ice field trip (Fig. 6.1) and the sampling and handling of sea ice in the field (Fig. 6.2). An ice drone has recently been developed that flies to a predetermined position on the ice, drills out a 25 cm long ice core with a diameter of 7 cm, and brings the ice core back to the operator where it is retrieved and sectioned (Carlson et al. 2019). The ice drone is especially useful when sampling thin ice that is inaccessible for safety reasons (Fig. 6.3).

6.1.1   Handling and Processing of Ice Samples

Sea ice is a complex, fragile matrix of ice crystals, liquids, dissolved gases, and biota. Some disturbance and loss of material is inevitable during collection and handling of ice samples, and there are advantages and disadvantages of different approaches for their processing. The issues can broadly be divided into (**1**) physical losses during collection and handling, (**2**) cell mortality during storage and thawing of samples, and (**3**) physiological acclimation that alters cellular processes and their activity during storage. Ideally, all samples would be fixed or metabolic activity determined immediately *in situ* on the ice, but there are many methodological limitations and logistical problems with Arctic field work that make this aim unrealistic. Loss of material begins during coring and affects cells attached to the delicate crystals in the skeletal layer of the ice and in some of the brine that is lost from ice cores during coring. The warmer the ice, the greater its porosity and permeability and the volume of brine that can be lost, but the loss is minimal in colder ice with brine

Fig. 6.1 A video shows the preparations before a sea ice field trip (https://doi.org/10.1007/000-05n)

Fig. 6.2 A video showing the sampling and handling of sea ice in the field (https://doi.org/10.1007/000-05m)

Fig. 6.3 A video showing the work and sampling on the thin ice using ice drone (Photograph by: Dan Carlson). Video: Stratoz Visuals – M.Skovby (https://doi.org/10.1007/000-05k)

volumes < 5%. When core sections are returned to the laboratory, treatments must be chosen that produce the most realistic data for a particular parameter. The sea ice sections are thawed at 1–3 °C over a maximum of 2 days, and in complete darkness to avoid either algal photosynthetic growth or pigment breakdown. Before thawing, each of the sea ice sections is weighed with a digital balance to the nearest 1.0 gram to calculate ice density by dividing with the calculated volume. Thawing of the samples can be carried out by adding sterile-filtered (0.2 μm) seawater into each container in a 1:1 or 1:2 (volume:volume) ratio to reduce osmotic stress when the ice algae residing in highly saline (>50–100) brine channels are thawed out in low (3–10) saline meltwater. Note that the volume of any filtered seawater added to the ice sections must be accurately recorded, as it is needed to determine dilution factors for determining ice algae cell numbers, nutrient and Chl *a* concentrations. Thawing in diluted seawater can require large volumes of filtered seawater which are not always readily available, but the method is essential for certain measurements (e.g. Campbell et al. 2019). Some recent studies have taken the approach of scraping bottom ice crystals with ice algae into a small container or cuvette, thawing the crystals within a few minutes in a few mL of filtered seawater, which is optional. The sample is processed instantly in the field when actual and immediate physiological conditions of the ice algae are needed, and to avoid any longer delay between sample collection and measurements (McMinn et al. 2010; Hancke et al. 2018).

There are challenges in knowing the exact volumes of sampled ice with this method, but it does allow immediate measurement and fixation. It is emphasized that researchers must carefully consider the aims of their studies to justify the compromises necessary for obtaining data that best provide useful insight to the processes under study. New developments such as novel *in situ* sensors (Long et al. 2012) as well as non-invasive remote sensing methods to determine ice algal biomass (Else et al. 2015, Forrest et al. 2019) may help to overcome some of the shortcomings in classical sea ice sampling methods.

6.1.2   Sackholes

The standard procedure for collecting liquid sea ice brines is drilling sackholes (Fig. 6.4). These are vertical holes in the ice drilled out by an ice corer but not to the bottom of the ice. The brine is allowed to drain into the hole and slowly fill it. Samples are collected from the hole using syringes or with a pump, and placed in pre-cleaned polyethylene containers. The sampled brine is typically analysed for nutrient content, bacteria, Chl *a*, and algae cells. Samples are also placed in the dark and returned to the laboratory in thermally insulated boxes. One obvious problem with the method is that brine water is draining out from the wall of the entire core hole with no vertical resolution, as when a core is sectioned described above. Another problem is that this method only collects organisms that are free-living in the brine, whereas the fraction of ice algae cells, bacteria, and other particulate material attached to the walls of the brine channels is not sampled.

6.2   Salinity, Brine and Brine Volume

The salinity of melted sea ice, also termed bulk salinity, is generally measured with a handheld electronic salinometer (to the nearest 0.1) such as the YSI Pro30 or other similar models. It is the conductivity of the sample that is measured and converted into a salinity, based on the measured temperature of the sample. With the bulk salinity and ice core temperatures measured immediately after retrieval it is now possible to calculate brine and gas volume fractions, density of the ice, brine salinity, and brine density as based on the Cox and Weeks relations (1983). Brine volume fraction (V_b/V) is calculated as:
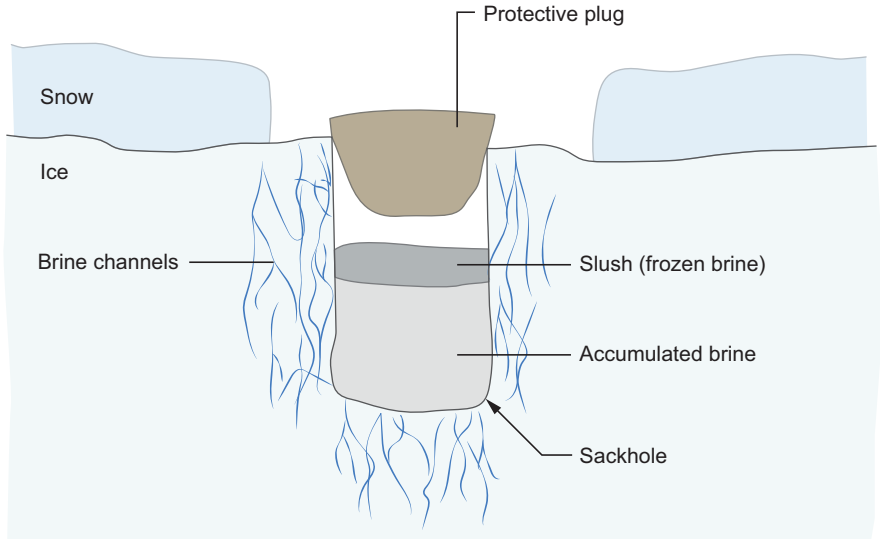
Fig. 6.4 Illustration of a sackhole. (Modified from: Miller et al. 2015)

$$\frac{V_b}{V} = \frac{\sigma \cdot S_{si}}{F_1(T)} \qquad (6.1)$$

and the gas volume fraction (V_a/V) as:

$$\frac{V_a}{V} = (1 - \left(\frac{\sigma}{\sigma_i}\right) + \sigma_i \cdot S_{si} \cdot (\frac{F_2(T)}{F_1(T)}) \qquad (6.2)$$

where σ is the bulk density (kg m^{-3}) of the ice, σ_i the density (kg m^{-3}) of pure ice, S_{si} is the bulk salinity, and $F_1(T)$ and $F_2(T)$ are coefficients depending on the temperature (T), tabulated in Cox and Weeks (1983). The density of pure ice is a function of the ice temperature given by:
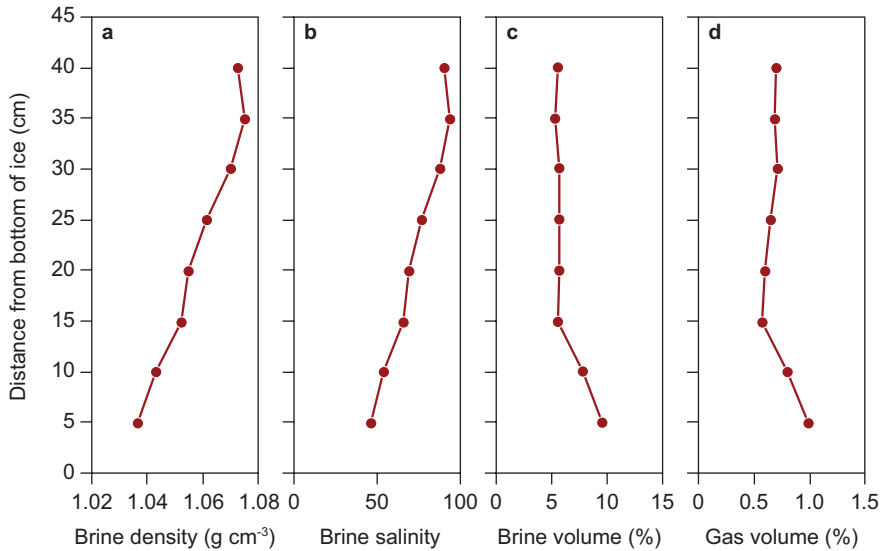
$$\sigma_i = 0.971 - 1.403 \cdot 10^{-4} \cdot T \qquad (6.3)$$

The salinity of the brine S_b for temperatures >-23 °C also depends on the ice temperature as:

$$S_b = \left(1 - \left(\frac{54.11}{T}\right)\right)^{-1} \cdot 1000 \qquad (6.4)$$

and brine density is:

$$\sigma_{br} = 1 + 0.0008 \cdot S_b \qquad (6.5)$$

Fig. 6.5 Brine density (**a**), brine salinity (**b**), brine volume fraction (**c**), and gas volume fraction (**d**) in an ice core, February 2018, Godthåbsfjord, SW Greenland, February

where T is temperature (°C), σ_i and σ_{br} are densities (kg m^{-3}), and S_b brine salinity. Examples of brine density, brine salinity, brine, and gas volume in a sea ice core are shown in Fig. 6.5. Density of the ice varies slightly compared to bulk salinity and temperature, and Fig. 6.6 is a nomogram of brine volume as functions of bulk salinity and temperature. At a bulk salinity of 5.0 and a temperature of −5.0 °C, the brine volume is about 5%, the known "rule of five" (Golden et al. 2007). A brine volume of 5% is also considered as the percolation threshold for fluid transport for sea ice with a columnar crystal structure (Fig. 5.21). The salinity of the brine in the channels is only governed by the temperature of the ice. Brine channels are clearly seen in this core (Fig. 6.7). Brine volumes can now be measured by Magnetic Resonance Scanning (MR-scanning) (Galley et al. 2015), but without access to these advanced methods must otherwise be calculated.

6.3 Transmittance and Light Attenuation

Transmittance is the ratio between irradiance measured after passing through a solid or liquid substance relative to the irradiance before passing the substance, and given as a number between 0.0 and 1.0 and sometimes in percent. Irradiance sensors employed for this purpose measure downwelling or upwelling irradiance across 180°, i.e. the hemisphere above or below the sensor. Irradiance is measured with a 2π cosine-corrected sensor such as the Li-Cor sensors, where cosine-corrected means the irradiance measured by a sensor (E_θ) is proportional to the cosine of the

Fig. 6.6 Nomogram of
brine volume (V_b/V) as a
function of bulk sea ice
salinity and temperature.
Black lines in nomogram
shows "rule of five".
(Modified from: Petrich
and Eicken 2017)
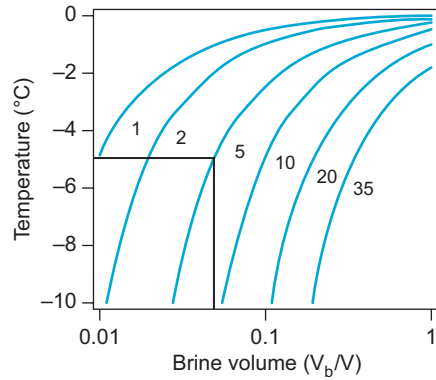
Fig. 6.7 Brine channels
(blue arrows) in an ice core
with a diameter of 90 mm.
(Photographs by: Authors)
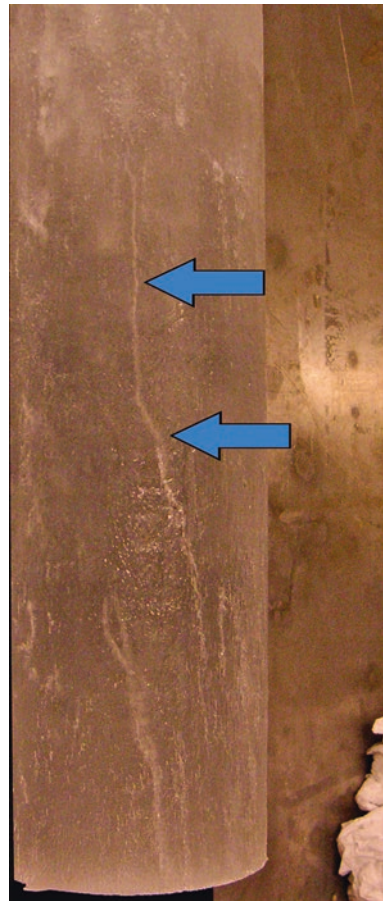
angle of the incident light (θ), following Lambert's cosine law $E_\theta = E_d \cdot \cos(\theta)$ (Fig. 6.8). The irradiance which is reflected and scattered back into space from a surface of snow or ice is upwelling irradiance, with the upwelling/downwelling as the albedo of the surface, which varies from around 0.8 and up for snow and around 0.5 for a snow-free sea ice (Perovich and Polashenski 2012). Transmittance can be determined for PAR, the interval of visible light (400–700 nm) of the electromagnetic spectrum, but can also be spectrally resolved for each wavelength across a spectrum from 320 to 920 nm (Fig. 6.9a). An example obtained near the North Pole in August 2012 shows a strong attenuation through 1.5 m thick ice, especially in the red part of the spectrum whereas blue-green light centered around 520 nm is least attenuated. Shorter wavelengths such as UV-A (315–400 nm) are also strongly attenuated (Fig. 6.9a-b). A second example of transmittance, likewise from the Arctic Ocean, emphasizes the strong spatial variation in transmittance with high values (0.12–0.15) under a melt pond, which reduces to around 0.03 outside the melt pond (Fig. 6.10) (Nicolaus et al. 2012). The diffuse attenuation coefficient of PAR, $K_d(PAR)$, describes the attenuation of PAR through a substance of known thickness, as in snow, sea ice, or between two or more depths in a water column. The d in $K_d(PAR)$ denotes that it is downwelling PAR whereas $K_u(PAR)$ is the diffuse attenuation coefficient of upwelling PAR as in a water column, for instance. The attenuation comprises both scattering and absorption of the irradiance in the medium. The $K_d(PAR)$ coefficient is derived from Lambert's law, which states that the intensity of incident irradiance (I_o), passing through a medium decreases exponentially with the thickness (z) of the medium:

$$I_z = I_o \cdot \exp^{(-K_d(PAR) \cdot z)} \qquad (6.6)$$

Here I_o is the incident light intensity (μmol photons m^{-2} s^{-1}) at the surface and I_z the intensity (μmol photons m^{-2} s^{-1}) at distance (z) (m) in the medium, and $K_d(PAR)$

Fig. 6.8 Lambert's cosine law states that downwelling irradiance (E_d) is proportional to the cosine to the angle of incidence, as for the variation in the sun's height above the horizon during a day and the year
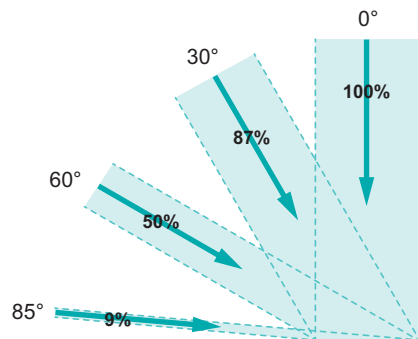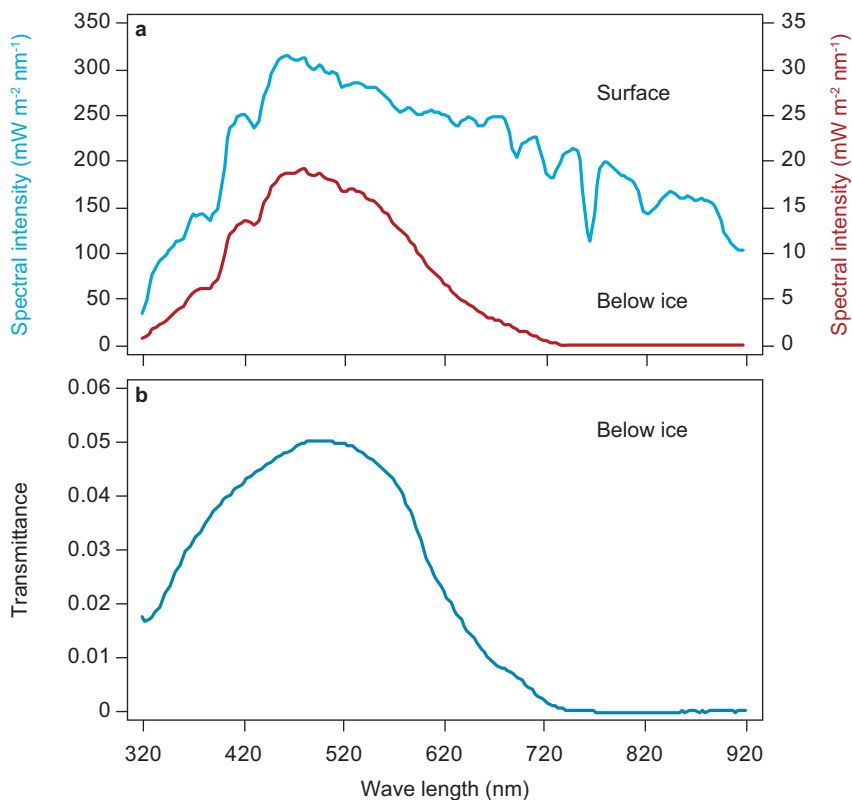
Fig. 6.9 Spectral irradiance at wavelengths between 320 and 920 nm at the surface (blue line) and below the ice (red line) (**a**), and transmittance (**b**) August 2012, Amundsen Basin, Arctic Ocean. (Unpublished data)

(m^{-1}) the diffuse attenuation coefficient. Rearranged with PAR to determine $K_d(PAR)$ results in:

$$K_d\left(PAR\right) = -\ln(\frac{PAR_z}{PAR_o})\,/\,z \qquad (6.7)$$

In the example (Fig. 6.11), transmittance is 0.05 of the snow (0.1 m thick) and ice package (0.5 m thick), which gives an under-ice irradiance of 30.0 µmol photons m^{-2} s^{-1} with a surface downwelling PAR of 600.0 µmol photons m^{-2} s^{-1}. $K_d(PAR)$ was derived for each of the components as snow = 11.9 m^{-1}, ice = 0.84 m^{-1}, and water = 0.32 m^{-1}, which are typical $K_d(PAR)$ values and emphasizes the strong attenuation in the snow. PAR and spectral under-ice irradiances must be obtained some distance away from holes drilled in the ice. An L-arm is often applied with the sensor head ideally >1.5 m away from the deployment hole in the ice to prevent

Fig. 6.10 Transmittance of short wave radiation (250–2500 nm) .in multi-year ice with melt-ponds as based on ROV measurements, August 2011, Arctic Ocean. Each spot represents one measurement. (Modified from: Nicolaus et al. 2012)
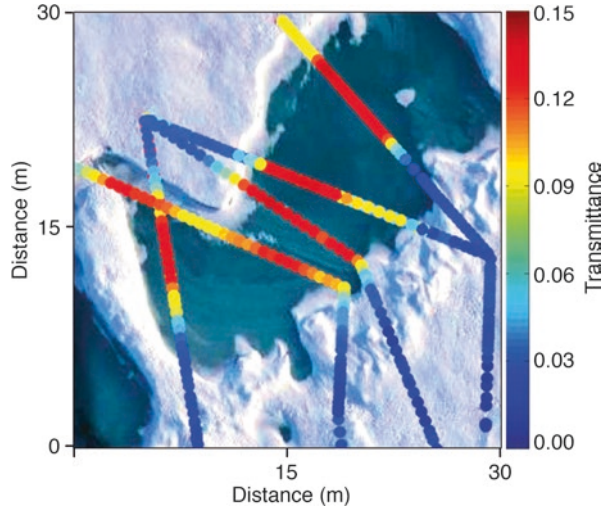
Fig. 6.11 Incident PAR, albedo, K_d(PAR) attenuation coefficients for snow, ice and seawater, March 2011, Kangerlussuaq, W Greenland
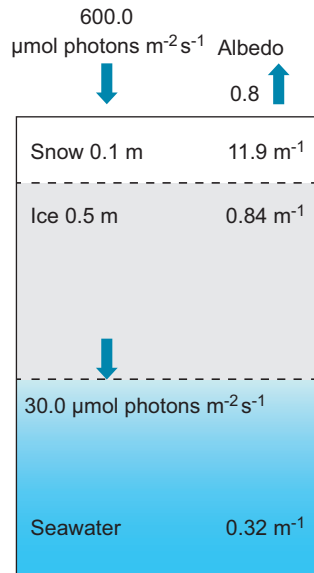
false light from above interfering with the measurements (Fig. 6.12). The hole is filled with snow and pieces of ice once the L-arm is in place. Concomitantly with the under ice measurements of PAR or spectral distribution of irradiance it is necessary to measure surface PAR or spectra, both to derive transmittance and to correct for changes in surface conditions by incoming clouds while measuring. An average of 10 measurements is a working standard for such measurements both above and

Fig. 6.12 L-arm mounted with a TriOS spectroradiometer for measuring spectral resolved irradiance below the ice. Distance between hole in the ice and point of measurement is 1.5 m. The L-arm is operated through a drilled hole and the arm unfolds below the ice and obtains a configuration as shown in the photo. (Photograph by: Authors)

below the ice. Albedo, the ratio between upwelling and downwelling irradiance, either PAR or spectrally resolved, is measured with the sensor head at a certain height (0.5–1.0 m) above the surface, and similarly with an average of 10 measurements.

6.4 Sea Ice Bacteria and Viruses – Methods and Sampling Issues

Bacteria are the most abundant heterotrophs in sea ice (Kaartokallio 2004; Mock and Thomas 2005; Deming and Collins 2017), and bacterial heterotrophy includes direct consumption of dissolved substrates and extracellular decomposition of dissolved and particulate matter (i.e. bacterial uptake). The density of bacteria in Arctic sea ice ranges from $4 \cdot 10^3$ mL^{-1} in winter surface ice (Collins et al. 2008) to $3 \cdot 10^7$ mL^{-1} in summer bottom ice (Krembs and Engel 2001). The diversity of prokaryotic organisms, Archaea and Eubacteria, includes more than 20 genera, with most of
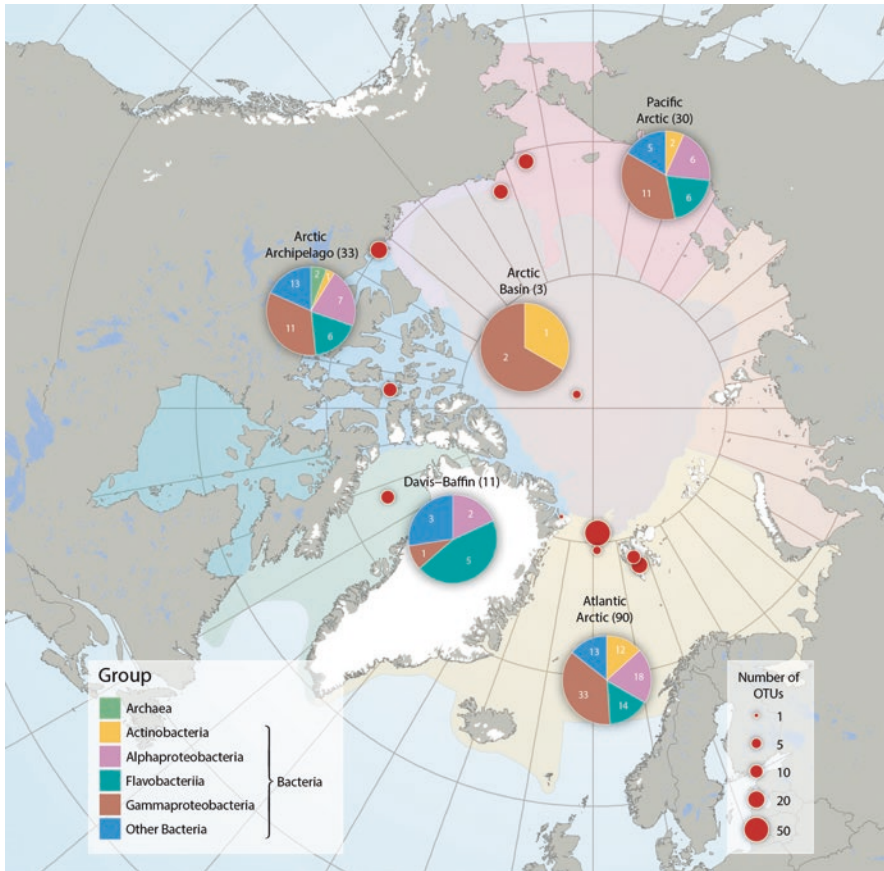
Fig. 6.13 Bacteria and Archaea across five Arctic areas based on number of operational taxonomic units (OTUs) or molecular species. (Courtesy: State of the Arctic Marine Biodiversity Report, https://www.caff.is/marine/marine-monitoring-publications/state-of-the-arctic-marine-biodiversity-report)

the isolated organisms being Gammaproteobacteria, Alphaproteobacteria and Bacteroidetes (Lizotte 2003; Kaartokallio et al. 2008; Collins and Deming 2011) (Fig. 6.13). These bacterial groups are psychrophilic, i.e. cold-adapted, and can degrade a broad spectrum of algal-derived organic substrates. Anoxic microzones also occur in sea ice where fermenting bacteria and anoxygenic phototrophic purple sulphur bacteria occur (Petri and Imhoff 2001). In the Baltic Sea (Kaartokallio 2001; Kaartokallio et al. 2007) and in Arctic sea ice (Rysgaard et al. 2008), active denitrifiers have also been found. Sea ice bacteria may be parasitic on eukaryotes or other bacteria or epiphytic on algae, particularly diatoms. The fraction of sea ice bacteria attached to particles, surfaces (e.g. sediment grains, detritus, ice crystal boundaries) or algae is close to 50% of the population (Junge et al. 2004), which is higher than the 10–15% in marine waters (Fenchel 1998). The density of

bacteriophages (viruses) is very high in sea ice compared to aquatic environments, where a typical virus to bacteria ratio is 10, but ratios in sea ice can range over several orders of magnitude (Collins and Deming 2011). Viruses can control bacterial population sizes in sea ice and also mediate lateral gene transfer (Feng et al. 2014).

6.4.1 Sampling Methods for Bacteria

When sampling sea ice to investigate the bacterial community, the ice is sectioned on-site using a sterile stainless steel saw, and transported back to the laboratory in sterile containers, then thawed in the dark at 1–3 °C. For frost flowers, brine skim or snow cover, sterile spatulas are used to collect the sample and handling is as described above and as in Sect. 6.1. Preferably, measurements of biogeochemical parameters, i.e. total inorganic carbon (TCO_2), Total alkalinity (TA), inorganic nutrients (phosphate, nitrate, nitrite, silicate, ammonium), dissolved organic carbon (DOC), dissolved organic nitrogen (DON), O_2 concentration, bulk salinity and temperature, should be included in the sampling program, depending again on the research questions under consideration.

6.4.2 Biomass, Community Structure, Bacterial Production and Bacterial Carbon Demand

Methods for determining the abundance, biomass and diversity of sea ice bacteria and viruses include: simple enumeration and epifluorescence microscopy (cell counts), culture work, flow cytometry, DNA sequencing technologies (i.e. amplicon sequencing and shotgun metagenomics), fluorescent *in situ* hybridization (FISH) or DNA fingerprinting techniques such as DGGE and T-RFLP (Deming 2010; Junge et al. 2004). To understand the mechanisms of microbial adaptation to the sea ice environment requires identification of the functional gene diversity. The most widely used method to identify the functional genomics in sea ice is metagenomic analysis and complete genome sequencing of isolated strains of sea ice microorganisms (Deming and Collins 2017). The primary method to determine sea ice bacterial production is by measuring incorporation of [³H]thymidine into DNA and using a conversion factor to relate DNA production to production of bacterial cells (Fuhrman and Azam 1982). The assessment of the bacterial production and carbon demand is based on a number of debatable assumptions. The conversion factor is not easy to measure routinely, but can be derived theoretically from assumptions of the extent of isotope dilution, thymidine content of bacterial DNA and the amount of DNA per cell (Fuhrman and Azam 1982), or empirically by comparing incorporation rates with increases in bacterial numbers (Kirchman et al. 1982a, b). Other factors affecting the conversion of thymidine incorporation into bacterial carbon production include the average bacterial cell size (Cell size) and the volume-specific carbon

content (C_{factor}), which multiplied provides the cell-specific carbon content (N_c) as (N_c = Cell size · C_{factor}), all of which are affected by environmental changes (Coveney and Wetzel 1988).

Bacterial production (BP) can be calculated as:

$$BP\left(\mu g\ CL^{-1}h^{-1}\right) = \frac{(DPM_{sample} \cdot N_{cells} \cdot N_c)}{(SA \cdot T_{inc} \cdot V_{filt})} \tag{6.8}$$

where DPM_{sample} is the average rate of isotope disintegrations per minute (DPM) for the live treatment subtracted from the average DPM for TCA-killed controls (DPM), N_{cells} (cells mol$^{-1\ 3}$H) is the conversion factor, N_c (μg C per cell) is the cell-specific carbon content, T_{inc} is the incubation period (hour), V_{filt} is the volume of the sub-samples (liter), and SA is the specific activity of the thymidine solution as disintegrations per minute (DPM mol^{-1}). None of these parameters are easy to measure, and therefore literature values are often applied to sea ice data. The [^{3}H]thymidine method also assumes that all bacteria assimilate exogenous thymidine and that eukaryotes do not. Uptake of [^{3}H]thymidine by eukaryotic microalgae has been observed (Rivkin 1986), but Fuhrman and Azam (1982) have shown that at low concentrations and relatively short incubation periods the uptake of [^{3}H]thymidine by eukaryotes can be assumed to be negligible.

Bacterial carbon demand (BCD) can be calculated as:

$$BCD\left(\mu g\ CL^{-1}h^{-1}\right) = \frac{BP}{BGE} \tag{6.9}$$

where BP is the bacterial production calculated as above and BGE is the bacterial growth efficiency. Note that, small changes in temperature would influence bacterial growth efficiency (2.5% decrease in bacterial growth efficiency per 1 °C temperature increase) and, hence, bacterial carbon demand (Rivkin and Legendre 2001).

6.5   Ice Algae Biomass Distributions

There is substantial temporal, geographical, and spatial variability in Arctic ice algal biomass. The temporal variability derives from the very low winter-early spring concentrations of 0.01 mg Chl *a* m^{-2} versus high biomass values of 80–130 mg Chl *a* m^{-2} during the spring algal bloom in the Canadian Arctic. The geographical variability in ice algal biomass is exemplified by the differences in the high (80–120 mg Chl *a* m^{-2}) Canadian Arctic (Fig. 1.4), and maximum biomasses in Greenland, which rarely exceed 6 mg Chl *a* m^{-2} as in Disko Bay, and are even lower in SW Greenland with 0.2 mg Chl *a* m^{-2} (Fig. 1.4). Spatial variation is here the variation in ice algal biomass at a specific location within a temporal frame of days, as measured in studies of biomass variation in relation to physical drivers such as irradiance (Rysgaard et al. 2001), snow thickness (Mundy et al. 2007), and bottom
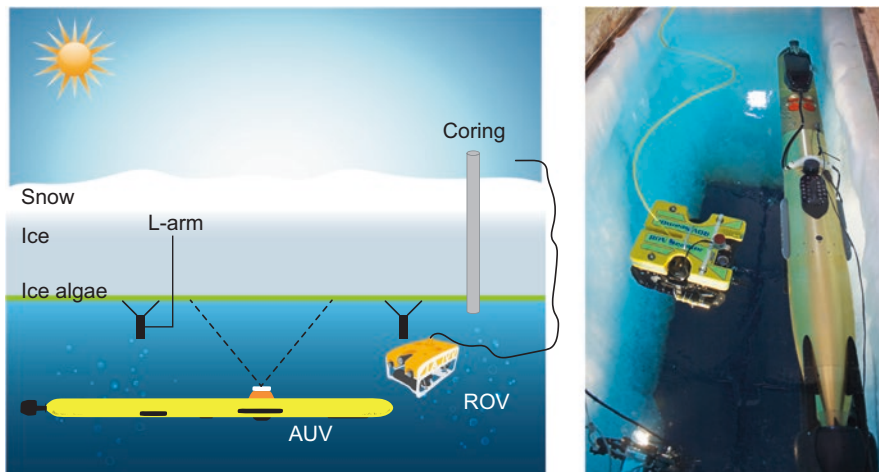
Fig. 6.14 Left diagram shows three methods for obtaining under-ice spectra or PAR: (1) an L-arm is applied to place the PAR or spectroradiometer sensor below the package of snow and ice, (2) a sensor is placed on the ROV (Remotely Operated Vehicle), or (3) a sensor is placed on an AUV (Autonomous Underwater Vehicle). Right photo shows ROV and AUV ready for deployment from the operation hole in the ice. (Photograph by: Alexander Forrest)

roughness (Lund-Hansen et al. 2016). See Cimoli et al. (2017a) for a comprehensive review of variability in algal biomass magnitude. Welch and Bergmann (1989) were able to predict ice algal biomass from sampling date and snow thickness as a proxy for accumulated light exposure over the growth season. They suggested that temporal ice algal biomass variability is driven by a "*head start*" mechanism, for example, between-site differences in spatial biomass variability resulting from small differences in early season snow cover, and potentially amplified, throughout the growth season. A variety of methods have been developed to study ice algal biomass distributions in sea ice, and they are either based on physical sampling of the ice or non-invasive methods such as under-ice remote sensing (Cimoli et al. 2017b). Coring is still the most widely used method to obtain samples of sea ice and specifically when a vertical resolution of parameters as nutrients, particulate matter, or Chl *a* is required to address the relevant scientific questions (Eicken et al. 2009). In comparison, remote sensing below the ice measures an optical signal that integrates over the entire column of the ice, as based on surface irradiance transmitted through the ice, but with no vertical resolution (Cimoli et al. 2017b). The clear advantage of applying remote sensing techniques in sea ice research is that significantly larger areas can be covered within a short time period compared to traditional coring, and they are non-invasive (Cimoli et al. 2017a). This is especially so if the measuring optical sensor is mounted on an AUV (Autonomous Underwater Vehicle) or ROV (Remotely Operated Vehicle) (Fig. 6.14) (Lund-Hansen et al. 2018). Remote sensing techniques for mapping ice algae at the bottom of the sea ice have developed considerably, but the principle is to locate an optical sensor below the ice and measure the transmitted spectrally resolved irradiance (Fig. 6.9). Irradiance passes through the
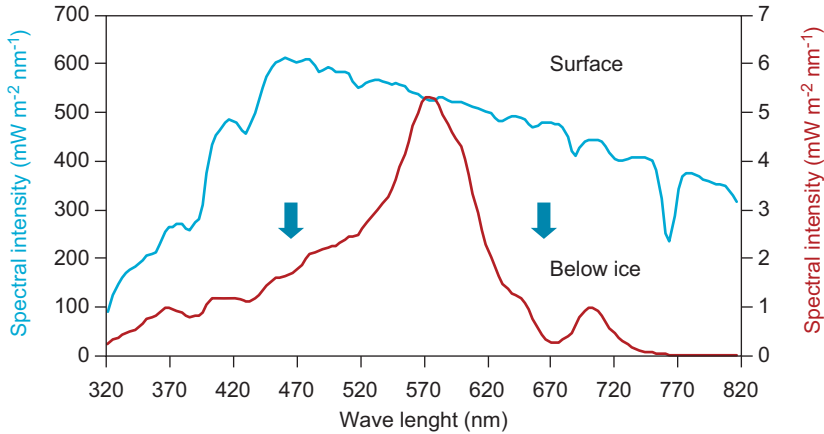
Fig. 6.15 Spectral irradiance at wavelengths between 320 and 820 at the surface (blue line) and below the ice (red line) where blue arrows indicate specific wavelengths of Chl *a* absorption peaks at 465 and 665 nm

snow and ice, and ice algae in the ice absorb or attenuate the irradiance at specific wavelengths. The attenuation changes the shape of the under-ice spectra such as for the Chl *a* pigment, which has two distinct absorption peaks – one in the blue (465 nm) and one in the red (665 nm) (Falkowski and Raven 2007). The higher the attenuation at these peaks, the higher the concentration of Chl *a* and thus algal biomass. Figure 6.15 shows surface and under-ice spectra from Cape Evans, Antarctica. There are some significant "lows" in transmitted irradiance around 465 nm and especially 665 nm related to the absorption by ice algae. This is clearly revealed by a comparison of corresponding spectra from the Arctic Ocean with low (~0.05 mg Chl *a* m^{-2}) concentrations at the ice bottom (Fig. 6.9a) to at bottom with high (15.2 mg Chl *a* m^{-2}) concentrations (Fig. 6.15). Maximum absorption is not always at specific wavelengths such as 465 nm or 665. Accordingly, a method has been developed to search a dataset of under-ice spectra for the best correlation between absorption at specific wavelengths and actually measured Chl *a*, for ice cores collected with conventional ice corer and analyzed for Chl *a* from the same area as covered by under-ice spectral measurements. This method termed NDI (Normalized Difference Index) is applied to correlate the variation in Chl *a* based on the relative absorption of irradiances at distinct wavelengths (Mundy et al. 2007):

$$\text{NDI} = \frac{\left[E_d\left(\lambda_1 \right) - E_d\left(\lambda_2 \right) \right]}{\left[E_d\left(\lambda_1 \right) + E_d\left(\lambda_2 \right) \right]} \tag{6.10}$$

where $E_d(\lambda_1)$ is downwelling (d) energy (E) (mW m^{-2} nm^{-1}), at a specific wavelength (λ_1) and here the wavelength with the strongest absorption related to Chl *a*, which in this example is 665 nm, and $E_d(\lambda_2)$ is a wavelength only affected by the attenuation of snow and ice and not by Chl *a* and is here 578 nm.

The variability in NDI is then only related to variability in absorption by Chl a, as variability related to snow and ice is taken into account by $E_d(\lambda_2)$ in the equation. In this example $E_d(665) = 0.34$ mW m^{-2} nm^{-1} and $E_d(578) = 5.67$ mW m^{-2} nm^{-1}, which equals an NDI of -0.89 for a specific Chl a concentration measured in the sea ice. A second spectrum at another place below the ice gives $E_d(665) = 1.5$ mW m^{-2} nm^{-1}, which shows that absorption by Chl a is relatively less as $E_d(665)$ is higher, as less energy is absorbed compared to the first spectrum. The $E_d(578) = 5.67$ mW m^{-2} nm^{-1} is equal to the first values, which equals an NDI $= -0.58$. The higher the value of the NDI, the lower the Chl a concentration. In this example $E_d(\lambda_1) = 665$ nm and $E_d(\lambda_2) = 578$ nm, but there are several other combinations and the total dataset (of all available wavelength pairs) is searched for the best combination of wavelengths in terms of the highest coefficient of determination (r^2) between NDI and Chl a. When the correlation is established we can take λ_1 and λ_2 at specific wavelengths from each of the 100 to 1000 or more spectrums from below the ice and calculate the Chl a concentration. The method was developed by Legendre and Gosselin (1991), and showed a high correlation ($r^2 = 0.75$) between Chl a and the irradiance ratio $E_d(671)/E_d(540)$ at wavelengths comparable to the example above. See Melbourne-Thomas et al. (2015) for a review of NDI methods and similar spectrum-based methods for mapping ice algae distributions. In a field study of PAR transmittance and snow depths we deployed a ROV, equipped with positioning cameras, PAR sensor and a TriOS spectroradiometer, and connected to a surface unit for data transmission and manoeuvring (Fig. 6.16). The ROV kept a constant vertical distance between sensor heads and bottom of the ice of 25 cm with the spacer poles (Fig. 6.16). Results from a 13 m long transect clearly demonstrate that PAR transmittance decreases with a high snow depth, and similarly for Chl a concentrations that also reduce under-ice irradiances (Fig. 6.17) (Lund-Hansen et al. 2018). A video shows the ROV deployed below the ice (Fig. 6.18). Maximum ice algal biomass concentrations are not always located at the bottom of the ice (Fig. 6.19), but can be distributed in a variety of ways in the ice core, as determined by the history and growth conditions of the ice (Fig. 6.20). The Station North core is likely multi-year ice where the Chl a maximum near 200 cm from the bottom likely relates to an ice bottom with high Chl a, but from previous years. The Godthåbsfjord ice developed during a cold period of 1–2 weeks in February, and homogenous vertical Chl a distribution most likely reflects that phytoplankton from the water column became incorporated into the ice during the freeze-up. Only the Kangerlussuaq core shows distinct high bottom-ice concentrations. When establishing an NDI correlation, as above, it must be considered where in the ice the biomass is actually located, and not just assume that most of biomass is located in the bottom of the ice. In a case like Godthåbsfjord (Fig. 6.20) Chl a must be measured and integrated for the whole core and applied when developing the NDI. An important concept of comparing optical sensors below the ice and sampling with an ice corer is the footprint, which is the size of the area of bottom ice or surface covered by the sensor or collected by the corer. The footprint of a KOVACS standard ice corer with a diameter of 0.09 m is 0.0064 m^2, equal to a square of $8.0 \cdot 8.0$ cm. The size of the footprint of an optical sensor, measuring downwelling irradiance, depends on the vertical distance between the sensor and
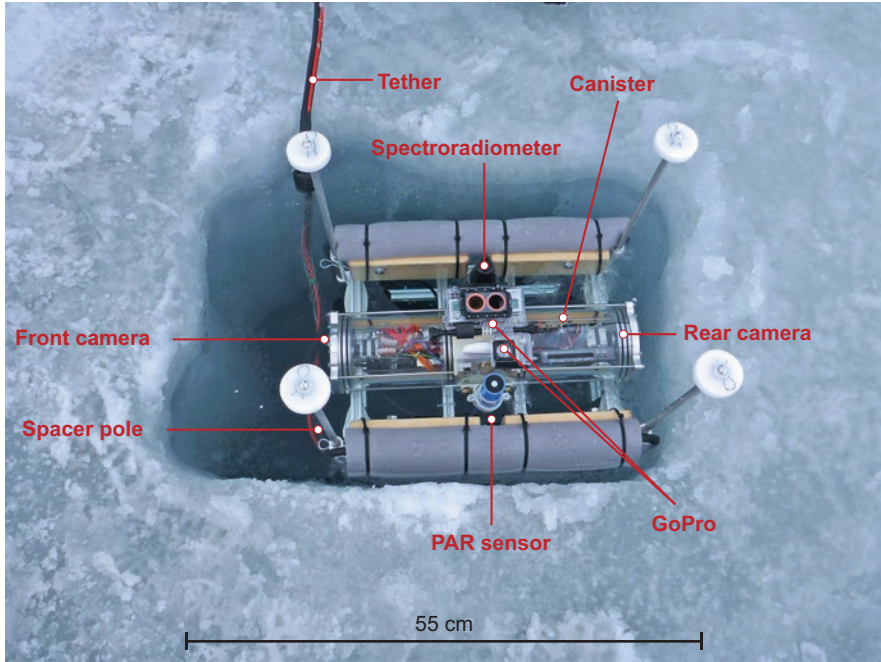
Fig. 6.16 Photo of the ROV in the ice with the sensors and cameras. (Modified from: Lund-Hansen et al. 2018)
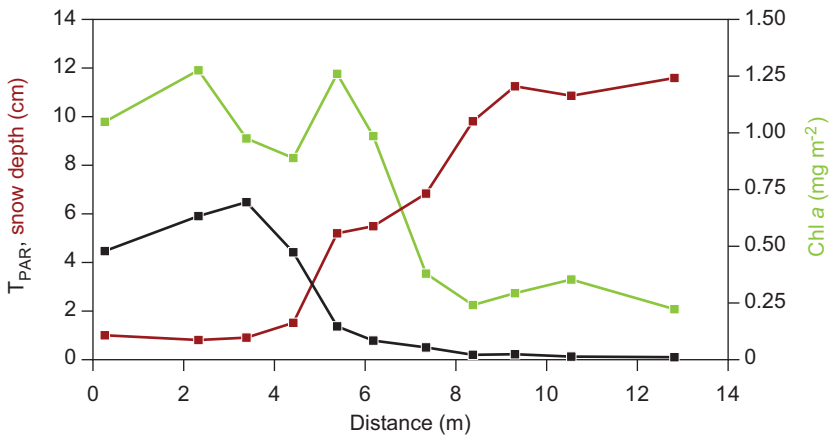
Fig. 6.17 PAR transmittance (black line), snow depth (red line), and Chl *a* (green line) along a transect. Note that PAR transmittance was multiplied by 100, and Chl *a* by 6 for scaling. (Modified from: Lund-Hansen et al. 2018)
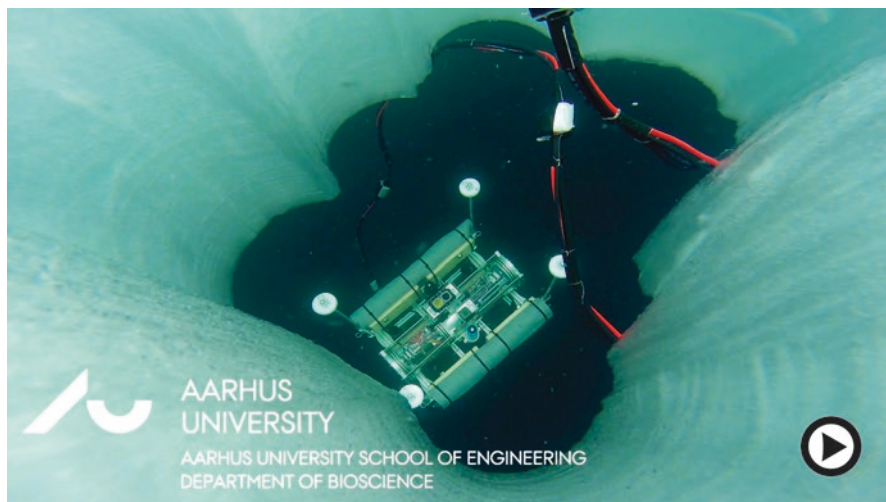
Fig. 6.18 A video shows the ROV deployed below the ice. Video: T. Juul and T. Eskildsen (https://doi.org/10.1007/000-05p)
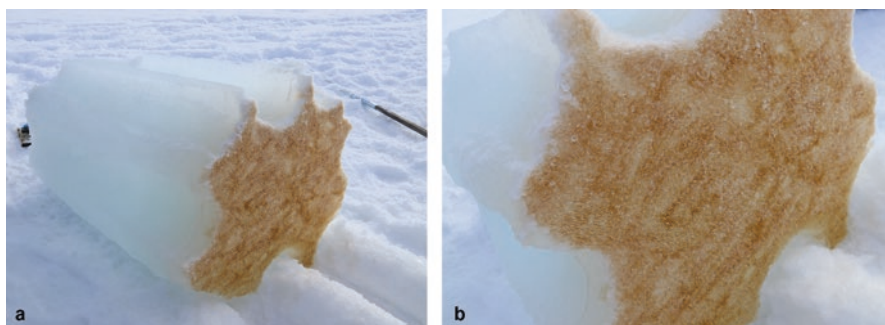
Fig. 6.19 A block of ice with a clear brown colouring due to the presence of ice algae, April, Svalbard (**a**), and a close up which clearly demonstrates an uneven distribution of the algae (**b**). Diameter of the block is about 40 cm. (Photograph by: Malin Daase)

the sea ice bottom. The fraction of the irradiance f(x,z) received by the sensor from within a radius (x) and a vertical distance (z) below a surface is:

$$f(x,z) = \sin^2 \cdot \left(\tan^{-1} \left(\frac{x}{z} \right) \right)$$

(6.11)

as shown by Nicolaus et al. (2012). An example: a sensor placed 0.25 m below the ice bottom receives 80% of the irradiance from within a circle of radius 0.5 m. Other parameters to consider when measuring bottom ice irradiance, both spectral and PAR, include dust and inorganic particles in the ice, brine channel size and geometry, ice temperature, CDOM, albedo, and ice algae to name the most important. Note
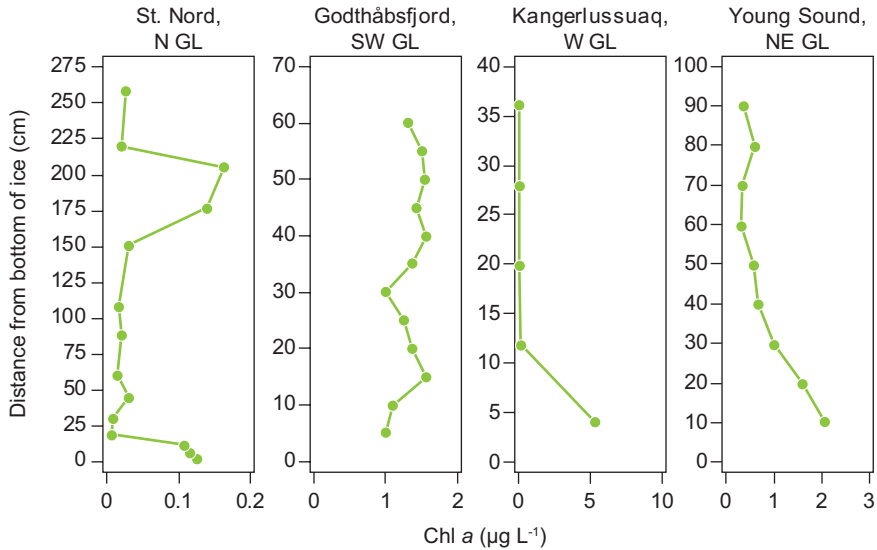
Fig. 6.20 Chl *a* concentrations in ice cores from different Greenland locations (GL)

that optical properties of the water column between the bottom of the sea ice and sensor head must also be considered with increased distances, as phytoplankton or sediment particles in the water will attenuate the irradiance before reaching the sensor.

6.5.1   Application of the Normalised Difference Index

At Cape Evans, Antarctica (Fig. 6.21) we deployed an AUV equipped with a Satlantic spectral radiometer measureing at six specific wavelengths (412, 470, 532, 565, 625, and 670 nm). The AUV followed a pre-programmed track below the ice operating with no surface contact covering under-ice flight paths up to 400 m long. The ice was about 1.9 m thick with a snow-free surface on the AUV paths, and PAR transmittance was low with an average of 0.004 reaching as low as 0.0015, and average under-ice PAR of only 2.4 μmol photons m^{-2} s^{-1}. Despite the low PAR values, ice algae biomasses were very high with an average of 31.4 mg Chl *a* m^{-2} and a maximum of 81.4 mg Chl *a* m^{-2}, which is probably related to the high sea ice surface area established by the platelet 3-D structure (Fig. 2.8). The NDI concept, described above, showed at Cape Evans a low ($r^2 = 0.31$) but significant ($p < 0.05$) correlation between log predicted (NDI – Chl *a*) and log observed (ice core – Chl *a*) (Fig. 6.22). This low correlation was supposedly related to the occurrence of the platelet ice and the challenges of sampling here for Chl *a* without losing any material. The NDI relation was based on under-ice spectra measured from the ice using
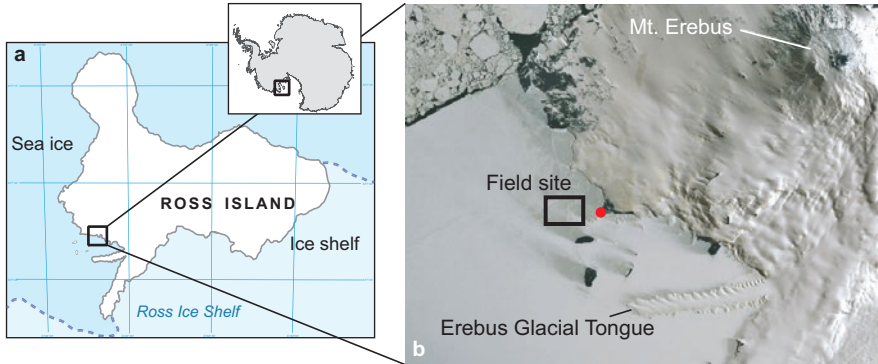
Fig. 6.21 Map of Ross Island in the Ross Sea where the blue dashed line is the border between the sea ice area and the Ross Ice Shelf (**a**), and satellite image of field site where the sea ice has begun to break up north of the field site (**b**). The Erebus Glacier Tongue is about 10 km long and about 1 km wide. (Modified from: Forrest et al. 2019)
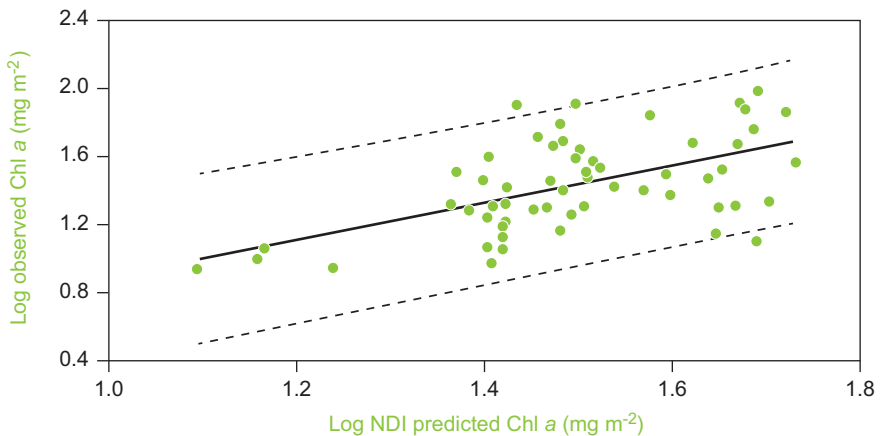
Fig. 6.22 Log observed Chl *a* against log NDI predicted Chl *a* with 95% confidence intervals (**a**) Cape Evans, November 2014, Antarctica. (Modified from: Forrest et al. 2019)

an L-arm (Fig. 6.12) combined with ice core sampling for Chl *a*. The subsequent NDI analyses showed that $E_d(\lambda_1) = 402$ nm and $E_d(\lambda_2) = 530$ nm were the best predictors of Chl *a*. The ratio was applied for the AUV dataset and used for mapping under-ice Chl *a*, and showed a strong variation in the spatial ice algae biomass distribution along the 350 m transect from an average background of 20 mg m^{-2} and up to 70 mg m^{-2} (Fig. 6.23). There was no clear relation between Chl *a* concentrations and under-ice topography except increased biomass at small protrusions at around 100, 150, 200, and 360 m. Work on the ice near Cape Evans is shown in Fig. 6.24.
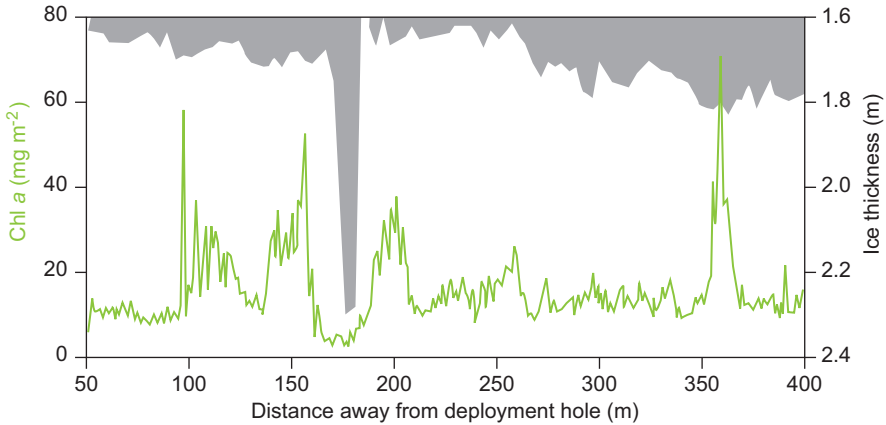
Fig. 6.23 GAVIA transect (350 m) with Chl *a* concentrations (green line) and ice thickness (grey colour), Cape Evans November 2014, Antarctica. (Modified from: Forrest et al. 2019)

Fig. 6.24 Work on sea ice and a 2 m thick block of sea ice with ice algae at the bottom, Cape Evans, Antarctica. (Photographs by: Authors)

6.6   Measuring Photosynthesis and Primary Production in Sea Ice

6.6.1   Methods Using Thawed Sea Ice

Photosynthesis and primary productivity of sea ice algae in thawed ice core samples can be measured with methods used for other aquatic microalgae. These were originally designed for free-living phytoplankton but can be suitable for ice algae, providing the sampling and handling problems discussed previously are recognised. Our understanding of photosynthesis and productivity in sea ice is based largely on these methods, and they will continue to be important even though there are new emerging methods such as microelectrodes (Else et al. 2015) and eddy covariance

(Attard et al. 2018) designed for *in situ* rather than thawed ice samples. The most widely used method to determine rates of inorganic carbon uptake in photosynthesis and the productivity of microalgae in liquid samples is the ^{14}C technique (e.g. Fernández-Méndez et al. 2015), originally developed by Steemann-Nielsen (1952). Primary production is determined in thawed ice samples at temperatures from 1 to 3 °C at different laboratory light intensities (minimum of 3 light intensities) and corrected with a dark incubation using trace amounts of radioactive $H^{14}CO_3^-$, which the algae assimilate and fix into their biomass. After incubations, algae in the sample are collected onto filters and these are placed in scintillation vials containing hydrochloric acid (1 M HCl) to remove labelled, unfixed inorganic carbon. Radioactivity inside the cells is then determined using a liquid scintillation counter. In parallel, total inorganic carbon (TCO_2) concentrations in melted sea ice are measured, e.g., as described by Rysgaard and Glud (2004). After liquid scintillation counting, counts are converted to potential primary production (PP_i in µg C L^{-1} h^{-1}) as:

$$PP_i = \frac{\left(DPM_{activity} \cdot TCO_{2\,seaice} \cdot F_{discr} \cdot M_C \right)}{\left(DPM_{added} \cdot T_{inc} \right)} \tag{6.12}$$

where $DPM_{activity}$ is the ^{14}C assimilated carbon corrected for carbon assimilated in the dark (DPM = disintegrations per minute), $TCO_{2\,sea\,ice}$ is the total concentration of dissolved inorganic carbon in the thawed sample (µmol L^{-1}), M_c is the molar mass of carbon (12.01 g mol^{-1}), F_{discr} is a discrimination factor of 1.05 to account for the differential assimilation of heavier ^{14}C vs ^{12}C, DPM_{added} is the specific activity of ^{14}C labelled medium (DMP L^{-1}) and T_{inc} the duration of the incubation (hours). The potential primary production (PP_i) (in the absence of photoinhibition) measured in the laboratory at different light levels is then plotted and fitted to the following function described by Platt et al. (1980):

$$PP\left(\mu g\ CL^{-1}h^{-1} \right) = P_{max} \cdot \left(1 - \exp\left(\frac{-\alpha \cdot E_{PAR}}{P_{max}} \right) \right) \tag{6.13}$$

where PP is the primary production, P_{max} (µg C L^{-1} h^{-1}) is the maximum photosynthetic rate at light saturation, α (µg C m^2 s µmol photons^{-1} L^{-1} h^{-1}) is the initial slope of the light curve and E_{PAR} (µmol photons m^{-2} s^{-1}) is the *in situ* hourly PAR irradiance at different sea ice depths which can be calculated using the attenuation coefficients. The onset of light saturation (i.e., the irradiance at which photosynthesis rate is reaching a maximum and becoming independent of irradiance) E_k (µmol photons m^{-2} s^{-1}) is then calculated as P_{max}/α (Fig. 3.16). Incubations using slices from sectioned sea ice cores allow description of profiles of primary productivity in the sea ice, and these can be integrated to convert the volumetric rates calculated above to productivity per unit area of sea ice. The photosynthesis-irradiance (P-*E*) response is the essential information for understanding the acclimation of algae to light availability and for estimating ice productivity, and most ^{14}C incubations involve sub-samples incubated over a range of laboratory light intensities in a specifically designed incubator (Fig. 6.25). The main theoretical debate with the ^{14}C
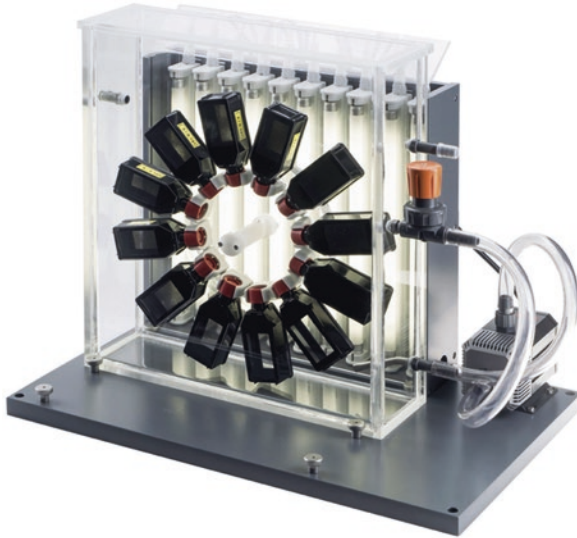
Fig. 6.25   The ICES incubator. An experimental set-up for a ^{14}C incubation experiment generating a photosynthesis-irradiance response curve requires an appropriate light source with incubation flasks at different irradiances for the P-E response. Neutral density filters placed between flasks and light source manipulate irradiances to desired values for constructing P-E curves. From bottom flask and going left clockwise the flasks are less and less transparent giving each flask a different light intensity inside the flasks containing the sample of melted ice or water with algae https://www.hydrobios.de/product/ices-incubator/

method is the extent to which it measures gross or net carbon uptake, or somewhere in-between. Considerable time can elapse before recently assimilated ^{14}C equilibrates with cell carbon pools and metabolism, so short incubations are usually interpreted as gross photosynthesis, given that little if any ^{14}C will be initially respired in mitochondria. Incubations long enough to allow complete equilibration to ensure net rather than gross uptake are often discouraged as this can also allow significant mortality and grazing of the incubated algae. A similar method that avoids the hazards of radioactive ^{14}C is to enrich the bottles of thawed ice with the stable carbon isotope ^{13}C rather than radioactive ^{14}C (Gradinger 2009), as a stable isotope does not emit ionising radiation, and ^{13}C poses no safety hazard to the user. The principle of the method is that the photosynthesising algae assimilate inorganic carbon from the known added amount of inorganic ^{13}C in the sample, and the algal ^{13}C content, measured on a mass spectrometer rather than a scintillation counter, provides the photosynthetic rate. Comparisons of the two methods usually show very close agreement between ^{14}C and ^{13}C methods, and it is generally agreed that ^{13}C, like ^{14}C, is a measure of gross rather than net photosynthesis (López-Sandoval et al. 2018). Photosynthetic activity and cellular acclimation to irradiance can also be measured with techniques based on variable chlorophyll fluorescence (Hawes et al. 2012; Manes and Gradinger, 2009). When chloroplasts are illuminated with photosynthetically active radiation (400–700 nm), they fluoresce, i.e., emit radiation of

longer wavelengths (680–760 nm). Fluorescence occurs in the Chl *a* associated with Photosystem II (PSII) in the chloroplast, and allows cells to safely dispose of the excess energy that cannot be used in photosynthesis and hence avoid it damaging the sensitive proteins that make up the photosynthetic apparatus. The proportion of the incoming light emitted by fluorescence is therefore variable dependent on photosynthetic activity, with most of the light fluorescing at low irradiances when photosynthesis rates are low, and less at higher irradiances when photosynthesis is using more of the incoming photons in photosynthetic electron transport. Figure 6.26 summarizes how variable chlorophyll fluorescence is measured by a pulse-amplitude modulated (PAM) fluorometer, a very sensitive instrument designed to explore the kinetics of chlorophyll fluorescence, thereby detecting stress in photosynthetic cells and how their activity changes as irradiance increases (Ralph and Gademann 2005). The photosystems are initially activated by a very weak ($E_{PAR} < 0.2$ μmol photons m^{-2} s^{-1}) light that, in a darkened sample with no active photosynthesis, establishes the absolute minimum fluorescence (F_0) of the sample, followed by a brief (0.2 sec) pulse of extreme ($E_{PAR} > 8000$ μmol photons m^{-2} s^{-1}) irradiance that will produce the maximum possible fluorescence (F_m) (Fig. 6.26a). The maximum possible fluorescence yield in such a dark-adapted sample is termed F_v/F_m:

$$\frac{F_v}{F_m} = \frac{\left(F_m - F_0\right)}{F_m}$$

$$(6.14)$$

and on theoretical grounds can be as high as 0.8 in completely healthy, unstressed cells. This is a very useful parameter for interpreting the condition of the algae, as it will be lowered by stresses such as cold temperatures, high salinities, high oxygen concentrations, and damage suffered due to exposure to prolonged excess irradiance (photoinhibition). It also develops seasonally, being very low (0.1) in early spring when ice algae first colonise the sea ice, rising to values > 0.6 at the peak of the spring bloom. If the algae are then exposed to higher irradiances (Fig. 6.26b), the minimum fluorescence is more active but the maximum fluorescence produced will be lower, because more of the photons are being used in photosynthesis, and the effective quantum yield termed Y(II) is also lower. Y(II) therefore decreases with increasing irradiance (Fig. 6.26c), and a photosynthesis-irradiance proxy curve can be derived by converting Y(II) to a photosynthetic electron transport rate in the chloroplast:

$$ETR = Y\left(II\right) \cdot A_f \cdot 0.5 \cdot E_{PAR}$$

$$(6.15)$$

where ETR is the electron transport rate (μmol electrons m^{-2} s^{-1}), A_f is the light absorption spectrum of chlorophyll in the sample, and E_{PAR} the irradiance. If A_f is unknown, it can be set as a constant and ETR is termed rETR (relative electron transport rate). PAM fluorescence-derived rETR-*E* curves have become a popular non-destructive and faster alternative to the ^{14}C method. PAM fluorescence instruments also offer an even faster P-*E* curve option, termed a rapid light curve (RLC). In this case the instrument measures how the fluorescence yield changes over a
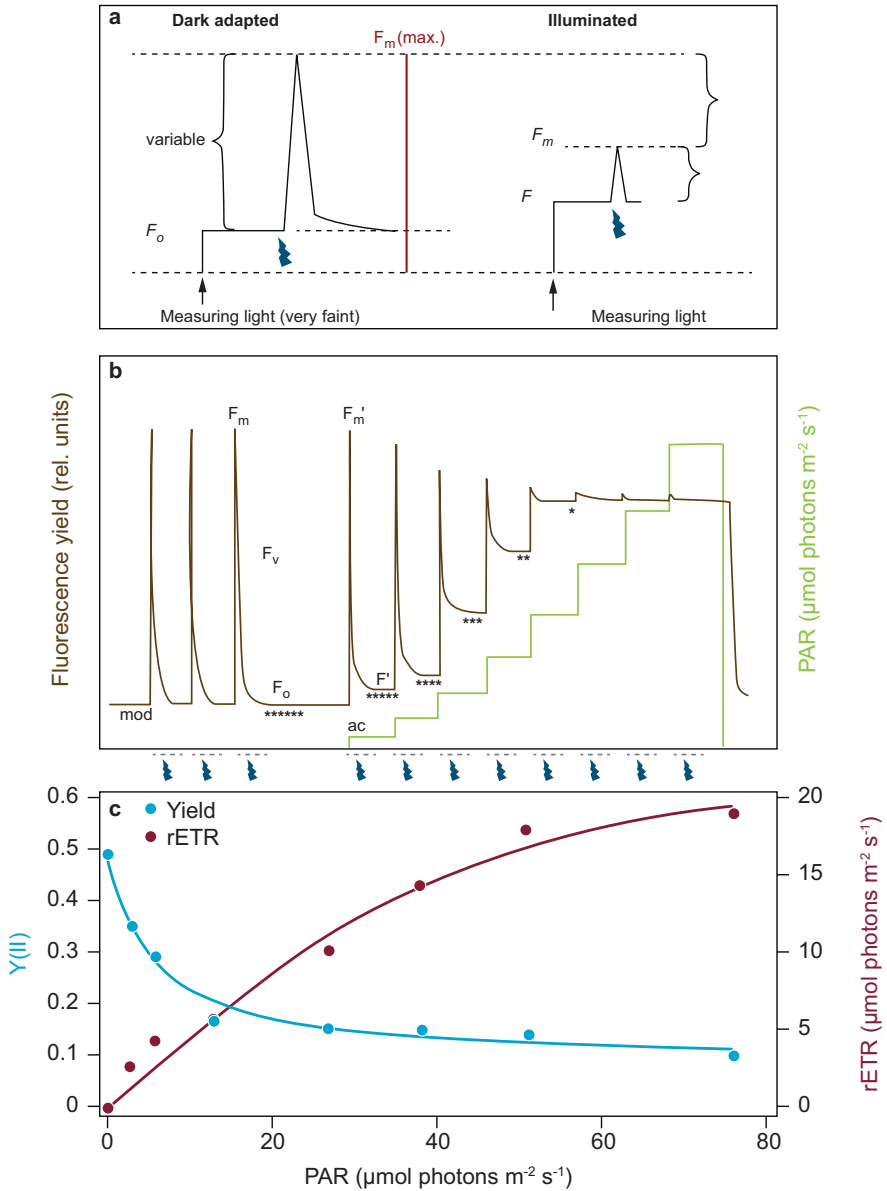
Fig. 6.26 Fluorescence kinetics in dark-adapted and illuminated cells in response to a saturating light pulse (blue flashes at the bottom) in a PAM-fluorometer. F_0 and F_m are the absolute minimum and maximum fluorescence in a dark-adapted (>30 min in darkness) sample, and F and F'_m are the corresponding yields in an illuminated sample (**a**), repeated pulses give progressively less fluorescence yield Y(II) at each increasing irradiance step, as more of the light is used in photosynthesis (**b**), and plot of the decreasing yield of Y(II) with increasing irradiance (blue line), and conversion of the Y(II) data to relative photosynthetic electron transport rates (rETR) (red line) in a P-E response for the rapid light curve (**c**). The number of asterisks at each light step in (**b**) represents the relative number of open reaction centers before each light pulse. Note that Y(II) is the effective quantum yield as compared to the maximum quantum yield F_v/F_m as the quantum yield of the dark-adapted sample

range of irradiances over a very short time period, usually less than 5 min per sample. Hence, the instrument is increasing the irradiance at a higher rate than the exposed algae can acclimate their photosynthetic machinery to at each new E_{PAR} setting. As discussed by Ralph and Gademann (2005), an RLC therefore cannot be used to provide the true P-*E* response of the organisms, but instead provides additional information about their instantaneous acclimation to the irradiance experienced before the RLC was applied. The same light response parameters derived from standard P-*E* curves described in Sect. 3.7 are derived in PAM fluorescence curves, except that the maximum rate of photosynthesis is ETR_{max} or $rETR_{max}$, the maximum light-saturated electron transport rate, rather than P_{max}. A detailed comparison of ^{14}C, O_2, and variable chlorophyll fluorescence (Phyto-PAM) derived photosynthesis parameters was carried out be Hancke et al. (2015).

6.6.2   Methods Using Non-Thawed Sea Ice

To avoid the disturbances associated with coring, methods have been developed to measure algal productivity from beneath the sea ice. These include measuring O_2 gradients in the diffusive boundary layer at the ice-water interface with O_2 microelectrodes or microoptodes (e.g., McMinn and Ashworth 1998; McMinn et al. 2007; Mock and Thomas 2005). Another novel development is the eddy covariance approach (Fig. 6.27). The principle is to mount the eddy-covariance instrumentation on the underside of undisturbed sea ice and quantify the flux of O_2 in and out of the ice, integrating over a much larger area than can be done by microsensor profiles

Fig. 6.27 An eddy covariance (EC) set-up that measures under-ice fluxes of O_2 and heat. The set-up consists of an acoustic Doppler velocimeter, O_2 microsensor temperature sensor, and a light meter (not shown). The measurements require an undisturbed light and flow regime with a footprint area of 20–100 m² upstream from the instrument. Green dots represent photosynthesizing ice algae at the bottom of the ice
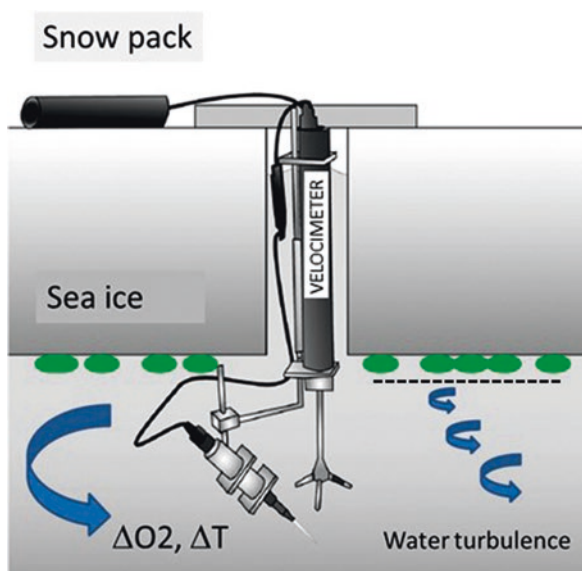
(Else et al. 2011, 2015). As shown in Fig. 6.27, the data necessary for the eddy covariance approach include a vertical profile of the flow of water along the ice, the concentration of O_2, as well as measurements of the temperature gradient, which describes the transfer rate. Recent studies using this approach suggest that the other methods under-estimate productivity compared to *in situ* eddy covariance (Attard et al. 2018). The major challenge for this method, and the reason it has not been more widely used, is the logistical difficulties, as the instrument must be installed by a diver. In addition, the O_2 fluxes at the ice-water interface are influenced not only by biotic processes i.e., photosynthetic production and respiration, but also by abiotic processes such as freezing and melting of the ice. For example, brine rich in O_2 could be rejected from the ice via the brine channels. Furthermore, it is challenging to define the footprint of this method which makes it difficult to relate eddy covariance data with other measurements, such as biomass estimates from ice coring or optical sensors.

6.6.3   Methods for Algal Quantification

Ancillary data for photosynthetic methods include sea ice Chl *a* content as well as concentrations of other pigments related to the photosynthetic machinery. These are all determined by collecting algae from thawed ice samples by concentrating material onto filters (usually 0.2 μm pore size) and extracting the filters in solvents. Using the Chl *a* content of the sample as a proxy for biomass is a long-standing practice in microalgal ecology, but this may not always be accurate as the algae can upregulate and downregulate their chlorophyll content in response to changing irradiances (Kühl et al. 2001). For that reason, it is also useful to have quantitative cell counts from the samples to compare against Chl *a*; for most of the larger algal species this can be based on simple microscopic counts of cells that have been concentrated in settling chambers (Utermöhl 1958). Smaller taxa that cannot be readily accounted for in standard microscopy are usually quantified by epifluorescence microscopy or by flow cytometry (Detmer and Bathmann 1997). These methods involve staining the small nano- and pico-plankton with a fluorescent dye and detecting them by their fluorescence including the Chl *a* autofluorescence (Marie et al. 2000).

6.7   Determination of Chl *a*

Chl *a* is the most commonly used proxy for viable algal biomass in sea ice and seawater. There are various techniques to measure chlorophyll, based on spectrophotometry and fluorometry. These are all determined from collecting algae in the thawed ice by filtering samples onto filters (usually 0.2–0.6 μm effective pore size glass fibre filters). The filters are then carefully folded with the algae inside, and

wrapped in aluminium foil for freezing unless they can be analysed immediately. A normal household deep freeze ($-18\ °C$) suffices for short periods but for longer storage a $-80°C$ freezer is more secure. The filters can also be placed in small glass containers with the solvent, and kept in the freezer until analysed. Be aware that Chl a can break down if kept on filters in a freezer for months. For extraction, filters are usually placed in a small volume of solvent (95% ethanol) in the dark for up to 24 h, or placed in a sonicator for faster extraction. Methanol and acetone can also be used as solvents, but ethanol is preferred. The extract is then vortexed and centrifuged, and chlorophyll content is analysed in a spectrophotometer or by a fluorometer. Chl a (µg Chl a L^{-1}) in a spectrophotometer can be calculated following Lorenzen (1967) and Strickland and Parsons (1972):

$$\mathrm{Chl}\ a = \mathrm{ethanol\ added} \times 29.1 \times \frac{\left(\left(A_{665} - A_{750}\right)_{-\mathrm{Acid}} - \left(A_{665} - A_{750}\right)_{+\mathrm{Acid}}\right)}{\mathrm{width} \times \mathrm{volume\ filtered}} \qquad (6.16)$$

with volume of ethanol added (mL), $A_{665} - A_{750}$ are absorbances at 665 and 750 nm without ($-$ Acid) and with ($+$ Acid), width is cuvette width (cm), and volume filtered (L). The factor 29.1 combines the absorption coefficient of Chl a and a factor for reduction in absorbance to initial Chl a concentration. After initial measurement of A_{665} and A_{750} at these wavelengths, acidifying with two drops of 1 N HCl ($+$ acid) in the cuvette breaks the Chl a down to pheophytin, and absorbance at A_{665} and A_{750} are read again. In sea ice ecology we then integrate the concentration over the length of the ice core or ice section and the units are then mg Chl a m^{-2}. The reason is that ice algae are not evenly distributed in the ice, often with high concentrations at the bottom of the ice. The ratio between the absorbance at 480 nm and 665 nm (480/665) may be used as an indicator for the nutrient status of the algae, i.e. are they nutrient-limited or not. If the ratio is > 2, the algae community in question is said to be nutrient-limited (Heath et al. 1990). Fluorometers are widely used in sea ice research, being more sensitive than spectrophotometer measurements, and are usually best for sea ice algae, as these can occur in very low concentrations (~0.001 mg Chl a m^{-2}). The extraction is performed similarly, and the calculation again uses the volumes of solvent and filtered sample. The measured fluorescence is integrated over the spectrum of chlorophyll rather than being wavelength-specific, but actual calculation of Chl a concentrations depends on the specific type or brand of fluorometer, and the manual must be consulted.

6.8   Fluorescence Imaging of Ice Algae

The problems associated with studying sea ice algal metabolism in melted ice samples are discussed above (Sects. 6.6 and 6.7), and particularly the highly unnatural condition of using liquid samples to study cells that, *in vivo,* are fixed in position in the ice-brine matrix. Clearly, methods that can measure algal distribution and metabolism in intact, non-melted ice samples are preferable. One such approach

that has provided considerable insight into the natural behaviour of ice algae during the last 10 years is fluorescence imaging, a variation of the variable chlorophyll fluorescence technique described in Sect. 6.6, based on pulse-amplitude modulated (PAM) fluorometry. This version of a PAM fluorometer, the Imaging-PAM fluorometer, designed to make two-dimensional images of chlorophyll fluorescence in flat plant leaves, can as well be applied to flat ice surfaces (Fig. 6.28). A detailed description of applying Imaging-PAM techniques in sea ice is given by Hawes et al. (2012) and applied in several studies (Lund-Hansen et al. 2013, 2016; Castrisios et al. 2018). The principle of the method is that, instead of thawing sections of ice cores, the intact sections are placed under the light source/camera apparatus as shown in Fig. 6.28. Great care is required in protecting the ice sample from light and cold or warm air temperatures during handling. Variable chlorophyll fluorescence is then measured largely as described in Sect. 6.6 for the Phyto-PAM method, by activating photosystems with a very weak, pulsed blue light, followed by a saturating light pulse. The difference and advantage of this method is that the important parameters F_0, F_v/F_m, and ETR (electron transport rate) are recorded as two-dimensional images of the photographed ice surface, rather than as a single number for a thawed, mixed sample. The method provides a spatial resolution of parameters with values of parameters in each pixel. The digital information in the images can then be converted to quantitative data that describe their spatial variation in the ice, and are more representative of the *in situ* condition than a melted sample. Moreover, images can be made of both horizontal surfaces (Fig. 6.28a, b) and vertical sections (Fig. 6.28c, d), allowing the spatial distribution of algae and their activity within the ice matrix to be determined three-dimensionally. The main disadvantage of the method is that it considerably less sensitive than the Phyto-PAM. It cannot be used to detect the very earliest production at low Chl *a* concentrations, or to investigate the low-biomass communities higher up in the ice, although the Imaging-PAM is applicable to the quantitatively important diatom communities occurring at the bottom of the sea ice. Fluorescence imaging provides a technique allowing measurement of photobiology that is certainly more natural than melted samples, although artefacts due to coring disturbance are still likely.

6.9   The IP$_{25}$ – A Proxy for Sea Ice Distributions and Food Web Studies

As described in Chap. 5, sea ice plays a significant role in Earth's climate specifically because much shortwave radiation is reflected back into space due to the high albedo of snow and ice (Perovich and Polashenski 2012). With less sea ice, incoming shortwave radiation from the sun will be absorbed in the water column and increase the temperature of the water column (Arrigo and Dijken 2015). There will be no summer ice in the Arctic in 2080, if the present rate of melting continues (Fig. 5.2b). An important question is then how sea extents were before satellite
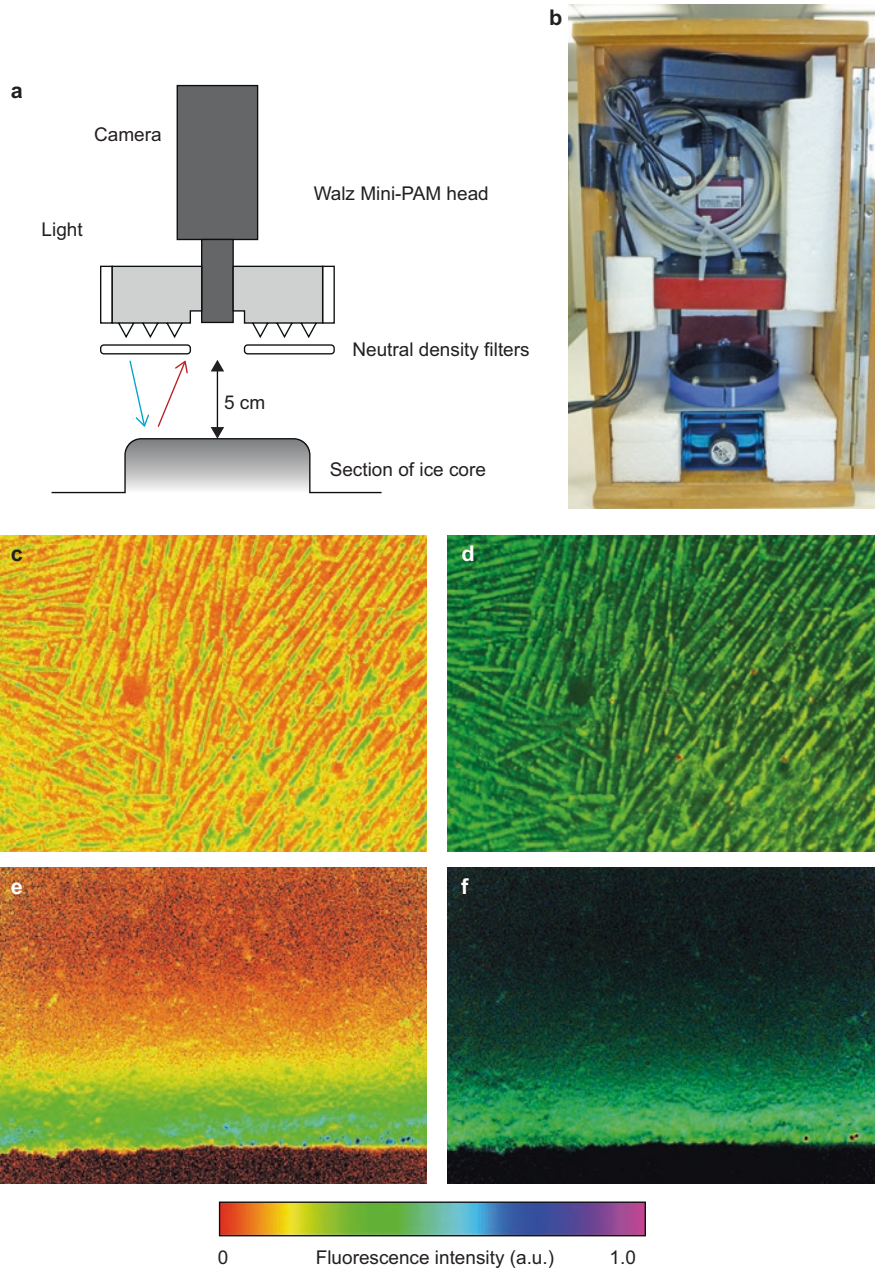
Fig. 6.28 The Walz Imaging-PAM instrument pulses the ice sample with blue light and the camera detects algal fluorescence at longer (red) wavelengths with neutral density filters to reduce illumination (**a**), and enclosing the entire apparatus in a light-proof box ensures dark-adapted conditions (**b**), and examples of images produced by Imaging-PAM fluorometry as: F_0 image of the bottom surface of an ice core, showing the distribution of live algae on the crystal structure (**c**), a similar image of F_v/F_m after a saturating pulse (**d**), F_0 image of transverse section through a core, showing vertical distribution of live algae in the lower 10–15 mm of the ice matrix (**e**), and a similar image of F_v/F_m (**f**). Images (30 · 23 mm) are false colour images with relative units. (Modified from: Hawes et al. 2012)
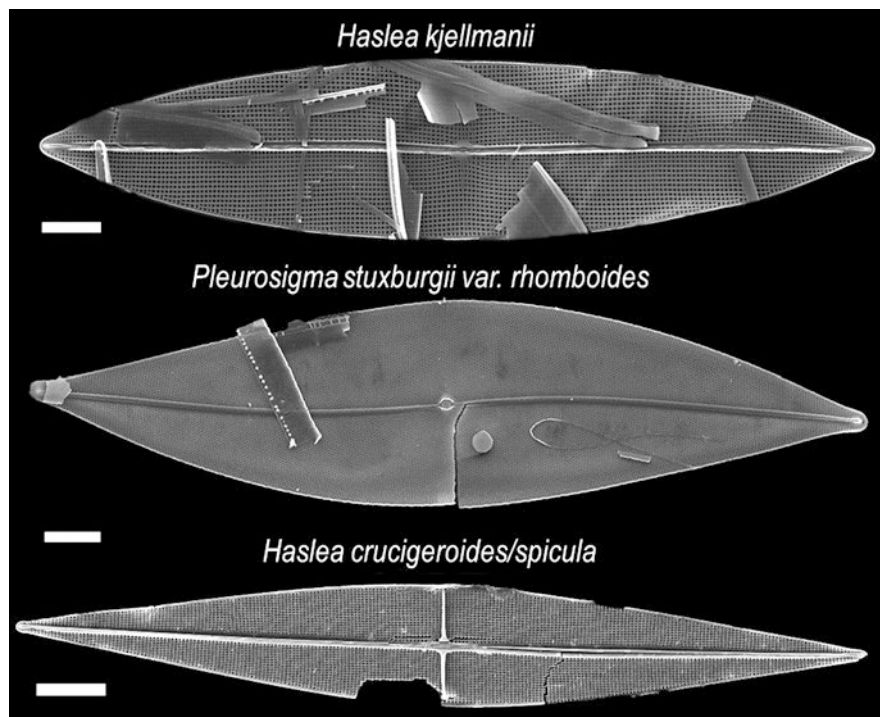
Fig. 6.29 Scanning electron micrographs of IP$_{25}$ -producing diatom species.. Scale bars 10 μm. (Micrographs by: T. Brown)

commencing in 1979, and even further back in time, where the geological record has shown a considerable variation in Arctic sea ice extent related to warmer and colder periods (Luoto et al. 2018). The main archive for reconstruction of past oceanographic environmental conditions is the sediment accumulated at the bottom of the oceans (Seibold and Berger 2017), where ocean water temperatures can be reconstructed based on the isotopic composition as $\partial O^{18}/\partial O^{16}$ of microorganisms deposited over time (Hanslik et al. 2010). An equivalent proxy for the occurrence of sea ice has just recently been identified: the IP$_{25}$ – short for Ice Proxy with 25 carbon atoms. The IP$_{25}$ is a highly-branched isoprenoid, an organic compound of fatty acids, which is synthesized or produced specifically by sea ice diatoms of the genera *Haslea* and *Pleurosigma* (Belt et al. 2007; Brown et al. 2014) (Fig. 6.29). IP$_{25}$ is a biomarker and preserved in the sediment record when algae are deposited, and presence or absence of IP$_{25}$ in the sediment core is applied as a proxy for the presence or absence of sea ice at the time of deposition. The IP$_{25}$ has proven to be an extremely important proxy for, among other things, establishment of sea ice and oceanographic conditions in the past, as shown by a study of previous sea ice extent in the
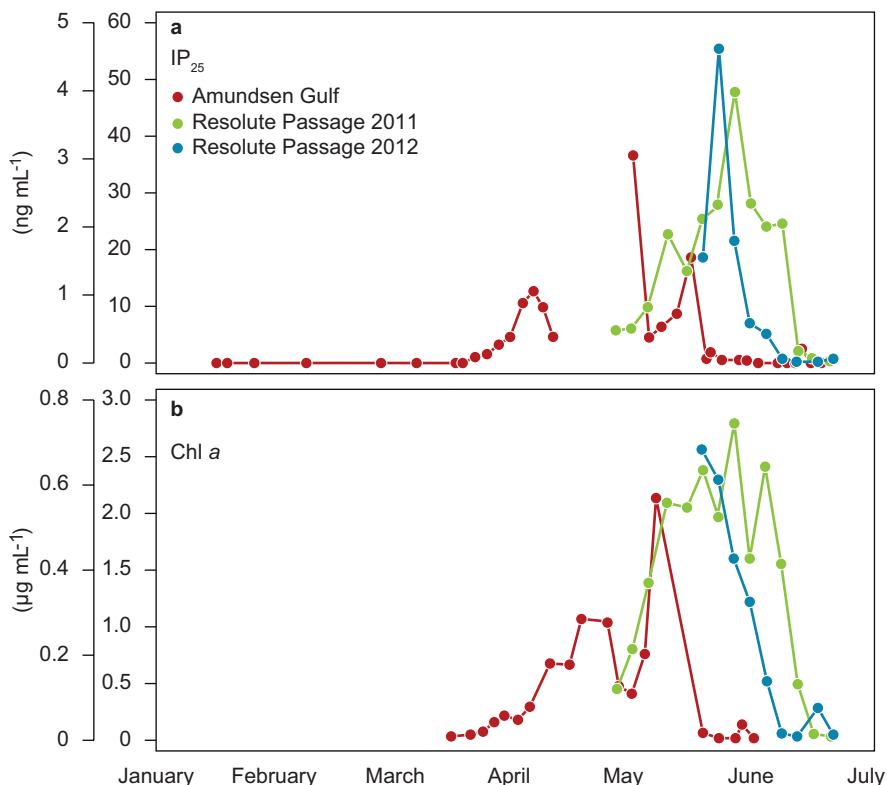
Fig. 6.30 Time series of IP$_{25}$ (**a**), and Chl *a* concentrations (**b**) from sea ice samples collected in the Amundsen Gulf in 2008 (red line), in Resolute Passage in 2012 (green line) and 2012 (blue line), NE Canadian Arctic. Note that inner ordinate scales apply for Resolute Passage 2012. (Modified from: Belt et al. 2013)

Bering Strait (Detlef et al. 2018). This organic compound has also proved useful in food web studies that have suggested that 70–100% of the diet of polar bears is sympagic-based (i.e., derived from carbon produced by ice algae), rather than pelagic-based (Brown et al. 2018). IP$_{25}$ has been applied in several trophic studies of sea ice-pelagic (Brown et al. 2017) and sea ice-pelagic-benthic coupling (Brown and Belt 2012), which have emphasized the importance of sea ice algae in Arctic ecosystems. Time-series during the ice algae spring bloom in the Canadian Arctic show positive correlations between Chl *a* and IP$_{25}$ (Fig. 6.29), which substantiates that IP$_{25}$ was synthesized by the ice algae. The specific IP$_{25}$ synthesizing algae were later identified as *Pleurosigma stuxbergi var: rhomboids*, *Haslea crucigeroides* and or *Haslea spicula*, and *Haslea kjelmanii* (Fig. 6.30) (Brown et al. 2014).

References

Arrigo, K. R., & Dijken, G. L. (2015). Continued increases in Arctic Ocean primary production. *Progress in Oceanography, 136*, 60–70. https://doi.org/10.1016/j.pocean.2015.05.002.

Attard, K. M., Søgaard, D. H., Piontek, J., Lange, B. A., Katlein, C., Sørensen, H. L., McGinnies, D. F., Rovelli, L., Rysgaard, S., Wenzhöfer, F., & Glud, R. N. (2018). Oxygen fluxes beneath Arctic land-fast ice and pack ice: Towards estimates of ice productivity. *Polar Biology, 41*, 2119–2134. https://doi.org/10.1007/s00300-018-2350-1.

Belt, S. T., Massé, G., Rowland, S. J., Poulin, M., Michel, C., & LeBlanc, B. (2007). A novel chemical fossil of palaeo sea ice: IP$_{25}$. *Organic Chemistry, 38*, 16–27. https://doi.org/10.1016/j.orggeochem.2006.09.013.

Belt, S. T., Brown, T. A., Ringrose, A. E., Cabedo-Sanz, P., Mundy, C. J., Gosselin, M., & Poulin, M. (2013). Quantitative measurement of the sea ice diatom biomarker IP$_{25}$ and sterols in Arctic sea ice and underlying sediments: Further considerations for palaeo sea ice reconstruction. *Organic Geochemistry, 62*, 33–45. https://doi.org/10.1016/j.orggeochem.2013.07.002.

Brown, T. A., & Belt, S. T. (2012). Identification of the sea ice diatom biomarker IP$_{25}$ in Arctic benthic macrofauna: Direct evidence for a sea ice diatom diet in Arctic heterotrophs. *Polar Biology, 35*, 131–137. https://doi.org/10.1007/s00300-011-1045-7.

Brown, T. A., Belt, S. T., Tatarek, A., & Mundy, C. J. (2014). Source identification of the Arctic sea ice proxy IP$_{25}$. *Nature Communications, 5*, 4197. https://doi.org/10.1038/ncomms5197.

Brown, T., Assmy, P., Hop, H., Wold, A., & Belt, S. T. (2017). Transfer of ice algae carbon to ice-associated amphipods in the high-Arctic pack ice environment. *Journal of Plankton Research, 39*, 664–674. https://doi.org/10.1093/plankt/fbx030.

Brown, T. A., Galicia, M. P., Thiemann, G. W., Belt, S. T., Yurkowski, D. J., & Dyck, M. G. (2018). High contributions of sea ice derived carbon in polar bear (*Ursus maritimus*) tissue. *PLoS One, 13*, e0191631. https://doi.org/10.1371/journal.pone.0191631.

Campbell, K., Mundy, C. J., Juhl, A. R., Dalman, L. A., Michel, C., Galley, R. J., Else, B. E., Geilfus, N. X., & Rysgaard, S. (2019). Melt procedure affects the photosynthetic response of sea ice algae. *Frontiers in Earth Science*. https://doi.org/10.3389/feart.2019.00021.

Carlson, D. F., Pasma, J., Jacobsen, M. E., Hansen, M. H., Thomsen, S., Lillethorup, J. P., Tirsgaard, F. S., Flythkjær, A., Melvad, C., Laufer, K., Lund-Hansen, L. C., Meire, L., & Rysgaard, S. (2019). Retrieval of ice samples using the Ice Drone. *Frontiers in Earth Science*. https://doi.org/10.3389/feart.2019.00287.

Castrisios, L., Martin, A., Müller, M. N., Kenneddy, F., Mcminn, A., & Ryan, K. G. (2018). Response of Antarctic sea-ice algae to an experimental decrease in pH: A preliminary analysis form chlorophyll fluorescence imaging of melting ice. *Polar Research, 37*. https://doi.org/10.1080/17518369.2018.1438696.

Cimoli, E., Meiners, K. M., Lund-Hansen, L. C., & Lucieer, V. (2017a). Spatial variability in sea-ice algal biomass: An under-ice remote sensing perspective. *Advances in Polar Science, 4*, 268–296. https://doi.org/10.13679/j.advps.2017.4.00268.

Cimoli, E., Lucieer, A., Meiners, K. M., Lund-Hansen, L. C., Kennedy, F., Martin, A., McMinn, A., & Lucieer, V. (2017b). Towards improved estimates of sea-ice algal biomass: Experimental assessment of hyperspectral imaging cameras for under-ice studies. *Annals of Glaciology, 58*, 68–77. https://doi.org/10.1017/aog.2017.6.

Collins, R. E., & Deming, J. W. (2011). Abundant dissolved genetic material in Arctic sea ice Part II: Viral dynamics during autumn freeze-up. *Polar Biology, 34*, 1831–1841. https://doi.org/10.1007/s00300-011-1008-z.

Collins, R. E., Carpenter, S. D., & Deming, J. W. (2008). Spatial heterogeneity and temporal dynamics of particles, bacteria, and pEPS in arctic winter sea ice. *Journal of Marine Systems, 74*, 902–917. https://doi.org/10.1016/j.jmarsys.2007.09.005.

Coveney, M. F., & Wetzel, R. G. (1988). Experimental evaluation of conversion factors for the [^{3}H] thymidine incorporation assay of bacterial secondary productivity. *Applied and Environmental Microbiology, 54*, 2018–2026.

Cox, G. F. N., & Weeks, W. F. (1983). Equations for determining the gas and brine volumes in sea-ice samples. *Journal of Glaciology, 29*, 306–316. https://doi.org/10.3189/S0022143000008364.

Deming, J. W. (2010). Sea ice bacteria and viruses. In D. N. Thomas & G. S. Dieckmann (Eds.), *Sea ice* (2nd ed., pp. 247–282). Oxford: Wiley Blackwell.

Deming, J. W., & Collins, R. E. (2017). Sea ice as a habitat for Bacteria, Archaea and viruses. In D. N. Thomas (Ed.), *Sea ice* (3rd ed., pp. 326–351). Oxford: Wiley Blackwell, 652 pp.

Detlef, H., Belt, S. T., Sosdian, S. M., Smik, L., Lear, C. H., Hall, I. R., Cabedo-Sanz, P., Husum, K., & Kender, S. (2018). Sea ice dynamics across the Mid-Pleistocene transition in the Bering Sea. *Nature Communications*. https://doi.org/10.1038/s41467-018-02845-5.

Detmer, A. E., & Bathmann, U. V. (1997). Distribution patterns of autotrophic pico- and nano-plankton and their relative contribution to algal biomass during spring in the Atlantic sector of the Southern Ocean. *Deep Sea Research Part II: Topical Studies in Oceanography, 44*, 299–320. https://doi.org/10.1016/S0967-0645(96)00068-9.

Eicken, H., Gradinger, R., Salganek, M., Shirasawa, D., Perovich, D. K., & Leppäranta, M. (2009). *Sea ice research techniques*. Alaska: University of Alaska Press.

Else, B. G. T., Papakyriakou, T. N., Galley, R. J., Drennan, W. M., Miller, L. A., Mucci, A., & Thomas, H. (2011). Wintertime CO_2 fluxes in an Arctic polynya using eddy covariance: Evidence of enhanced air-sea gas transfer during ice formation. *Journal of Geophysical Research, 116*. https://doi.org/10.1029/2010JC006760.

Else, B. G. T., Rysgaard, S., Attard, K., Cambell, K., Crabeck, O., Galley, R. J., Geilfus, N.-X., Lemes, M., Lueck, R., Papakyriakou, T., & Wang, F. (2015). Under-ice eddy covariance flux measurements of heat, salt, momentum, and dissolved oxygen in an artificial sea ice pool. *Cold Regions Science and Technology, 119*, 158–168. https://doi.org/10.1016/j.coldregions.2015.06.018.

Falkowski, P. G., & Raven, J. A. (2007). *Aquatic photosynthesis: Second edition*. Princeton: Princeton University Press, 488 pp.

Fenchel, T. (1998). Formation of laminated cyanobacterial mats in the absence of benthic fauna. *Aquatic Microbial Ecology, 14*, 235–240. https://doi.org/10.3354/ame014235.

Feng, S., Powell, S. M., Wilson, R., & Bowman, J. P. (2014). Extensive gene acquisition in the extremely psychrophilic bacterial species *Psychroflexus torquis* and the link to sea-ice eco-system specialism. *Genome Biology and Evolution, 6*, 133–148. https://doi.org/10.1093/gbe/evt209.

Fernández-Méndez, M., Katlein, C., Rabe, B., Nicolaus, M., Peeken, I., Bakker, K., Flores, H., & Boetius, A. (2015). Photosynthetic production in the central Arctic Ocean during the record sea-ice minimum in 2012. *Biogeosciences, 12*, 3525–3549. https://doi.org/10.5194/bg-12-3525-2015.

Forrest, A. L., Lund-Hansen, L. C., Sorrell, B., Bowden-Floyd, I., Lucieer, V., Cossu, R., Lange, B. A., & Hawes, I. (2019). Exploring spatial heterogeneity of Antarctic sea ice algae using an autonomous underwater vehicle mounted irradiance sensor. *Frontiers in Earth Science, 7*, 169–172. https://doi.org/10.3389/feart.2019.00169.

Fuhrman, J. A., & Azam, F. (1982). Thymidine incorporation as a measure of heterotrophic bacterioplankton production in marine surface waters: Evaluation and field results. *Marine Biology, 66*, 109–120.

Galley, R. J., Else, B. G. T., Geilfus, N.-X., Hare, A. A., Isleifson, D., Barber, D. G., & Rysgaard, S. (2015). Imaged brine inclusions in young sea ice – Shape, distribution and formation timing. *Cold Regions Science and Technology, 111*, 39–48. https://doi.org/10.1016/j.coldregions.2014.12.011.

Golden, K. M., Eicken, H., Heaton, A. L., Miner, J., Pringle, D. J., & Zhu, J. (2007). Thermal evolution of permeability and microstructure in sea ice. *Geophysical Research Letters, 34*. https://doi.org/10.1029/2007GL030447.

Gradinger, R. (2009). Sea-ice algae: Major contributors to primary production and algal biomass in the Chukchi and Beaufort Seas during May/June 2002. *Deep Sea Research Part II Topical Studies in Oceanography, 56*, 1201–1212. https://doi.org/10.1016/j.dsr2.2008.10.016.

Hancke, K., Dalsgaard, T., Sejr, M. K., Markager, S., & Glud, R. N. (2015). Phytoplankton productivity in an Arctic fjord (West Greenland): Estimating electron requirements for carbon fixation and oxygen production. *PLoS One, 10*. https://doi.org/10.1371/journal.pone.0133275.

Hancke, K., Lund-Hansen, L. C., Lamare, M. L., Pedersen, S. H., King, M. D., Andersen, P., & Sorrell, B. K. (2018). Extreme low light requirement for algae growth underneath sea ice: A case study from Station Nord, NE Greenland. *Journal of Geophysical Research, 123*, 985–1000. https://doi.org/10.1002/2017JC013263.

Hanslik, D., Jakobsson, M., Backman, J., Björck, S., Sellén, E., O'Regan, M., Fornaciari, E., & Skog, G. (2010). Quaternary Arctic Ocean sea ice variations and radiocarbon reservoir age corrections. *Quaternary Science Reviews, 29*, 3440–3441. https://doi.org/10.1016/j.quascirev.2010.06.011.

Hawes, I., Lund-Hansen, L. C., Sorrell, B. K., Nielsen, M. H., Borzák, R., & Buss, I. (2012). Photobiology of sea ice algae during initial spring growth in Kangerlussuaq, West Greenland: Insights from imaging variable chlorophyll fluorescence of ice cores. *Photosynthesis Research, 112*, 103–115. https://doi.org/10.1007/s11120-012-9736-7.

Heath, M. R., Richardson, K., & Kiørboe, T. (1990). Optical assessment of phytoplankton nutrient depletion. *Journal of Plankton Research, 12*, 381–396. https://doi.org/10.1093/plankt/12.2.381.

Junge, K., Eicken, H., & Deming, J. W. (2004). Bacterial activity at −2 to −20°C in Arctic wintertime sea ice. *Applied and Environmental Microbiology, 70*, 550–557. https://doi.org/10.1128/AEM.70.1.550-557.2004.

Kaartokallio, H. (2001). Evidence for active microbial nitrogen transformations in sea ice (Gulf of Bothnia, Baltic Sea) in midwinter. *Polar Biology, 24*, 21–28. https://doi.org/10.1007/s003000000169.

Kaartokallio, H. (2004). Food web components, and physical and chemical properties of Baltic Sea ice. *Marine Ecology Progress Series, 273*, 49–63. https://doi.org/10.3354/meps273049.

Kaartokallio, H., Kuosa, H., Thomas, D. N., Granskog, M. A., & Kivi, K. (2007). Biomass, composition and activity of organism assemblages along a salinity gradient in sea ice subjected to river discharge in the Baltic Sea. *Polar Biology, 30*, 183–197. https://doi.org/10.1007/s00300-006-0172-z.

Kaartokallio, H., Tuomainen, J., Kuosa, H., Kuparinen, J., Martikainen, P. J., & Servomaa, K. (2008). Succession of sea-ice bacterial communities in the Baltic Sea fast ice. *Polar Biology, 31*, 783–793. https://doi.org/10.1007/s00300-008-0416-1.

Kirchman, D., Ducklow, H., & Mitchell, R. (1982a). Estimates of bacterial growth from changes in uptake rates and biomass. *Applied and Environmental Microbiology, 44*, 1296–1307.

Kirchman, D., Sigda, J., Kapuscinski, R., & Mitchell, R. (1982b). Statistical analysis of the direct count method for enumerating bacteria. *Applied and Environmental Microbiology, 44*, 376–382.

Krembs, C., & Engel, A. (2001). Abundance and variability of microorganisms and transparent exopolymer particles across the ice-water interface of melting first-year sea ice in the Laptev Sea (Arctic). *Marine Biology, 138*, 173–185. https://doi.org/10.1007/s002270000396.

Kühl, M., Glud, R. N., Borum, J., Roberts, R., & Rysgaard, S. (2001). Photosynthetic performance of surface-associated algae below sea ice as measured with a pulse amplitude-modulated (PAM) fluorometer and O_2 microsensors. *Marine Ecology Progress Series, 223*, 1–14. https://doi.org/10.3354/meps223001.

Legendre, L., & Gosselin, M. (1991). In situ spectroradiometric estimation of microalgal biomass in first-year sea ice. *Polar Biology, 11*, 113–115. https://doi.org/10.1007/BF00234273.

Lizotte, M. P. (2003). The microbiology of sea ice. In D. N. Thomas & G. S. Dieckmann (Eds.), *Sea ice. An introduction to its physics, chemistry, biology and geology*. Blackwell Science, 401 pp. https://doi.org/10.1002/9780470757161.ch6

Long, M. H., Koopmans, D., Berg, P., Rysgaard, S., Glud, R. N., & Søgaard, D. H. (2012). Oxygen exchange and ice melt measured at the ice-water interface by eddy correlation. *Biogeosciences, 9*, 1957–1967. https://doi.org/10.5194/bg-9-1957-2012.

López-Sandoval, D. C., Huertas, A., & Agusti, S. (2018). The ^{13}C method as a robust alternative to ^{14}C-based measurements of primary productivity in the Mediterranean Sea. *Journal of Plankton Research, 40*, 544–554. https://doi.org/10.1093/plankt/fby031.

Lorenzen, C. J. (1967). Determination of chlorophyll and pheo-pigments: Spectrophotometric equations. *Limnology and Oceanography, 12*, 343–346. https://doi.org/10.4319/lo.1967.12.2.0343.

Lund-Hansen, L. C., Hawes, I., Sorrell, B. K., & Nielsen, M. H. (2013). Removal of snow cover inhibits spring growth of Arctic ice algae through physiological and behavioral effects. *Polar Biology, 37*, 471–481. https://doi.org/10.1007/s00300-013-1444-z.

Lund-Hansen, L. C., Hawes, I., Nielsen, M. H., & Sorrell, B. K. (2016). Is colonization of sea ice by diatoms facilitated by increased surface roughness in growing ice crystals? *Polar Biology, 40*, 593–602. https://doi.org/10.1007/s00300-016-1981-3.

Lund-Hansen, L. C., Juul, T., Eskildsen, T. D., Hawes, I., Sorrell, B., Melvad, C., & Hancke, K. (2018). A low-cost remotely operated vehicle (ROV) with an optical positioning system for under-ice measurements and sampling. *Cold Regions Science and Technology, 151*, 148–155. https://doi.org/10.1016/j.coldregions.2018.03.017.

Luoto, T. P., Ojala, A. E. K., Arppe, L., Brooks, S. J., Kurki, E., Oksman, M., Wooller, M. J., & Zajaczkowski, M. (2018). Synchronized proxy-based temperature reconstructions reveal mid- to late Holocene climate oscillations in High Arctic Svalbard. *Journal of Quaternary Science, 33*, 93–99. https://doi.org/10.1002/jqs.3001.

Manes, S. S., & Gradinger, R. (2009). Small scale vertical gradients of Arctic ice algal photophysiological properties. *Photosynthesis Research, 102*, 53–66. https://doi.org/10.1007/s11120-009-9489-0.

Marie, D., Simon, N., Guillou, L., Partensky, F., & Vaulot, D. (2000). Flow cytometry analysis of marine picoplankton. In R. A. Diamond & Demaggio (Eds.), *In living color*. Berlin: Springer, 734 pp. https://doi.org/10.1007/978-3-642-57049-0_34.

McMinn, A., & Ashworth, C. (1998). The use of oxygen microelectrodes to determine the net production by an Antarctic sea ice algal community. *Antarctic Science, 10*, 39–44. https://doi.org/10.1017/S0954102098000066.

McMinn, A., Ryan, K. G., Ralph, P. J., & Pankowski, A. (2007). Spring sea ice photosynthesis, primary productivity and biomass distribution in eastern Antarctica, 2002-2004. *Marine Biology, 151*, 985–995. https://doi.org/10.1007/s00227-006-0533-8.

McMinn, A., Martin, A., & Ryan, K. (2010). Phytoplankton and sea ice algal biomass and physiology during the transition between winter and spring (McMurdo Sound, Antarctica). *Polar Biology, 33*, 1547–1552. https://doi.org/10.1007/s00300-010-0844-6.

Melbourne-Thomas, J., Meiners, K. M., Mundy, C. J., Schallenberg, C., Tattersall, K. L., & Dieckmann, G. S. (2015). Algorithms to estimate Antarctic sea ice algal biomass from under-ice irradiance spectra at regional scales. *Marine Ecology Progress Series, 536*, 107–121. https://doi.org/10.3354/meps11396.

Miller, L. A., Fripiat, F., Else, B. G. T., Bowman, J. S., Brown, K. A., Collins, R. E., Ewert, M., Fransson, A., Gosselin, M., Lannuzel, D., Meiners, K. M., Michel, C., Nishioka, J., Nomura, D., Papadimitriou, S., Russell, L. M., Sørensen, L. L., Thomas, D. N., Tison, J.-L., van Leeuwe, M. A., Vancoppenolle, M., Wolff, E. W., & Zhou, J. (2015). Methods for biogeochemical studies of sea ice: The state of the art, caveats and recommendations. *Elementa Science of the Anthropocene, 3*, 1–53. https://doi.org/10.12952/journal.elementa.000038.

Mock, T., & Thomas, D. N. (2005). Recent advances in sea-ice microbiology. *Environmental Microbiology, 7*, 605–619. https://doi.org/10.1111/j.1462-2920.2005.00781.x.

Mundy, C. J., Ehn, J. K., Barber, D. G., & Michel, C. (2007). Influence of snow cover and algae on the spectral dependence of transmitted irradiance through Arctic landfast first-year sea ice. *Journal of Geophysical Research, 112*. https://doi.org/10.1029/2006JC003683.

Nicolaus, M., Katlein, C., Maslanik, J., & Hendricks, S. (2012). Changes in Arctic sea ice result in increasing light transmittance and absorption. *Geophysical Research Letters, 39*. https://doi.org/10.1029/2012GL053738.

Perovich, D. K., & Polashenski, C. (2012). Albedo evolution of seasonal Arctic sea ice. *Geophysical Research Letters, 39*. https://doi.org/10.1029/2012GL051432.

Petri, R., & Imhoff, J. F. (2001). Genetic analysis of sea-ice bacterial communities of the Western Baltic Sea using an improved double gradient method. *Polar Biology, 24*, 252–257. https://doi.org/10.1007/s003000000205.

Petrich, C., & Eicken, H. (2017). Overview of sea ice growth and properties. In D. N. Thomas (Ed.), *Sea ice*. (3rd ed., pp. 1–41). Oxford: Wiley Blackwell, 652 pp. https://doi.org/10.1002/9781118778371.ch1.

Platt, T., Gallegos, C. L., & Harrison, W. G. (1980). Photoinhibition of photosynthesis in natural assemblages of marine phytoplankton. *Journal of Marine Research, 38*, 687–701.

Ralph, P. J., & Gademann, R. (2005). Rapid light curves: A powerful tool to assess photosynthetic activity. *Aquatic Botany, 82*, 222–237. https://doi.org/10.1016/j.aquabot.2005.02.006.

Rivkin, R. B. (1986). Incorporation of tritiated thymidine by eucaryotic microalgae. *Journal of Phycology, 22*, 193–198. https://onlinelibrary.wiley.com/doi/abs/10.1111/j.1529-8817.1986.tb04163.x.

Rivkin, R. B., & Legendre, L. (2001). Biogenic carbon cycling in the upper ocean: Effects of microbial respiration. *Science, 291*, 2398–2400. https://doi.org/10.1126/science.291.5512.2398.

Rysgaard, S., & Glud, R. (2004). Anaerobic N_2 production in Arctic Sea Ice. *Limnology and Oceanography, 49*, 86–94. https://doi.org/10.4319/lo.2004.49.1.0086.

Rysgaard, S., Kühl, M., Glud, R. N., & Hansen, J. W. (2001). Biomass, production and horizontal patchiness of sea ice algae in a high-Arctic fjord (Young Sound, NE Greenland). *Marine Ecology Progress Series, 223*, 15–26. https://doi.org/10.3354/meps223015.

Rysgaard, S., Glud, R. N., Sejr, M. K., Blichner, M. E., & Stahl, H. J. (2008). Denitrification activity and oxygen dynamics in Arctic sea ice. *Polar Biology, 31*, 527–537. https://doi.org/10.1007/s00300-007-0384-x.

Seibold, E., & Berger, W. (2017). *The sea floor. An introduction to marine geology*. Berlin, Heidelberg, New York: Springer, 267 pp.

Steemann-Nielsen, E. S. (1952). The use of radio-active carbon (C^{14}) for measuring organic production in the sea. *ICES Journal of Marine Science, 18*, 117–140. https://doi.org/10.1093/icesjms/18.2.117.

Strickland, J. D. H., & Parsons, T. R. (1972). A practical handbook of seawater analysis. *Fisheries Research Board of Canada, 167*, 1–310.

Utermöhl, H. (1958). Zur Vervollkommung der quantitativen Phyto-plankton Methodik. *Mitteilungungen Der Internationale Vereinigung für Limnologie, 9*, 1–39.

Welch, H. E., & Bergmann, M. A. (1989). Seasonal development of ice algae and its prediction from environmental factors near Resolute, N.W.T., Canada. *Canadian Journal of Fisheries and Aquatic Sciences, 46*, 1793–1804. https://doi.org/10.1139/f89-227.

Glossary

Absorption The process by which irradiance is absorbed by water, biota, ice, sediments, and dust in the ice.

Acclimation Phenotypic adjustments of individual organisms to specific environmental conditions that lead to improved performance or tolerance of stress.

Adaptation Evolutionary adjustment of the genetic basis of organism traits that enhance performance in a specific environment**.**

Aggregates Attached or free–floating mats of algae found beneath the sea ice, in melt ponds, frozen into the sea ice or sinking to the bottom of the sea floor.

Albedo Fraction of the incident radiation reflected by a surface, i.e. reflected/incident.

Algae Autotrophic, eukaryotic photosynthetic organisms with chlorophyll *a* and other photosynthetic pigments, ranging from unicellular groups, e.g., some diatoms, to large, macroscopic forms, such as giant kelp.

Allelopathy Release of substances into the environment that inhibit germination or growth of other plants.

Allochthonous Externally derived organic carbon or organic matter sources in an ecosystem, c.f. autochthonous.

Archaea A domain of heterotrophic, single-celled prokaryotic organisms, genetically distinct from bacteria and often found in extreme environments.

Autochthonous Organic carbon or matter produced within an ecosystem, c.f. allochthonous.

Autotrophic The ability to use energy from light (photoautotrophic) or from oxidation of inorganic compounds (chemoautotrophic) to convert inorganic carbon (usually CO_2) to organic matter, c.f. heterotrophic.

Bacteria A large domain of prokaryotic microorganisms, most of which are heterotrophic and typically a few micrometres in length.

Benthos Organisms living on the seafloor, such as mussels and bivalves.

Biota The bacterial, plant and animal life in a specific area at a given time.

Brine channels mm-sized channels within the sea ice containing *brine* (concentrated seawater), and an important habitat for sea ice biota.

Brine drainage   Drainage of brine out of the sea ice into the underlying seawater column due to gravity.

Brine expulsion   The flow of liquid brine towards the underside of the sea ice driven by the freezing of the ice, which results in pressure build-up in the brine pockets.

Brine salinity   Salinity of the brine in the brine channels of sea ice.

Brine skim   A highly saline skim of brine that is formed on the sea surface in newly forming sea ice.

Bulk salinity   Salinity of a melted sample of sea ice.

Carbon dioxide (CO_2)   A trace gas, currently present at a concentration of 410 ppm in the atmosphere, having risen from pre-industrial levels of approx. 280 ppm. Most global CO_2 is dissolved in the oceans and reacts with water to form bicarbonate (HCO_3^-) and carbonate ions (CO_3^{2-}). Under typical seawater conditions, HCO_3^- is the dominant (86.5%) form, whereas dissolved free CO_2 (0.5%) and CO_3^{2-} (13%) are present in lower concentrations.

Carotenoids   Accessory photosynthetic pigments, generally responsible for absorbing additional light for photosynthesis and protecting chloroplast proteins from photodamage.

Cell membrane   The biological membrane that separates the interior of all cells from the outside environment. It is made of a lipid bilayer interspersed with proteins, making it selectively permeable to ions and organic molecules.

Centric diatoms   Radially symmetrical diatoms, often of low mobility, c.f. pennate.

Chlorophyll   Green pigments in the photosynthetic membranes of autotrophs that trap the energy of sunlight for photosynthesis. They exist in several forms of which the most common is chlorophyll *a*.

Chlorophyll *a*   The most common form of chlorophyll, predominant in all oxygen–evolving photosynthetic organisms. It is abbreviated as Chl *a*. Often used as a proxy for biomass in microscopic algal populations.

Chlorophyll *b*   A form of chlorophyll restricted to green plants, Chlorophyta and Euglenophyta.

Chlorophyll *c*1 and *c*2   Forms of chlorophyll found in many microalgae, including diatoms and dinoflagellates, as well as brown macroalgae.

Chlorophyta   The green algae, a division of algae characterised by Chl *a* and Chl *b* as their predominant photosynthetic pigments.

Chromophoric dissolved organic matter (CDOM)   Photoactive substances of the dissolved organic matter (DOM), with strong absorption in the blue and ultraviolet parts of the spectrum.

Ciliates   Motile protozoans characterized by hair-like organelles called cilia that generate movement by beating.

Conductivity   A measure of the ionic concentration of a liquid, based on its ability to conduct electricity.

Copepods   A subclass of Crustacea, usually planktonic, often being an important component of the sympagic fauna.

Cryophilic   See **psychrophilic**.

Cryoprotectants   Chemical substances that protect cells or tissue from damage when freezing.

Cryotolerant   Tolerant of low temperatures.

Cysts   Resting or dormant stages of an organism that allow them to survive unfavourable environmental conditions. Especially common in prokaryotes.

Desalination   The process by which salt ions are expelled from the freezing ice as there is no place for other ions being incorporated into the crystal lattice of water.

Diatinoxanthin and diadinoxanthin   Xanthophyll pigments in diatoms, the inter-conversion of which in the chloroplast help avoid serious damage from excess radiation. Often abbreviated Dtx and Ddx.

Diatoms   A major group of algae, characterised by a silica cell wall termed a frustule. Among the most common types of phytoplankton, they are usually the dominant biomass of the ice algae community. They are unicellular, and often exist as chains or colonies.

DIC   Dissolved inorganic carbon. See **TCO_2**.

Diffusive boundary layer (DBL)   The thin layer of non-moving water between a solid structure and the moving bulk water, e.g., between the bottom of the sea ice and its underlying seawater. It is a mm-thick layer where the transport of dissolved substances is solely by molecular diffusion compared to much faster turbulent mixing in the bulk water above or below the DBL. The DBL restricts the exchange of gases and nutrients between the ice and the water.

Dinoflagellates   A large group of autotrophic, flagellate eukaryotes that are common in both phytoplankton and sea ice algal communities.

Dissolved organic carbon (DOC)   Organic molecules of varied origin and composition dissolved in water in all aquatic ecosystems. DOC in marine waters generally results from decomposition of dead organic matter, especially plants. DOC is a food supplement supporting the growth of bacteria and plays an important role in the global carbon cycle through the microbial loop.

Dissolved organic matter (DOM)   The organic matter fraction in solution that passes through a 0.45 μm filter.

Dissolved organic nitrogen (DON)   A mixture of dissolved compounds ranging from simple amino acids to complex humic substances.

Eddy covariance   A technique for measuring oxygen exchange between seawater and a surface such as the sediment or sea ice, based on water turbulence and diffusion of gases in the diffusive boundary layer. Can be used to determine primary production or nutrient uptake and release of intact sea ice.

Eubacteria   The 'true' bacteria, single-celled prokaryotic microorganisms found in almost all ecosystems throughout the world, c.f. Archaea and eukaryotes.

Exponential growth   Growth of microorganisms whereby the cell number doubles within a fixed time period.

Extracellular polymeric substances (EPS)   High-molecular weight compounds secreted by microorganisms into their environment. In sea ice, EPS can function as cryoprotectants, or as external reserves of hydrolysable organic compounds, to depress the freezing point and to provide a physical buffer against encroaching ice crystals.

First-year ice   Sea ice consisting of no more than one winter's ice growth. It develops from young ice and is usually >30 cm thick.

Flagellate   Motile organisms with one or more flagella. Flagella-bearing species are common in all algal groups except the Cyanophyceae, Rhodophyceae, Phaeophyceae and Bacillariophyceae.

Fluorescence   Photons re-emitted from chloroplasts at a longer wavelength when electrons in photosystems return to the ground state. Chlorophyll fluorescence can be used to estimate algal biomass in a water column or on the underside of sea ice, and the variable chlorophyll fluorescence of photosystems can be used to quantify photosynthetic state and activity.

Frazil ice   Loose, randomly oriented ice crystals forming in supercooled water. Often a precursor to sea ice formation.

Freeboard   The vertical distance between the water table and the surface of the ice. Negative freeboard occurs when the water table is higher than the ice surface, typically when the weight of snow on top of the ice presses the ice surface downwards into the water column.

Frost flowers   Clusters of saline ice crystals that have a dendritic and branched structure. Frost flowers form at the interface between a warm ice surface and a cold atmosphere in conditions of low surface wind speeds.

Fucoxanthin   An accessory pigment in the chloroplasts of some algal groups including diatoms, that assist in light harvesting in the yellow to blue range of the spectrum, allowing greater light absorbance in aquatic environments.

F_0 Minimal fluorescence yield of photosynthesis after dark adaptation of an algal sample.

F_v/F_m The maximum quantum yield of photosynthesis of dark-adapted photosynthetic organisms, a widely used indicator of their photosynthetic activity, health and stress.

Global carbon budget   The sum of all exchanges (inflows and outflows) of carbon compounds between the earth's carbon reservoirs in the carbon cycle.

Halocline   A strong change in salinity at a specific depth, and develops due to stratification of seawater into layers of different salinity.

Halophile   An organism that thrives in highly saline water, e.g., in brine channels or salt lakes.

Halotolerant   The ability to withstand large changes in salinity.

Herbivore   An organism living by plant-based food subsistence.

Heterotrophic   Describes all organisms that obtain carbon for their organic synthesis by metabolising organic material. Includes animals, fungi, some algae, most bacteria, c.f. autotrophic.

HPLC   Abbreviation for high performance liquid chromatography, a method applied to separate and identify cellular pigments.

Infiltration layer   A layer in sea ice that develops by flooding of the sea ice surface by seawater and often due to the weight of the overlying snow.

Ikaite ($CaCO_3 \cdot 6H_2O$)   An unstable hexahydrate polymorph of $CaCO_3$, which begins to precipitate at $-2.2\ °C$ and dissolves at temperatures above $4\ °C$.

In situ   On site or in position.

Intracellular   Occurring or functioning within a cell.

IP$_{25}$ The abbreviation for ice proxy with 25 carbon atoms, a highly-branched iso-prenoid or fatty acid produced specifically by ice algae and used to detect fossil ice algae in sediments and applied in food web studies.

Irradiance   The radiant energy flux received per m^{-2} with the units W m^{-2}. Spectral irradiance is accordingly the energy or power resolved per wavelength (nm) with the units W m^{-2} nm^{-1}. The term is also used as synonym for PAR (Photosynthetic Active Radiation).

Light compensation point (E_c)   The irradiance at which the rate of CO_2 assimilation in photosynthesis is balanced by CO_2 released by respiration.

Light harvesting complex (LHC)   A complex of molecules including chlorophyll, accessory pigments and proteins of the chloroplast thylakoid membrane, which absorbs quanta of photons and transfers their excitation energy to chloroplast photosystems.

Light saturation   The irradiance range over which the rate of CO_2 assimilation in photosynthesis reaches a maximum and becomes independent of irradiance.

Leads   Open linear areas of open water in sea ice caused by stress fractures in the ice.

MAAs   Mycosporine-like amino acids that ice algae can synthesize as a protective compound against high ultraviolet radiation.

Meiofauna   Small multicellular animals living within the brine channel network, typically collected on a 20 μm sieve after completely thawing ice samples.

Melt ponds   Accumulation of pools of meltwater on the surface of the sea ice, mainly due to melting of snow, but also the underlying sea ice. Melt ponds absorb solar radiation rather than reflecting it as ice does and thereby have a significant influence on the sea ice albedo and earth's radiation balance.

Metazoa   Multicellular animals with two or more tissue layers, with a high degree of coordination between different cell types, and usually a nervous system, c.f. protozoa.

Motile   Capable of movement.

Multi-year ice   Sea ice consisting of more than a single year's growth. It can reach an age of 5–6 years.

NDI   Normalized difference index. An index based on absorption by Chl *a* at specific wave lengths, relative to absorption of snow and ice in the visible spectrum, allowing estimates of biomass from remote sensing methods.

Nekton   The community of organisms in a body of water able to swim actively against a current, as opposed to plankton, which is carried passively by water movement.

Nilas   A crust of sea ice up to 10 cm thick, typically an intermediate stage between new ice structures such as frazil and pancake ice and the formation of young sea ice proper.

Osmolytes   Dissolved ions or organic solutes within a cell that prevent osmotic shock by maintaining osmotic pressure within the cell to avoid cell lysis (too much internal pressure) or shrinkage (too little internal pressure).

Osmoprotectants   Solutes or molecules that help organisms survive extraordinary osmotic stress.

Osmotic shock   A sudden change in the solute concentration around a cell that causes a change in the movement of water across its cell membrane. In environments with high concentrations of salts, water is drawn out of the cells. This can be avoided by the incorporation of osmolytes.

Pancake ice   Approximately circular ice formations from 30 cm to 3 m in diameter and up to 10 cm thick, with raised and rimmed edges caused by collisions with other ice pieces.

PAR   See **Photosynthetically active radiation**.

p**CO$_2$**   The partial pressure of CO_2 in the atmosphere or when dissolved in water.

Pelagic   Organisms (including plankton and nekton) that swim or drift in the water column.

Pennate diatom   Bilaterally symmetrical, elongated diatoms, usually motile, c.f. centric.

Peridinin   An important carotenoid accessory pigment in dinoflagellates.

Permeability   The ability of a material such as ice to allow fluids (gases or liquids) to diffuse or flow through its pore spaces and brine channels.

pH   A scale used to specify how acidic or basic a water-based solution is. The pH of seawater plays an important role in the ocean's carbon cycle; pH measurement in seawater is complicated by its chemical properties.

Photoinhibition   A decline in photosynthetic efficiency upon exposure to high irradiance or UV radiation. A transient or dynamic photoinhibition is associated with protection of the photosynthetic apparatus, or longer-lasting photoinhibition implies photodamage (destruction of the photosynthetic apparatus).

Photon   A discrete unit of light that describes its particle-like properties (quantum), as opposed to its wavelike properties.

Photosynthesis   The process by which green plants and some unicellular organisms convert incoming sunlight into organic material from CO_2 and water.

Photosynthetically active radiation (PAR)   Radiation that can drive photosynthesis; the spectral range of solar radiation from 400 to 700 nanometres, similar to visible light. The unit of PAR is μmol photons $m^{-2}\,s^{-1}$.

Photosystem   A unit of pigments and proteins embedded in the membranes of the chloroplast where the excitation energy from absorbed photons is transferred to an electron.

Phytoplankton   The photosynthetic organisms of the plankton, and which are freely advected with the water masses.

Picophytoplankton   The fraction of the photosynthetic phytoplankton between 0.2 and 2 μm.

Platelet ice   Ice consisting of plates 1–10 mm thick, formed by freezing of seawater that has been supercooled below an ice shelf or glacier. Platelet ice can form metre-thick free-floating layers below the sea ice or can be frozen into the bottom of growing sea ice.

Polynya   An area of open water surrounded by sea ice. In this area, new sea ice is produced and frequently blown away, thereby allowing new ice to form repeatedly.

POM   Particulate organic matter. Organic particles <2 mm size in the water column or sea ice.

Porosity   A measure of the void volume of sea ice and hence the volume of the brine channels relative to the total volume.

Precipitation   Formation of a solid from solution by chemical or physical processes.

Pressure ridges   Angular blocks of sea ice that accumulate on the ice surface due to collisions between ice floes caused by currents and wind.

Primary production   The production of organic material (carbon) from inorganic carbon sources (CO_2 and HCO_3^-) by photosynthesis, termed primary as this is the basic step in almost all food webs.

Protists   Eukaryotic, unicellular or colonial organisms which form no distinct tissues. A paraphyletic, taxonomically diverse group including both autotrophs and heterotrophs.

Protozoa   Single-celled heterotrophic, eukaryotic organisms, c.f. metazoa.

Psychrophillic organisms   Organisms that have optimal growth rates at temperatures usually below 15 °C, and which cannot grow above 20 °C.

Psychrotolerant organisms   Organisms that have optimum growth rates at temperatures above 20 °C but can tolerate and, in the case of bacteria, grow at colder temperatures.

Pycnocline   A boundary in oceanography separating two water layers of different densities. The formation of a pycnocline may result from changes in salinity or temperature. Because the pycnocline is extremely stable, it acts as a barrier for surface processes.

Remote sensing   Measuring from a distance without direct hands-on involvement, such as with satellites measuring sea ice extent or spectroradiometers measuring spectral composition of the irradiance below the ice.

Respiration   Cellular metabolic processes that degrade organic matter and produce energy as ATP with CO_2 as a waste product.

Sackholes   Holes drilled partially through the sea ice for bulk sampling of brine water.

Salinity   The total mass of salts in 1 kg of seawater, dimensionless by definition although units such as ppm (parts per million), ‰, or PSU (Practical Salinity Unit) are often seen in the literature.

Scattering   The physical process by which photons are forced to deviate from a straight trajectory due to features such as particles, bubbles and density differences in water and sea ice.

Secondary production   Production of new organic matter by herbivores, carnivores or detritus feeders (c.f. primary production). In sea ice ecosystems, this is largely consumption of organic material such as ice algae by zooplankton or ingestion of phytoplankton by benthic organisms.

Skeletal layer   A crystalline layer a few mm thick at the bottom of the sea ice where actively growing ice crystals protrude into the seawater and where most of the ice algae biomass is usually located.

Stratification   Separation of water masses with different properties, e.g., different salinity (halocline), density (pycnocline), and temperature (thermocline), forming layers that act as barriers to water mixing.

Supercooled or undercooled water   Water with a temperature below its freezing point but still in the liquid phase.

Sympagic   Organisms or ecosystems associated with ice, including sea ice and other ice environments such as glaciers.

TA   Total alkalinity, a measure of the charge balance in seawater and in natural seawater at pH > 8, with units of μmol kg^{-1} seawater.

TCO$_2$ In seawater, CO_2 exists as three inorganic forms: dissolved CO_2, HCO_3^- and CO_3^{-2}. The sum of the concentration of these forms is the total dissolved inorganic carbon, abbreviated TCO$_2$, in units of μmol kg^{-1} seawater.

Thermocline   The plane of maximum rate of decrease or increase in temperature with depth in a water body, usually seen at a specific water depth and forming a barrier between layers during stratification.

Transmittance   The ratio between irradiance just below a package of ice or snow, for instance, and downwelling irradiance at surface of the ice or snow.

Ultraviolet radiation   The part of the electromagnetic spectrum with wavelengths from 100 nm to 400 nm, outside the visible or photosynthetically active spectrum, and therefore potentially harmful to sea ice algae and other biota. Abbreviated as UVR, and comprises UV-A (400–320 nm), UV-B (320–280 nm), UV-C (280–100 nm).

Xanthophyll   Broad term referring to a wide-range of yellow-coloured accessory pigments to photosynthesis in chloroplasts.

Zooplankton   Floating and drifting animal life in aquatic environments, comprising those organisms unable to swim against a current, c.f. nekton.